# Fatigue Life Prediction of Adhesively-Bonded Fiber-Reinforced Polymer Structural Joints under Spectrum Loading Patterns

THÈSE N$^{O}$ 5573 (2012)

PRÉSENTÉE LE 19 DÉCEMBRE 2012
À LA FACULTÉ DE L'ENVIRONNEMENT NATUREL, ARCHITECTURAL ET CONSTRUIT
LABORATOIRE DE CONSTRUCTION EN COMPOSITES
PROGRAMME DOCTORAL EN STRUCTURES

ÉCOLE POLYTECHNIQUE FÉDÉRALE DE LAUSANNE

POUR L'OBTENTION DU GRADE DE DOCTEUR ÈS SCIENCES

PAR

Roohollah SARFARAZ KHABBAZ

acceptée sur proposition du jury:

Prof. J.-P. Lebet, président du jury
Prof. T. Keller, Dr A. Vasilopoulos, directeurs de thèse
Prof. J.-F. Molinari, rapporteur
Prof. T. Philippidis, rapporteur
Prof. W. Van Paepegem, rapporteur

ÉCOLE POLYTECHNIQUE
FÉDÉRALE DE LAUSANNE

Suisse
2012

*To my parents and my wife Assieh*

# Preface

Fiber-reinforced polymer (FRP) composites are increasingly used in engineering structures thanks to their advantageous material properties such as high specific strength, high insensitivity to frost and de-icing salts, and short installation times, with minimum traffic interference in the case of bridge construction. Advances in pultrusion technology allow the production of large-scale structural components at acceptable costs for civil infrastructure applications and adhesive bonding constitutes a material-tailored connection technology for joining these large-scale components.

Since FRP structures are light in weight compared to their live loads, the repetitive loading to which they are subjected raises the question of the fatigue behavior of such structures and, in particular, their adhesively-bonded connections. The work presented by Roohollah Sarfaraz Khabbaz in this doctoral thesis is a continuation of the work of Ye Zhang (EPFL doctoral thesis No. 4662, 2010). While Ye Zhang focused on constant amplitude loading, the main topic of this work is joints subjected to spectrum loading patterns (or variable amplitude loading). Variable amplitude loading offers a much closer representation of the loading of real structures.

I would like to acknowledge the support provided for this research project by the Swiss National Science Foundation, Fiberline Composites A/S, Denmark (pultruded laminate supplier), and Sika AG, Zurich (adhesive supplier).

Prof. Dr. Thomas Keller

# Abstract

New load-bearing structures made of fiber-reinforced polymer (FRP) composites comprise adhesively-bonded joints, which are components vulnerable to fatigue failure. These structural components are frequently subjected to complex cyclic loading histories during their service life and the development of reliable methodologies for prediction of their fatigue life under variable amplitude loading patterns is therefore essential. Experimental investigations on FRP laminates showed significant effects of spectrum loading on the fatigue life. However, scientific efforts to study the fatigue behavior of adhesively-bonded FRP joints are mainly focused on constant amplitude fatigue loading and many loading parameters involved in the variable amplitude spectrums have not yet been investigated.

The aim of this research is to understand the fatigue behavior of adhesively-bonded FRP joints under different loading patterns and establish a reliable methodology for the fatigue life prediction of these structural components. The fatigue response of a typical adhesively-bonded structural joint, a double-lap joint, was experimentally investigated under different loading patterns including constant amplitude, block and variable amplitude loading. The development of fatigue cracks during the lifetime and their correlation with the observed failure modes and applied cyclic load were analyzed. The experimental investigations revealed the loading parameters that significantly influence fatigue behavior and that therefore must be considered in the fatigue life prediction methodology.

A new semi-empirical S-N formulation was developed to characterize the constant amplitude fatigue life and overcome the deficiencies of the fatigue models commonly used for composite materials. Based on the experimental investigation results, two phenomenological formulations were proposed in order to model the loading parameters that affect fatigue life. A new constant life diagram was developed to model the effect of mean stress on fatigue life and its accuracy was assessed using the experimental data. Also, a method was proposed to take into account the load interaction effects under variable amplitude loading.

A fatigue life prediction methodology was established using the newly developed models and implemented in the form of a computational tool to predict the fatigue life of adhesively-bonded FRP joints. The variable amplitude fatigue life predictions obtained using this methodology correlated fairly well with the experimental results and proved its effectiveness in real applications.

**Keywords:** Bonded joints; Pultruded laminates; Fatigue life prediction; Block loading; Variable amplitude loading; S-N curve; Constant life diagram.

# Résumé

Les nouvelles structures porteuses fabriquées en polymères renforcés avec des fibres (FRP) présentent des joints collés susceptibles d’une rupture à la fatigue. Ces éléments structuraux sont habituellement soumis à des charges cycliques complexes pendant la durée de vie de la structure. Le développement de méthodes fiables pour la prédiction de la durée de vie à la fatigue des joints soumis à des charges cycliques d’amplitude variable s’avère donc indispensable. Des recherches expérimentales réalisées sur des laminés FRP ont montré un effet significatif de la forme du spectre de charge sur la durée de vie à la fatigue. Cependant les efforts scientifiques pour étudier le comportement à la fatigue de joints FRP collés sont fondamentalement centrés dans des charges de fatigue d’amplitude constante et beaucoup de paramètres intervenant dans les spectres de charges d’amplitude variable n’ont pas encore été investigués.

L’objectif de ce projet est de comprendre le comportement à la fatigue des joints collés en FRP soumis à différents spectres de charges et d’établir une méthodologie fiable pour la prédiction de la durée de vie à la fatigue de ces éléments structuraux. La réponse à la fatigue d’un joint collé typique, le joint collé à double recouvrement, a été expérimentalement investigué pour des spectres de charge d’amplitude constante, des spectres en block et des spectres d’amplitude variable. Le développement de fissures de fatigue pendant la durée de vie du joint et sa corrélation avec les modes de rupture observés et la charge cyclique appliquée ont été analysés. Les investigations expérimentales ont mis en évidence les paramètres de chargement influençant significativement le comportement à la fatigue et qui doivent être donc considérés dans la méthodologie pour la prédiction de la durée de vie à la fatigue.

Une nouvelle formulation S-N semi-empirique a été développée afin de caractériser la durée de vie à la fatigue sous spectre de charge d’amplitude constante et de surmonter les déficiences des modèles de fatigue habituellement utilisés pour les matériaux composites. A partir des résultats expérimentaux, deux formulations ont été proposées afin de modéliser les paramètres de chargement influençant la durée de vie à la fatigue. Un nouveau “constant life diagram” a été développé pour modéliser l’effet de la contrainte moyenne dans la durée de vie à la fatigue et son exactitude a été évaluée en utilisant les résultats expérimentaux. Une méthode a été aussi proposée pour tenir en compte les effets d’interaction sous chargement d’amplitude variable.

Les nouveaux modèles développés ont permis d’établir une méthodologie pour la prédiction de la durée de vie à la fatigue. Cette méthodologie a été implémentée sous la forme d’un programme informatique pour prédire la durée de vie à la fatigue des joints FRP collés. Les prédictions de la durée de vie à la fatigue sous spectre de chargement d’amplitude variable obtenues à partir du modèle étaient en accord avec les résultats expérimentaux et ont ainsi prouvé l’efficacité du modèle pour des applications réelles.

**Mots clés:** Joints collés; Laminés pultrudés; Prédiction de la durée de vie à la fatigue; Spectre de charge en block; Spectre de charge d’amplitude variable; Courbe S-N; “Constant life diagram”.

# Acknowledgments

In the course of my doctoral research, I have received encouragement and support from many different people. I would like to express my gratitude to all those who provided me with the circumstances to complete this thesis.

First and foremost, I would like to express my gratitude to my thesis directors: Prof. Thomas Keller for providing me with such an opportunity to do this research project and for his guidance and support and Dr. Anastasios P. Vassilopoulos for his regular supervision, fruitful and rich discussions, and his encouragement and recommendations during the difficult times of this project.

I would also like to acknowledge the exceptional sources that supported this project:

- The Swiss National Science Foundation for funding the project (Grant No 200020-121756).
- Fiberline Composites A/S, Denmark for supplying the pultruded laminates
- Sika AG, Zurich for supplying the adhesive.

I wish to express my thanks to the thesis defense committee for the time and effort they devoted to reading and evaluating my thesis: Prof. Jean-Francois Molinari, Director of the Computational Solid Mechanics Laboratory (LSMS), EPFL, Switzerland; Prof. Theodore Philippidis, Department of Mechanical Engineering & Aeronautics, University of Patras, Greece; Prof. Wim Van Paepegem, Department of Materials Science and Engineering, Ghent University, Belgium; and Prof. Jean-Paul Lebet, Head of the Steel Structures Laboratory (ICOM), EPFL, Switzerland, President of the jury.

The incredible team in the laboratory (IIC-EPFL) for their continuous help and support, Sylvain Demierre for his technical coordination and contribution to experimental set-ups; Gilles Guignet for his useful help with experimental set-ups and development of data acquisition programs, Patrice Gallay, Roland Gysler, Gérald Rouge, and Léa Frédérique Dubugnon for their precise work for the preparation of experimental samples and François Perrin for his unfailing help and support.

I would also like to thank those who provided incredible technical support, Mrs. Margaret Howett for the diligent English correction of the thesis, Mrs. Magdalena Schauenberg for all the administrative coordination and my colleague Carlos Pascual Agullo for converting the English abstract into the French (résumé).

I would like to thank my current colleagues in CCLab – EPFL, Dr. Julia de Castro, Moslem Shahverdi, Michael Osei-Antwi, Carlos Pascual Agullo, Wei Sun, Kyriaki Goulouti, Haifeng Fan, and Myrsini Angelidi as well as my ex-colleagues, Dr. Behzad Dehghan Manshadi, Dr. Omar Moussa, Dr. Ye Zheng, Dr. Yu Bai and Dr. Erika Schaumann, for their help and support and for providing a friendly environment.

I would like also to thank my friends for their support, and last but not least, my sincere gratitude goes to my family for their support and love, particularly my parents for the extraordinary sacrifices throughout my life, my wife to whom I am indebted for her tireless support and understanding and my in-laws for their exceptional encouragement.

# Nomenclature

## *Abbreviation*

ASTM − American Society for Testing and Materials
BL − Block Loading
BR − Boerstra
CA − Constant Amplitude
C-C − Compression-Compression
CFRP − Carbon Fiber Reinforced Polymer
CLD − Constant Life Diagram
CSM − Chopped Strand Mat
DCB − Double Cantilever Beam
DLJ − Double Lap Joint
ESS − equivalent static strength
FCG − Fatigue Crack Growth
FRP − Fiber Reinforced Polymer
GFRP − Glass Fiber Reinforced Polymer
HCF − High-Cycle Fatigue
H-L − High-Low loading sequence
HLR − High Loading rate
HR − Harris
K-S − Kolmogorov-Smirnov
KW − Kawai
K-W − Kruskal-Wallis
LCF − Low-Cycle Fatigue
LEFM − Linear Elastic Fracture Mechanics
L-H − Low-High loading sequence
LLR − Low Loading rate
LR − Linear
PEEK − Poly Ether Ether Ketone
PNL − Piecewise Nonlinear

POLY − Polynomial

PWL − Piecewise Linear

S.L. − Significance Level

SERR − Strain Energy Release Rate

SLERA − Strength Life Equal Rank Assumption

SSE − Sum of Squared Errors

T-C − Tension-Compression

T-T − Tension- Tension

UCL − Ultimate Compressive Load

UCS − Ultimate Compressive Stress

UTL − Ultimate Tensile Load

UTS − Ultimate Tensile Stress

VA − Variable Amplitude

WISPER − Wind turbine reference spectrum

***Notations (Chapter 3)***

$\sigma$ − Stress variable

$\sigma_e$ − Endurance limit

$\sigma_u$ − Ultimate strength

$\sigma_{\min}$ − Minimum cyclic stress

$\sigma_{\max}$ − Maximum cyclic stress

$\sigma_{eq}$ − Equivalent static strength

$\sigma_a$ − Stress amplitude

$\Delta\sigma$ − Stress range

$\alpha_f$ − Shape parameter of Weibull distribution

$\beta$ − Scale parameter of Weibull distribution

$R$ − Stress ratio ($R=\sigma_{\min}/\sigma_{\max}$) or Load ratio ($R=F_{\min}/F_{\max}$)

$\psi$ − $\psi = R$ for $-\infty < R < 1$, $\psi = 1/R$ for $1 < R < \infty$

$\theta$ − Off-axis angle

$fr$ − Frequency of cyclic loading

$N_f$ − Number of cycles to failure

$N_{cyclic}$ − Lower limit for the low cycle fatigue life

$N_{LCF}$ − Upper limit for the low cycle fatigue life

$\rho$ − Density of composite material

$A_{cr}$ − Cross-sectional area of specimen

$E$ − Elastic Young's modulus

$E_0$ − Young's modulus corresponding to static loading

$E_1$ − Young's modulus measured at first cycle

$E_N$ − Young's modulus measured at N-th cycle

$F$ − Load

$F_{max}$ − Maximum cyclic load

$F_{min}$ − Minimum cyclic load

$P_N(N)$ − Probability of failure

$R_N(N)$ − Probability of survival

$a, A, b, B, m, c, d, D, f, S, \alpha, \delta, r, m_2, K, a_{LCF}, b_{LCF}, a_{HCF}, b_{HCF}, g, Q, S_0, x, y$ − Parameters of S-N models

**_Basic fatigue terminology_**

The basic fatigue terminology for constant amplitude loading patterns is schematically presented in the following figure. The load ratio ($R$-ratio) is defined as the ratio of minimum to maximum cyclic load ($R=F_{\text{min}}/F_{\text{max}}$). $F_{\text{mean}}$, $F_{\text{amp}}$, and $\Delta F$ denote mean load, load amplitude, and load range respectively and $f$ denotes the frequency of cyclic load.

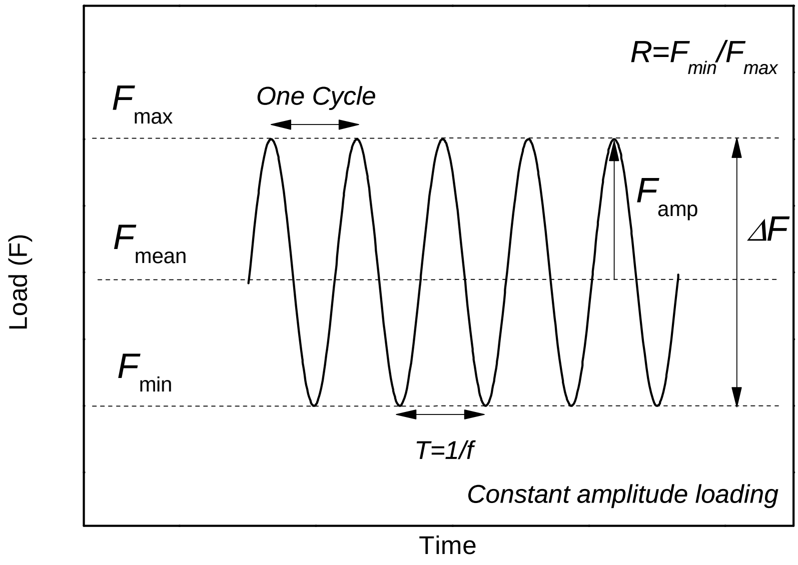

# Table of Contents

**Preface** **v**

**Abstract** **vii**

**Résumé** **ix**

**Acknowledgment** **xi**

**Nomenclature** **xiii**

**1. Introduction** **1**

1.1. Motivation 1

1.2. Objectives 4

1.3. Investigation method 4

1.4. Thesis organization 5

1.5. References 8

**2. Experimental investigations** **11**

2.1. Material description 11

2.2. Specimen geometry and fabrication 14

2.3. Experimental set-up and instrumentation 15

2.3.1. Quasi-static experiments 15

2.3.2. Constant amplitude experiments 15

2.3.3. Block loading experiments 16

2.3.4. Variable amplitude experiments 19

2.4. References 20

**3. Constant amplitude loading 21**

3.1. Introduction 21

3.2. Experimental results and discussion 25

3.2.1. Quasi-static investigation 25

3.2.2. Fatigue investigation 27

3.2.2.1.Failure modes 27

3.2.2.2.Fatigue life 27

3.2.2.3.Stiffness degradation 31

3.2.2.4.Fracture mechanics 34

3.3. S-N formulations for composites 41

3.4. Application of S-N formulations to experimental data 44

3.4.1. Selection of the appropriate S-N formulations 44

3.4.2. Assumptions of the selected models – validation methods 45

3.4.3. Model application – Validation of hypotheses 47

3.4.3.1.Linear or linearized fatigue models 49

3.4.3.2.Pooling scheme 52

3.4.3.3.Wear-out model 55

3.4.4. Effect of static strength data 58

3.5. Conclusions 62

3.6. References 65

**4. Hybrid S-N formulation 69**

4.1. Introduction 69

4.2. Disadvantages of commonly used S-N models 73

4.3. The hybrid S-N formulation 76

4.4. Comparison with existing fatigue models 79

4.4.1. Glass fiber-reinforced laminates 80

4.4.2. Carbon fiber-reinforced laminates 85

4.4.3. Hybrid glass-carbon fiber-reinforced laminates 85

4.4.4. Short fiber-reinforced laminates 87

4.4.5. Pultruded fiber-reinforced adhesively-bonded joints 87

4.5. Discussion 88

4.6. Conclusions 90

4.7. References 91

**5. Mean load effect 95**

5.1. Introduction 95

5.2. Experimental results 97

5.2.1. Failure modes 97

5.2.2. Fatigue life 98

5.2.3. Constant life diagram 101

5.3. Modeling 102

5.4. Results and discussion 105

5.5. Conclusions 111

5.6. References 112

**6. Block loading 115**

6.1. Introduction 115

6.2. Experimental results 117

6.2.1. Failure modes 117

6.2.2. Block loading results 118

6.3. Discussion 122
    6.3.1. Loading sequence effect 122
        6.3.1.1. Tensile loading 122
        6.3.1.2. Compressive loading 124
        6.3.1.3. Failure mode and sequence effect 127
        6.3.1.4. Modeling issues 128
    6.3.2. Load transition effect 129
6.4. Conclusions 130
6.5. References 131
**7. Variable amplitude loading 135**
7.1. Introduction 135
7.2. Experimental results 138
    7.2.1. Failure mode 138
    7.2.2. Fatigue life and crack propagation 138
7.3. Modified fatigue life prediction methodology 145
    7.3.1. Cycle-counting methods 145
    7.3.2. S-N formulations 146
    7.3.3. Constant life diagrams 147
    7.3.4. Damage summation 148
    7.3.5. Effect of frequent load transition 149
7.4. Results and discussion 151
7.5. Conclusions 154
7.6. References 155
**8. Conclusions and future work 159**
8.1. Conclusions 159

8.1.1. Experimental investigations 159

8.1.2. Analytical investigations 161

8.2. Original contributions 163

8.3. Recommendations for future research 164

8.3.1. Modeling of fatigue-creep interaction 164

8.3.2. Investigation of loading parameters 165

8.3.3. Development of damage accumulation models 165

**Annex 1. *CCfatigue software*** **167**

**Annex 2. Pultruded GFRP laminates** **177**

**Annex 3. Double-lap joints quasi-static loading** **187**

**Curriculum Vitae** **195**

# 1 Introduction

## 1.1. Motivation

Engineering structures are subjected to complex loading histories combining cyclic thermal/humidity and mechanical loading. These loading patterns are frequently of variable amplitude and cause damage in the material that eventually leads to functional and/or structural integrity problems. Adhesively-bonded fiber-reinforced polymer (FRP) joints represent a critical element in numerous engineering structures nowadays, and they must therefore be able to transfer the developed stresses (of a complex nature) from one part of the structure to another. One of the scientific research community's key objectives is thus the development of reliable methodologies for the fatigue life prediction of adhesively-bonded FRP joints under realistic loading patterns, and this requires an extensive study of the fatigue behavior of these joints.

The behavior of structural FRP joints under fatigue loads has already been examined, mainly in relation to bolted joints in automotive and aerospace applications [1-3]. Although bolted and bonded joints have their advantages and disadvantages, adhesively-bonded joints are preferred for permanent connections in FRP civil engineering structures [4-8]. This type of joint offers cost-effective structures with uniform geometrical shapes without the need for cutting fastener holes in the FRP adherends, resulting in a material-adapted stress transfer. Also, it is more appropriate for corrosion-resistant lightweight structures since no metallic parts are used and, due to the absence of moving parts, adhesively-bonded joints exhibit very good fatigue behavior.

The scientific research performed on the fatigue of FRP composite joints is mainly restricted to constant amplitude (CA) loading. The aim of these investigations was to explore the basic fatigue characteristics of bonded FRP joints, e.g. failure mechanisms, fatigue limit, and effect of environmental conditions [5, 9]. However, most structural components such as joints are subjected to stochastic loading patterns that introduce more complex phenomena such as load interaction effects (e.g. load sequence and overload effects) than constant amplitude loading. The experimental fatigue studies on composite laminates showed significant effects due to the load interactions. The effect of loading sequence was examined for different composite materials and its detrimental or beneficial contribution to the fatigue life was found to be material-dependent [10-21]. As far as adhesively-bonded FRP joints are concerned, only a small number of articles focused on the subject of block and variable amplitude fatigue loading [22-23]. These experimental investigations mainly concentrated on the fatigue crack initiation phase and the total life and little information regarding crack propagation under variable amplitude (VA) loading was provided.

In order to quantify fatigue damage in FRP materials and structures, in addition to crack development, other measures such as cyclic stress, cyclic strain, remaining stiffness, and remaining strength were used by scientists as damage metrics. Among the proposed damage metrics, two quite popular approaches for the fatigue life prediction of materials are the phenomenological stress-life theory, which is a macroscopic approach, and fracture mechanics theory that focuses on fatigue crack growth. The first approach is based on the establishment of reliable S-N curves and the modeling of fatigue life using a number of macroscopic fatigue data, while the second is derived from accurate measurements of the developed fatigue crack and its correlation with a fracture mechanics parameter such as strain energy release rate.

Macroscopic, classic stress-life prediction methods have the advantage that they can be used to predict the variable amplitude fatigue life of any composite material or structure based on only a small amount of static and constant amplitude fatigue data. They cannot, on the other hand, be used to predict the fatigue life of any other material or structural component or joint, since they do not comprise any information about the geometry (stacking sequence of a laminate, or geometry of an adhesively-bonded joint) or substrate materials and adhesive of the examined system. Fracture mechanics can be employed for VA fatigue life prediction irrespective of the joint configuration. However, to establish a credible fracture failure criterion that takes into account the effect of different fracture modes and their interactions on the fatigue life, an extensive experimental program is required. The literature review shows few reports on the modeling of the fatigue life of adhesively-bonded joints based on the aforementioned approaches. These models are mainly based on crack propagation measurements under constant amplitude fatigue loading patterns and only during the last few years has the fatigue behavior been investigated under more realistic loading conditions in order to develop and evaluate the theoretical models [22, 23].

In spite of the recent investigations into the topic, many parameters involved in cyclic loading have not yet undergone detailed and systematic analysis. The anisotropy of composite materials in addition to the joint geometry can lead to different failure modes under cyclic loading, e.g. different failure modes under tensile or compressive fatigue loading and different locations of failure. Also several loading parameters such as the mean load and the load sequence effects may affect the fatigue behavior of bonded FRP joints, similarly to their influence on composite laminates. The lack of consistent experimental data for bonded FRP joints under CA, VA and block loading, as an intermediate phase between CA and VA, also hinders the development of credible models. However, the feasibility of fatigue crack monitoring during the initiation and propagation phases in bonded joints compared to composite laminates enables a correlation to be established between CA and VA fatigue behavior and consequently the development of reliable fatigue life prediction models.

The aim of this PhD thesis was to attempt to deal with these unresolved problems and recommend new, more reliable design methods for adhesively-bonded FRP joints under operational loading patterns. The classic stress-life prediction method was used as the theoretical basis for this investigation. Full-scale structural joints subjected to constant, block, and variable amplitude loading were also used to understand the fatigue behavior under different loading conditions. This work was conducted in parallel with another PhD project focused on the fracture mechanics of the same material system. These projects, supported by the Swiss National Science Foundation (Grant No. 200020-121756), were intended to provide some experimental data in order to establish an appropriate methodology for the fatigue life prediction of structural FRP joints under realistic loading patterns.

## 1.2. Objectives

The main purpose of this research is the experimental investigation of the fatigue behavior of structural adhesively-bonded joints and the establishment of a fatigue life prediction methodology under realistic loading conditions based on quasi-static and constant amplitude fatigue data. The specific objectives include the following:

1. Understand the behavior of the examined materials and structural joints under complex fatigue loading patterns:
    a. Characterization of the mechanical behavior of the constituent materials (GFPR laminates and adhesive) under quasi-static loading.
    b. Characterization of the behavior of structural joints under quasi-static loading, constant amplitude fatigue, and variable amplitude fatigue.
    c. Characterization of the loading interaction effects (load sequence, overload, etc.) on the fatigue behavior of structural joints.
2. Develop theoretical models for:
    a. The interpretation of fatigue data obtained from structural adhesively-bonded FRP joints.
    b. The formulation of constant life diagrams based on fatigue data gathered from experiments under different loading patterns.
    c. Considering the effect of load interactions on the life of structural joints.
    d. The establishment of a phenomenological life prediction methodology combining research findings from the previous steps (a-c).

## 1.3. Investigation method

To achieve the aforementioned objectives, an extensive experimental program was carried out in order to understand the behavior of the examined bonded joints under different loading conditions. Initially, specific experimental data were gathered to form the basis for the development of the theoretical models. Semi-empirical and phenomenological models were developed to characterize and to take into account the parameters involved in the fatigue behavior of the examined bonded joints. Finally, fatigue failure data under selected loading conditions were used for validation of the developed models. The research project flow chart is shown in Fig. 1.1.

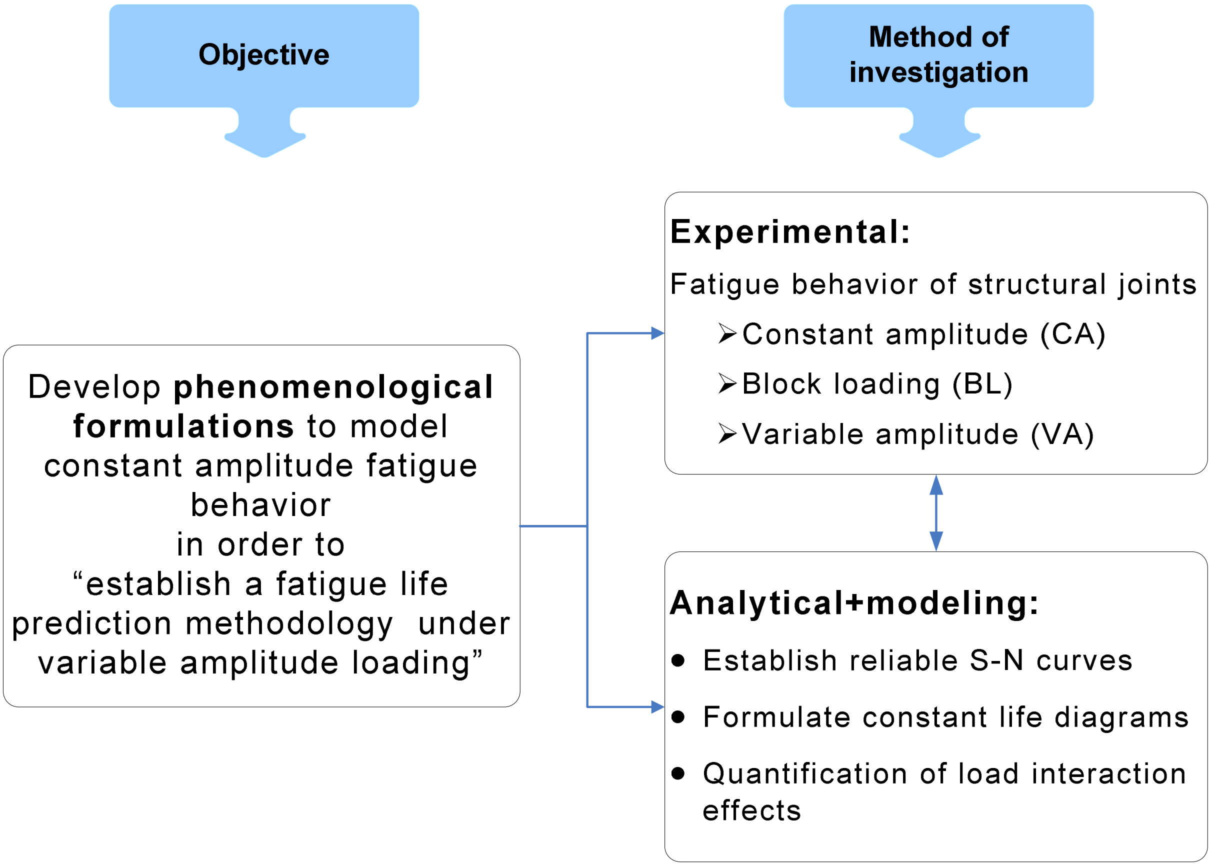
Objective
Method of investigation
Experimental:
Fatigue behavior of structural joints
➢Constant amplitude (CA)
➢Block loading (BL)
➢Variable amplitude (VA)
Develop phenomenological formulations to model constant amplitude fatigue behavior in order to "establish a fatigue life prediction methodology under variable amplitude loading"
Analytical+modeling:
● Establish reliable S-N curves
● Formulate constant life diagrams
● Quantification of load interaction effects

Fig. 1.1. Research project flow chart

The method of investigation is detailed in the following steps:

1. The quasi-static experiments were performed on the constituent materials (pultruded GFRP substrates and epoxy adhesive systems) and the structural joints under investigation.
2. The constant amplitude fatigue behavior of joints was investigated under tensile, compressive, and reversed fatigue.
3. The applicability of the developed models for characterizing the constant amplitude fatigue behavior of composite materials was investigated.
4. The effect of the *R*-ratio (the ratio of the minimum to maximum applied cyclic load) was experimentally studied. The existing formulations for composite materials were applied to model this effect and their strengths and shortcomings were discussed.
5. The stress-life approach was used to predict the variable amplitude fatigue life of bonded joints based on the models developed in previous steps and the established design tool.

6. The structural response of joints under a variable amplitude loading spectrum was experimentally investigated. The prediction accuracy of the applied methodology was evaluated using these experimental data.

## 1.4. Thesis organization

The present thesis is comprised of eight chapters that were organized in order to address the objectives referred to in Section 1.2 as follows:

- **Chapter 1**: The significance of the fatigue analysis of adhesively-bonded composite joints in structural design is discussed and the investigations performed in this field are briefly reviewed. The knowledge gap for the reliable fatigue design of these structural elements is extracted from the state –of –the art to define the research objectives. The method of investigation, including the experimental and theoretical analyses, designed to achieve the defined objectives, is described. The overall content of the thesis is also summarized in this chapter.
- **Chapter 2**: The details of the experimental investigation are presented. The properties of the constituent materials of structural joints, joint configurations, and the fabrication process are described. The planned experimental program consisting of quasi-static and fatigue loading experiments is elaborated. The loading set-up, experimental conditions and measuring systems employed to collect the experimental data are explained.
- **Chapters 3**: The fatigue response of adhesively-bonded pultruded GFRP double-lap joints was investigated under different loading patterns and experimental results were obtained for three different applied load ratios: $R$=0.1, $R$=10, and $R$=-1. The failure mode, fatigue life, stiffness degradation, and fracture mechanics of the examined joint configuration were studied. The constant amplitude fatigue behavior was modeled by a number of conceptually different phenomenological S-N formulations in order to investigate their appropriateness for accurate modeling of lifetime from the very low cycle fatigue to the high cycle fatigue regions. Based on an extensive review, appropriate fatigue formulations that take into account the probabilistic nature of lifetime measurements were selected and their fundamental assumptions examined.
- **Chapter 4**: A semi-empirical S-N formulation for the modeling of the constant amplitude fatigue behavior of the examined bonded joints is introduced based on the well-known fatigue models for metallic and composite materials. The new S-N model

is a hybrid formulation combining the two existing models in order to improve their modeling accuracy in the low and high cycle fatigue regions. This formulation was applied to a number of fatigue databases for different composite materials and structural elements in order to simulate their fatigue behavior. The modeling accuracy of the hybrid model was compared to the accuracy of commonly used S-N models for composite materials.

- **Chapter 5**: The effect of mean load on the fatigue behavior of the joints under constant amplitude loading was experimentally investigated. The joints were examined under nine different load ratios ($R$) representing pure tension, compression, and combined tension-compression fatigue loading. The characteristics of the constant life diagram developed for the examined bonded joints are thoroughly discussed. A phenomenological formulation is proposed and its accuracy evaluated by comparisons with the derived experimental data.
- **Chapter 6**: The effect of loading sequence was experimentally investigated by applying different tensile and compressive block loading patterns. The observed failure modes were compared with failure modes under constant amplitude loading. A significant load sequence effect observed for both tensile and compressive loading was associated with the crack propagation rates and their dependence on loading type. The effect of the number of load transitions in a multi-block loading spectrum was also studied by using different loading sequences. The influence of this loading parameter compared to the sequence effect was discussed.
- **Chapter 7**: The variable amplitude fatigue behavior of bonded joints was experimentally investigated. The acceleration or retardation in the crack propagation rate due to the load interaction effects was thoroughly investigated by monitoring crack propagation during the variable amplitude loading. The variable amplitude fatigue life of the joints was predicted using classic fatigue life prediction methodology. The previously developed models for characterizing the fatigue behavior of the examined joints were employed together with the linear Palmgren-Miner’s rule for prediction of fatigue life under variable amplitude loading patterns. A simple modification was incorporated into the applied methodology to take into account the load interaction effects involved under variable amplitude loadings.
- **Chapter 8**: The conclusions derived from experimental and theoretical investigations are presented. The original contributions of the present work to the research topic are

also highlighted in this chapter. Finally some recommendations regarding future work to complement this research are given.

## 1.5. References

1. Demuts E. Fatigue spectrum sensitivity of composite joints, Composites, 1983;14(1):27–33.
2. Schön J, Nyman T. Spectrum fatigue of composite bolted joints, Int J Fatigue, 2002;24(2):273–279.
3. Schön J. Spectrum fatigue of composite bolted joints-small cycle elimination, Int J Fatigue, 2006;28(1):73–78.
4. Burgueño R, Karbhari VM, Seible F, Kolozs RT. Experimental dynamic characterization of an FRP composite bridge superstructure assembly, Compos Struct, 2001;54(4):427–444.
5. Keller T, Tirelli T. Fatigue behavior of adhesively connected pultruded GFRP profiles, Compos Struct, 2004;65(1):55–64.
6. Keller T, Gürtler H. Quasi-static and fatigue performance of a cellular FRP bridge deck adhesively bonded to steel girders, Compos Struct, 2005;70(4):484-496.
7. Keller T, Zhou A. Fatigue behavior of adhesively bonded joints composed of pultruded GFRP adherends for civil infrastructure applications, Compos Part A-Appl S, 2006;37(8):1119–1130.
8. Zhang Y, Vassilopoulos AP, Keller T. Stiffness degradation and life prediction of adhesively-bonded joints for fiber-reinforced polymer composites, Int J Fatigue, 2008;30(10-11):1813–1820.
9. Zhang Y, Vassilopoulos AP, Keller T. Environmental effects on fatigue behavior of adhesively-bonded pultruded structure joints, Compos Sci Technol, 2009;69(7–8):1022–1028.
10. Van Paepegem W, Degrieck J. Effects of load sequence and block loading on the fatigue response of fibre-reinforced composites, Mech Adv Mater Struct, 2002;9(1):19–35.
11. Han KS, Abdelmohsen MH. Fatigue Life Scattering of RP/C, Int J of Vehicle Design, Technological advances in Vehicle Design Series, SP6, Designing with Plastics and Advanced Plastic Composites, 1983;218–227.

12. Hwang W, Han KS. Cumulative damage models and multi-stress fatigue life prediction, J Compos Mater, 1986;20(2):125–153.
13. Lee CH, Jen MHR. Fatigue response and modelling of variable stress amplitude and frequency in AS-4/PEEK composite laminates, Part 1: Experiments, J Compos Mater, 2000;34(11):906–929.
14. Gamstedt EK, Sjögren BA. An experimental investigation of the sequence effect in block amplitude loading of cross-ply laminates, Int J Fatigue, 2002;24(2-4):437–446.
15. Broutman LJ, Sahu S. A new theory to predict cumulative fatigue damage in fibre-glass reinforced plastics, In: Composite materials: testing and design (2nd Conference), pp. 170–188, ASTM STP 497, American Society for Testing and Materials, Philadelphia (1972).
16. Yang JN, Jones DL. Load sequence effects on the fatigue of unnotched composite materials, In: Fatigue in Fibrous Composite Materials, KN. Lauraitis (Ed.), pp. 213–231, ASTM STP 723, American Society for Testing and Materials, Philadelphia (1981).
17. Found MS, Kanyanga SB. The influence of two-stage loading on the longitudinal splitting of unidirectional carbon-epoxy laminates, Fatigue Fract Engng Mater Struct, 1996;19(1):65–74.
18. Otani N, Song DY. Fatigue life prediction of composite under two-step loading, J Mater Sci, 1997;32(3):755–760.
19. Bartley-Cho J, Lim SG, Hahn HT, Shyprykevich P. Damage Accumulation in Quasi isotropic Graphite/Epoxy Laminates under Constant-Amplitude Fatigue and Block Loading, Compos Sci Technol, 1998;58(9):1535–1547.
20. Wahl NW, Mandell JF, Samborsky DD. Spectrum fatigue lifetime and residual strength for fiberglass laminates in tension, ASME Wind Energy Symposium, AIAA-2001-0025, ASME/AIAA, 2001, pp. 1–11.
21. Hosoi A, Kawada H, Yoshino H. Fatigue characteristic of quasi-isotropic CFRP laminates subjected to variable amplitude cyclic loading of two-stage, Int J Fatigue, 2006;28(10 SPEC. ISS.):1284–1289.
22. Erpolat S, Ashcroft IA, Crocombe AD, Abdel-Wahab MM. A study of adhesively bonded joints subjected to constant and variable amplitude fatigue, Int J Fatigue, 2004;26(11):1189–1196.

23. Erpolat S, Ashcroft IA, Crocombe AD, Abdel-Wahab MM. Fatigue crack growth acceleration due to intermittent overstressing in adhesively bonded CFRP joints, Compos Part A-Appl S, 2004;35(10):1175–1183.

# 2 Experimental investigations

## *Abstract*

*The details of the experimental investigation are presented. The properties of the constituent materials of structural joints, joint configurations, and the fabrication process are described. The planned experimental program consisting of quasi-static and fatigue loading experiments is elaborated. The loading set-up, experimental conditions and measuring systems employed to collect the experimental data are explained.*

## 2.1. Materials description

Pultruded GFRP laminates, supplied by Fiberline A/S, Denmark, consisted of E-glass fibers and isophthalic polyester resin were used for fabrication of bonded joints. The fiber architecture of the laminates is shown in Fig. 2.1. The laminate comprises two mat layers on each side and a roving layer in the middle, with a thin layer of polyester veil on the outer surfaces of the laminate. Each mat layer comprises a woven fabric stitched to a chopped strand mat (CSM). An estimation of the nominal thickness of each layer derived by optical microscopy is also given in Fig. 2.1.

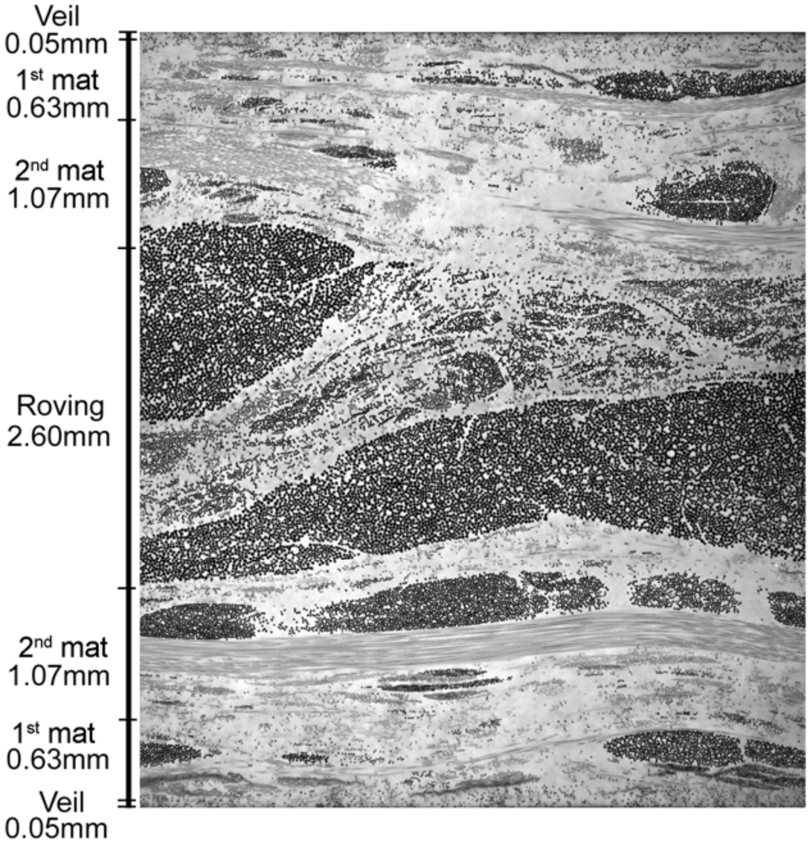
Veil
0.05mm
1st mat
0.63mm
2nd mat
1.07mm
Roving
2.60mm
2nd mat
1.07mm
1st mat
0.63mm
Veil
0.05mm

Fig. 2.1. Microscopic view of laminates (cross section perpendicular to pultrusion direction)

The fiber content, determined by burn-off experiments (Fig. 2.2) according to test method I – procedure G of the ASTM D3171-09, was 43.2 vol.% based on the fiber density of 2560 kg/m$^3$ specified by the manufacturer. The burn-off tests were carried out on three specimens cut from the long laminates and kept for 5 hours at 600°C in an electric oven.

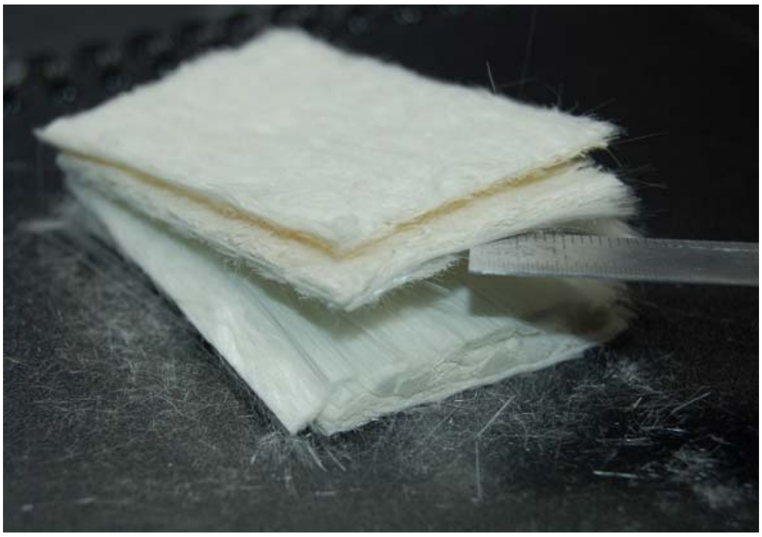

Fig 2.2. Typical architecture of laminates after burn off

The longitudinal strength and Young's modulus of the GFRP laminate were obtained from tensile experiments, according to ASTM D3039-08, as being 307.5±4.7 MPa and 25.1±0.5 GPa respectively. The details of the experimental data for different specimens are presented in Table 2.1.

Table. 2.1. Longitudinal tensile test results for pultruded laminates

| | Specimen No. | | |
|---|---|---|---|
| | 1 | 2 | 3 |
| Maximum tensile load [kN] | 77.24 | 78.56 | 76.34 |
| Maximum tensile strength [MPa] | 305.04 | 312.94 | 304.51 |
| Tensile modulus of elasticity [GPa] | 24.63 | 24.90 | 25.63 |
| Poisson's ratio | 0.23 | 0.24 | 0.23 |

A two-component epoxy adhesive system (Fig. 2.3) was used (Sikadur 330, Sika AG Switzerland) as the bonding material. The tensile strength of the adhesive was 38.1±2.1 MPa and the stiffness 4.6±0.1 GPa. The epoxy showed an almost elastic behavior and a brittle failure under quasi-static tensile loading [1].

Sikadur®- 330
1 Kg Comp. B
Sikadur®- 330
4 Kg Comp. A

Fig. 2.3. Sikadur®-330 two components epoxy adhesive

## 2.2. Specimen geometry and fabrication

Symmetric adhesively-bonded double-lap joints composed of pultruded GFRP laminates bonded using an epoxy adhesive system were fabricated for entire experimental program. All surfaces subjected to bonding were mechanically abraded (to a depth of approximately 0.3 mm) in order to increase roughness, and then chemically degreased using acetone. An aluminum frame was employed to assist the alignment of the laminates. The thickness of the adhesive was controlled by using 2-mm thick spacers embedded in the bonding area. The specimens were kept for at least 10 hours at 30 °C and at least 3 days in laboratory conditions to ensure full curing of the adhesive.

Two different joint configurations were prepared; one with a total length of 410 mm, see Fig. 2.4, and used only for tensile loading, and another with a reduced total length of 350 mm, which was used when compressive loads were applied to avoid any buckling of the joints. To achieve the latter configuration, the free length of the “inner laminate” was reduced from 100 mm to 40 mm without changing the bonding and gripping length. These dimensions were selected after preliminary testing and modal analysis using the finite element software ANSYS, v.10, which indicated that this length reduction sufficed to prevent the buckling of the laminates. Moreover, the finite element stress analysis showed that there is no change in the stress field close to the bonded area due to the decreased laminate length. The bond line was kept constant at 50 mm for both joint configurations.

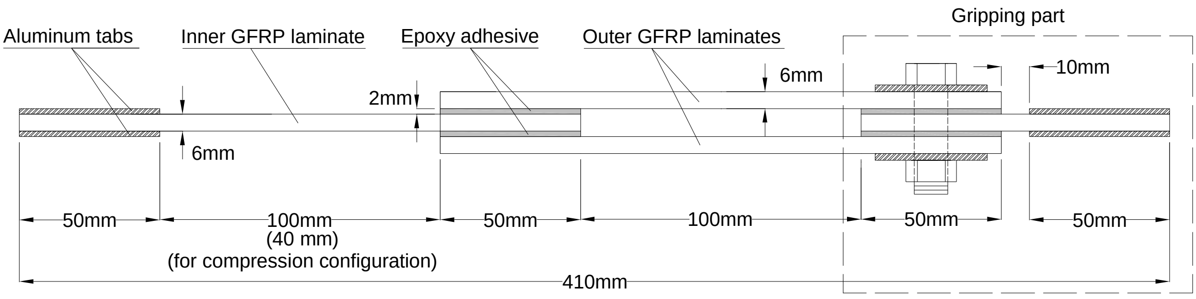

Fig. 2.4. DLJ geometry

The gripping areas at both sides of the specimen were also 50-mm long to allow load transfer through shear. Aluminum tabs were used to avoid crushing of the laminate by the wedges of the testing frame. The gripping part (shown on the right side of the specimen in Fig. 2.4) was designed to adapt the thickness of the specimen to the opening of the jaw faces of the machine. A bolted connection was used in addition to bonding to prevent any failure in the gripping part. No failure or crack initiation was observed in the gripping part of all specimens during the entire experimental program.

## 2.3. Experimental set-up and instrumentation

All experiments were carried out on an INSTRON 8800 servohydraulic machine under laboratory conditions (23±5°C and 50±10% RH). The designed bonded joints were experimentally investigated under Quasi-static loading, constant amplitude fatigue, block loading, and variable amplitude loading as is detailed in the following,

### 2.3.1. Quasi –static experiments

Quasi-static tensile and compressive experiments were performed under two different loading modes: A displacement-control mode with a ramp rate of 1 mm/min – designated the low loading rate (LLR) – and a load-control mode with a ramp rate of around 350 kN/s – designated the high loading rate (HLR). The loading rate selected for the load-control mode is similar to the highest loading rate applied during fatigue loading. Five specimens under tensile loading and LLR and three samples per loading condition for the other cases, i.e. tension-HLR, compression-HLR and compression-LLR, were examined.

### 2.3.2. Constant amplitude experiments

Fatigue experiments were performed under load control, using a constant amplitude sinusoidal waveform, at a frequency of 10 Hz. It has already been shown [2] that the fatigue performance of similar specimens is not affected by the frequency when it lies in the range between 2 and 10 Hz. Three load ratios, the ratio of the minimum to maximum applied cyclic load ($R=F_{min}/F_{max}$), were selected to simulate tension-tension ($R$=0.1), reversed ($R$=-1) and compression-compression ($R$=10) loading. The fatigue experimental program was designed to derive experimental data that cover the entire lifetime between one cycle and five million cycles. Seven load levels for $R$=0.1 and five load levels for $R$=-1 and $R$=10 were selected. At least three specimens were tested at each load level in order to also obtain information regarding the scatter of the fatigue life. The specimens were labeled accordingly, e.g. R018503 represents the third specimen (R0185**03**) loaded at a level of 85% (R01**85**03) of the ultimate tensile load under $R$=0.1 (**R01**8503).

One specimen per load level at $R$=10 and 0.1 was instrumented on one side by two crack gages (HBM crack gage-type RDS20, Fig. 2.5a) which cover the whole bonding length and monitor crack initiation and propagation during the fatigue life (see Fig. 2.5b). Preliminary results proved that the cracks initiate and propagate in a similar way along the two sides of the bond line of each specimen. The crack gages included 20 parallel wires with a pitch of 1.15 mm placed perpendicular to the adhesive layer. As the crack propagated, the wires were progressively broken and the electrical resistance of the gage increased. A Labview application and a multi-channel electronic measurement unit (HBM-Spider8) were used for data acquisition. The fatigue crack was optically monitored during the test at $R$=-1 using a 40x microscope due to the different possible locations for crack initiation and propagation.

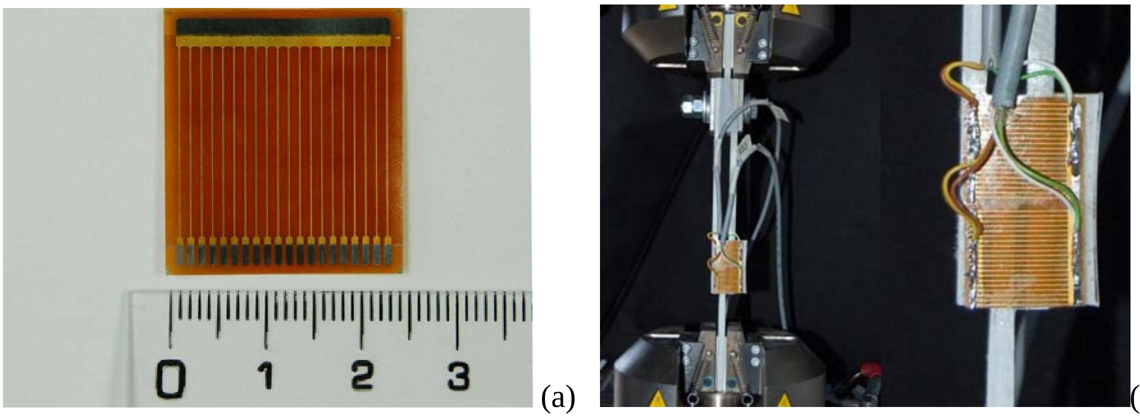

(a) (b)

Fig. 2.5. HBM crack gage-type RDS20 (a) and DLJ instrumented with two crack gages (b)

### 2.3.3. Block loading experiments

The block loading experiments were carried out under load control, using a sinusoidal waveform, at a frequency of 10 Hz. The loading sequence effect in a two-block loading and the effect of load level transitions in a multi-block loading were investigated. Since the load ratio ($R$) can also affect the results, it was kept constant for tension ($R$=0.1) and compression ($R$=10) loading blocks and only the load levels were altered.

The experimental program shown in Table 2.2 was employed for the investigation of the loading sequence effect. The program consisted of two-block loading sequences with transitions from low to high (L-H) and high to low (H-L) load levels under $R$-ratios 0.1 and 10, representative of tensile and compressive fatigue respectively. A schematic representation of the applied loads is given in Fig. 2.6a for the L-H and in Fig. 2.6b for the H-L loading sequences.

Two types of loading blocks with different load levels were applied under each $R$-ratio. The load levels in the block loading sequences were chosen based on the availability of fracture data in the CA database. The length of the first loading block in terms of number of cycles ($n_1$) was predetermined as being equal to 25-35% of the constant amplitude fatigue life of the joints ($N_1$). After completion of the first step ($n_1$), the second loading block was applied up to failure, which resulted in $n_2$. The Two specimens were examined under each loading sequence.

Table 2.2. Experimental program for investigation of loading sequence effect

| $R$ | Sequence | Nominal load level under 1st block (up to 25-35% of fatigue life) [% of UTL or UCL] | Nominal load level under 2nd block (up to failure) [% of UTL or UCL] |
|---|---|---|---|
| 0.1 | L-H | 50[a] | 80 |
|  |  | 40 | 70 |
|  | H-L | 80 | 50 |
|  |  | 70 | 40 |
| 10 | L-H | 60[b] | 70 |
|  |  | 65 | 80 |
|  | H-L | 70 | 60 |
|  |  | 80 | 65 |

[a] Nominal % of Ultimate Tensile Load (UTL=27.7±2.2 kN)
[b] Nominal % of Ultimate Compressive Load (UCL=-27.1±1.9 kN)

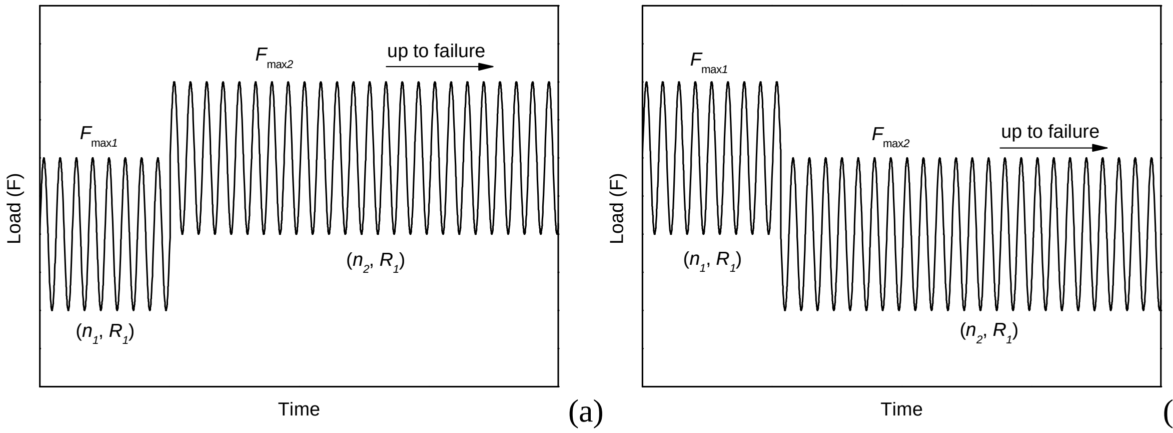

(a) (b)

Fig. 2.6. Schematic representation of applied two-block loading sequences (a) L-H sequence (b) H-L sequence

Also for two more specimens under tension loading, the length of the first block was equal to 50% of the CA fatigue life. The specimens were labeled accordingly, e.g. R01F30B704002 represents the second specimen (R01F30B7040**02**) loaded at the nominal level of 70%, followed by the level of 40% (R01F30**B7040**02) of the ultimate tensile load (UTL) under *R*=0.1 (**R01**F30B704002) and the length of the first loading block was equal to 25-35% of the constant amplitude fatigue life of the joints under the first load level (R01**F30**B704002). The letter “x” is also used in labels to designate a group of specimens with partially similar conditions, e.g. R01F**xx**B7040**xx** refers to all specimens loaded under *R*=0.1 and the loading sequence 70% to 40% of the UTL. One specimen per loading sequence was instrumented on one side by two crack gages to monitor crack initiation and propagation during the fatigue life The experimental program used for investigation of the effect of number of transitions is summarized in Tables 2.3 and 2.4. A schematic representation of the applied loads is shown in Figs. 2.7a-b. Each loading sequence in Figs. 2.7a-b is composed of two load levels with the same *R*-ratio but different length and was applied repeatedly until specimen failure.

Table 2.3. Experimental program for investigation of transition effect at *R*=0.1

| | 1st load level (Nominal % of UTL) | $n_1$ | 2nd load level (Nominal % of UTL) | $n_2$ |
|---|---|---|---|---|
| High Transition | 70 | 10 | 40 | 2914 |
| | 40 | 2914 | 70 | 10 |
| Low Transition | 70 | 100 | 40 | 29140 |
| | 40 | 29140 | 70 | 100 |

The length of the blocks was predetermined to provide the same amount of partial damage ($n_i/N_i$), based on the linear damage accumulation model, according to the CA fatigue data, i.e. $n_1/N_1 = n_2/N_2$. Accordingly when the number of cycles in the first block is increased, i.e. at *R*=0.1 from 10 to 100 cycles, the length of the second block also increases by the same ratio, e.g. from 2914 to 29140 cycles (see Table 2.3).

Table 2.4. Experimental program for investigation of transition effect at *R*=10

| | 1st load level (Nominal % of UCL) | $n_1$ | 2nd load level (Nominal % of UCL) | $n_2$ |
|---|---|---|---|---|
| High Transition | 70 | 10 | 60 | 374 |
| | 60 | 374 | 70 | 10 |
| Low Transition | 70 | 1000 | 60 | 37400 |
| | 60 | 37400 | 70 | 1000 |

Two specimens were examined under each loading sequence with different starting loading block. The letters “L” and “H” used for specimen labeling e.g. R01B4070**H**01 denote the low and high number of transition experiments respectively.

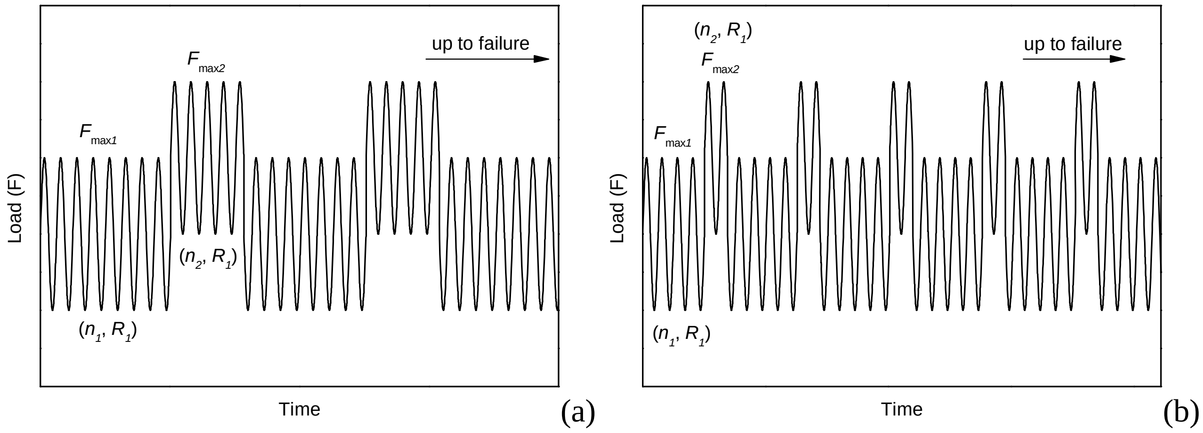

Fig. 2.7. Schematic representation of applied multi-block loading sequences (a) low transition (b) high transition

### 2.3.4. Variable amplitude experiments

The VA loading experiments were performed under load control, using a standard loading spectrum at a constant frequency of 10 Hz. Keeping the frequency constant during the whole spectrum imposed different loading rates depending on the amplitude of each cycle and thus loading rates similar to constant amplitude experiments

The spectrum used was the WISPERX time series developed for wind turbine applications [3]. The WISPERX spectrum is very well documented, optimized in terms of length, and also includes a variety of load amplitudes, mean loads, and overloads. It represents a short version of WISPER (wind turbine reference spectrum) and reduces experimental time to a tenth. WISPERX is a row of integers ranging from -24 to 39 indicating load reversal points and is composed of 25663 reversals i.e. 12831 cycles. The WISPERX spectrum was applied using the INSTRON WaveMatrix$^{TM}$ software application v1.5.

To obtain the desired maximum applied loads ($F_{max}$), representing four load levels at 22, 20, 18, and 16 kN, each of the spectrum integers was multiplied by appropriate factors. The scaled spectra were repeatedly applied to the specimens up to failure. At least three specimens were examined under each load level to obtain information regarding fatigue life scatter. The specimens were labeled accordingly, e.g. WX1603 represents the third specimen loaded at the maximum load level of 16 kN under the WISPERX loading spectrum. One specimen per load level was instrumented on one side with two crack gages to monitor crack initiation and propagation during the fatigue life.

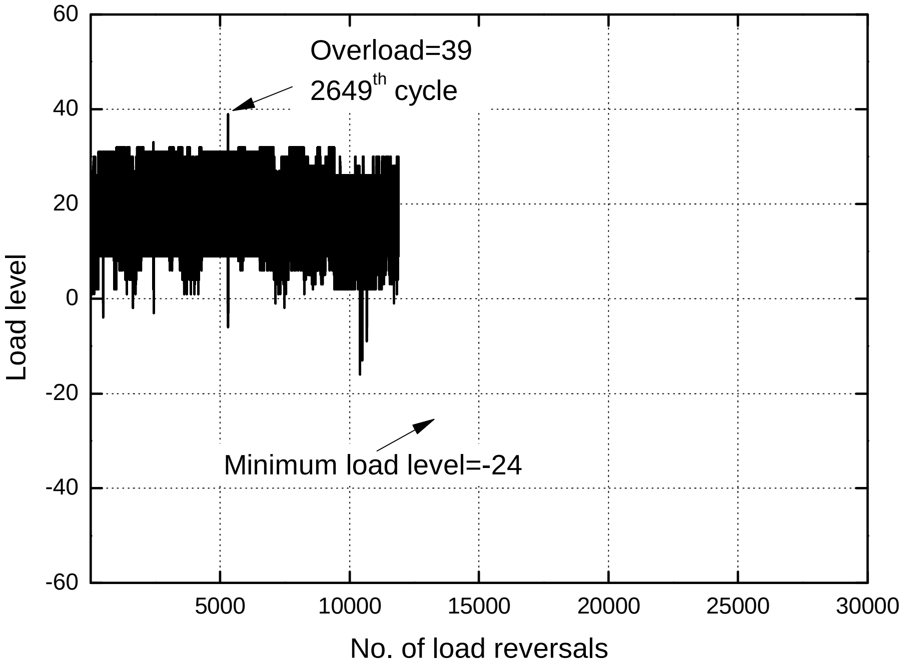

Fig. 2.8. WISPERX spectrum

## 2.4. References

1. De Castro J, Keller T. Ductile double-lap joints from brittle GFRP laminates and ductile adhesives. Part I: experimental investigation. Compos Part B – Eng, 2008;39(2):271–281.
2. Zhang Y, Vassilopoulos AP, Keller T. Environmental effects on fatigue behavior of adhesively-bonded pultruded structure joints. Compos Sci Technol, 2009;69(7–8):1022–1028.
3. ten Have AA. WISPER and WISPERX: Summary paper describing their backgrounds, derivation and statistics, American Society of Mechanical Engineers, Solar Energy Division, 1993, p. 169 -178.

# 3 Constant amplitude loading

## *Abstract*

*The fatigue response of adhesively-bonded pultruded GFRP double-lap joints was investigated under different loading patterns and experimental results were obtained for three different applied load ratios: R=0.1, R=10, and R=-1. The failure mode and the fatigue life of the examined joint configuration are affected by the different loading type. A decrease in joint stiffness was observed being different under tensile and compressive loading. Independent of the failure mode, similar crack development was observed, characterized by an initial and final region of accelerated propagation, and a middle part of linear, and slower, crack propagation, corresponding to around 80% of the fatigue life. Considerable differences were observed for the derived fatigue crack growth curves under different load ratios. The constant amplitude fatigue behavior was modeled by a number of conceptually different phenomenological S-N formulations in order to investigate their adequacy for accurate modeling of lifetime from the very low cycle fatigue to the high cycle fatigue regions. Based on an extensive review, appropriate fatigue formulations that take into account the probabilistic nature of lifetime measurements were selected and their fundamental assumptions examined. The modeling results were similar for all selected fatigue formulations with the derived S-N curves exhibiting differences mainly in the low and high cycle fatigue regimes. The formulations insensitive to the scatter in the experimental data were found to be the most appropriate models.*

## 3.1. Introduction

The adhesively-bonded FRP joints have been used in civil engineering applications and their quasi-static and constant amplitude fatigue behavior have been investigated, e.g. [1-5]. Full-scale structural adhesively-bonded joints composed of pultruded GFRP laminates and epoxy adhesive were investigated under tensile constant amplitude fatigue loading [2, 5-7]. The questions relating to the developed failure mechanisms, the fatigue limit and the environmental effects have been discussed in [2, 6]. The applicability of stiffness degradation and fracture mechanics models to these types of structures has also been examined in [5, 7].

Despite the vast number of scientific publications concerning the fatigue of FRP composite joints under constant amplitude loading, numerous aspects related to their behavior under realistic loading patterns require further examination. One of these aspects is the effect of the mean stress and the application of compressive loading components on the life of the examined joints. All experimental studies performed to date are based on tensile fatigue loads mainly because they have focused on joints with metal substrates, e.g. [8], in which a cohesive or an adhesive failure is exhibited. A significant mean stress effect was reported in [8] and a linear Goodman diagram has been shown to be appropriate for representing this effect. However, there is no evidence that the fatigue behavior of the examined joints is the same under compressive loads, a loading pattern that is very common during the operation of a structure. This phenomenon can be more pronounced for pultruded FRP joints in which cracks in the adherend – which are generally not unidirectional – lead the failure process, see [2-7].

For composite laminates, traditionally the experimentally obtained fatigue data are plotted on the S-N plane (cyclic stress vs. number of cycle) and fitted by an appropriate mathematical equation (the S-N curve) to simulate the exhibited behavior. For uniaxial loading, the established S-N curves for metals, usually the power law equation according to the formulation first introduced by Basquin in 1910 [9], were initially adopted for composites as well. Nevertheless, the complicated damage mechanisms that develop in fiber-reinforced composite laminates and composite structural elements under fatigue loading make the adoption of a universal S-N model very difficult. Moreover, the effect of loading parameters such as the mean stress and the frequency of loading on the fatigue life of composites was more pronounced when compared to metals, see e.g. [10-12], forcing the development of more complicated empirical S-N models that are able to take into account the effect of more parameters on the fatigue life, e.g. [13-17]. Although these models seem promising, their empirical nature is a disadvantage as their predictive ability is strongly affected by the selection of a number of parameters that must be estimated or even, in some cases, assumed.

Alternative S-N formulations that include information concerning damage were also proposed. Several S-N models for the description of the fatigue life of composites were introduced based on strength or stiffness degradation, e.g. [14-20]. For the fatigue life of adhesively-bonded composite joints, fracture mechanics modeling is preferred. Damage tolerant design allowables, corresponding to predetermined crack lengths, can be derived in this way, see e.g. [7]. However, the need for extended experimental input and the limitation of the derived models to the examined databases hinder their common acceptance. Bi-linear [21] and multi-parameter [22] models were also introduced in order to appropriately cover the entire lifetime of polymer matrix composites exhibiting different behaviors in the low-cycle fatigue (LCF) and high-cycle fatigue (HCF) regimes.

It is also known that composite materials exhibit high scatter that can extend to one decade of fatigue life or more. Methods appropriate for the derivation of S-N curves that take into account the probabilistic nature of the fatigue properties of the examined materials have been established to permit the derivation of S-N curves with some statistical significance based on limited datasets e.g. [23-25]. These statistical methods are also based on a deterministic S-N equation for the representation of fatigue data. However, they assume that the fatigue data for each load level follow a normal [23] or Weibull [24] statistical distribution instead of considering the mean or median fatigue lives for the modeling. In addition, the methods introduce assumptions that also allow the run-outs (data from specimens that did not fail during loading) to be considered in the analysis [24, 25] together with the static strength data [25].

However, the use of static strength data for the derivation of fatigue curves (as fatigue data for 1 or ¼ cycle) is arguable and no complete study on this subject exists. Previous publications, e.g. [26], showed that static strength data should not be a part of the S-N curve, especially when they have been acquired under strain rates much lower than those used in fatigue loading. The use of static strength data in the regression leads to incorrect slopes of the S-N curves as presented in [26]. On the other hand, the exclusion of static strength data, although improving the description of the fatigue behavior, introduce errors in the lifetime predictions when the low-cycle regime is important, as for example for loading spectra including only a few high-load cycles. In another study [27] inclusion of static strength data improved the simulation of the low-cycle fatigue life especially when the power law model was used. The authors [27] justified the mixing of static strength data with the corresponding fatigue data, based on the observation that most polymers and composites fail under fatigue due to the same mechanism as under static loading. Kensche [28] also included the static strength data in the fatigue analysis of GFRP materials due to the strong effect of the static strength on the fatigue life estimation in the low-cycle region. However, Echtemeyer and coworkers [29] found that the static strain to failure of GFRP laminates with different resins and architectures can vary while the laminates show the same fatigue characteristics and concluded that the static and fatigue performances of materials are not necessarily interrelated.

Despite the vast number of research articles concerning the modeling of the constant amplitude fatigue life of composite laminates, the fatigue behavior of adhesively-bonded joints is usually modeled by the power law formulation. The fatigue behavior of different types of bonded joints with metallic adherends, where the failure modes are mainly cohesive or interfacial failure, has been characterized with the power law model [8, 30, 31]. In the case of adhesively-bonded joints with FRP substrates, the failure mode is usually more complicated and the adherends can be involved in the fatigue failure, see e.g. [32] where a fiber tear failure occurred. Nevertheless, the power law model was used for composites as well, see e.g. in [33] for studying the effect of the design parameters of single-lap joints comprising carbon/epoxy laminates and epoxy adhesive. However, deviations between the S-N data and the power law model for FRP bonded and bolted joints have been reported, see e.g. [34]. Concerning joints comprised by pultruded FRP laminates, both the exponential and wear-out [25] models were used for the fatigue life modeling [2, 6]. Newly introduced computational techniques such as artificial neural networks or genetic programming [35-37] can also be used for the estimation of accurate S-N curves for bonded FRP joints as was shown in [38]. The literature review revealed that there is no universal theoretical model able to accurately describe the constant amplitude fatigue behavior of adhesively-bonded FRP joints yet available.

The fatigue behavior of adhesively-bonded pultruded FRP Double-Lap Joints (DLJs) under different constant amplitude loading patterns, including tensile, compressive and reversed (combination of tensile and compressive) loading has been experimentally investigated in this chapter to form the basis for further investigation of their behavior under realistic loading patterns. The failure process of the examined joints was thoroughly investigated and analyzed. The stiffness fluctuations during loading were recorded and analytically presented. Linear Elastic Fracture Mechanics (LEFM) theory was used for the interpretation of fracture mechanics data acquired during the experiments in order to describe the different failure modes observed under tensile and compressive loading.

The fatigue life was simulated using load-life curves (similar to the *S-N* curves used for composite laminates). The applicability of phenomenological S-N types that are known and commonly used for the modeling of composite laminates to the examined double-lap adhesively-bonded FRP joints is investigated. After an extensive review of the available S-N formulations for composite materials, the fatigue behavior of the examined joints under tension, compression and reversed fatigue loading is investigated. The most appropriate S-N models are selected and their assumptions and limitations are presented via a detailed statistical analysis of the available experimental datasets. The influence of the data scatter and the introduction of static strength data on the modeling accuracy are thoroughly investigated.

## 3.2. Experimental results and discussion

### 3.2.1. Quasi-static investigation

The examined DLJs showed an almost linear load-elongation behavior up to a brittle failure under both tension and compression independent of the applied loading rate. Similar behavior was reported in [32, 39] for DLJs of the same material under tension loading. The ultimate tensile load (UTL), ultimate compressive load (UCL), and the stiffness for all the examined cases are given in Table 3.1. At these load levels the tensile stress in laminates with the nominal cross section 240 mm$^2$ (40 mm x 6 mm) was between 100 to 125 MPa, almost one third of the tensile strength of pultruded laminates, showing that the failure is solely attributed to the bonding area.

Table 3.1. Quasi-static data

| | UTL or UCL[kN] | Stiffness [kN/mm] |
|---|---|---|
| Tension (Low Loading Rate) | 25.5±0.97 | 23.1±0.20 |
| Tension (High Loading Rate) | 27.7±2.17 | 24.6±0.28 |
| Compression (Low Loading Rate) | -29.0±1.07 | 30.5±0.39 |
| Compression (High Loading Rate) | -27.1±1.92 | 30.2±0.46 |

The joint stiffness was defined as the slope of the load-displacement curve in the range of 0 to 10 kN where no crack formed in the bond line. The higher joint stiffness under compression is due to the reduced length of the inner laminate. The difference between the results obtained from both applied loading rates was insignificant, comparable to the scatter of the results. Therefore, it was concluded that the loading rate effect is not a significant parameter for the quasi-static strength of the examined DLJs.

The observed failure mode was a fiber-tear failure as presented in Fig. 3.1 for a specimen tested under tensile loads. A dominant crack initiated from the joint corner of one of the bond lines – the upper in this figure – between the adhesive and the inner laminate and then shifted deeper, between the first and the second mat layers of the inner laminate, and propagated along this path up to failure. The cracks observed along the lower bond line and at the right side of the inner laminate of the specimen shown in Fig. 3.1 are secondary cracks that occurred only after the failure of the specimen. The same failure mode was observed for double-lap joints composed of similar materials as documented in [32].

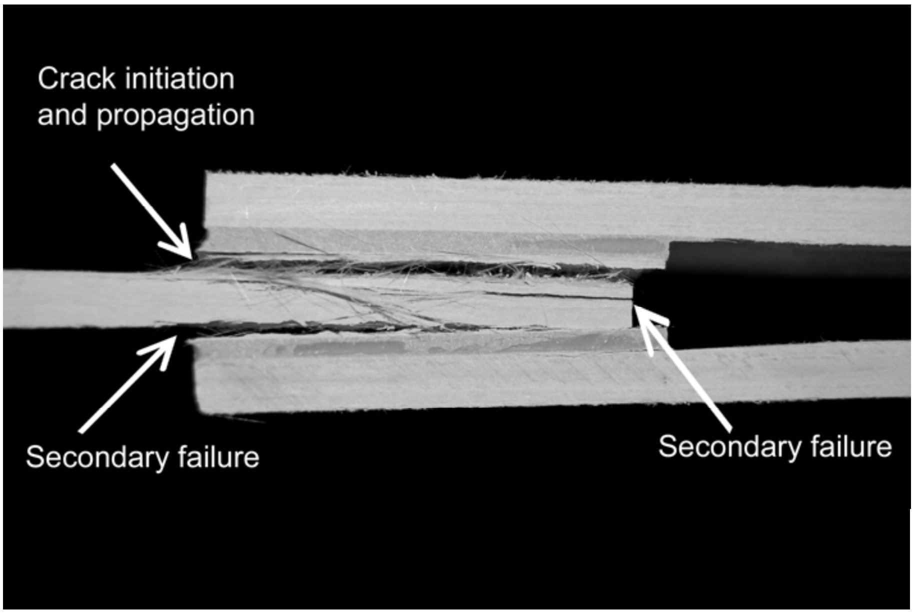
Crack initiation
and propagation
Secondary failure
Secondary failure

Fig. 3.1. DLJ failure mode under tension loading

A different failure mode was observed for the specimens examined under compression loading as shown in Fig. 3.2. The dominant crack initiated and propagated from the right side of the inner laminate (as shown in Fig. 3.2) inside the roving layer.

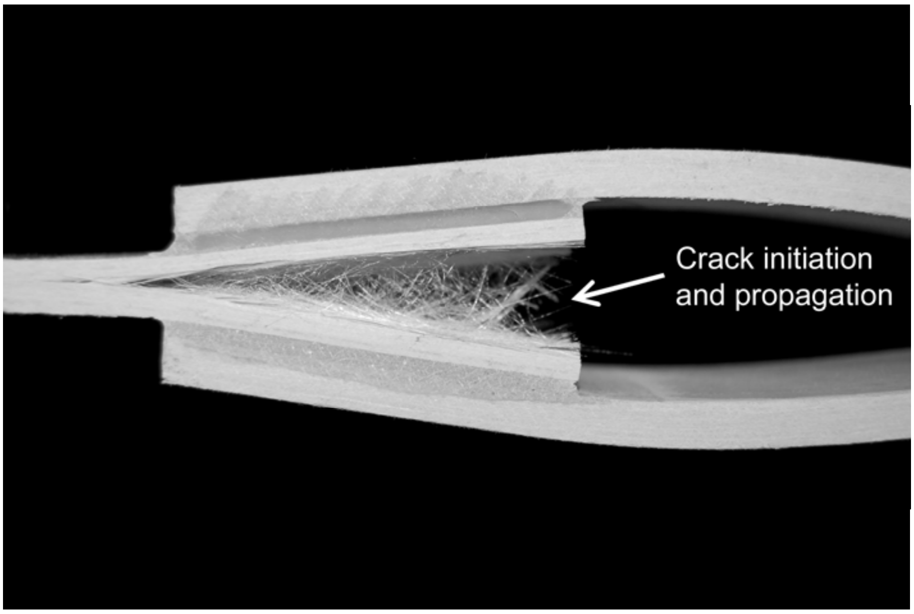
Crack initiation
and propagation

Fig. 3.2. DLJ failure mode under compression loading

## 3.2.2. Fatigue investigation

### 3.2.2.1. Failure modes

Different failure modes were observed for the three applied load ratios. Under tensile fatigue loading (T-T), i.e. a load ratio of 0.1, the failure mode was similar to that observed under quasi-static tension failure (see Fig. 3.1); a crack occurred only in one of the joint bond lines for all the applied load levels. Similarly, for compression-compression (C-C) fatigue, i.e. $R$=10, the crack, as for the compression quasi-static failure, occurred within the roving layer of the inner laminate (see Fig. 3.2). Under tension-compression (T-C) fatigue ($R$=-1), different failure modes were observed. In most of the examined cases, the failure process was similar to T-T mode. For some of the examined specimens, in addition to the dominant crack along one of the bond lines, a smaller crack of approximately 1 mm was observed in the middle of the inner laminate at a similar location as for C-C loading. However, during the fatigue life the dominant crack was propagating and leading the failure process, while the crack created by the compressive component of the applied cyclic load remained short up to the failure of the joint.

### 3.2.2.2. Fatigue life

The fatigue loading matrix and detailed results, Number of cycles to failure ($N_f$) and to crack initiation ($N_i$), for the three different load ratios are presented in Tables 3.2-3.4. The tensile stress in pultruded laminates at the highest maximum load level (22.8 kN) was around 30% of tensile strength of laminates. This value was very close to the endurance limit (25% of tensile strength) of similar material according to [42] and therefore showing that the fatigue failure is solely attributed to failure of bonded joint. The fatigue life of joints under the applied load ratios is plotted against the maximum applied cyclic load ($F_{max}$) in Fig. 3.3 for comparison. The lines that simulate the fatigue behavior are based on a power law relationship as follows:

$$F_{\max} = AN^{B} \tag{3.1}$$

where $F_{\max}$ is the maximum load, $N$, the number of cycles and $A$, $B$ are model parameters that can be obtained after fitting Eq. (3.1) to the experimental data. The values of parameters $A$ and $B$ as estimated by a linear regression analysis are given in Table 3.5. The $F$-$N$ curve for $R$=-1 shows the highest slope (-0.1038) of the three curves, exhibiting the sensitivity of the examined joints to reversed loading.

Table 3.2. Fatigue data at $R$=0.1

| Specimen ID | Nominal load level [% of UTL] | $F_{\max}$ [kN] | $N_f$ | $N_i$ | $N_i/N_f$ (%) |
|---|---|---|---|---|---|
| R018501 | 85 | 22.8 | 217 | – | – |
| R018502 | | | 415 | – | – |
| R018503 | | | 864 | – | – |
| R018504[a] | | | 261 | 1 | 0.38 |
| R018001 | 80 | 21.6 | 1083 | – | – |
| R018002 | | | 799 | – | – |
| R018003 | | | 720 | – | – |
| R018004[a] | | | 1229 | 1 | 0.08 |
| R017001 | 70 | 19.2 | 9493 | – | – |
| R017002 | | | 5773 | – | – |
| R017003 | | | 5043 | – | – |
| R017004[a] | | | 16624 | 1 | 0.01 |
| R016001 | 60 | 16.8 | 7132 | – | – |
| R016002 | | | 11873 | – | – |
| R016003 | | | 82646 | – | – |
| R016004[a] | | | 85025 | 261 | 0.31 |
| R015001 | 50 | 14.4 | 154191 | – | – |
| R015002 | | | 131493 | – | – |
| R015003 | | | 169674 | – | – |
| R015004 | | | 231260 | – | – |
| R015005[a] | | | 124195 | 1967 | 1.58 |
| R014501 | 45 | 13.2 | 187063 | – | – |
| R014502 | | | 299261 | – | – |
| R014503 | | | 183874 | – | – |
| R014504[a] | | | 215718 | 1680 | 0.78 |
| R014001 | 40 | 12.0 | 1317105 | – | – |
| R014002 | | | 2173519 | – | – |
| R014003 | | | 1309163 | – | – |
| R014004[a] | | | 1581478 | 18603 | 1.18 |

[a] specimens instrumented by crack gages

Table 3.3. Fatigue data at $R$=10

| Specimen ID | Nominal load level [% of UCL] | $F_{\max}$ [kN][b] | $N_f$ | $N_i$ | $N_i/N_f$ (%) |
|---|---|---|---|---|---|
| R109001 | 90 | 26.1 | 32 | _ | _ |
| R109002 | | | 235 | _ | _ |
| R109003[a] | | | 385 | 1 | 0.26 |
| R108001 | 80 | 23.2 | 1144 | _ | _ |
| R108002 | | | 13623 | _ | _ |
| R108003 | | | 6222 | _ | _ |
| R108004 | | | 2766 | | |
| R108005[a] | | | 944 | 45 | 4.77 |
| R107001 | 70 | 20.3 | 116281 | _ | _ |
| R107002 | | | 57472 | _ | _ |
| R107003 | | | 121639 | _ | _ |
| R107004[a] | | | 44821 | 2370 | 5.29 |
| R106501 | 65 | 18.9 | 308732 | _ | _ |
| R106502[a] | | | 278641 | 38170 | 13.70 |
| R106503 | | | 58755 | _ | _ |
| R106001 | 60 | 17.4 | 2490433 | _ | _ |
| R106002 | | | 4363735 | _ | _ |
| R106003[a] | | | 2240724 | 22047 | 0.98 |

[a] specimens instrumented by crack gages

[b] absolute value

The effect of the load ratio on the fatigue life of the examined joints can also be demonstrated if the fatigue data is plotted on the "mean-amplitude" ($F_m$-$F_a$) plane. Although under static loading the examined joints exhibited the same strengths for tension and compression (see Table 3.1), their fatigue strength is greater under compression as shown in Fig. 3.4. The typical linear Goodman diagram derived from the experimental data under $R$=-1 is presented in Fig. 3.4. In this diagram, each set of points represents the projection of the power law model at given fatigue lives onto the mean-amplitude load plane. The lines represent the constant life contours, i.e. each one corresponds to the same number of cycles.

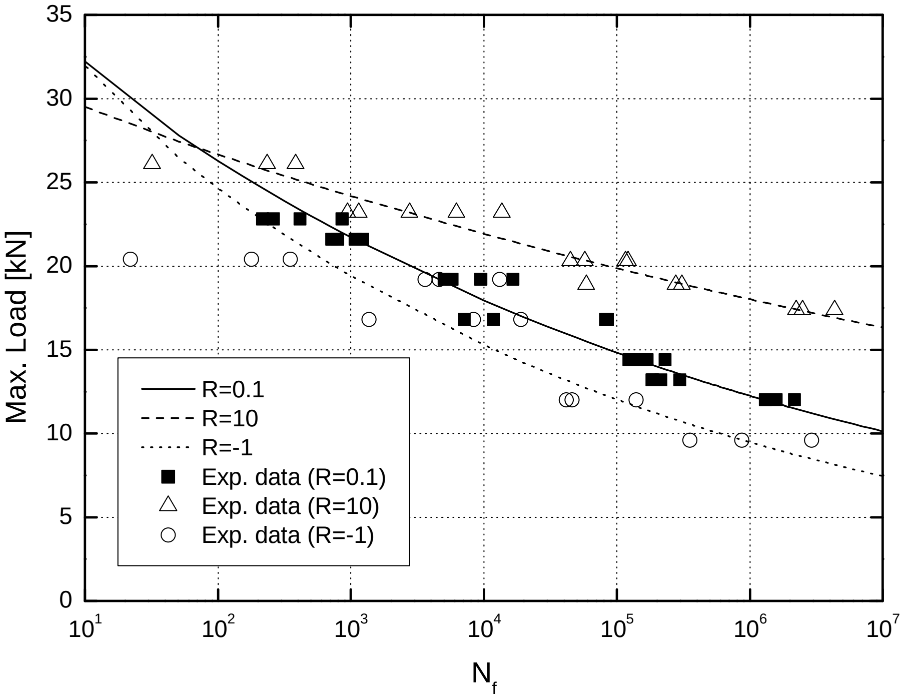

Fig. 3.3. Comparison of load-life data at different *R*-ratios

Table 3.4. Fatigue data at *R*=-1

| Specimen ID | Nominal load level [% of UTL] | $F_{max}$ [kN] | $N_f$ | $N_i$ | $N_i/N_f$ (%) |
|---|---|---|---|---|---|
| R-17501 | 75 | 20.4 | 180 | – | – |
| R-17502 | | | 352 | – | – |
| R-17503 | | | 22 | 1 | 4.55 |
| R-17001 | 70 | 19.2 | 4628 | – | – |
| R-17002 | | | 13173 | – | – |
| R-17003 | | | 3632 | 1 | 0.03 |
| R-16001 | 60 | 16.8 | 19087 | – | – |
| R-16002 | | | 1370 | – | – |
| R-16003 | | | 8372 | 1 | 0.01 |
| R-14001 | 40 | 12 | 41726 | – | – |
| R-14002 | | | 46269 | – | – |
| R-14003 | | | 140176 | 700 | 0.50 |
| R-13501 | 35 | 9.6 | 354021 | – | – |
| R-13502 | | | 2920391 | – | – |
| R-13503 | | | 874667 | 5000 | 0.57 |

Table 3.5. Estimated material constants of Eq. (3.1) for all load ratios

|  | $R$ = -1 | $R$ =0.1 | $R$ =10 |
|---|---|---|---|
| $A$ [kN] | 39.77 | 38.49 | 32.45 |
| $B$ | -0.1038 | -0.0828 | -0.0426 |

However, the diagram shows that the linear model is unable to accurately model the fatigue life of the examined joint configurations at $R$=0.1 and 10, especially in the high cycle regime. The linear model overestimates the fatigue life under $R$=0.1, while it underestimates the $F$-$N$ curve for $R$=10, especially for longer fatigue lifetimes.

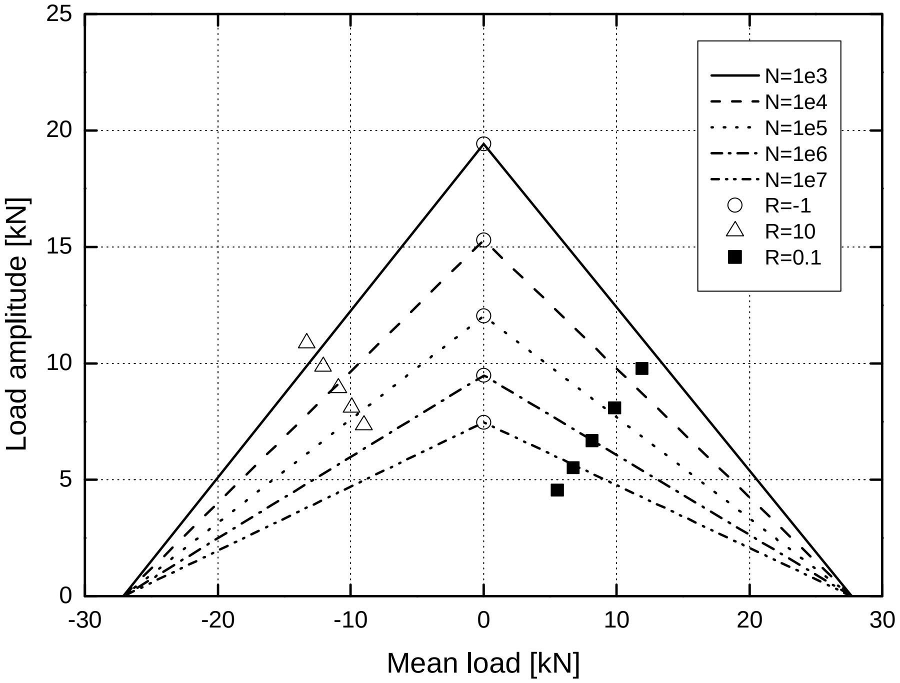

Fig. 3.4. Linear Goodman diagram

More sophisticated models, like those previously developed for composite laminates and presented in [40, 41], are necessary to accurately describe the behavior of the examined joints under different loading conditions. The presentation of the constant life diagram formulations and their application to the available experimental data is extensively discussed in Chapter 5.

### *3.2.2.3. Stiffness degradation*

Stiffness degradation was also recorded during fatigue life since stiffness can be used as a non-destructive damage metric for evaluation of the structural integrity of constructions and permits the establishment of fatigue design allowables, which can be easily implemented in design codes, as described in [5]. The slope of the load-displacement loops, calculated by fitting a linear equation to a set of 1 to 10 consecutive hysteretic loops depending on load level at approximately every 1/40 of the fatigue life, was used to describe the structural stiffness of the examined joints.

In theory, stiffness degradation results from crack propagation and degradation of laminate stiffness. However, previous studies on similar adherends [42] showed that degradation of laminate stiffness is almost insignificant at the level of the loads applied here and the degradation can therefore be attributed solely to crack propagation.

The stiffness degradation results for different load levels of the examined load ratios are shown in Figs. 3.5-3.7. Average stiffness degradation values obtained from load-displacement measurements of the three to five specimens tested per load level are presented. The differences in the initial values can be attributed to the small geometry tolerances and the scatter of the experimental results.

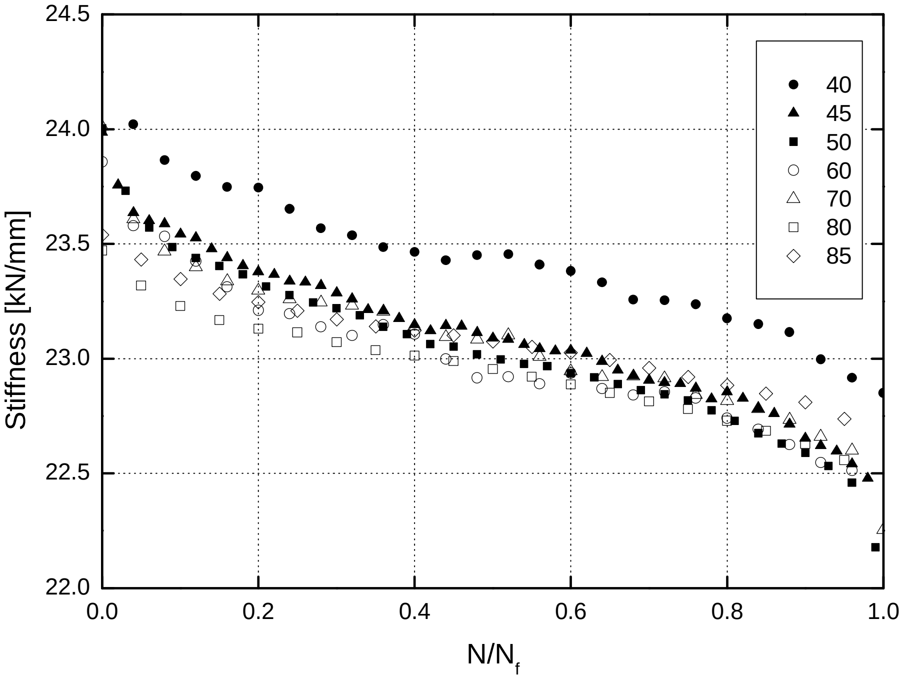

Fig. 3.5. Stiffness degradation curves at *R*=0.1

Independent of load ratio and load level, a similar trend was observed for all the curves; a rapid stiffness degradation at the beginning and up to 10% of the total life, an almost linear and less steep stiffness degradation in the range of 10-90% of life and a very rapid drop after 90% of total life, related to the final failure of the joint. The degradation of the joints that were loaded under *R*=0.1 and -1 was around 8% up to failure (see Figs. 3.5, 3.6), while the value was less than 2% for joints tested under pure compressive loading. This behavior is in agreement with the observed failure modes of the specimens.

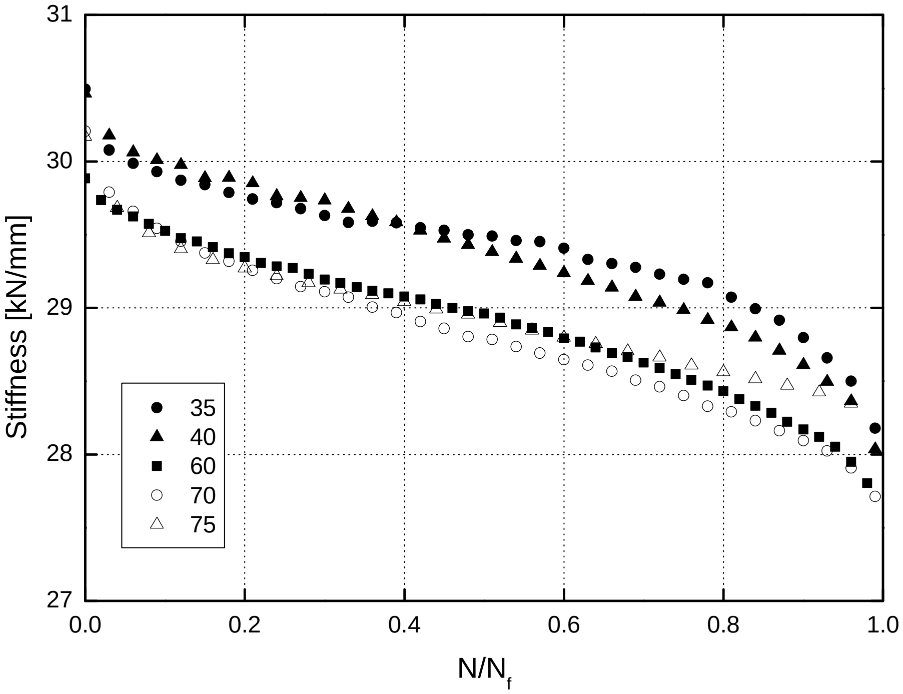

Fig. 3.6. Stiffness degradation curves at *R*=-1

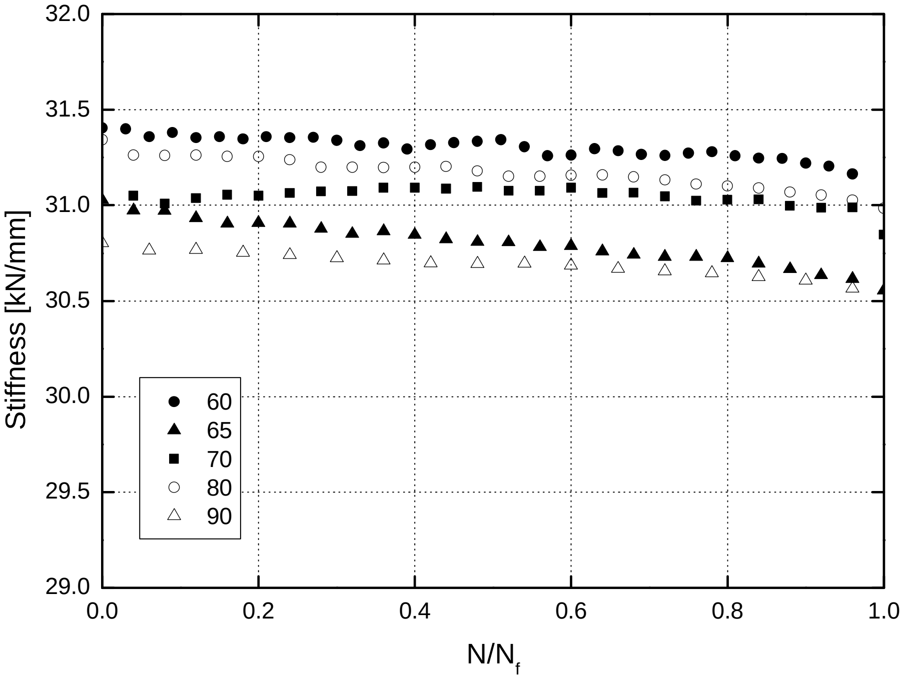

Fig. 3.7. Stiffness degradation curves at *R*=10

### 3.2.2.4. Fracture mechanics

As shown in Tables 3.2-3.4, the crack initiated early in the fatigue life of all the examined cases independent of load level. Nevertheless a trend was apparent in the average of ($N_i/N_f$) for different *R*-ratios since initiation was observed later in the lifetime in the case of C-C fatigue loading (0.62±0.54 for *R*=0.1, 5.00 ±4.78 for *R*=10, 1.13±1.72 for *R*=-1). The crack lengths, measured by crack gages or the visual method (for *R*=-1), vs. the normalized number of cycles are given in Figs. 3.8-3.10 for the three types of loading. A common trend was observed: rapid crack propagation at the beginning and end of fatigue life, with a significantly lower rate between 10 and 90% of fatigue life.

This behavior concurs with the joint stiffness degradation trends shown in Figs. 3.5-3.7. Under load conditions of *R*=0.1 and 10, another trend is also apparent in Figs. 3.8 and 3.10. The specimens tested at higher load levels exhibited faster crack propagation up to around 10% of the fatigue life.

The strain energy release rate (SERR), *G*, can be calculated based on linear elastic fracture mechanics (see Eq. 3.2). According to this theory, for a double-lap joint with width *B*, and an existing crack of length, *a*, the strain energy release rate is a function of the applied load, *F*, and the rate of the compliance change, *dC/da*:

$$G = \frac{F^2}{2B}\frac{dC}{da} \tag{3.2}$$

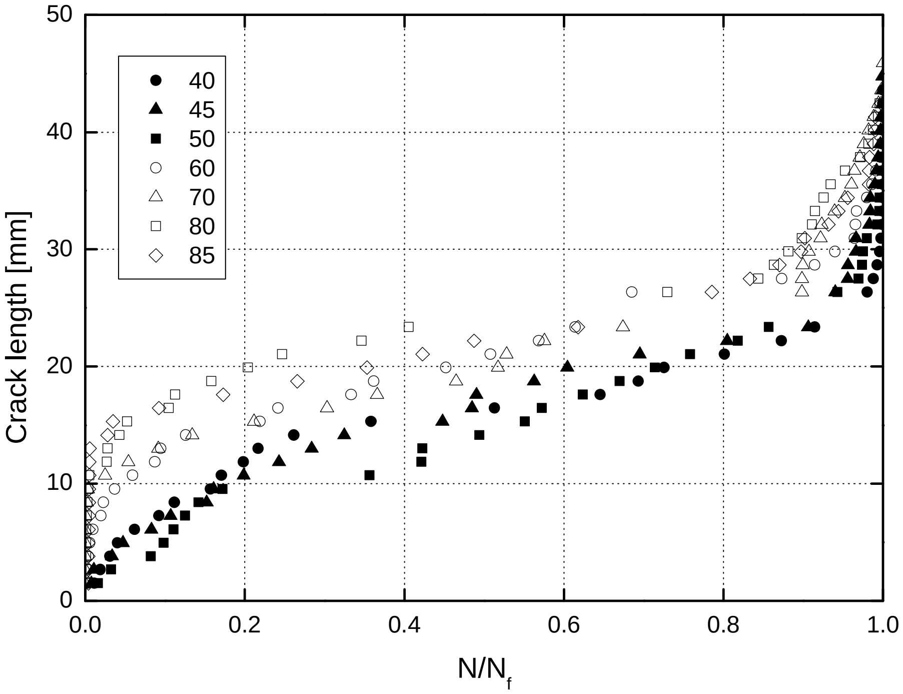

Fig. 3.8. Crack length vs. normalized number of cycles at *R*=0.1

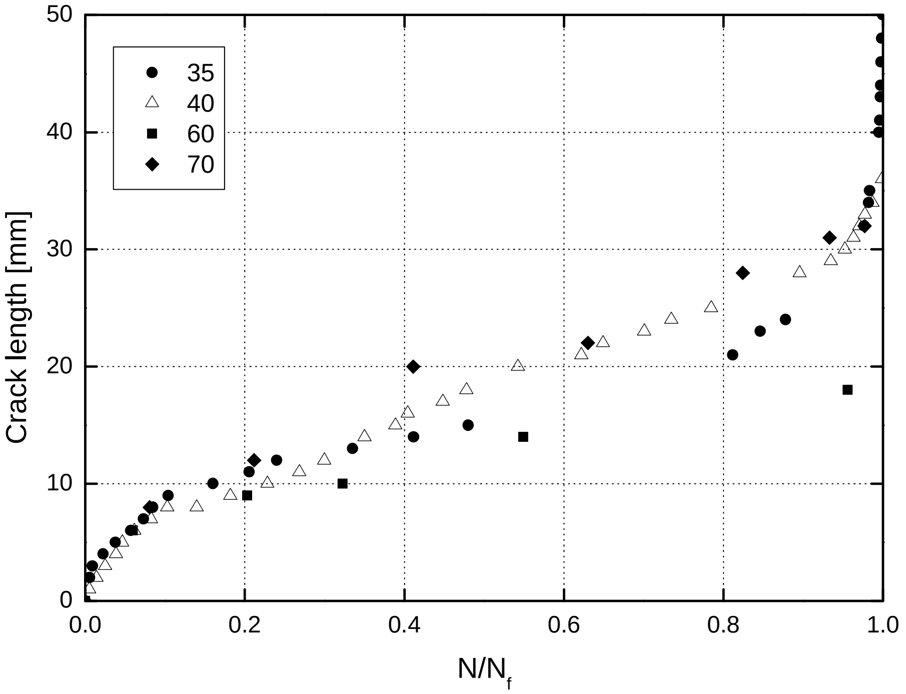

Fig. 3.9. Crack length vs. normalized number of cycles at *R*=-1

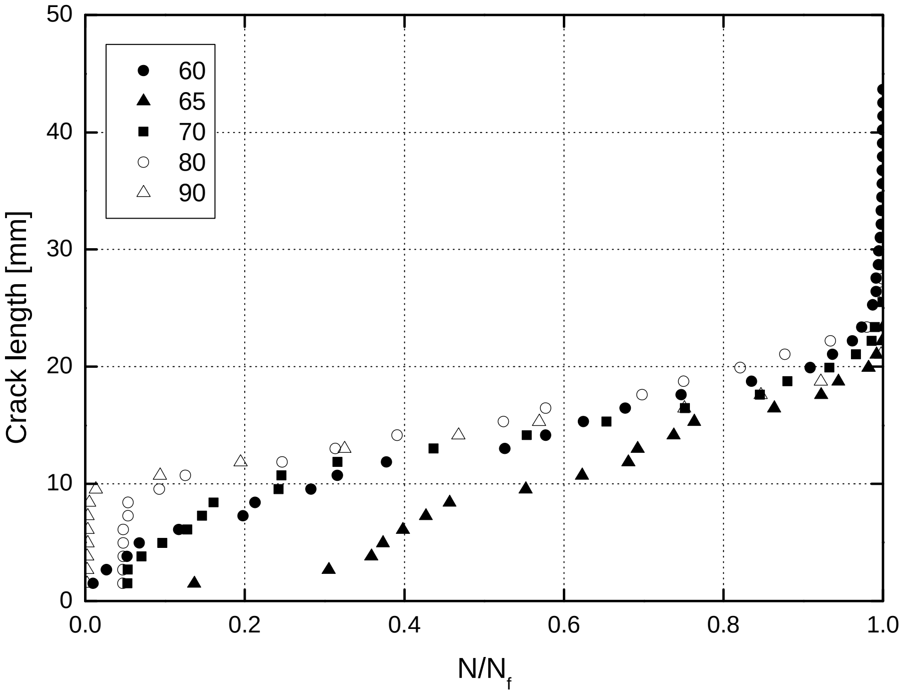

Fig. 3.10. Crack length vs. normalized number of cycles at *R*=10

For cyclic loading, the maximum value of the strain energy release rate during one fatigue cycle can be deduced accordingly:

$$G_{\max} = \frac{F_{\max}^2}{2B}\frac{dC}{da} \tag{3.3}$$

where $F_{max}$ is the maximum cyclic load applied during the fatigue cycle. The joint compliance vs. the crack length is given in Figs. 3.11-3.13.

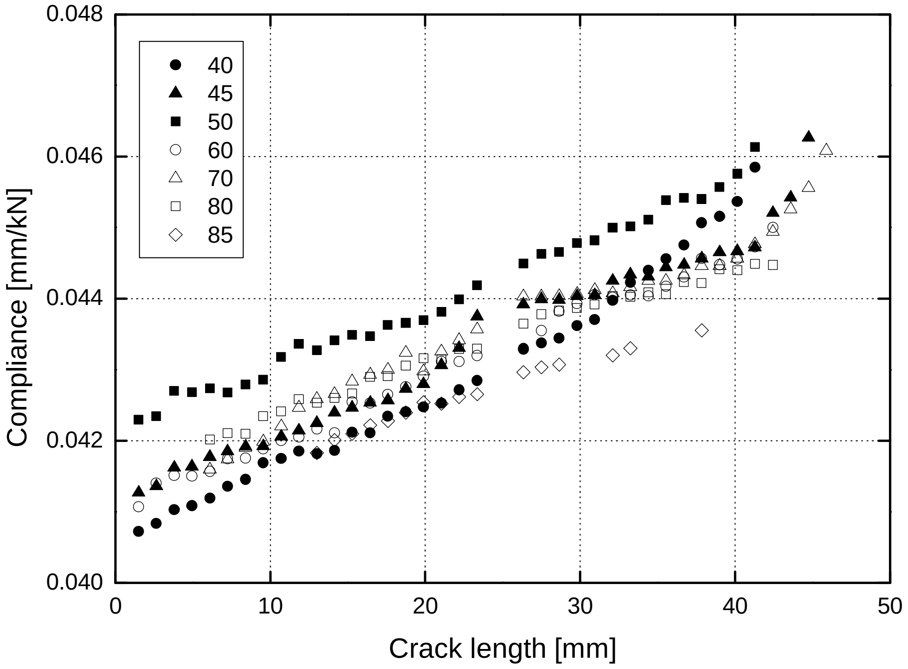

Fig. 3.11. Compliance vs. crack length at $R$=0.1

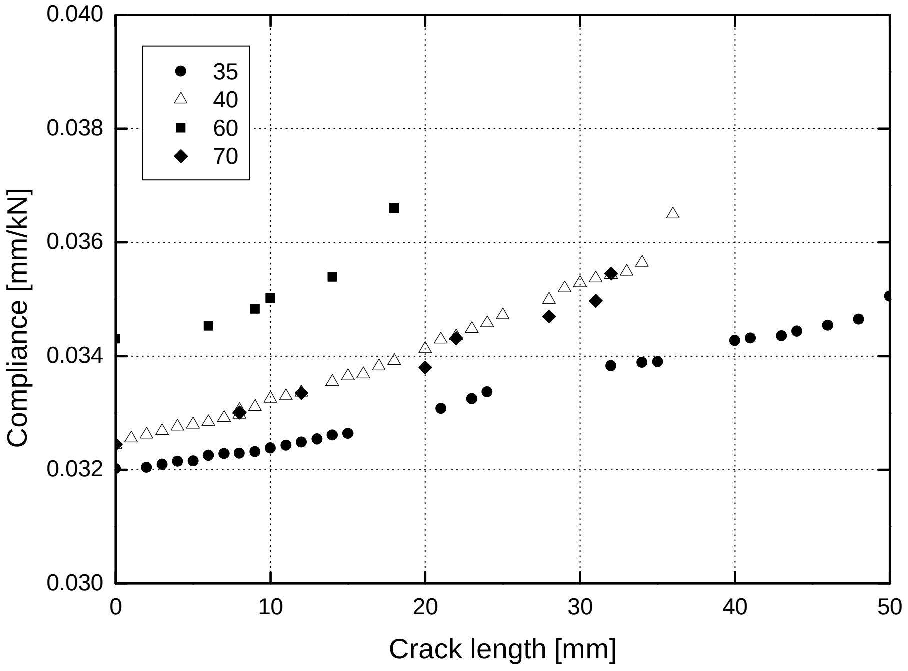

Fig. 3.12. Compliance vs. crack length at $R$=-1

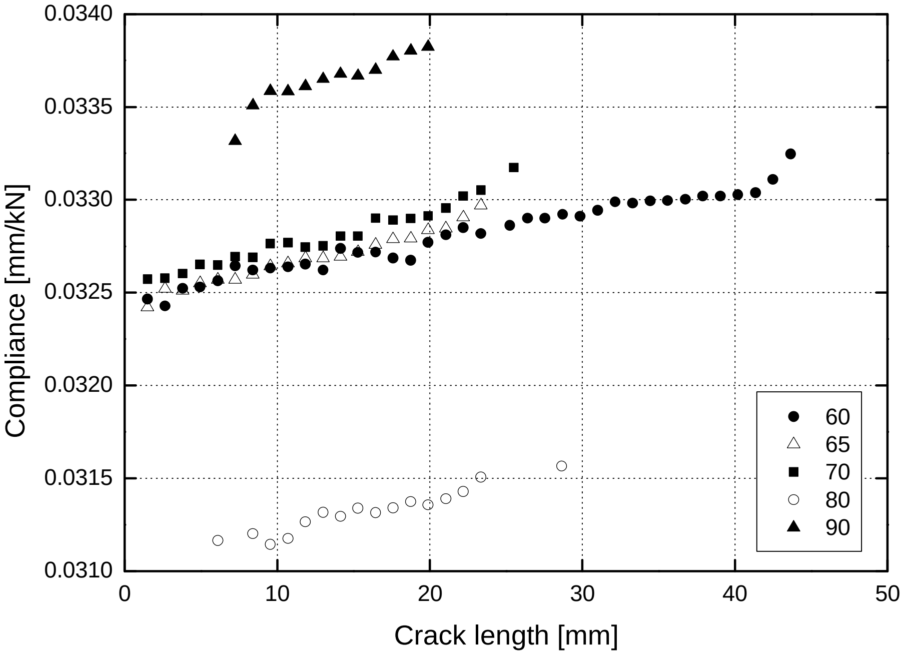

Fig. 3.13. Compliance vs. crack length at $R$=10

As shown, in the crack length range between 10 and 25 mm, corresponding to approximately 10% to 90% of fatigue life, the relationship between compliance and crack length is linear, with a slope which is almost independent of the applied load level under each load ratio. Thus, for each loading case, the average values of *dC/da*, as shown in Table 3.6, were used for the derivation of the maximum SERR by means of Eq. (3.3).

Table 3.6. Compliance change rate under different load ratios (average of all load levels)

| | $R$ = -1 | $R$ = 0.1 | $R$ = 10 |
|---|---|---|---|
| *dC/da* [1/*N*] | 9.04e-8 | 8.83e-8 | 1.73e-8 |
| Standard deviation | 0.14e-9 | 7.32e-9 | 4.79e-9 |

If $G_{\max}$ is plotted against the crack propagation rate, *da/dN*, on logarithmic axes to derive the Fatigue Crack Growth (FCG) graphs, the major part of the relationship is linear and can be simulated by the following equation:

$$\frac{da}{dN} = D\left(G_{\max}\right)^{m} \qquad (3.4)$$

where $D$ and $m$ are fitting parameters, dependent on the loading conditions. In previous studies [43, 44], $D$ and $m$ were considered as material parameters with values independent of joint configuration and loading conditions. However, as was proved earlier [7] this argument fails to produce reliable life prediction results.

The secant method and incremental polynomial fitting (according to ASTM E647) were used to calculate the crack propagation rate. According to the secant or point-to-point technique, the crack propagation rate can be determined by calculating the slope of a straight line connecting two contiguous data points on the *a*-*N* curve. The incremental polynomial method fits a second-order polynomial to sets of a specified number of successive data points, usually 3, 5, 7 or 9. The slope of the determined equation at any point corresponds to the crack propagation rate. The secant method is simple and accurately represents experimental data, but is sensitive to scatter in the latter [45]. The incremental polynomial method can reduce scatter but involves the risk of masking real effects, especially when only small data sets are available [45]. The curve is expected to become smoother when more points are used for the calculations, but there is a risk of inadequate modeling, usually at the start or end of the lifetime.

Both methods were applied, as seen in Figs. 3.14-3.16 for representative specimens for all loading conditions. The secant method showed high sensitivity to the scatter while increasing the number of points in the polynomial method effectively decreased this sensitivity without changing the actual trend of experimental data (see e.g. Fig. 3.16). The crack growth rate was almost constant in the range of 10 to 90% for all load ratios and load levels. Hence, in this range, the slope of the fitted line to the experimental data on the *a*-*N* curve was considered as the crack propagation rate.

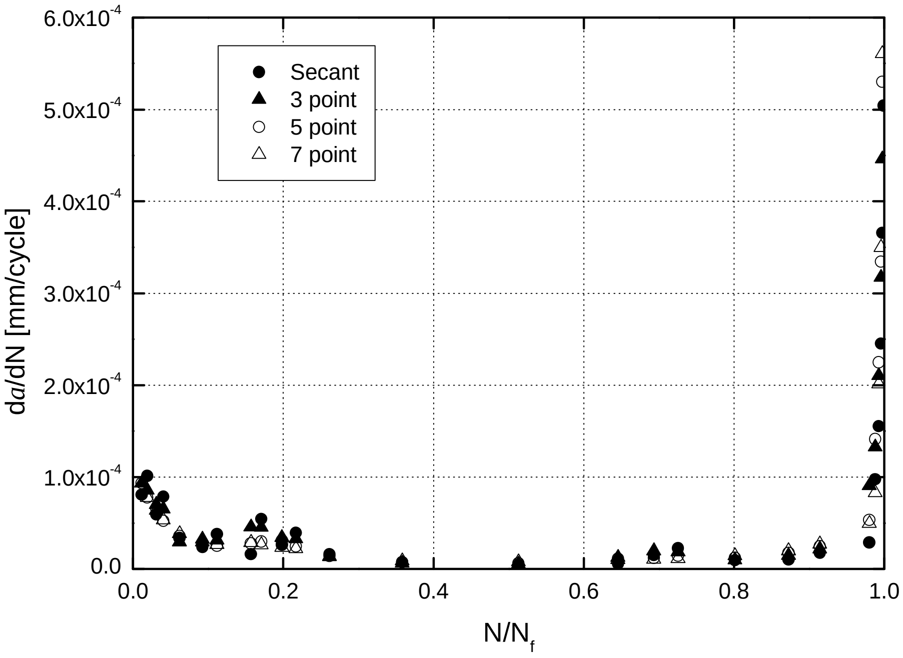

Fig. 3.14. Comparison of secant method and incremental polynomial method for estimation of crack growth rate at *R*=0.1

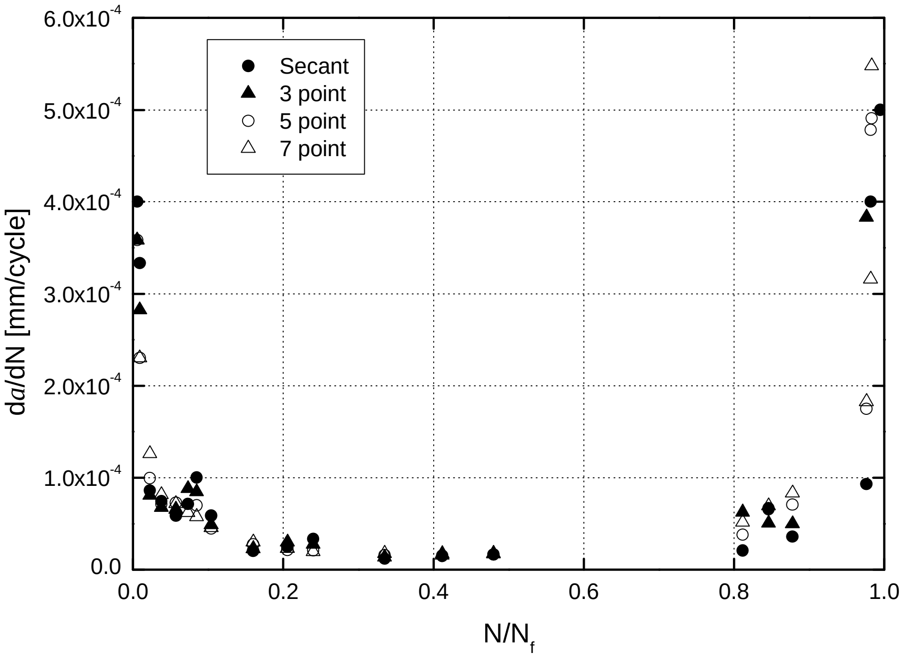

Fig. 3.15. Comparison of secant method and incremental polynomial method for estimation of crack growth rate at *R*=-1

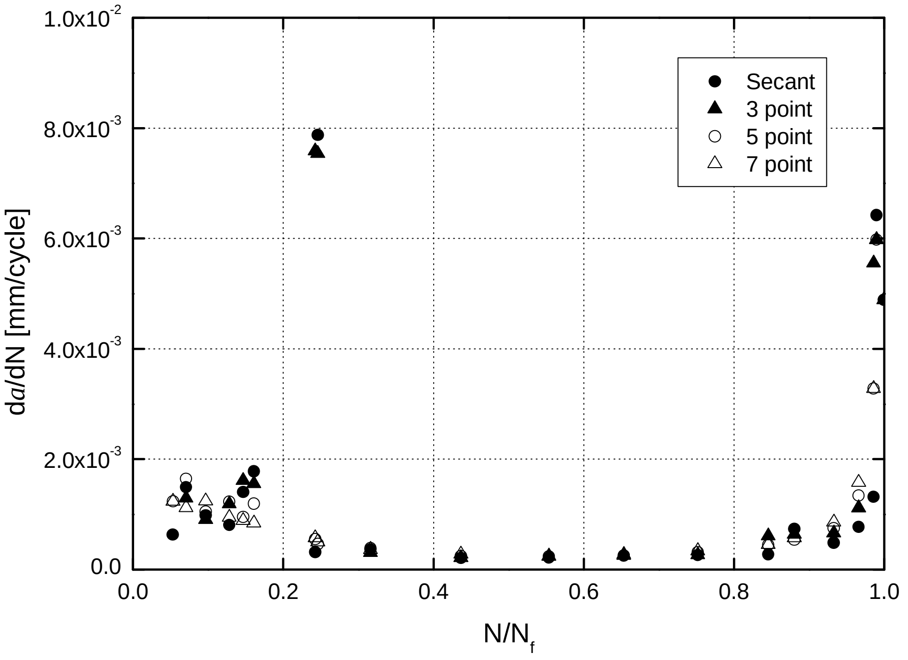

Fig. 3.16. Comparison of secant method and incremental polynomial method for estimation of crack growth rate at *R*=10

The FCG curves for all the examined load ratios are presented in Fig. 3.17 and the parameters of the plotted FCG curves are given in Table 3.7.

Table 3.7. Estimated constant parameters of Eq. (3.4) and corresponding $R^2$

| | $R$ = -1 | $R$ =0.1 | $R$ =10 |
|---|---|---|---|
| $D$ | 1.95e-13 | 3.92e-18 | 3.35e-24 |
| $m$ | 4.012 | 5.700 | 10.239 |
| $R^2$ | 0.99 | 0.92 | 0.95 |

The results prove that the relationship between $G_{\max}$ and ($da/dN$) is highly dependent on the load ratio. A steeper curve with lower strain energy release rate value corresponds to $R$=10, under which specimens failed due to a crack propagating through the roving layer of the inner laminate without significant fiber bridging.

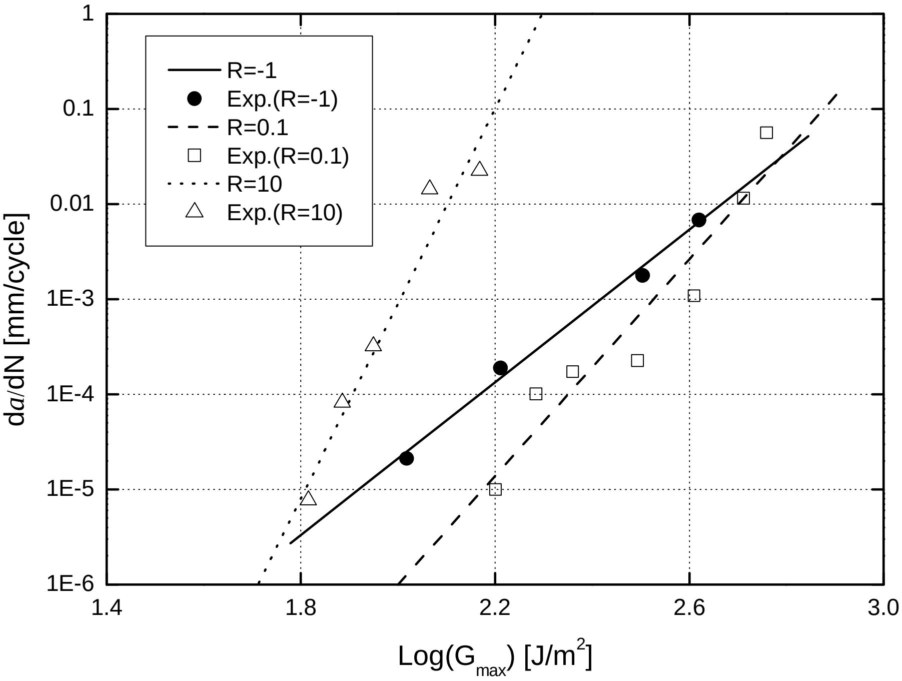

Fig. 3.17. Comparison of developed FCG curves for all load ratios

The dominant cracks for $R$=0.1 and -1 propagated through the mat layers with a considerable amount of fiber bridging. The lower slope of the derived FCG curve for $R$=-1 compared to the $R$=0.1 results from the closing of the crack during the compressive part of the cycles under reversed loading. The crack closure breaks the fibers that cause the fiber bridging and consequently reduces the energy required for subsequent crack propagation.

In Fig. 3.18, the FCG curve under $R$=0.1 is also compared with the results reported in [7] for double-lap joints under the same load ratio and with similar material and failure mode (open triangles). Theoretically, these results should be corroborated well by the latest ones;

however, a shift of the previous FCG curve towards the left (less $G_{\max}$ for the same *da/dN*) is obvious in Fig. 3.18. The main reason for this difference is the method used for calculation of the fracture parameter, $G_{\max}$, and the rate of crack growth, (*da*/*dN*). Based on the process followed in [7] these parameters were calculated using the entire set of the measured fracture mechanics data (crack lengths of 4.6 to 80 mm) and not only the linear part. If the linear part of the crack propagation is used, the results become similar to the latest ones, as shown in Fig. 3.18 (modified set).

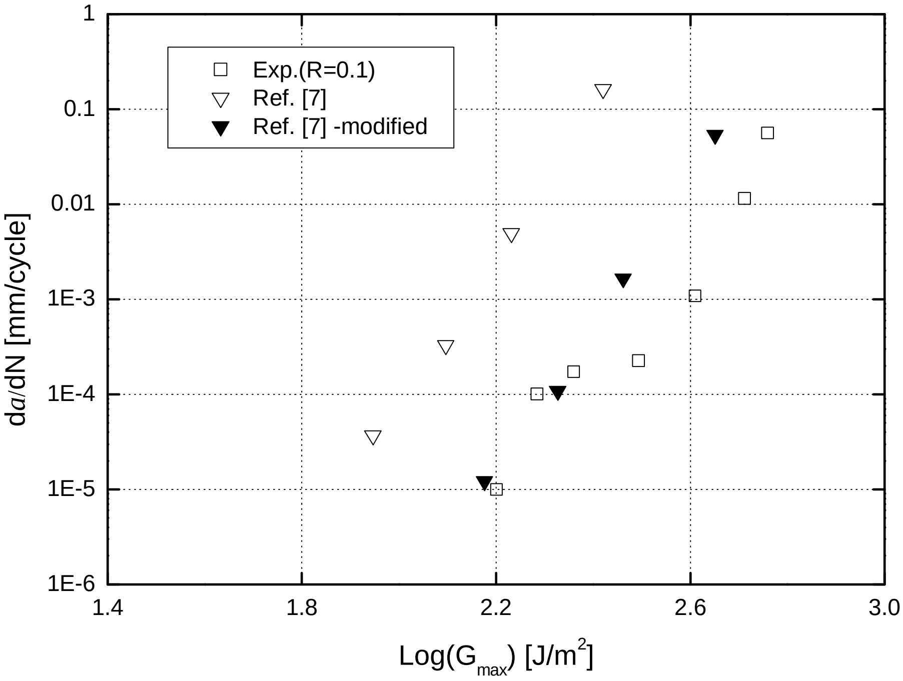

Fig. 3.18. Comparison of FCG curve under *R*=0.1 with reported results in [7]

## 3.3. S-N formulations for composites

The power law form, initially established by Basquin in 1910, Eq. (3.5), usually fits the data well when a high number of cycles is involved [46], although its performance is often poor in the LCF region.

$$\sigma = bN_f^{-a} \tag{3.5}$$

Eqs. (3.6) and (3.7) have been established for metals in order to improve the Basquin formulation for the entire fatigue life range by introducing the endurance limit ($\sigma_e$) and a constant parameter (*B*) which control the S-N curve in the high- and low-cycle fatigue regions respectively.

$$\sigma = bN_f^{-a} + \sigma_e \tag{3.6}$$

$$\sigma - \sigma_e = b\left(N_f + B\right)^{-a} \tag{3.7}$$

Several phenomenological models that take into account parameters affecting the fatigue behavior such as the stress ratio, frequency, temperature, and fiber direction, as well as models that consider the probabilistic nature of the fatigue properties of composite materials were introduced. Jarosch and Stepan [13] incorporated an additional term into the power law formulation that considers the stress ratio effect on fatigue life, Eq. (3.8), to characterize the fatigue life of glass fiber reinforced epoxy material used in rotor blades.

$$\sigma = a + b\big/N_f^{\,x} - c\Big/\left(\left(1-R\right)/\left(1+R\right)\right)^y \tag{3.8}$$

This model was used by Sims and Brogdon [46] to characterize the fatigue behavior of S-glass/epoxy and graphite/epoxy laminates. The effect of the stress ratio on fatigue life was also addressed by Mandell [28], who suggested a model for GFRP laminates, Eq. (3.9).

$$\sigma = UTS\left(1 - DLogN_f\right),\ D = F(material, R) \tag{3.9}$$

Parameter *D* is a function of the stress ratio and is different for each examined material. Appel and Olthoff [28] established an estimation of parameter *D* after analyzing data from literature, Eq. (3.10).

$$\sigma = UTS\left(1 - DLogN_f\right)\ D = 0.015\left(1-R\right) + 0.08 \tag{3.10}$$

However, the evaluation of this model showed that predictions are reliable for tension-tension fatigue, but become optimistic for higher load levels under reversed loading.

Attempts to introduce damage mechanics into the process of S-N derivation were also reported. Strength degradation due to fatigue loading was considered a valid measure for the development of S-N curve formulations [14-18]. According to the latter, fatigue failure is assumed when the residual strength decreases to the same level as the maximum applied cyclic stress. Sendeckyj [17] established a model on this basis in the form of Eq. (3.11).

$$\sigma_{eq} = \sigma_a\left(1 + \left(N_f - 1\right)f\right)^S \tag{3.11}$$

The model consists of two parameters, *S* (the slope of the S-N curve) and *f* (the asymptotic slope of the S-N curve at low stress levels), which can be constants or functions of stress ratio. Different alternatives for *S* and *f* provide a variety of models such as the classic power law model for *S* and *f* =1, the wear-out model for constant *S* and *f* or a model in which both *S* and *f* are functions of the stress ratio. Subsequent models were also developed based on strength degradation. The effect of the stress ratio was included in the model developed by D'Amore et al. [14], Eq. (3.12).

$$N_f = \left(1 + \frac{1}{\alpha(1-R)}\left(\frac{\beta}{\sigma_{\max}}\left|\ln[1-P_N(N)]\right|^{\frac{1}{\alpha_f}} - 1\right)\right)^{1/\delta} \tag{3.12}$$

The effect of frequency was incorporated in [15, 16] in the form of Eqs. (3.13) and (3.14) respectively.

$$(\sigma_u/\sigma_{\max} - 1)(\sigma_u/\sigma_{\max})^{0.6-\psi|\sin\theta|}\left(fr^{\delta}\Big/(1-\psi)^{1.6-\psi|\sin\theta|}\right) = \alpha\left(N_f{}^{\delta} - 1\right) \tag{3.13}$$

$$N_f{}^{\delta} - 1 = \frac{1}{\alpha}(\Delta\sigma/\sigma_u)^{-r}\left(\rho A_{cr}\, fr^2/E\right)^{-m}(1-\sigma_{\max}/\sigma_u) \tag{3.14}$$

Fatigue models have also been developed based on the stiffness degradation of the material. Hwang and Han [19] for example established an S-N model based on the fatigue modulus concept, Eq. (3.15).

$$N_f = \left(B(1-\sigma_a/\sigma_u)\right)^c \tag{3.15}$$

Philippidis and Vassilopoulos [20] introduced a stiffness-based S-N curve, designated Sc-N curve, Eq. (3.16), for the modeling of GFRP laminates.

$$\sigma_a = E_0\left((1-E_N/E_1)/KN\right)^{1/c} \tag{3.16}$$

Bi-linear and sigmoid S-N formulations were also introduced, e.g. [21, 22, 34, 47, 48], for the modeling of experimental datasets showing different behaviors in low- and high-cycle fatigue regimes. Harik and coworkers [21, 47] proposed a bi-linear model for unidirectional GFRP laminates to describe the low- and high-cycle fatigue regions, Eq. (3.17).

$$\sigma = \frac{\sigma_{\max}}{\sigma_u} = \begin{cases} a_{LCF} + b_{LCF} L\log N_f,\ for: N_{cyclic} \le N_f \le N_{LCF} \\ a_{HCF} + b_{HCF} L\log N_f,\ for: N_{LCF} \le N_f \le N_f \end{cases} \tag{3.17}$$

According to Eq. (3.17) the fatigue data must be divided into two groups and the fitting is performed separately for each group. Sarkani et al. [34] reported a deviation between the S-N data and the power law model for FRP bonded and bolted joints. They found a good match between the experimental data and a two-segment power law equation however, still based on the subjective classification of the fatigue data into the LCF and HCF regimes. Sigmoid models like the one developed by Xiong and Shenoi [22], Eq. (3.18), and Mu et al [48], Eq. (3.19), provide algebraic fitting equations that cover the entire fatigue life range, but require greater numbers of fatigue data to adequately estimate the increased number of model parameters.

$$F_\sigma(\sigma)=1-\exp\left(-\left(\left(10^{c\left(\log N_f\right)^m}(\sigma-S_0)+S_0\right)\Big/\beta\right)^{\alpha_f}\right) \tag{3.18}$$

$$\sigma=(1-c)\Big/\left((1-a)+ae^{-b\left(LogN_f\right)}\right)+c \tag{3.19}$$

All the aforementioned models consider deterministic equations for simulation of the fatigue life of the examined composite materials. However, with appropriate statistical analysis of the fatigue data, they can be applied to characterize probabilistic fatigue behaviors. Several methods have been established for characterizing the scatter in fatigue data and developing reliable models to estimate fatigue life with a specific probability of failure. Analysis of numerous datasets showed that the static and fatigue strength data for composite materials follow a Weibull or a (Log)-normal statistical distribution. The parameters of the selected distribution can be estimated by fitting the fatigue data (presumably the number of cycles to failure at each stress level, e.g. [23, 24] (Eqs. (3.20-3.22)).

$$LogN_f=a+b\sigma \tag{3.20}$$

$$LogN_f=c+dLog\sigma \tag{3.21}$$

$$\sigma=K\left(\left(-\ln R_N(N)\right)^{1/\alpha_f g}\right)N_f^{-1/g} \tag{3.22}$$

Alternatively, the selected distributions can fit the static strength data based on the assumption that the fatigue strength follows the same distribution, e.g. [14, 22], or a set of equivalent static strengths that have been previously produced following an iterative process, like the one presented in [25] (see Eq. (3.23)).

$$\sigma_a=\beta\left(-lnR_N(N)\right)^{\frac{1}{\alpha_f}}\left((N-A)Q\right)^{-m} \tag{3.23}$$

S-N formulations containing information regarding the reliability of the simulation normally emerge from this process. The estimated (usually by using maximum likelihood estimators) distribution parameters are used as the S-N model parameters and the S-N curves can be easily derived for different reliability levels, depending on any design needs.

## 3.4. Application of S-N formulations to experimental data

### 3.4.1. Selection of the appropriate S-N formulations

Four models were selected from among the reviewed formulations and their applicability for the interpretation of the available fatigue data was extensively investigated. The power law and the exponential are the most popular models for the derivation of S-N curves since they are fairly accurate and their parameters can be estimated easily through linear regression, or even hand calculations. The power law model (also called the Log-Log model) and the exponential (called Lin-Log) are designated by ASTM in [23]. The S-N curves resulting from the application of these models correspond to the mean or median fatigue life of the examined specimens, although a process for the derivation of confidence bounds is also described in [23]. Other models like the Whitney's pooling scheme [24] and the wear-out model as used by Sendeckyj [25], although necessitating complicated fitting procedures for derivation of the model parameters, were used here to derive S-N curves that take into account the probabilistic nature of the fatigue properties of composite materials. Both models result in a power curve model able to derive S-N curves for different reliability levels. Both the pooling scheme and the wear-out methods assume that the experimental data follow a Weibull distribution, in contrast to ASTM methods that are based on a Log-Normal distribution for representation of the fatigue life.

The application of other models presented was limited due to the implemented assumptions, or because of an increased need for experimental data, and therefore these models were excluded from further analysis in this work. For example, Eqs. (3.9) and (3.10) are limited to tensile fatigue, the endurance limit (not easily derived for all materials) is required for the models of Stromeyer and Palmgren, Eqs. (3.6) and (3.7), and information regarding stiffness degradation is necessary for the application of Eqs. (3.15) and (3.16).

### 3.4.2. Assumptions of the selected models – validation methods

The linear regression models assume a linear relationship (the linearity hypothesis) between the logarithm of fatigue life, $Log(N_f)$, and the stress (Eq. (3.20) or the logarithm of stress (Eq. (3.21)) when $Log(N_f)$ is the dependent variable and the stress parameter, $\sigma$, is the independent variable. Statistical analysis of the fatigue data is performed under two conditions [23]: the logarithms of the fatigue lives, $Log(N_f)$, are normally distributed and their variance is constant over the entire range of the independent variable, $\sigma$, i.e. $Log(N_f)$ exhibits the same scatter at high and low load levels.

The linearity hypothesis is evaluated by calculating a statistical index [23] (the linearity index) for each set of fatigue data and comparison of this index to a critical value corresponding to a 5% significance level (S.L.). This critical value is obtained from standard tables and is a function of the total number of fatigue data and the number of stress levels

[23]. However, the other assumption concerning the distribution of the fatigue lives for each load level cannot be properly examined due to the limited number of data at each load level.

A two-step process that allows the generation of an S-N curve with some statistical value, Eq. (3.22), without resorting to an extremely large database is presented in [24]. Based on an alternative to the wear-out model approach for the fatigue characterization of composite materials proposed by Hahn and Kim [49], this process involves two basic assumptions: (1) a classic power law representation of the S-N curve [13], and (2) a two-parameter Weibull distribution of time-to-failure. According to the process, a Weibull distribution is fitted to estimate the characteristic number of cycles at each stress level. The fatigue life at each stress level is normalized by each characteristic value and a relatively large database emerges comprising the normalized data. This new dataset is designated the pooled dataset. A second Weibull distribution is fitted to the pooled data set to derive the appropriate model parameters. The adequacy of the Weibull distribution at each load level cannot be properly evaluated due to the limited number of data. However, the fitting quality of the distribution to the pooled dataset can be examined by using appropriate goodness of fit tests, like the Kolmogorov-Smirnov (K-S) test [50].

The wear-out model as used by Sendeckyj [25] is based on the ‘Strength Life Equal Rank Assumption’ or SLERA, introduced by Hahn and Kim [51], stating that a specimen of a certain rank in the static strength probability distribution has the same rank in the fatigue life distribution. In other words, the application of the wear-out model is valid as long as no competing failure modes are observed during fatigue life, or even between the fatigue and the static loading. According to [25] the S-N curve is described by a deterministic equation of any type, e.g. exponential, power law, etc., although the power law representation was selected in the original publication. Based on the SLERA and by using adequate fatigue model parameters, all fatigue data can be converted into equivalent static strength (ESS) data by means of Eq. (3.11). A two-parameter Weibull distribution is then fitted to the resulting set of equivalent static strength data to estimate the model parameters.

For validation of the model, the fitting quality of the Weibull distribution is examined by the Kolmogorov-Smirnov (K-S) goodness of fit test. Additionally, the method introduced in [25] prescribes a process (application of a Kruskal-Wallis (K-W) goodness of fit test) for evaluation of the fitting quality of the resulting S-N curve. The accuracy is also evaluated qualitatively by studying the dispersion of the ESS data along the probability plot. The uniform dispersion of ESS data corresponding to each stress level along the probability plot without any segregation shows the model can uniformly transform the fatigue data into the equivalent static strength dataset.

### 3.4.3. Model application ─ Validation of hypotheses

The four selected fatigue models were applied to the available experimental data and the results are presented in Figs. 3.19-3.21. The *CCfatigue* software (see Annex A1) was used for the estimation of all S-N curves. Although the designation "S-N" curves was preserved for convenience, the fatigue data refer to applied load and not to stress levels since use of a stress value is not meaningful for joints.

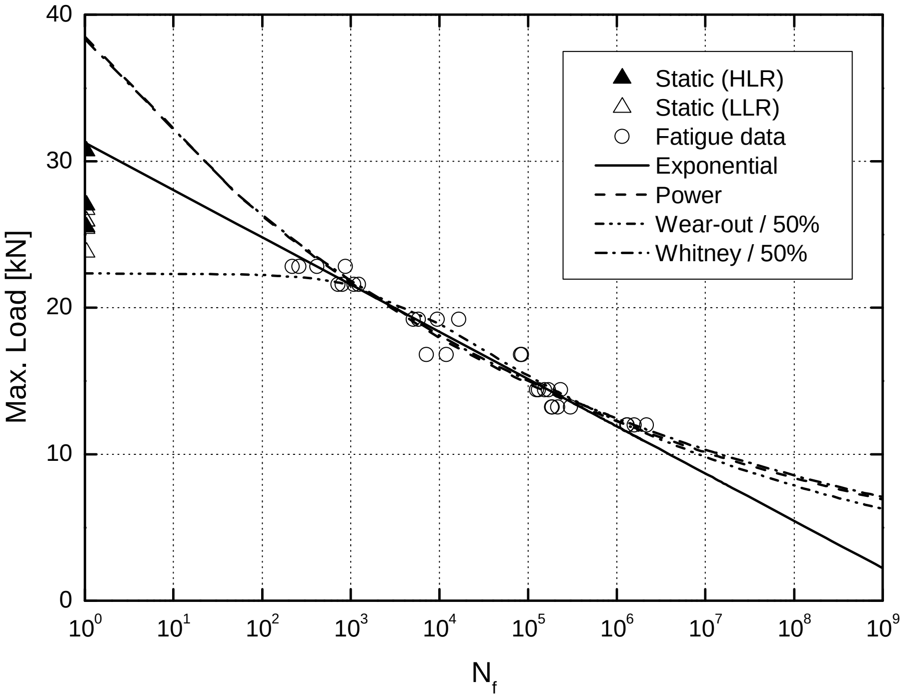

Fig. 3.19. Comparison of derived S-N curves with experimental data for *R*=0.1 (excluding static data)

Table 3.8. Estimated material constants for different models (excluding static data)

| | Exponential, Eq. (3.20) | | Power law, Eq. (3.21) | | Whitney, Eq. (3.22) | | | Sendeckyj, Eq. (3.23) | | | |
|---|---|---|---|---|---|---|---|---|---|---|---|
| *R* | *a* | *b* | *c* | *d* | *K* | *1/g* | $\alpha_f$ | *m* | *Q* | $\alpha_f$ | $\beta$ |
| 0.1 | 9.69 | -0.310 | 19.14 | -12.07 | 38.93 | 0.081 | 1.95 | 0.098 | 0.0005 | 22.60 | 22.70 |
| -1 | 8.64 | -0.292 | 15.41 | -9.63 | 37.33 | 0.092 | 1.14 | 0.129 | 0.0002 | 11.56 | 20.15 |
| 10 | 14.50 | -0.475 | 35.50 | -23.49 | 32.65 | 0.042 | 1.41 | 0.048 | 0.0021 | 36.15 | 26.30 |

The static strength data were not used for estimation of the model parameters, shown in Table 3.8. However, both LLR and HLR loading rates results are presented in the figures for information purposes.

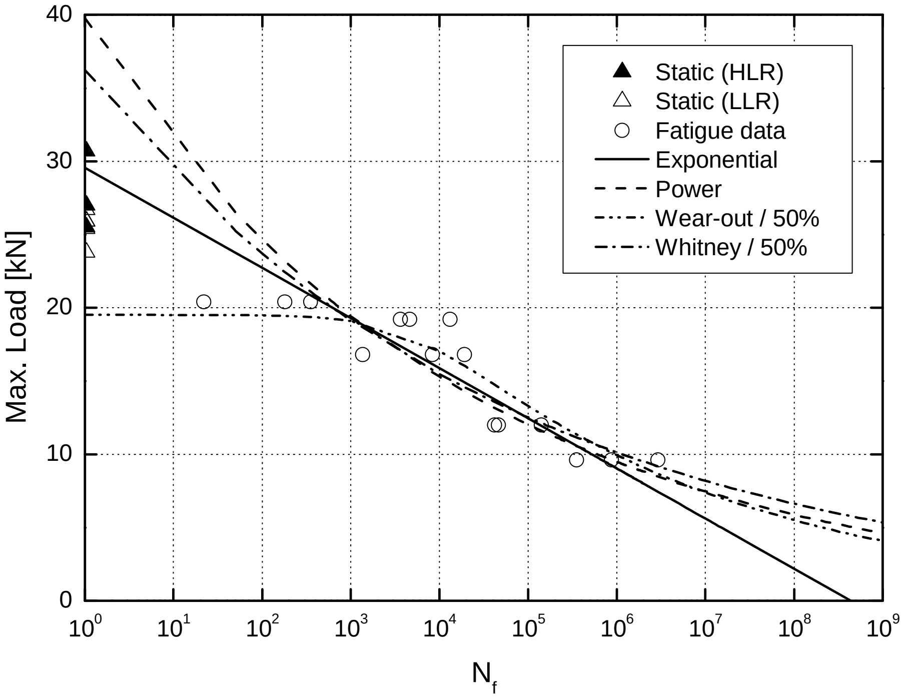

Fig. 3.20. Comparison of derived S-N curves with experimental data for *R*=-1 (excluding static data)

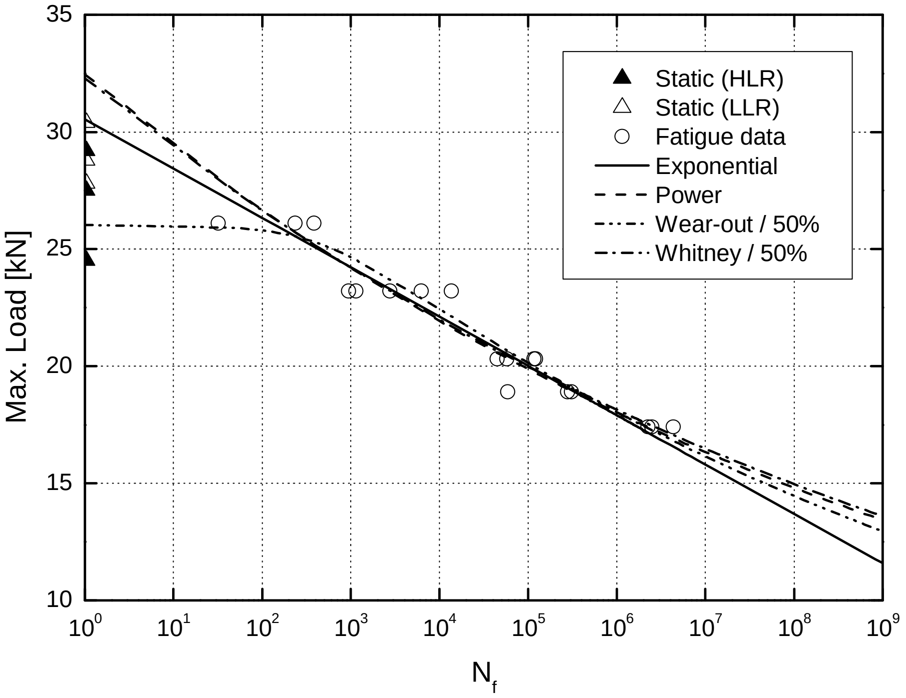

Fig. 3.21. Comparison of derived S-N curves with experimental data for *R*=10 (excluding static data)

#### *3.4.3.1 Linear or linearized fatigue models*

The calculated linearity indices and the corresponding critical values at the 5% S.L. are given in Table 3.9. The linearity hypothesis is not rejected except in the case of *R*=-1 where the linearity index values are higher than the critical values for both the exponential and power models. The rejection of the linearity hypothesis results from the significant scatter in fatigue life under the load ratio of *R*=-1, which is clearly apparent in Figs. 3.22 and 3.23.

Table 3.9. Calculated indices for evaluation of linear models (excluding static data)

| *R* | Linearity index for Eq. (3.20) | Linearity index for Eq. (3.21) | Critical linearity index corresponding to 5% S.L. |
|---|---|---|---|
| 0.1 | 1.85 | 2.38 | 2.66 |
| -1 | 4.87 | 5.21 | 3.71 |
| 10 | 0.84 | 0.69 | 3.41 |

S.L. : Significance level

Comparison of the calculated 95% confidence bands around the mean S-N curves at different *R*-ratios also shows a wider interval for *R*=-1, which clearly indicates its higher scatter. The higher scatter at *R*=-1 is a consequence of the inconsistent crack initiation and propagation exhibited by the examined joints under this kind of cyclic loading. Monitoring of the crack during the fatigue experiments in Section 3.2.2.1 showed that under tension-tension or compression-compression fatigue loading only a single crack initiated and propagated up to failure. Nevertheless, in some cases under tension-compression, in addition to the dominant crack, other smaller cracks initiated in different locations of the bonded joints.

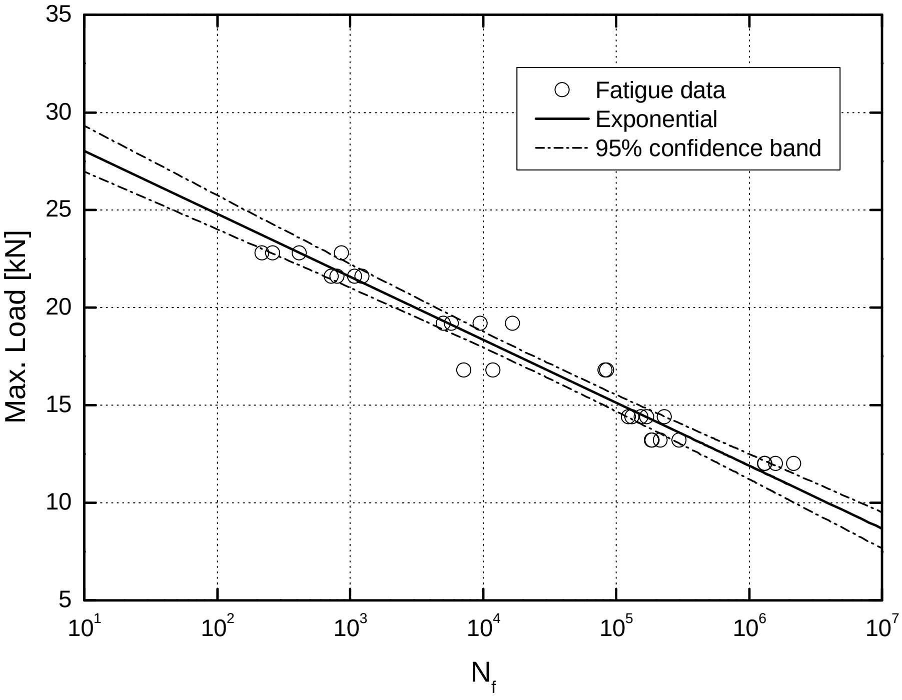

a)

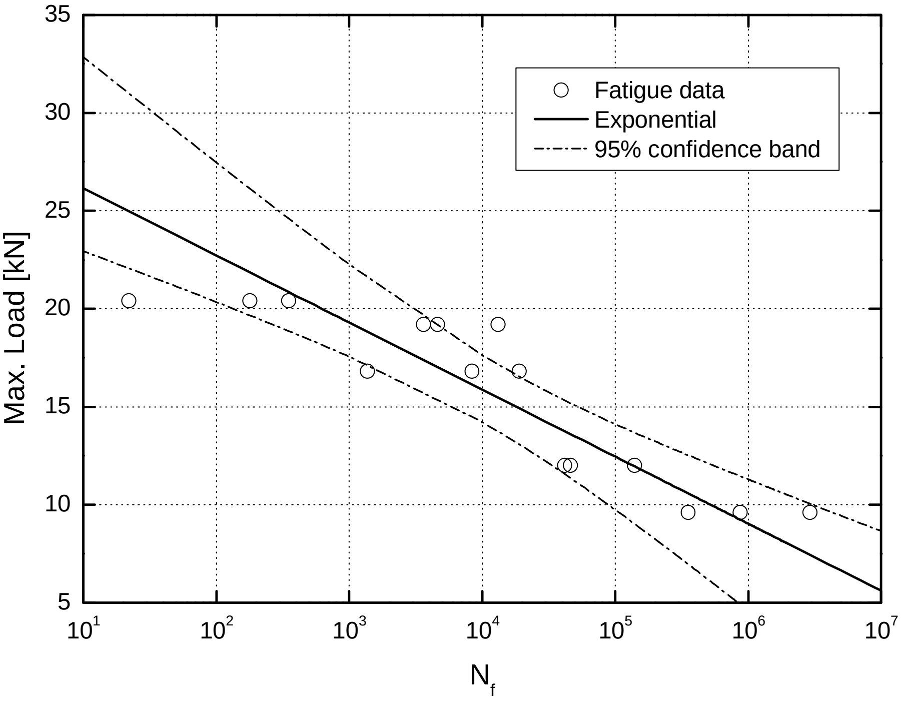

b)

Fig. 3.22, continued in next page

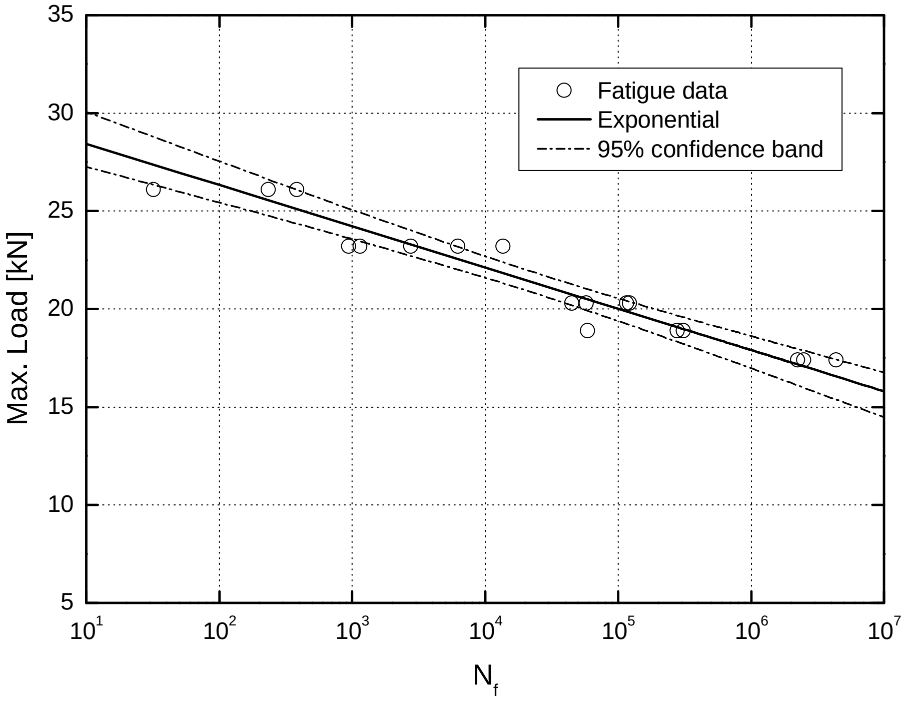

c)

Fig. 3.22. Derived exponential curves and corresponding 95% confidence bands for a) $R$=0.1, b) $R$=-1, and c) $R$=10 (excluding static data)

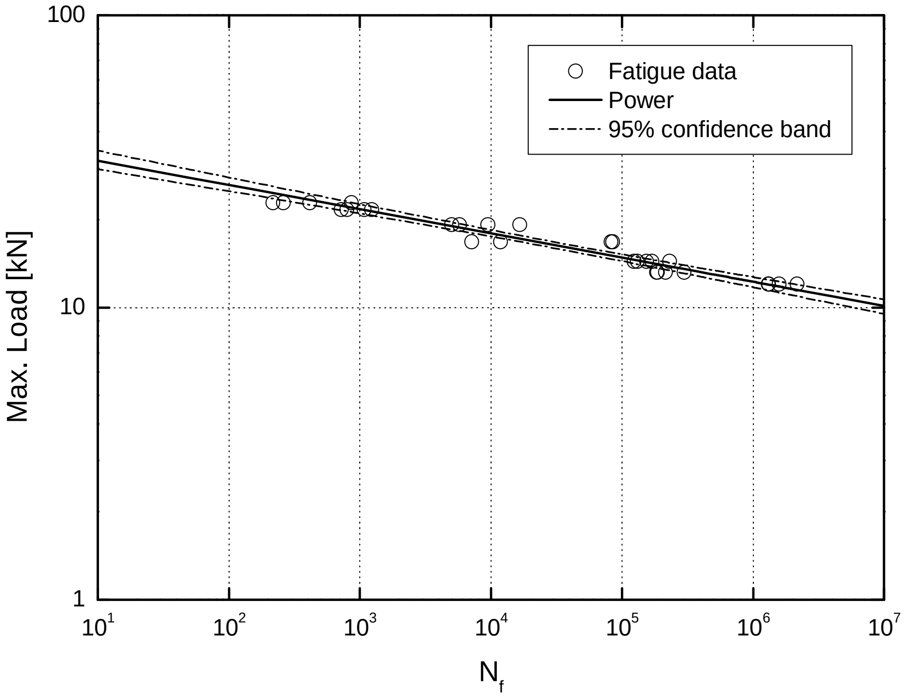

a)

Fig. 3.23, continued in next page

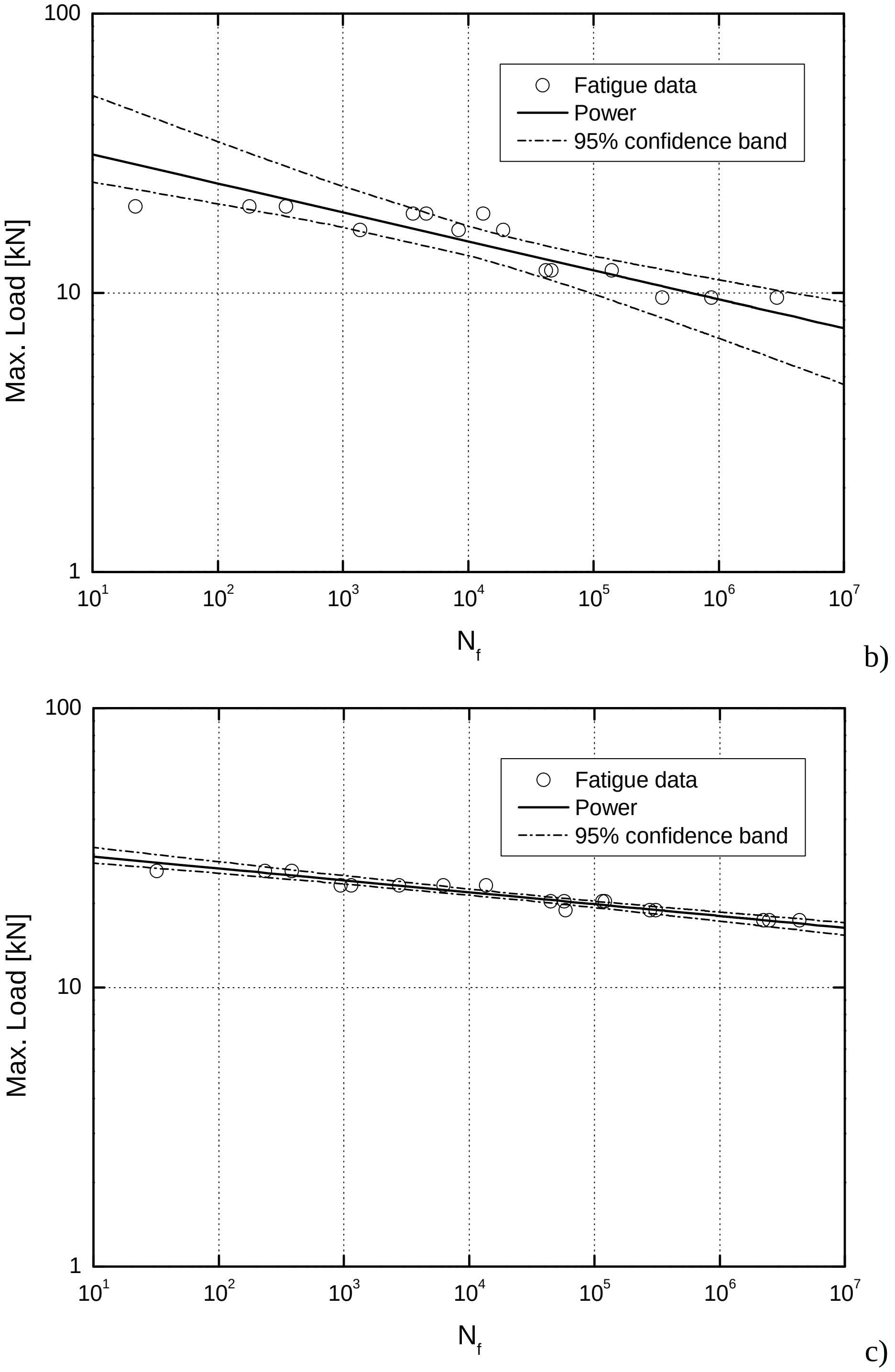

Fig. 3.23. Derived power curves and corresponding 95% confidence bands for a) *R*=0.1, b) *R*=-1, and c) *R*=10

### *3.4.3.2 Pooling scheme*

A Kolmogorov-Smirnov (K-S) goodness of fit test was performed to examine the validity of the Weibull distribution of the pooled data. Results for all three examined cases are presented in Table 3.10, where it is shown that the null hypothesis is not rejected for any *R*-ratio.

Table 3.10. Kolmogorov-Smirnov (K-S) statistics and corresponding critical values for all *R*-ratios (pooled data excluding static data and ESS data, test for Weibull distribution)

| *R* | $H_{KS}$ for pooled data | $H_{KS}$ for ESS data | $H_{cr}$ corresponding to 5% S.L. |
|---|---|---|---|
| 0.1 | 0.9184 | 0.3631 | 1.3593 |
| -1 | 0.4702 | 0.8822 | 1.3592 |
| 10 | 0.5315 | 0.4055 | 1.3561 |

S.L. : Significance level

In all examined cases, the K-S statistical indices ($H_{KS}$) are lower than the critical values ($H_{cr}$) at the 5% S.L. The agreement between the distribution of the pooled data and the estimated Weibull distribution is demonstrated in Fig. 3.24. The curves that have been plotted above and below the theoretical Weibull distribution correspond to the 5% S.L. band. If the cumulative step function of the pooled data crosses this band at any point, the null hypothesis at the 5% S.L. is rejected [50]. As can be seen in Fig. 3.24, although the Weibull distribution fits better to pooled data at *R*=-1 and *R*=10, the main assumption of Whitney's method is not rejected for any *R*-ratio and remains valid for the fatigue reliability analysis of the examined bonded joint.

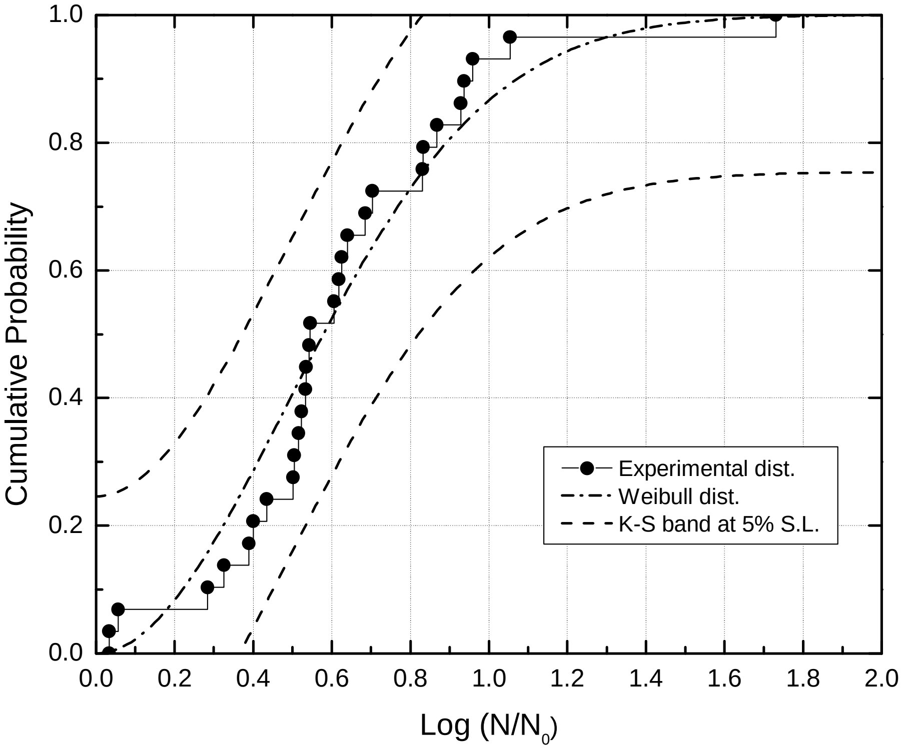

a)

Fig. 3.24, continued in next page

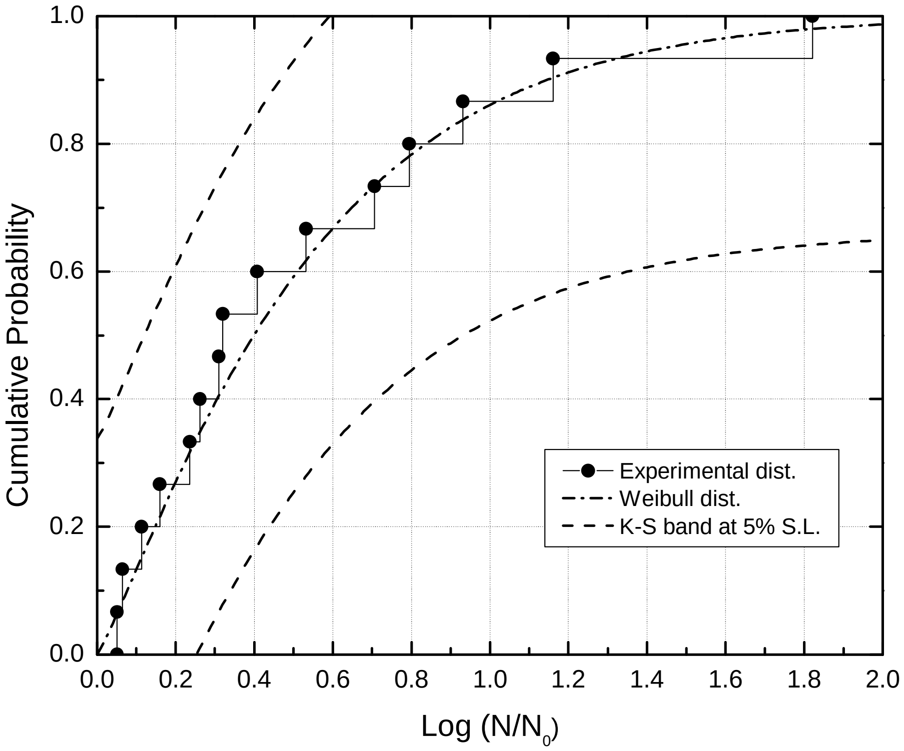

b)

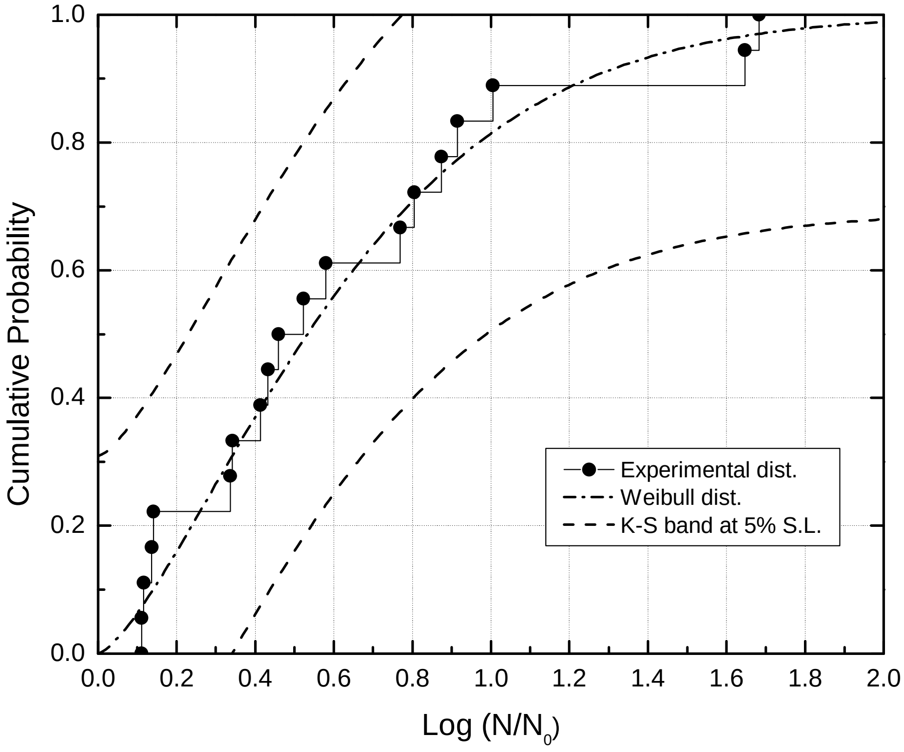

c)

Fig. 3.24. Comparison of cumulative distribution of pooled data excluding static data and estimated Weibull distribution and corresponding K-S bands at 5% S.L. for a) *R*=0.1, b) *R*=-1, and c) *R*=10. (S.L. : Significance level)

### *3.4.3.3. Wear-out model*

There are two requirements that must be fulfilled in order to evaluate the fitting quality of the wear-out model [25]: The main hypothesis – the equivalent static strength follows a Weibull distribution – must be validated, and a goodness of fit test must be performed to evaluate the fitting quality of the wear-out model to the data.

A K-S goodness of fit test was used to examine whether the ESS data followed a Weibull distribution. The cumulative distribution of the ESS data, corresponding to the model parameters $m$ and $Q$ given in Table 3.8, is compared with the fitted Weibull distribution in Fig. 3.25. The ESS data are fitted by the Weibull distribution for $R$=0.1 and 10 more accurately than the fatigue data collected under $R$=-1. However, the null hypothesis is not rejected at 5% S.L. for any $R$-ratio since the $H_{KS}$ statistical indices are lower than the corresponding critical values, $H_{cr}$, see Table 3.10.

The K-W goodness of fit test for validation of the fitting of the derived S-N curve was also performed as described in [25]. The qualitative evaluation was carried out via the graphical representation of the probability of survival plots for the ESS data and the obtained Weibull distributions (see Fig. 3.25). Each symbol corresponds to one load level. The dispersion of the symbols along the probability plot indicates the quality of fitting.

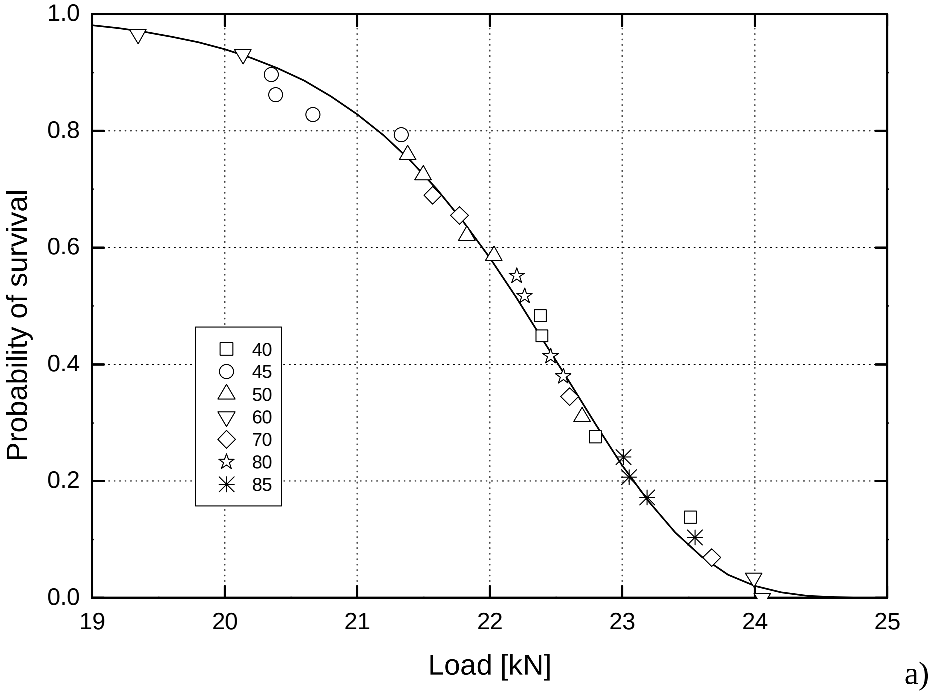

Fig. 3.25, continued in next page

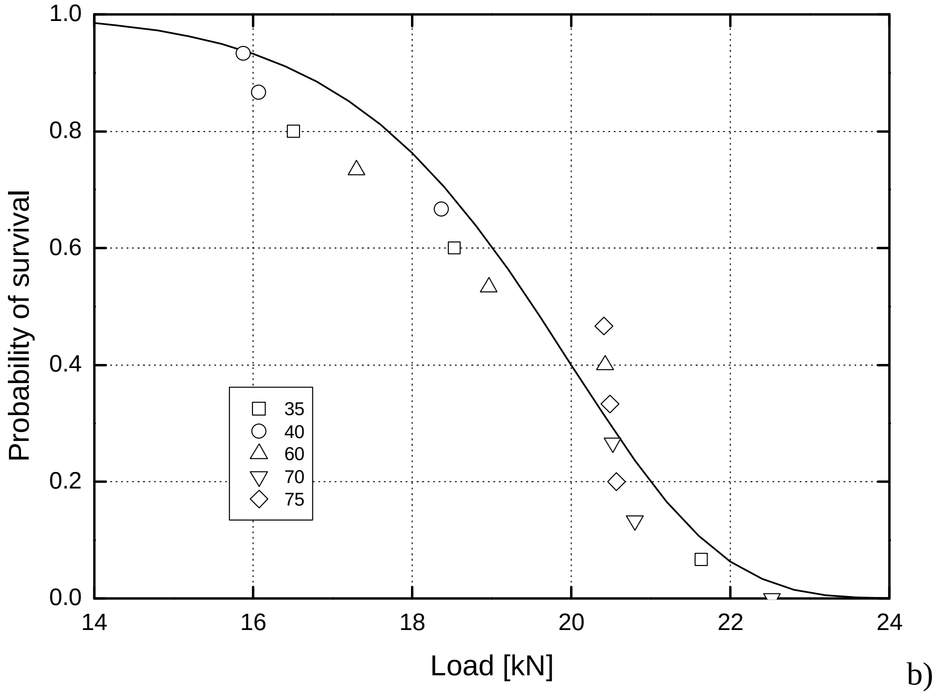

b)

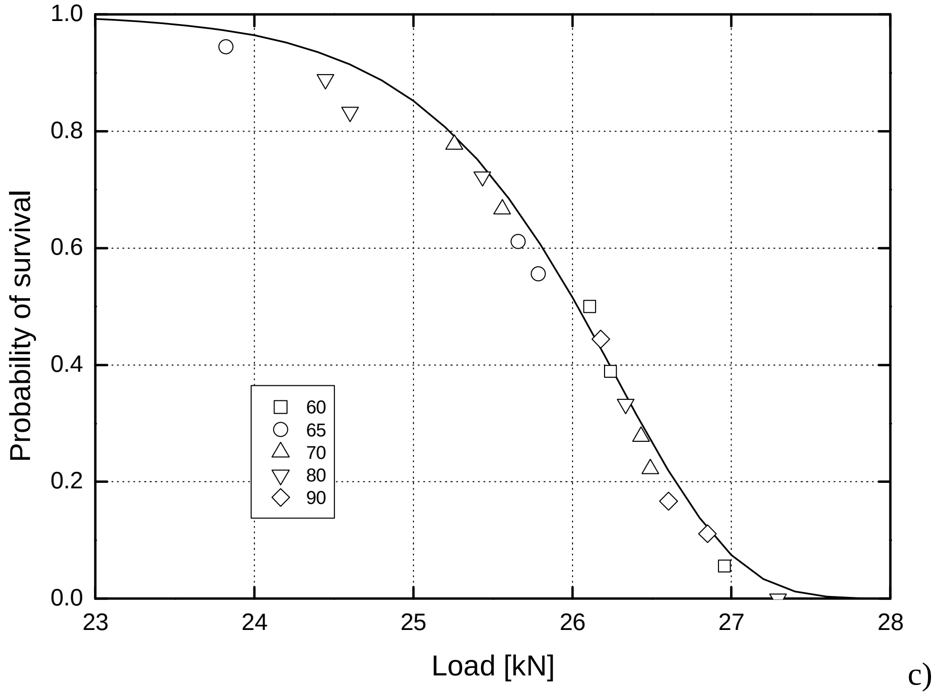

c)

Fig. 3.25. Probability-of-survival plot for Equivalent Static Strength (ESS) data excluding static data and estimated Weibull distribution (solid curve) for a) *R*=0.1, b) *R*=-1, and c) *R*=10 (numbers in the legends stand for nominal maximum cyclic load level as percentage of UTS for R=0.1 and R=-1 and UCS for R=10)

As can be seen in Fig. 3.25, there is some tendency for segregation of the symbols for *R*=0.1 and -1 which shows that the model is not very well fitted to the experimental data. The segregation is more pronounced at *R*=0.1 where the star symbols lie to the right of up triangles or circles are congregated on the left of other symbols except down triangles (Fig. 3.25a) and it is less noticeable for $R$=-1 for which the circles are segregated on the left side of the plot (Fig. 3.25b). However for $R$=10 the symbols are well interspersed, which shows a good fitting of the model to the fatigue data. The K-W statistical indices ($H_{KW}$) were calculated for each $R$-ratio (see Table 3.11). The degree of freedom corresponds to the number of different load levels in each fatigue dataset. The comparison of the $H_{KW}$ statistical indices and the corresponding critical values at the 5% S.L. (taken from Table A4 in [52]) confirms the above-mentioned qualitative results. The $H_{KW}$ approaches the given critical value for $R$=0.1 indicating poor fitting. The $H_{KW}$ for $R$=-1 is higher than the K-W statistic for $R$=10 (both datasets have the same degree of freedom) showing that the fitting is better for $R$=10.

Table 3.11. Kruskal-Wallis statistics and corresponding critical values for all $R$-ratios (excluding static data)

| $R$ | Degree of freedom | $H_{KW}$ | $H_{cr}$ corresponding to 5% S.L. |
|---|---|---|---|
| 0.1 | 6 | 12.20 | 12.59 |
| -1 | 4 | 6.47 | 9.49 |
| 10 | 4 | 4.90 | 9.49 |

S.L. : Significance level

All the examined fatigue models are appropriate for the modeling of the material behavior in the region between $10^3$ and $10^6$ cycles (see Figs. 3.19-3.21). Nevertheless, they show significant disparities outside this region, where no experimental data exist and the models must extrapolate their predictions to simulate the material behavior. In the very LCF region, close to one cycle, the wear-out model predicts the lowest maximum load followed by the exponential model, while the other two methods that rely on a power S-N formulation predict very high loads, even higher than the static strength (ultimate load) of the examined joints. The S-N curves derived by the Whitney’s pooling scheme and the power law model are similar as long as the scatter of the examined fatigue dataset is low (e.g. for $R$=0.1 and $R$=10). When the scatter is higher, e.g. for $R$=-1, the difference in the derived curves is more pronounced (see Fig. 3.20) although still not significant. On the other hand, in the HCF region, the life estimation from the exponential model is very conservative compared to all other models and becomes unrealistic since it predicts a finite life under zero load. The rest of the examined model predictions follow the trend of the experimental data.

### 3.4.4. Effect of static strength data

Static strength data (representing fatigue data for one cycle) were used to investigate whether this data can improve the accuracy of the applied model in the LCF region. S-N curves for all three datasets, derived by including the HLR static strength data together with the fatigue data for estimation of the model parameters, are shown in Figs. 3.26-3.28. The estimated model parameters are given in Table 3.12. The linearity hypothesis of the new linear curves was rejected for all the *R*-ratios at the 5% S.L. (see Table 3.13) but the hypothesis of the Weibull distribution of the pooled and ESS data was not rejected (Table 3.14).

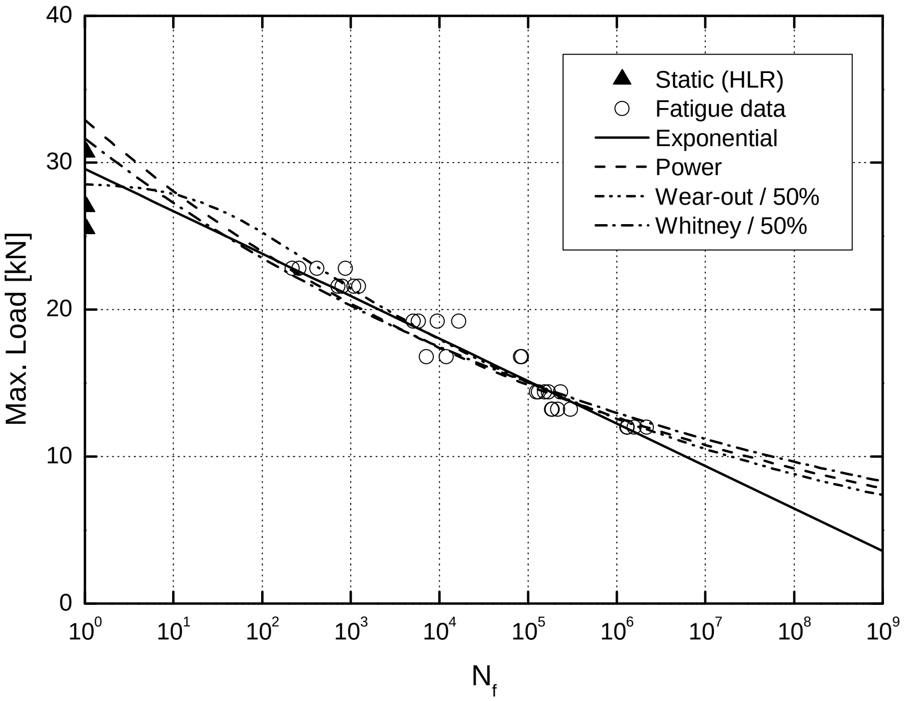

Fig. 3.26. Comparison of derived S-N curves with experimental data for *R*=0.1 (including static data)

Table 3.12. Estimated material constants for different models (including static data)

| | Exponential, Eq. (3.20) | | Power law, Eq. (3.21) | | Whitney, Eq. (3.22) | | | Sendeckyj, Eq. (3.23) | | | |
|---|---|---|---|---|---|---|---|---|---|---|---|
| *R* | *a* | *b* | *c* | *d* | *K* | *1/g* | $\alpha_f$ | *m* | *Q* | $\alpha_f$ | $\beta$ |
| 0.1 | 10.24 | -0.346 | 21.94 | -14.46 | 31.99 | 0.064 | 2.06 | 0.078 | 0.0386 | 17.86 | 29.11 |
| -1 | 8.88 | -0.311 | 18.02 | -11.98 | 30.83 | 0.075 | 1.27 | 0.112 | 0.0071 | 8.83 | 27.21 |
| 10 | 15.95 | -0.551 | 41.47 | -28.14 | 29.33 | 0.033 | 1.55 | 0.045 | 0.0179 | 29.44 | 28.27 |

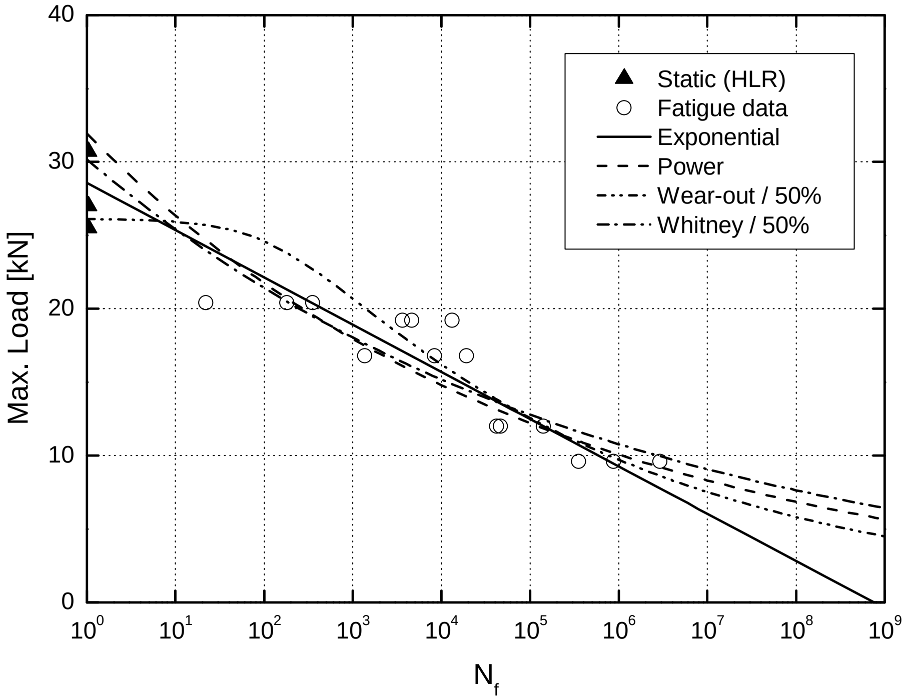

Fig. 3.27. Comparison of derived S-N curves with experimental data for *R*=-1 (including static data)

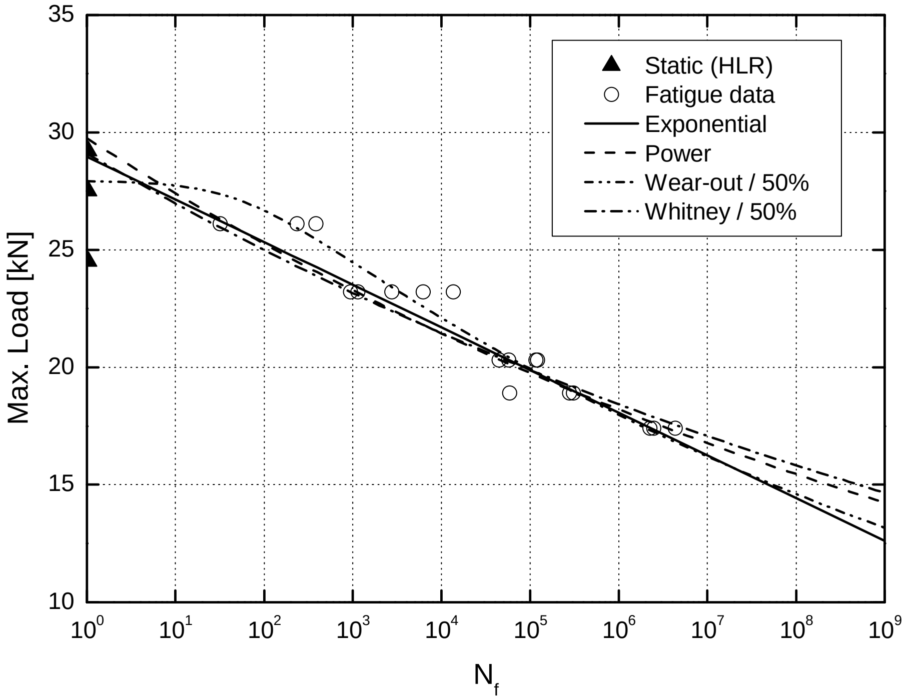

Fig. 3.28. Comparison of derived S-N curves with experimental data for *R*=10 (including static data)

Table 3.13. Calculated indices for evaluation of linear models (including static data)

| $R$ | Linearity index for Eq. (3.20) | Linearity index for Eq. (3.21) | Critical linearity index corresponding to 5% S.L. |
|---|---|---|---|
| 0.1 | 6.91 | 16.97 | 2.51 |
| -1 | 4.82 | 9.02 | 3.26 |
| 10 | 8.98 | 11.26 | 3.06 |

S.L. : Significance level

Table 3.14. Kolmogorov-Smirnov (K-S) statistics and corresponding critical values for all $R$-ratios (pooled data including static data and ESS data, test for Weibull distribution)

| $R$ | $H_{KS}$ for pooled data | $H_{KS}$ for ESS data | $H_{cr}$ corresponding to 5% S.L. |
|---|---|---|---|
| 0.1 | 0.8630 | 0.9257 | 1.3563 |
| -1 | 0.4234 | 0.6601 | 1.3561 |
| 10 | 0.5158 | 0.4551 | 1.3565 |

S.L. : Significance level

Table 3.15. Kruskal-Wallis statistics and corresponding critical values for all $R$-ratios (including static data)

| $R$ | Degree of freedom | $H_{KW}$ | $H_{cr}$ corresponding to 5% S.L. |
|---|---|---|---|
| 0.1 | 7 | 12.32 | 14.07 |
| -1 | 5 | 8.88 | 11.07 |
| 10 | 5 | 2.63 | 11.07 |

S.L. : Significance level

The goodness of fit procedure for the wear-out model was also performed for the new S-N curves (Fig. 3.29). As shown in Fig. 3.29, the quality of fitting was significantly improved by including the static data as the different symbols were interspersed well along the theoretical estimated probability-of-survival curves with a relatively low tendency for segregation of symbols. The comparison of the calculated $H_{KW}$ statistical indices shown in Table 3.15 with the critical values at 5% S.L. and with the corresponding $H_{KW}$ indices of Table 3.11 confirms this improvement. This behavior was expected since the wear-out model was based on the Strength Life Equal Rank Assumption that is valid as long as failure modes do not differ between the static and fatigue loading. This assumption is validated for the examined joint configuration under the given loading conditions as presented in Section 3.2.2.1.

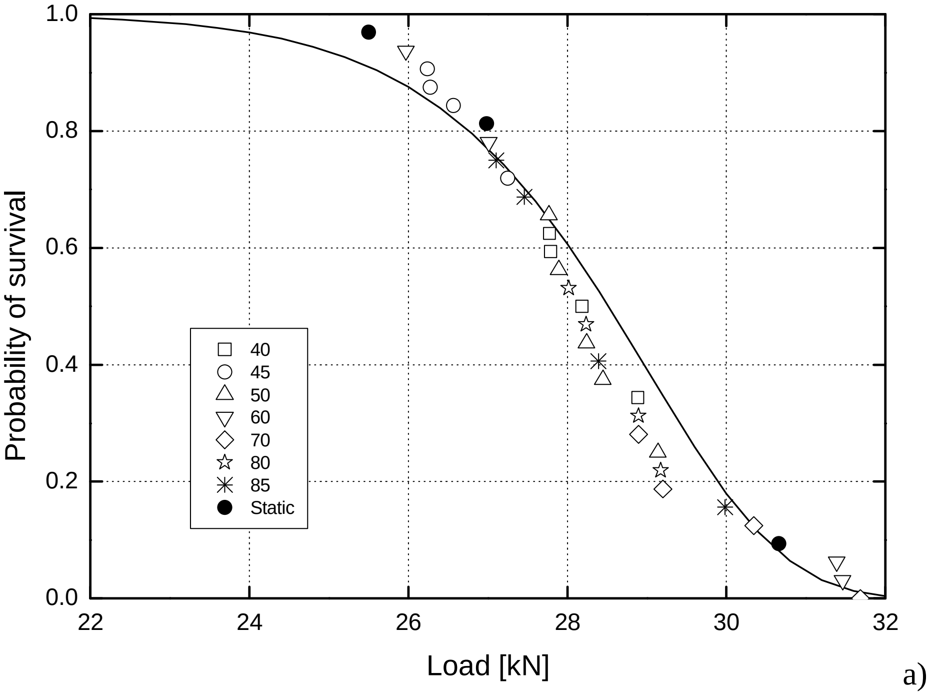

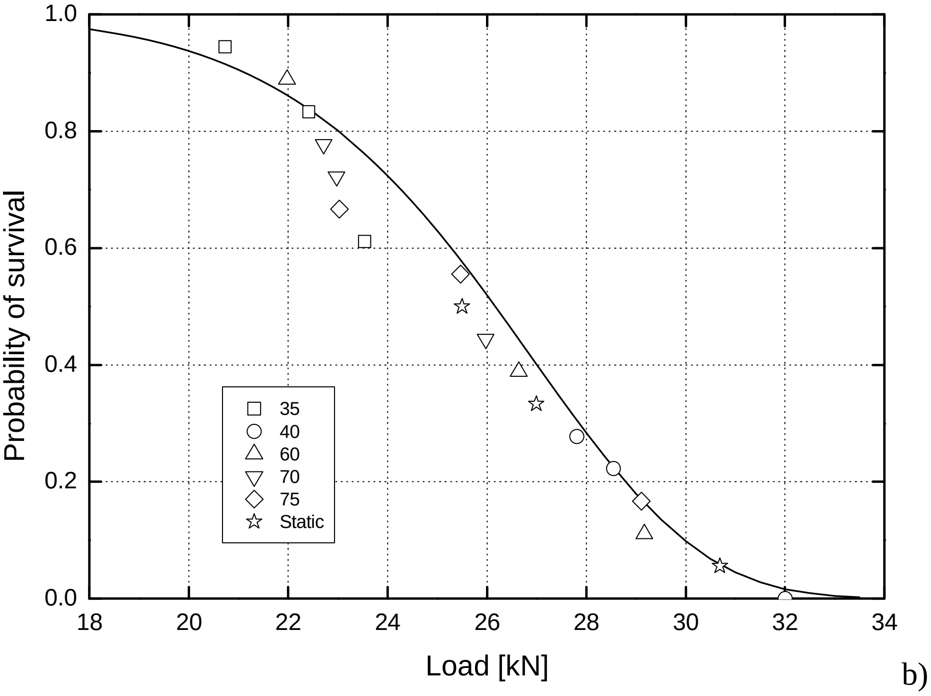

Fig. 3.29, continued in next page

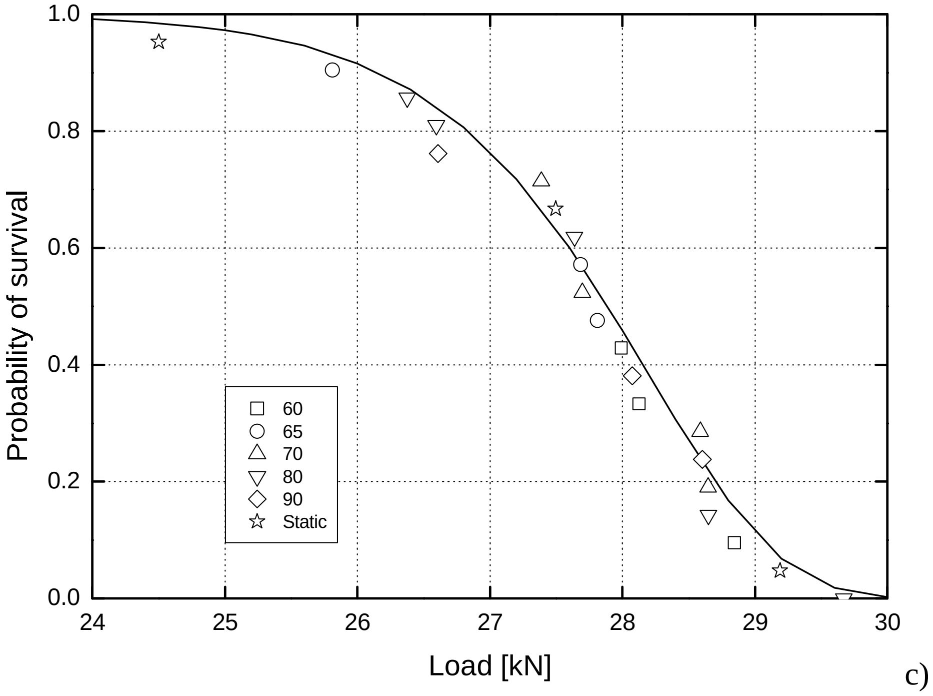

Fig. 3.29. Probability-of-survival plot for Equivalent Static Strength (ESS) data including static data and estimated Weibull distribution (solid curve) for a) *R*=0.1, b) *R*=-1, and c) *R*=10 (numbers in the legends stand for nominal maximum cyclic load level as percentage of UTS for R=0.1 and R=-1 and UCS for R=10)

Although the S-N curves based on the wear-out model were improved in the LCF region, and the overall quality of fitting was enhanced, use of the static strength data did not improve the results obtained using the other methods. The resulting S-N curves (shown in Figs. 3.26-3.28) simulate the fatigue behavior better at very LCF but fail to accurately follow the trend of the fatigue data in the HCF region. In general, inclusion of the static strength data in the analysis leads to lower slopes of the derived S-N curves resulting in non-conservative estimation of life in the HCF region.

## 3.5. Conclusions

The fatigue behavior of adhesively-bonded pultruded GFRP double-lap joints was experimentally examined under load ratios of 0.1, -1, and 10 in order to investigate the effect of different load ratios on fatigue life, stiffness degradation and crack propagation. The results showed that the change in load ratio significantly affected the fatigue behavior of the examined adhesively-bonded joints. The conclusions of this work will form the basis for further investigation of the effect of realistic loading patterns on the response of the same structural joints. The applicability of known and commonly accepted phenomenological fatigue models for characterizing the constant amplitude fatigue behavior of adhesively-bonded GFRP joints has also been examined in this chapter. A concise review was performed for the selection of the most appropriate methods. Four models were chosen, based on their simplicity, the need for limited datasets, and their ability to take into account the probabilistic nature of the fatigue properties of composite materials. The following conclusions can be drawn from this chapter:

- The examined joints exhibited different behavior under quasi-static tension and compression loading. A fiber-tear failure was observed under tensile loading. The failure of the specimens was dominated by cracks in the mat layers of the inner laminate. Under compression, failure occurred in the roving layer in the middle of the inner laminate. A similar failure was observed and similar stiffness derived under low or high loading rates without significant change in the strength of the examined joints, independent of loading condition.
- The fatigue failure mode of DLJs under load ratios of 0.1 and -1 were found to be similar to the failure mode observed under quasi-static tension loads. The failure of specimens at $R$=10 was similar to the compressive quasi-static failure mode.
- The examined DLJs were found to be more sensitive to tensile than to compressive fatigue loads. When fatigue data are represented on the $F_{\max}$-$N$ plane, the curve corresponding to $R$=-1 lies below the other two, while the $F_{\max}$-$N$ curve corresponding to $R$=10 exhibits the lowest slope. The simple linear Goodman diagram cannot accurately describe the mean load effect on fatigue life. More sophisticated phenomenological models may provide better results.
- All fatigue models were appropriate for the modeling of fatigue behavior between $10^3$-$10^6$ cycles. However, different behaviors are predicted by the models when they extrapolate in the low- and high-cycle fatigue regions. The power model and Whitney pooling scheme, in contrast to the wear-out model which is very conservative at LCF, estimate very high fatigue strength in this region. However, all three are similar in the HCF region. On the other hand, the exponential model exhibited a good behavior at LCF while it underestimates the fatigue life in the HCF region.
- The influence of including the static strength data for derivation of S-N curves was investigated. Comparison of S-N curves indicated the improvement in fatigue life estimation in the LCF region when the static data were included in the fatigue

analysis. However, the slopes of the power law and Whitney curves were negatively affected by this modification and the use of static data for the derivation of the S-N curves is, therefore, not recommended. The fitting quality of the wear-out model was improved by including the static data in the fatigue analysis. This behavior was found reasonable since the model was developed based on the relationship between static and fatigue data. However comparison of the S-N curves for different *R*-ratios showed that the quality of fitting was strongly affected by the scatter of data since the model parameters are adjusted based on the distribution of fatigue life.

- The exponential and power law models were found to be the most appropriate, since they are simple and relatively insensitive to the scatter in the experimental data. Nevertheless, none of the studied models can adequately characterize the fatigue behavior of the examined bonded GFRP joints over the entire life range and thus new models must be developed for this purpose.

## 3.6. References

1. Burgueno R, Karbhari VM, Seible F, Kolozs RT. Experimental dynamic characterization of an FRP composite bridge superstructure assembly. Compos Struct, 2001;54(4):427-444.
2. Keller T, Tirelli T. Fatigue behavior of adhesively connected pultruded GFRP profiles. Compos Struct, 2004;65(1):55–64.
3. Keller T, Gürtler H. Quasi-static and fatigue performance of a cellular FRP bridge deck adhesively bonded to steel girders. Compos Struct, 2005;70(4):484-496.
4. Keller T, Zhou A. Fatigue behavior of adhesively bonded joints composed of pultruded GFRP adherends for civil infrastructure applications. Compos Part A – Appl S, 2006;37(8):1119-1130.
5. Zhang Y, Vassilopoulos AP, Keller T. Stiffness degradation and fatigue life prediction of adhesively-bonded joints for fiber-reinforced polymer composites. Int J Fatigue, 2008;30(10–11):1813–1820.
6. Zhang Y, Vassilopoulos AP, Keller T. Environmental effects on fatigue behavior of adhesively-bonded pultruded structure joints. Compos Sci Technol, 2009;69(7–8):1022–1028.
7. Zhang Y, Vassilopoulos AP, Keller T. Fracture of adhesively-bonded pultruded GFRP joints under constant amplitude fatigue loading. Int J Fatigue, 2010;32(7):979–987.

8. Crocombe AD, Richardson G. Assessing stress and mean load effects on the fatigue response of adhesively bonded joints. Int J Adhes Adhes, 1999;19(1):19-27.
9. Weibull W. Fatigue testing and the analysis of results, pp. 143-181, Pergamon Press, Oxford, 1961.
10. Mandell JF, Meier U. Effect of stress ratio, frequency and loading time on the tensile fatigue of glass-reinforced epoxy, O’Brian TK. (Ed.), pp. 55-77, ASTM STP 813, American society for testing and materials, Philadelphia, 1982.
11. Rotem A. Load frequency effect on the fatigue strength of isotropic laminates, Compos Sci Technol, 1993;46(2):129-138.
12. Ellyin F, El-Kadi H. Effect of stress ratio on the fatigue of unidirectional glass fibre/epoxy composite laminae. Composites 1994;25(10):917-24.
13. Jarosch E, Stepan A. Fatigue properties and test procedures of glass reinforced plastic rotor blades, J Am Helicopter Soc, 1970;15(1):33-41.
14. D'Amore A, Caprino G, Stupak P, Zhou J, Nicolais L. Effect of stress ratio on the flexural fatigue behaviour of continuous strand mat reinforced plastics, Sci Eng Compos Mater, 1996;5(1):1-8.
15. Epaarachchi JA, Clausen PD. An empirical model for fatigue behavior prediction of glass fibre-reinforced plastic composites for various stress ratios and test frequencies, Compos Part A-Appl S, 2003;34(4):313-326.
16. Qiao P, Yang M. Fatigue life prediction of pultruded E-glass/polyurethane composites, J Compos Mater, 2006;40(9):815-837.
17. Sendeckyj GP. Life prediction for resin matrix composite materials, In: K.L. Reifsnider, Editor, Fatigue of composite materials, pp. 431-483, Elsevier, Amsterdam, 1990.
18. Chou PC, Croman R. Degradation and sudden-death models of fatigue of graphite/epoxy composites. Composite materials: testing and design (fifth conference), Tsai SW. (Ed.), pp. 431-454, ASTM STP 674, American society for testing and materials, Philadelphia, 1979.
19. Hwang W, Han KS. Fatigue of composites - fatigue modulus concept and life prediction, Compos Mat, 1986;20(2):154-165.
20. Philippidis TP, Vassilopoulos AP. Fatigue design allowables for GFRP laminates based on stiffness degradation measurements. Compos Sci Technol 2000;60(15):2819–28.

21. Harik VM, Klinger JR, Bogetti TA. Low-cycle fatigue of unidirectional composites: Bi-linear S-N curves, Int J Fatigue, 2002;24(2-4):455-462.
22. Xiong JJ, Shenoi RA. Two new practical models for estimating reliability-based fatigue strength of composites, J Compos Mater, 2004;38(14):1187-1209.
23. Standard practice for statistical analysis of linear or linearized stress-life (S-N) and strain-life (ε-N) fatigue data, E 739-10, Annual book of ASTM standards, ASTM.
24. Whitney JM. Fatigue characterization of composite materials. In: Fatigue in fibrous composite materials, Lauraitis KN. (Ed.), pp. 133-151, ASTM STP 723, American society for testing and materials, Philadelphia, 1981.
25. Sendeckyj GP. Fitting models to composite materials fatigue data. In: Test methods and design allowables for fibrous composites, Chamis CC. (Ed.), pp. 245-260, ASTM STP 734, American Society for Testing and Materials, 1981.
26. Nijssen RPL, Krause O, Philippidis TP. Benchmark of lifetime prediction methodologies, Optimat blades technical report, 2004, OB_TG1_R012 rev.001, http://www.wmc.eu/public_docs/10218_001.pdf
27. Mandell JF. Fatigue behavior of short fiber composite materials, In: K.L. Reifsnider, Editor, Fatigue of composite materials, pp. 232-333, Elsevier, Amsterdam, 1990.
28. Kensche ChW. (ed.), Fatigue of materials and components for wind turbine rotor blades, European Comission, Directorate-General XII, Science, Research and Development (1996), ISBN 92-827-4361-6.
29. Echtermeyer AT, Hayman E, Ronold KO. Comparison of fatigue curves for glass composite laminates, In: Design of composite structures against fatigue: applications to wind turbine blades, RM. Mayer(Ed.), pp. 209-226, Mechanical Engineering Publications Limited, 1996.
30. Krenk S, Jönsson J, Hansen LP. Fatigue analysis and testing of adhesive joints, Eng Fract Mech, 1996;53(6):859-872.
31. Nolting AE, Underbill PR, Duquesnay DL. Fatigue behavior of adhesively bonded aluminium double strap joints, Journal of ASTM International, 2008;5(5):1-12.
32. Zhang Y, Keller T. Progressive failure process of adhesively bonded joints composed of pultruded GFRP. Compos Sci Technol, 2008;68(2):461–470.
33. Quaresimin M, Ricotta M. Fatigue behaviour and damage evolution of single lap bonded joints in composite material, Compos Sci Technol, 2006;66(2):176-187.
34. Sarkani S, Michaelov G, Kihl DP, Beach JE. Stochastic Fatigue Damage Accumulation of FRP Laminates and Joints, J Struct Eng, 1999; 125(12):1423-1431.

35. Vassilopoulos AP, Georgopoulos EF, Dionysopoulos V. Artificial neural networks in spectrum fatigue life prediction of composite materials, Int J Fatigue, 2007;29(1):20-29.
36. Vassilopoulos AP, Georgopoulos EF, Keller T. Comparison of genetic programming with conventional methods for fatigue life modelling of FRP composite materials, Int J Fatigue, 2008;30(9):1634-1645.
37. Vassilopoulos AP, Bedi R. Adaptive neuro-fuzzy inference system in modeling fatigue life of multidirectional composite laminates, Comput Mater Sci 2008;43(4):1086-1093.
38. Vassilopoulos AP, Keller T. Modeling of the fatigue life of adhesively-bonded FRP joints with genetic programming, Proceedings of the 17th International Conference on Composite Materials (ICCM17), pp. F13:13, Edingburgh, UK, July 27-31, 2009.
39. De Castro J, Keller T. Ductile double-lap joints from brittle GFRP laminates and ductile adhesives. Part I: experimental investigation. Compos Part B – Eng, 2008;39(2):271–281.
40. Vassilopoulos AP, Manshadi BD, Keller T. Influence of the constant life diagram formulation on the fatigue life prediction of composite materials. Int J Fatigue, 2010;32(4):659–669.
41. Vassilopoulos AP, Manshadi BD, Keller T. Piecewise non-linear constant life diagram formulation for FRP composite materials. Int J Fatigue, 2010;32(10):1731–1738.
42. Keller T, Tirelli T, Zhou A. Tensile fatigue performance of pultruded glass fiber reinforced polymer profiles. Compos Struct, 2005;68(2):235–245.
43. Hadavinia H, Kinloch AJ, Little MSG, Taylor AC. The prediction of crack growth in bonded joints under cyclic-fatigue loading. I. Experimental studies. Int J Adhes Adhes, 2003;23(6):449–461.
44. Abdel-Wahab MM, Ashcroft IA, Crocombe AD, Smith PA. Finite element prediction of fatigue crack propagation lifetime in composite bonded joints. Compos Part A – Appl S, 2004;35(2):213–222.
45. Ashcroft IA, Shaw SJ. Mode I fracture of epoxy bonded composite joints: 2. Fatigue loading. Int J Adhes Adhes, 2002;22(2):151–167.
46. Sims DF, Brogdon VH. Fatigue behavior of composites under different loading modes, ASTM STP 636, Reifsnider KL, Lauraitis KN. Ed., American society for testing and materials, Philadelphia, 1977, pp. 185-205.

47. Harik VM, Bogetti TA. Low cycle fatigue of composite laminates: A damage-mode-sensitive model, J Compos Mater, 2003;37(7):597-610.
48. Mu P, Wan X, Zhao M. A new S-N curve model of fiber reinforced plastic composite, Key Eng Mat, 2011;462-463:484-488.
49. Hahn HT, Kim RY. Proof testing of composite materials, J Compos Mater, 1975;9:297-311.
50. Massey FJ. The Kolmogorov-Smirnov test for goodness of fit, J Am Stat Assoc, 1951;46:68–78.
51. Hahn HT, Kim RY. Fatigue behavior of composite laminate, J Compos Mater, 1976;10:156-180.
52. Sheskin DJ. Handbook of parametric and nonparametric statistical procedures, Appendix: Table A4, 2nd edition, Chapman & Hall/CRC, London, 2000.

# 4 Hybrid S-N formulation

### *Abstract*

*A semi-empirical S-N formulation for the modeling of the constant amplitude fatigue behavior of composite materials and structures is introduced in this paper. The new S-N formulation is based on the commonly used exponential and power law fatigue models. It is a hybrid formulation combining the two existing models in order to improve their modeling accuracy in the low and high cycle fatigue regions. This formulation was applied to a number of fatigue databases for different composite materials and structural elements in order to simulate their fatigue behavior. The modeling accuracy of the hybrid model was compared to the accuracy of commonly used S-N models for composite materials. As proved, the hybrid model performs better in the majority of the examined cases and is able to overcome the disadvantages of previously developed models without introducing any complexity in the fitting procedure.*

## 4.1. Introduction

Significant research efforts have been devoted to understanding the fatigue behavior of fiber-reinforced polymer (FRP) composite materials and the development of techniques for modeling the fatigue life and prediction of the material’s behavior under different conditions. One of the most explicit and straightforward ways to represent experimental fatigue data is the S-N diagram. It is preferred to other approaches for the modeling of the fatigue life of FRP composite materials, e.g. those based on stiffness degradation, or crack propagation measurements during lifetime, since it requires input data (applied load and corresponding cycles to failure) that can be collected using very simple recording devices.

Usually, fatigue data for preliminary design purposes are gathered in the region of fatigue cycles ranging between $10^3$ and $10^7$. However, depending on the application, high- or low-cycle fatigue regimes can be of interest. Additional data are needed in such cases to avoid the danger of poor modeling due to extrapolation into unknown spaces. Although for the high-cycle fatigue (HCF) regime long-term and time-consuming fatigue data must be acquired, the situation seems easier for low-cycle fatigue (LCF) where static strength data can apparently be used in combination with the fatigue data. However, when the static strength data are considered in the analysis, other problems arise. As reported in [1, 2] for typical composite material systems, static strength data should not be a part of the S-N curve, especially when they have been acquired under strain rates much lower that those used in fatigue loading. The use of static data in the regression leads to incorrect slopes of the S-N curves as presented in [1]. On the other hand, although excluding static strength data improves the description of the fatigue behavior, it introduces errors in the lifetime predictions when the low-cycle regime is important, as for example for loading spectra with a low number of high-load cycles. Therefore the use of static strength data for the derivation of fatigue curves (such as fatigue data for 1 or ¼ cycle) is arguable.

A common S-N behavior of FRP laminates has been described by the wear-out model in [3] as a power curve that flattens at high applied cyclic stress levels. In another work by Salkind [4] this change of slope at the LCF regime is attributed to the sensitivity of FRP composites to high strain ranges that occurred under high stress levels. A comparative study by Mandell [5] on short fiber-reinforced composites showed that the S-N data for chopped glass strand polyester laminates follow a different trend. The behavior can be appropriately simulated by a linear curve in the semi-logarithmic scale, although at the HCF regime the presence of run-outs causes a decrease in the slope of the S-N curve. Detailed analysis of fatigue data with computational tools, like genetic programming, see e.g. [6] showed that a multi-slope curve fits better the fatigue behavior of typical composite laminates.

A review of articles on the fatigue behavior of composite materials shows that the mechanism of fatigue failure can alter with changes in the cyclic stress level [7-11] explaining the variation in the S-N curve slope. Different fatigue behavior was identified at high and low stress levels for an injection-molded polysulfone matrix composite reinforced by short glass and carbon fibers [7]. The experimental results showed a significant change in the S-N curves at around $10^3$ to $10^5$ cycles.  Different fatigue responses under high- and low-stress levels has also been reported in [8-9] for carbon/PEEK laminates where the dominant failure changes from fiber to matrix damage when the cyclic load level is decreased. Investigation of the fatigue behavior of glass/polyester $[0/(\pm45)_2/0]_T$ composite laminates [10] showed a significant difference in the stiffness degradation at failure (it was found to be higher for lower stress levels), although no difference was identified in the fracture surfaces. Miyano et al. [11] reported different failure modes under low- and high-stress levels in conically-shaped FRP joint systems, proved by observation of the fracture surfaces and a lower slope of the S-N curve at high stress levels.

With this variety of behaviors exhibited by composite materials, the selection of the fatigue model that is established by fitting a mathematical equation to the experimental data becomes of paramount importance for any fatigue analysis. The fatigue model reflects the behavior of the experimental data in theoretical equations which are subsequently used during design calculations. A number of different types of fatigue models (or types of S-N curves) have been presented in the literature, with the most "famous" being the empirical exponential (Lin-Log) and power (Log-Log) relationships. Based on these, it is assumed that the logarithm of the loading cycles is linearly dependent on the cyclic stress parameter, or its logarithm. Fatigue models determined in this way do not take different stress ratios or frequencies into account, i.e. different model parameters should be determined for different loading conditions. Also, they do not take into account any of the failure mechanisms that develop during the failure process. Other more sophisticated fatigue formulations that also take the influence of stress ratio and/or frequency into account have also been reported [12-13]. A unified fatigue function that permits the representation of fatigue data under different loading conditions (different $R$-ratios) in a single two-parameter fatigue curve was proposed by Adam et al. [12]. In another work by Epaarachchi et al. [13], an empirical model that takes into account the influence of the stress ratio and loading frequency was presented and validated against experimental data for different glass fiber-reinforced composites. Although these models seem promising, their empirical nature is a disadvantage as their predictive ability is strongly affected by the selection of a number of parameters that must be estimated or even, in some cases, assumed.

Experimental evidence showed that the commonly used models are not appropriate for fitting material behavior from the LCF to the HCF region, see for example [14-15]. Sarkani et al. [14] reported a deviation between the power S-N curve and the experimental data points obtained for bonded and bolted FRP joints. Similar experimental evidence is provided by Harik et al [15] for GFRP laminates. Bilinear models, in the logarithmic [14] and semi-logarithmic [15] scales, were introduced in both works to separately fit the material fatigue behavior in different (LCF and HCF) regions. The disadvantage of these approaches is the need for fatigue data in all regions for the fitting of model parameters and therefore their inability to extrapolate any result, since they simply resemble fitting procedures. In addition to this, the resulting S-N curve equations are not continuous since different model parameters are estimated for low-cycle and high-cycle fatigue, and the selection of the data subsets corresponding to each group has to be performed based on the experience of the user, and they are therefore not practical for integration into design methodologies.

Other models, able to derive multi-slope S-N curves, are available. However, they require more data in all the examined life regions, since they are only fitting equations that simulate material behavior by adjusting a number of fitting parameters. Mu et al. [16] proposed a multi-slope model comprising three parameters for modeling the fatigue behavior of composite materials. However, the model is based purely on the fitting of a logistic function to the experimental data and therefore its results cannot be extrapolated outside the range of existing experimental data.

Methods based on damage mechanics, therefore having a physical background, also exist. A typical example is the wear-out model adopted by Sendeckyj [3]. The wear-out model was initially introduced by Halpin et al. [17] for composite materials based on metal crack growth concepts. However, owing to objections to the dominant crack assumption for composites, the model has been reviewed and modified by a number of authors considering residual strength as the damage metric. The form of the wear-out model adopted by Sendeckyj is based on the ‘Strength Life Equal Rank Assumption’ or SLERA, introduced by Hahn and Kim [18], stating that a specimen of a certain rank in the static strength probability distribution has the same rank in the fatigue life distribution. In other words, application of the wear-out model is valid as long as no competing failure modes are observed during fatigue life, or even between the fatigue and static loading.

Methods for the S-N curve modeling of composite materials, also appropriate for the derivation of S-N curves that take into account the probabilistic nature of the fatigue properties of composite materials, have been established to permit the derivation of S-N curves with a given statistical significance based on limited datasets e.g. [3, 19]. These statistical methods (presented in detail in [20]) are also based on a deterministic S-N equation for representation of the fatigue data; however a more complicated process, compared to the simple regression analysis, is followed for the estimation of model parameters, which in one of the presented models (wear-out) leads to a multi-slope S-N curve.

The disadvantages of the common S-N formulations are summarized and demonstrated in the following by modeling the fatigue behavior of a wide variety of composite material systems. An alternative S-N formulation is established based on the commonly used exponential and power S-N fatigue models in order to resolve their shortcomings and appropriately simulate the fatigue life of several composite materials and composite structural elements from the LCF to the HCF region. The modeling ability of the introduced formulation is evaluated by comparison of the derived S-N curves with the existing fatigue data and resulting curves from popular existing fatigue models.

## 4.2. Disadvantages of commonly used S-N models

The exponential and power fatigue models are commonly used for the interpretation of composite material fatigue data due to the nature of these models that are straightforward, not based on any assumptions, and easily applied, even on limited databases, in order to derive a reliable estimate of fatigue life. The estimation of the model parameters is based on linear regression analysis that can be performed by simple hand calculations.

Comparison between the S-N curves derived from the two fatigue models shows that the performance of the exponential model is superior to that of the power model in the LCF region, while the power model is more accurate in the HCF region. In the LCF region, the power model curve almost always overestimates the fatigue strength of the material. On the other hand, the exponential fatigue model underestimates the lifetime for large numbers of cycles and occasionally estimates finite life as being at zero stress level. This behavior is shown in Fig. 4.1 for the typical constant amplitude fatigue data of composite materials (in this case E-glass/polyester laminates [21]).

The aforementioned low accuracy of the power model in the LCF region can be improved by including the static strength data in derivation of the power S-N curve, considering them as fatigue data. However, the simultaneous treatment of static and fatigue data may result in an incorrect slope which affects the entire range of the lifetime, as presented in Fig. 4.2.

The wear-out model [3] is capable of deriving multi-slope reliability-based S-N curves that fit quite accurately the available static strength and fatigue data. However, it has the drawback of the quite complicated optimization process required in order to estimate the model parameters. A detailed analysis reveals several other disadvantages including the sensitivity of the model parameter estimation to the exhibited scatter of the fatigue data and the inability of the model to extrapolate the life modeling to the LCF region when no available data (static strength or LCF fatigue data) exist.

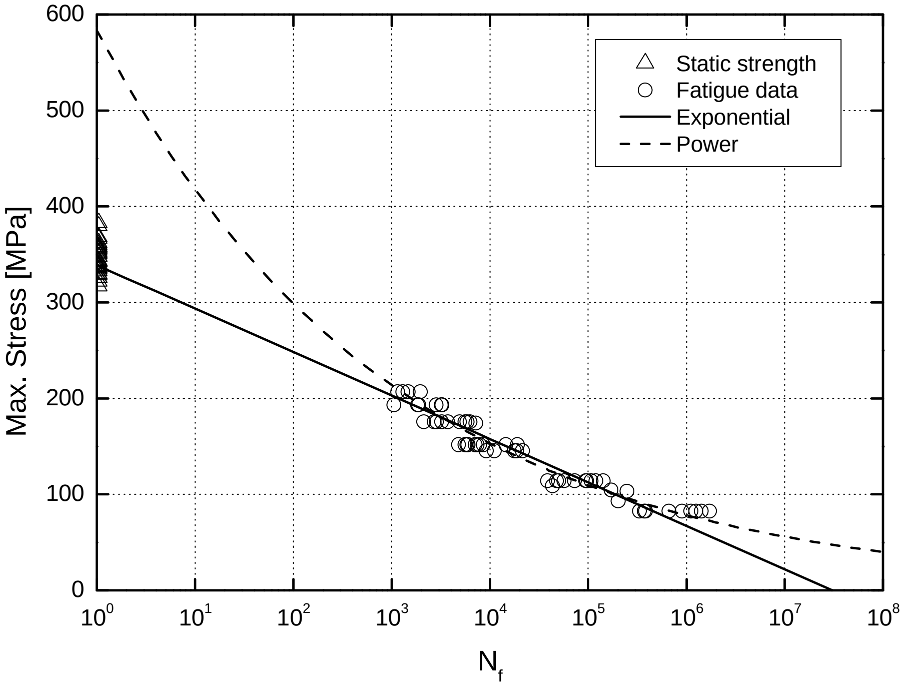

Fig. 4.1. Comparison of exponential and power curves for [0/+45/90/-45/0]$_S$ E-glass/vinylester laminate fatigue data [21] (excluding static data)

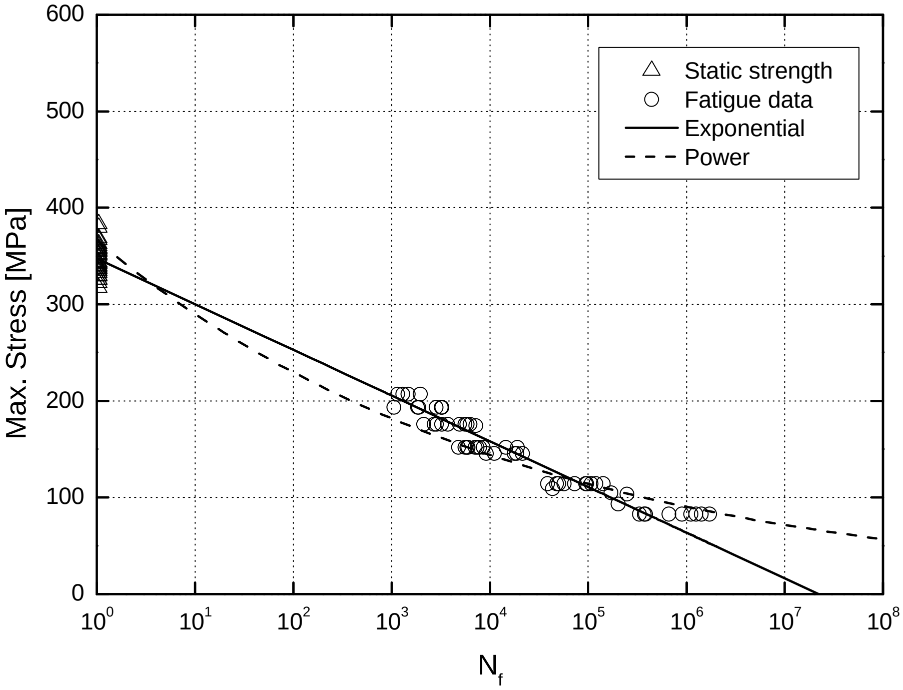

Fig. 4.2. Comparison of exponential and power curves for [0/+45/90/-45/0]$_S$ E-glass/vinylester laminate fatigue data [21] (including static data)

This drawback is demonstrated by modeling a set of constant amplitude fatigue data for $[\pm 45]_{2S}$ T300/5208 graphite/epoxy composite laminates with 57 fatigue data points distributed at five stress levels [22]. The wear-out model was applied using all the available data and also after censoring the two data points (at the 140-MPa stress level, open symbols in Figs. 4.3 and 4.4) that do not seem to follow the observed trend.

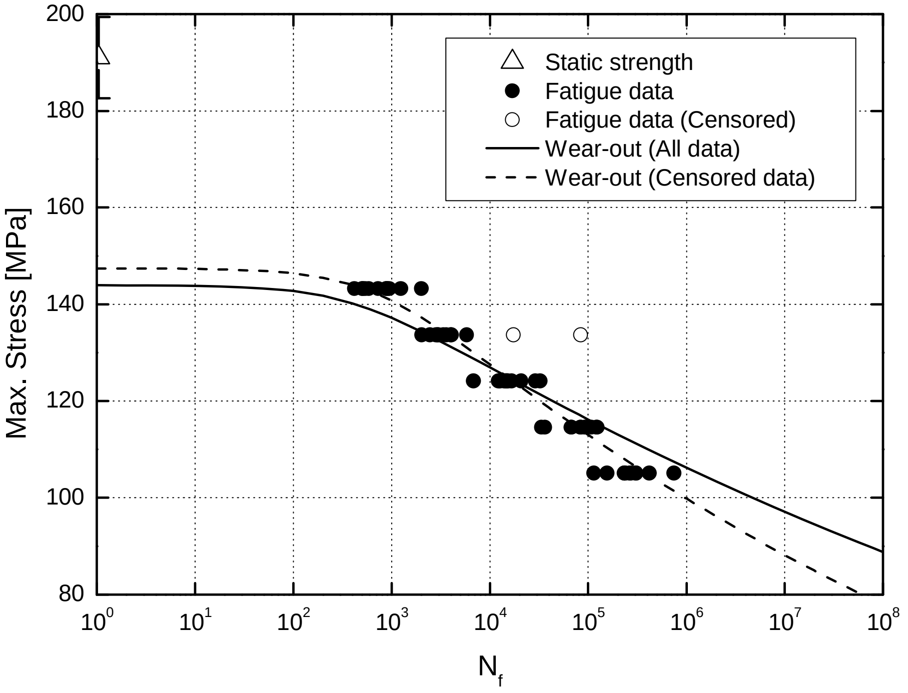

Fig. 4.3. Comparison of S-N curves derived by wear-out model for $[\pm 45]_{2S}$ graphite/epoxy laminates [22] (censored and uncensored fatigue data)

These two points were assumed as being outliers in the given data set. The derived S-N curves based on the wear-out model, presented in Fig. 4.3, are very different in both the LCF and the HCF regions. The slope of the S-N curve across the intermediate cycle fatigue region (ca. $10^3$-$10^6$) was also considerably altered by censoring only these two of the 57 available data points. On the other hand, no significant changes were made to the S-N curve derived by using the power fatigue model (see Fig. 4.4) when the entire or the censored data set was used. The average ultimate tensile strength, 191 MPa, with a standard deviation of ±8.4 MPa is shown in the figure at $N_f=1$, but was not used for estimation of the model parameters.

The new hybrid model was developed taking into account this remarkable stability of the linear regression models (exponential and power). The aim was to retain their advantages, but at the same time improve their weaknesses to appropriately model the fatigue life of composite materials in the LCF and the HCF regions.

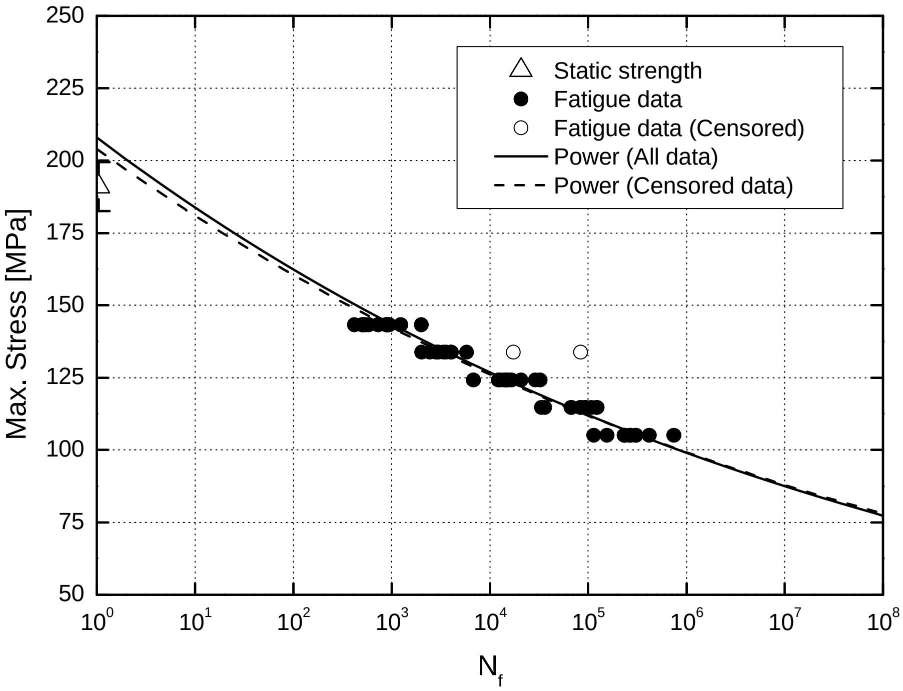

Fig. 4.4. Comparison of S-N curves derived by power model for $[\pm45]_{2S}$ graphite/epoxy laminates [22] (censored and uncensored fatigue data)

## 4.3. The hybrid S-N formulation

The hybrid S-N formulation is a semi-empirical one based on the commonly used exponential and power law models presented in Eqs. (4.1, 4.2).

$$\sigma = A + BLog\left(N_f\right) \qquad \text{(Exponential fatigue model)} \qquad (4.1)$$

$$\sigma = CN_f^D \qquad \text{(Power fatigue model)} \qquad (4.2)$$

where $\sigma$ is the stress parameter (it can be maximum cyclic stress, amplitude or stress range), $N_f$ denotes the number of cycles to failure, while $A$, $B$, $C$, and $D$ are the fatigue model parameters that can be derived by linear regression analysis, after fitting the equations to the experimental fatigue data.

The introduced formulation resembles the exponential model for LCF, while it is mutated to the power model, through a transition region, for longer lifetimes. This combination of the exponential and power models derives a formulation that adequately simulates the fatigue behavior of the examined composite material across the entire lifetime, from LCF to HCF. The hybrid S-N formulation is given in Eq. (4.3):

$$\sigma = f_1\left(N_f\right)\left[A + BLog\left(N_f\right)\right] + f_2\left(N_f\right)\left[CN_f^D\right] \qquad (4.3)$$

where, in addition to the aforementioned parameters, two weighting functions, $f_1(N_f)$ and $f_2(N_f)$, are included to control the transition from the exponential to the power curve model:

$$f_1\left(N_f\right)=\left[\frac{1}{1+\left(N_f/N_{trans}\right)^2}\right] \tag{4.4}$$

$$f_2\left(N_f\right)=\left[\frac{-1}{1+\left(N_f/N_{trans}\right)^2}+1\right] \tag{4.5}$$

A schematic plot of the fluctuations of these two empirical functions vs. the logarithm of the number of cycles is shown in Fig. 4.5. These sigmoid functions define the time and the rate of transition between the two basic fatigue models in order to avoid any singularity between the low and high cycle fatigue regions.

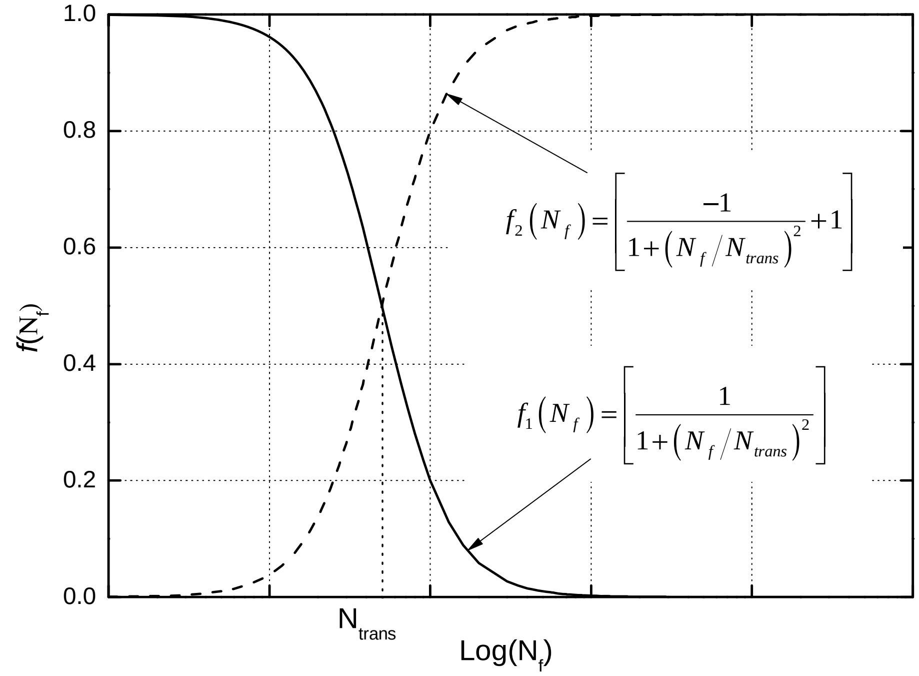

Fig. 4.5. Applied weighting functions in hybrid model

The transition number of cycles, $N_{trans}$, controls the moment of transition and is defined as the shortest lifetime among the examined sample of constant amplitude fatigue data. A sensitivity analysis was performed in order to assess the effect of the $N_{\mathrm{trans}}$ selection (between the shortest and the longest life at the highest stress level) on the model accuracy. The derived hybrid curves with different values for $N_{trans}$, showed that the accuracy of the model is not sensitive to the assumed value of $N_{trans}$. Although differences were observed, depending on the scatter of the experimental data, they were limited to the transition region. These differences did not affect the LCF and HCF regions and consequently the overall accuracy of the model. Therefore, for consistency, the shortest lifetime was used in all examined cases and it is recommended to use this value for the model derivation.

Substitution of the weighting functions, Eqs. (4.4, 4.5), into Eq. (4.3) and the rearranging of the latter results in the hybrid model formulation:

$$\sigma = CN_f^D + \left[\frac{1}{1+\left(N_f/N_{trans}\right)^2}\right]\left[A+BLog\left(N_f\right)-CN_f^D\right] \tag{4.6}$$

with parameters *A*, *B*, *C*, and *D* being the same as those resulting from fitting the exponential and power models separately and $N_{trans}$ equal to the shortest experimentally derived fatigue life, as defined above.

The form of the hybrid model is schematically presented in Fig. 4.6 and compared to the form of the exponential and power models. As described earlier, for low numbers of cycles, the hybrid model coincides with the exponential fatigue model and gradually mutates to the power fatigue model via a transition region determined by the weighting functions $f_1(N_f)$ and $f_2(N_f)$.

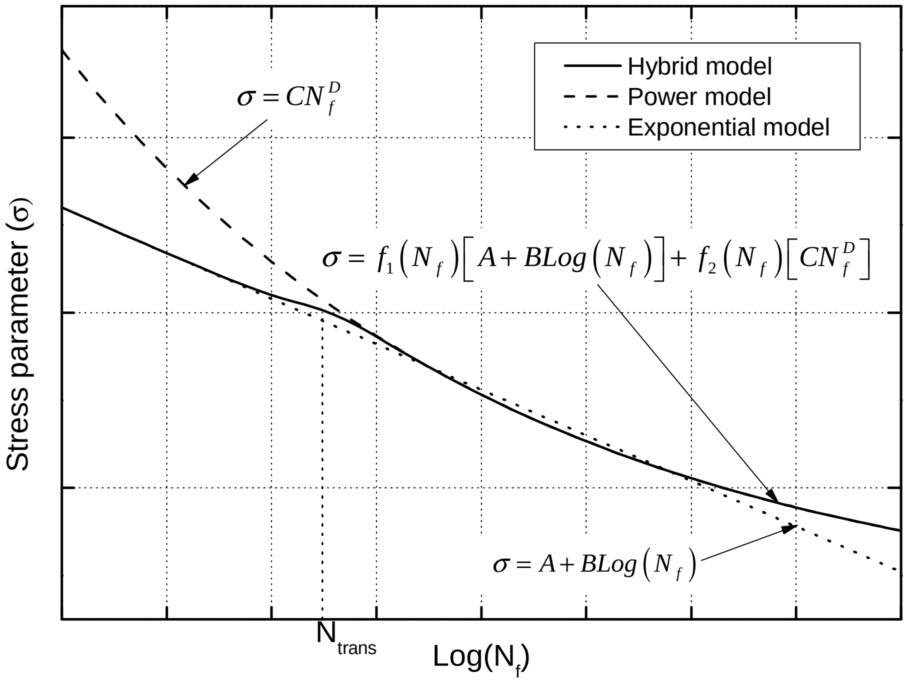

Fig. 4.6. Scheme of hybrid model in comparison with exponential and power models

## 4.4. Comparison with existing fatigue models

The modeling ability of the hybrid S-N formulation was validated by its application to a number of fatigue databases from different composite material systems and the evaluation of the fitting quality. The examined material databases include continuous and short glass and carbon fiber laminates combined with various polymer resins, and composite structures. Other commonly used fatigue models were also applied to the same material databases and their modeling accuracy was compared to the modeling accuracy of the hybrid model. The exponential and power curve models that were combined in order to derive the hybrid formulation were used for comparisons. In addition, the wear-out fatigue model [3], able to derive multislope S-N curves, was used.

The comparison of the results was based on graphical comparison of the derived S-N curves and a quantification of the fitting quality using the sum of squared errors (*SSE*). The *SSE* was calculated for each curve by defining the error as the difference between the logarithms of the estimated and experimental cyclic stress values. The *SSE* values were normalized by the maximum error value for each material as presented in Table 4.1.

Table 4.1. Calculated normalized sum of squared errors for derived S-N curves

| | **Normalized sum of squared errors (*SSE*)** | | | |
|---|---|---|---|---|
| | **Exponential** | **Power law** | **Wear-out** | **Hybrid** |
| Fig. 4.7 | 0.080 | 1.000 | 0.090 | 0.037 |
| Fig. 4.8 | 0.598 | 0.250 | 1.000 | 0.311 |
| Fig. 4.9 | 1.000 | 0.201 | 0.034 | 0.016 |
| Fig. 4.10 | 0.120 | 0.232 | 1.000 | 0.116 |
| Fig. 4.11 | 0.317 | 1.000 | 0.247 | 0.109 |
| Fig. 4.12 | 0.333 | 0.152 | 1.000 | 0.130 |
| Fig. 4.13 | 0.392 | 0.922 | 1.000 | 0.369 |
| Fig. 4.14 | 0.618 | 0.702 | 1.000 | 0.305 |
| Fig. 4.15 | 1.000 | 0.444 | 0.987 | 0.717 |
| Fig. 4.16 | 0.348 | 1.000 | 0.562 | 0.329 |
| Average | 0.481 | 0.590 | 0.692 | **0.244** |
| Standard deviation | ±0.323 | ±0.370 | ±0.418 | **±0.210** |

The *SSE* is calculated by the following equation:

$$SSE = \sum_{i=1}^{n} \left( Log\left(\sigma_{exp}\right) - Log\left(\sigma_{est}\right) \right)^2 \tag{4.7}$$

where $\sigma_{exp}$ and $\sigma_{est}$ are the experimental and estimated cyclic stresses corresponding to the same number of cycles and $n$ is the number of experimental data. The static data were not included in the processes for the derivation of the S-N curves. However, since fatigue strength data in the LCF region do not exist in most of the available databases, static data were used for calculation of the *SSE*, considered as being fatigue strength data corresponding to specimens that failed after one cycle ($N_f$ =1). The *CCfatigue* software was used for estimation of the fatigue model parameters and derivation of the S-N curves.

### 4.4.1. Glass fiber-reinforced laminates

Numerous fatigue databases for glass fiber-reinforced laminates with different matrix resins and stacking sequences exist in the literature. Typical cases for which adequate constant amplitude fatigue data exist were selected and are examined here. The first examined database comprises data from constant amplitude fatigue loading applied to woven roving E-glass/vinylester laminates with a stacking sequence of $[0/+45/90/-45/0]_S$ (according to the fabric warp direction in each layer) [21]. The comparison of the hybrid S-N curve with those derived using the other three methods is shown in Fig. 4.7 for the fatigue data obtained under tension-tension fatigue, at stress ratio $R=\sigma_{min}/\sigma_{max}$=0.1.

It is evident that the hybrid S-N curve is the most appropriate, since it adequately simulates the fatigue behavior, covering all regions, from very low cycle to high cycle fatigue. This figure also demonstrates the problems presented by the other methods. The exponential model results in a linear S-N curve on the semi-logarithmic plane, which is very conservative at the HCF regime. In this case it predicts failure under zero load after around $3 \times 10^7$ cycles, which is physically impossible. On the other hand, the power model does not exhibit this behavior in the HCF region, but, overestimates the fatigue strength at the LCF regime. For example, at $N_f$ =10 the fatigue strength estimated by the power model is 417.5 MPa and for one cycle approaches 600.0 MPa, while the tensile strength of the examined material equals 346.8±15.8 MPa. The S-N curve derived based on the wear-out model also underestimates the life in the LCF region. Nevertheless, this result is to be expected when this model is applied without the use of the static strength data. Comparison of the calculated error indices (*SSE*) given in Table 4.1 also shows that the hybrid formulation (*SSE*=0.037) performs better than the other models.

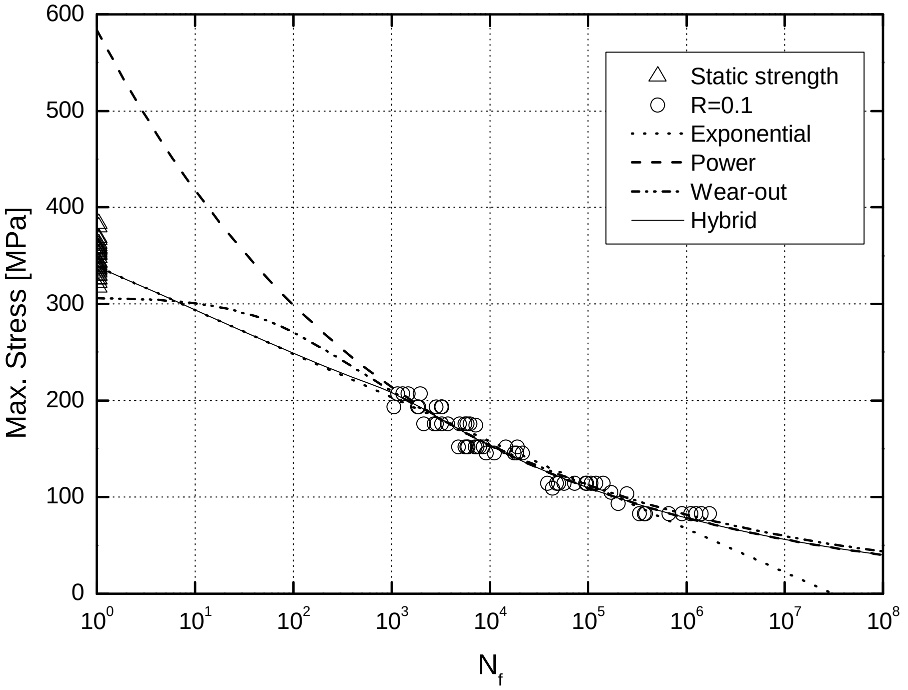

Fig. 4.7. Comparison of hybrid model with other S-N curves for $[0/+45/90/-45/0]_S$ E-glass/vinylester laminate fatigue data [21]

Three datasets were selected from the DOE/MSU composite material fatigue database [23]. The first comprises results from the constant amplitude fatigue loading of multidirectional E-glass/polyester laminates with stacking sequence of $[90/0/\pm45/0]_S$, encoded in DOE/MSU as DD16 material. The subset containing results from experiments performed under $R$=0.1 was used for the demonstration of the selected fatigue model application. The comparison of the modeling accuracy of the examined fatigue models, shown in Fig. 4.8, reveals a significant deviation between the experimental results and the wear-out models at the LCF regimes and the exponential model in the high cycle fatigue. The hybrid and power curves follow the trend of the experimental data at HCF and are in good agreement with static strength data although the power model overestimates and the hybrid underestimates the life in the LCF region.

The second material system from the DOE/MSU database is for $[0/\pm45]_4$ E-glass/polyester laminates tested at $R$=0.1 designated Material N. Although a limited number of fatigue data (16 data) is available, they cover a very large range of fatigue lifetime, between 20 and 8 million cycles. The derived S-N curves, shown in Fig. 4.9, prove the inability of the exponential fatigue model to properly simulate the real trend of the fatigue data. In the range between $10^3$ and $10^5$ cycles, the exponential model overestimates the fatigue life, while for cycles of more than $5x10^5$ it significantly underestimates the fatigue life, also indicating failure under zero load after $10^7$ cycles.

On the other hand, the power fatigue model is appropriate, but only for cycle numbers larger than $10^2$. Below this limit, in the LCF region, the power model considerably overestimates the fatigue strength as also shown in Fig. 4.9.

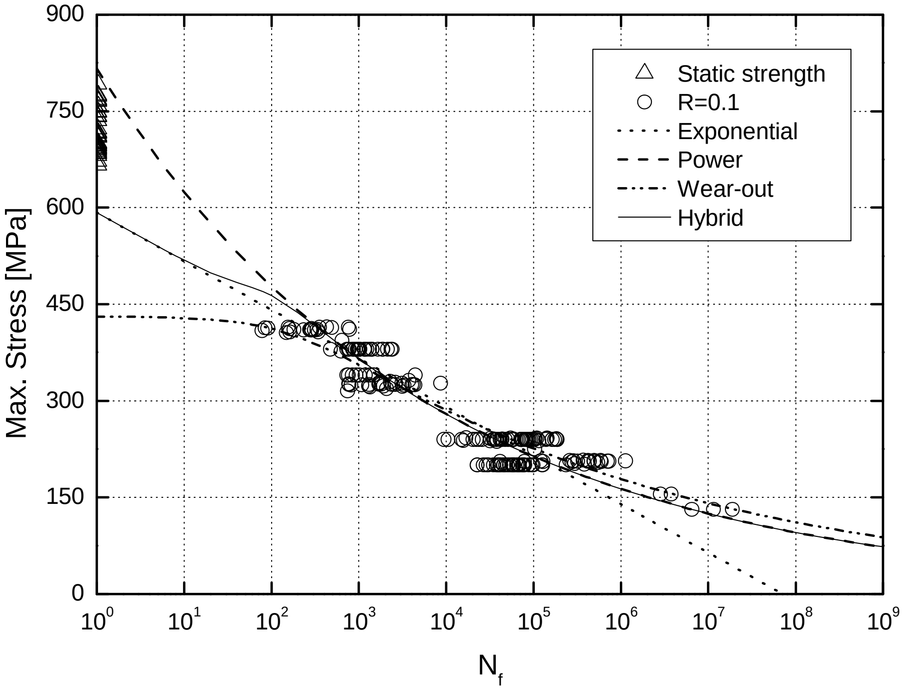

Fig. 4.8. Comparison of hybrid model with other S-N curves for $[90/0/\pm45/0]_S$ E-glass/polyester laminate fatigue data [23]

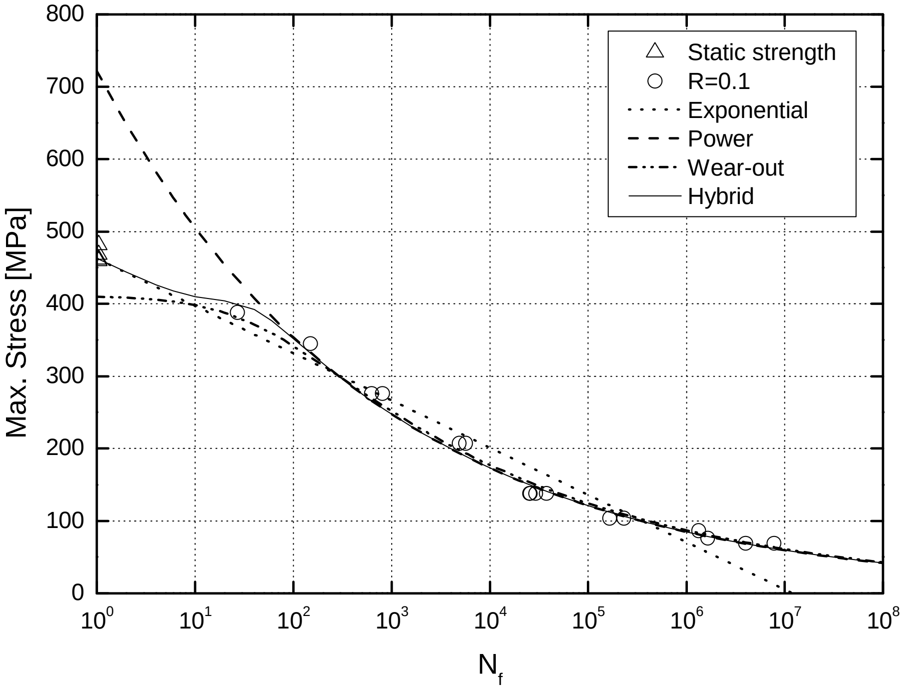

Fig. 4.9. Comparison of hybrid model with other S-N curves for $[0/\pm45]_4$ E-glass/polyester laminate fatigue data [23]

The S-N curve derived according to the wear-out method and the newly introduced hybrid model almost coincides in this case, showing differences only at the LCF regime where the hybrid model is more accurate, as it converges to the static strength data for very low cycle numbers. The calculated statistical indices shown in Table 4.1 confirm that the hybrid model provides the most accurate S-N curve.

The third dataset from the DOE/MSU database relates to a material designated 208 Fiber Strand and composed of 45 S-glass fibers and iso-polyester resin. This dataset includes data points covering a very wide cycle range ($10^3$-$10^{10}$ cycles). The same comments as for Fig. 4.9 concerning the modeling of the HCF apply to Fig. 4.10. All models, except the exponential, simulate well the exhibited fatigue behavior in this region. In the LCF region, the wear-out model underestimates and the power model overestimates the fatigue behavior. On the other hand, the hybrid and exponential models predict static strength values well within the range of the experimental scatter.

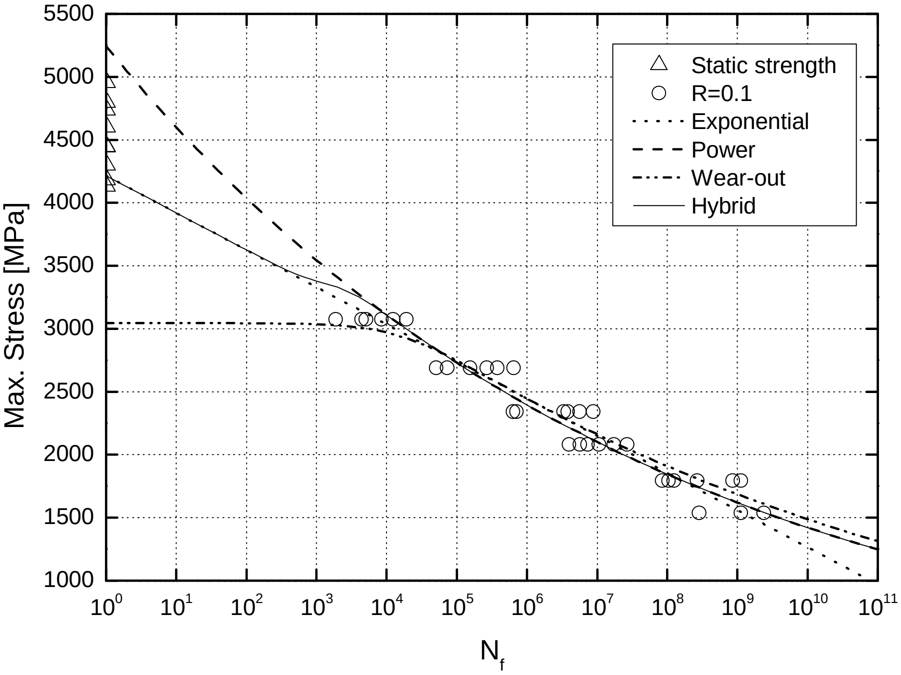

Fig. 4.10. Comparison of hybrid model with other S-N curves for fiber strand glass/iso-polyester fatigue data [23]

The fatigue models were also used for the simulation of the fatigue behavior of $[(\pm 45)_8/0_7]_S$ E-glass/polyester laminates under tension-tension ($R$=0.1) loading (see Fig. 4.11), retrieved from the FACT database [24]. The dataset includes fatigue data points corresponding to a life of only a few cycles to more than 100 million cycles. Again, the hybrid model is fairly accurate across the entire range of cycles, while the power and wear-out models fail to accurately simulate fatigue life in the LCF region and the exponential model provides only a rough averaging of the experimental data in this case. The lowest error index (*SSE*=0.109) was obtained for the hybrid formulation.

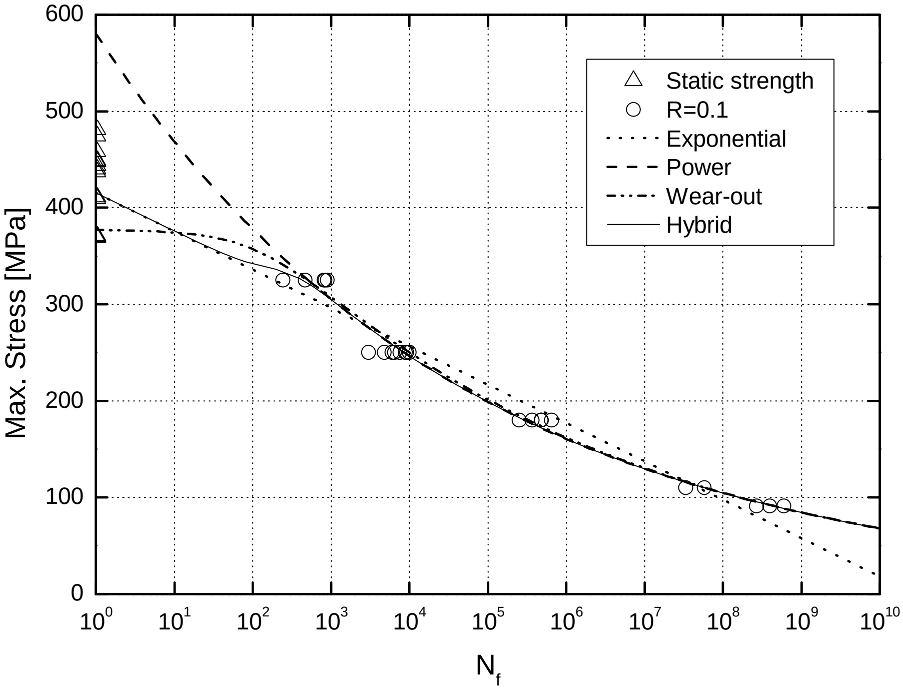

Fig. 4.11. Comparison of hybrid model with other S-N curves for $[(\pm45)_8/0_7]_S$ E-glass/polyester laminate fatigue data [24]

The S-N curves derived for a $[\pm45]_{2S}$ glass/epoxy material system loaded under $R$=0.1 [25] are compared in Fig. 4.12. The hybrid and power fatigue models perform well in this case – the former resulting in a lower *SSE* (0.130) than the latter (0.152). However, the wear-out model overestimates the fatigue strength in the LCF region in contrast to the results shown in Figs. 4.7-4.11 while the exponential model performs well only until ca. $10^5$ cycles and then becomes conservative.

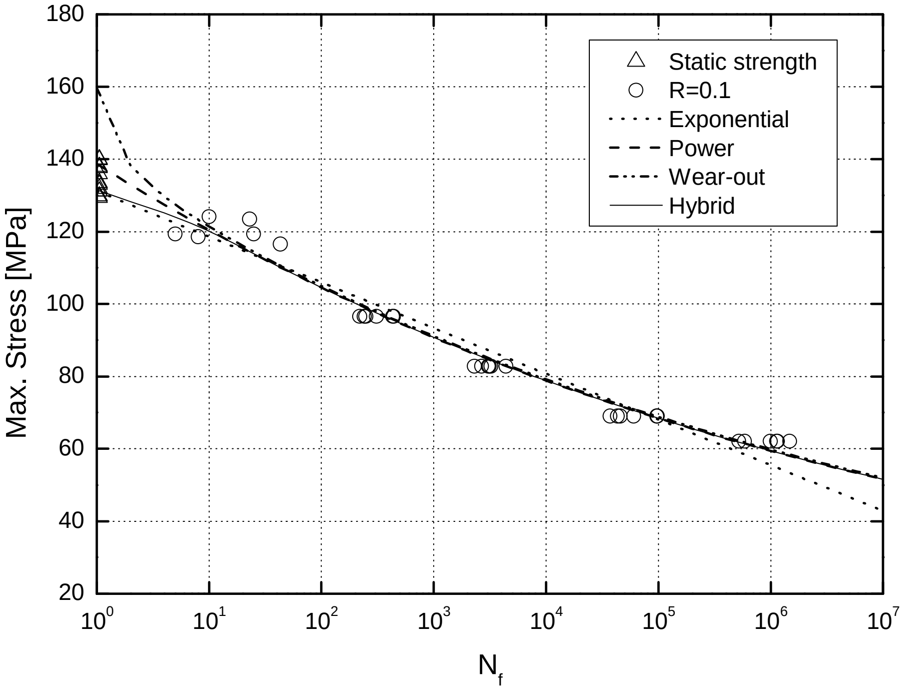

Fig. 4.12. Comparison of hybrid model with other S-N curves for $[\pm45]_{2S}$ glass/epoxy laminate fatigue data [25]

### 4.4.2. Carbon fiber-reinforced laminates

The constant amplitude fatigue data for graphite/epoxy $[90/+45/-45/0]_S$ laminates [26], was also selected for the evaluation of the hybrid model. The fatigue experiments were performed under tension-tension fatigue, $R$=0.1. As shown in Fig. 4.13 the comment regarding Fig. 4.10 also applies in this case and therefore similar *SSE* indices (see Table 4.1) were calculated for the exponential and hybrid models due to the similarity of the curves at HCF where fatigue data are available. As already pointed out, the wear-out model exhibits high sensitivity to the scatter of fatigue data and fails to accurately simulate the behavior in the LCF region when static strength and LCF data are not used for estimation of the model parameters. In the examined case the wear-out model significantly underestimates the fatigue life in the LCF region.

### 4.4.3. Hybrid glass-carbon fiber-reinforced laminates

Hybrid glass-carbon fiber-reinforced laminates are used in various engineering domains, like wind turbine rotor blades, in order to improve the modulus and strength and also decrease density and fatigue sensitivity compared to glass-reinforced polymers [27, 28]. A set of fatigue data from hybrid glass-carbon/epoxy laminates was used for the assessment of the new model [23]. The laminates were composed of 0° carbon and ±45 glass prepreg laminae with stacking sequence of $[\pm45/0_4]_S$ tested in the transverse direction under stress ratio $R$=-1 (coded P2BT in DOE database). The differences between the derived S-N curves at HCF are not significant (see Fig. 4.14) except for that derived by the exponential model, which is conservative.

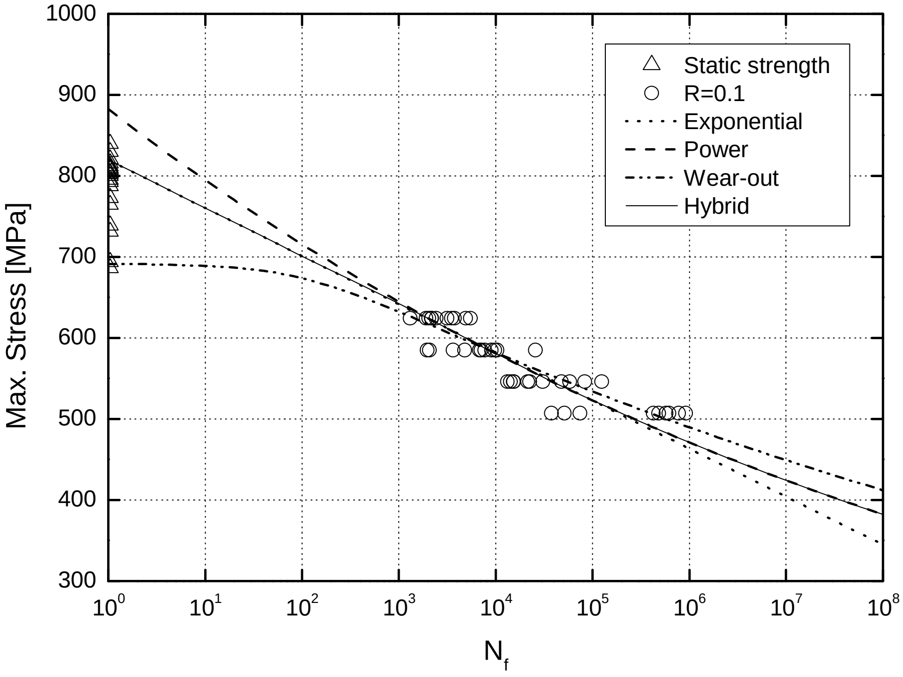

Fig. 4.13. Comparison of hybrid model with other S-N curves for $[90/+45/-45/0]_S$ graphite/epoxy laminate fatigue data [26]

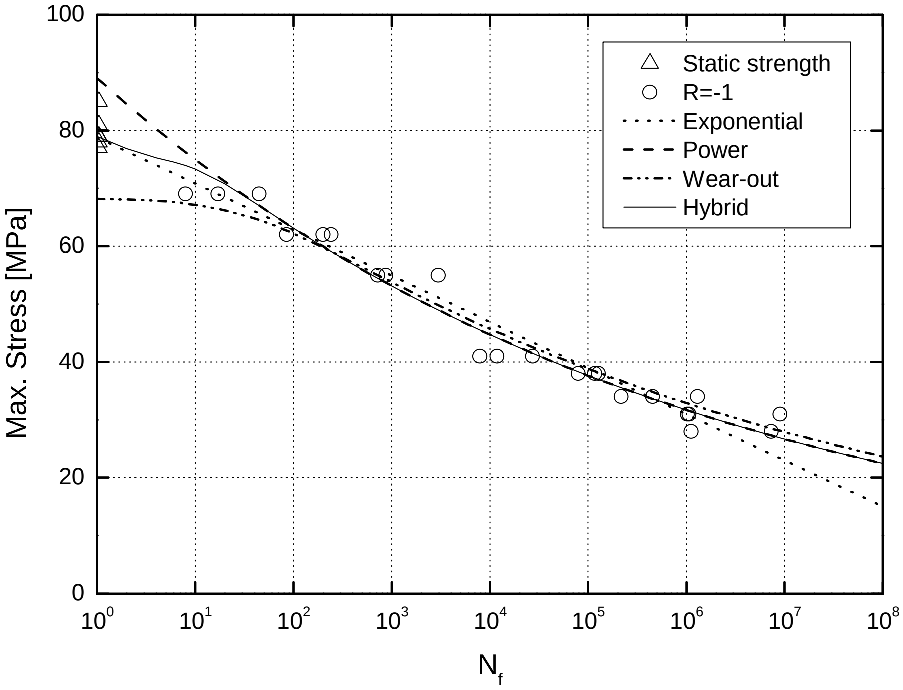

Fig. 4.14. Comparison of hybrid model with other S-N curves for hybrid $[\pm 45/0_{4C}]_S$ glass-carbon/epoxy laminate fatigue data [23]

However it can be observed that only the hybrid and exponential models converge with the static strength data, while the power and wear-out models predict higher and lower static strength respectively.

### 4.4.4. Short fiber-reinforced laminates

Short fiber-reinforced composites are used for the fabrication of numerous parts used in the automotive and aerospace industries for example [5]. The applicability of the hybrid formulation was examined by modeling the fatigue behavior of injection-molded fiber glass-reinforced PEEK thermoplastic polymer composite laminates [5]. The resulting S-N curves, shown in Fig. 4.15, prove that the hybrid, wear-out and power models appropriately simulate the behavior in the HCF region. Only the power fatigue model converges with the static strength data, with the wear-out model being more conservative than the rest. The minimum value for the *SSE*, 0.444, was estimated for the power model. The maximum *SSE* is calculated for the exponential model, which again estimates very low fatigue strength in the HCF region.

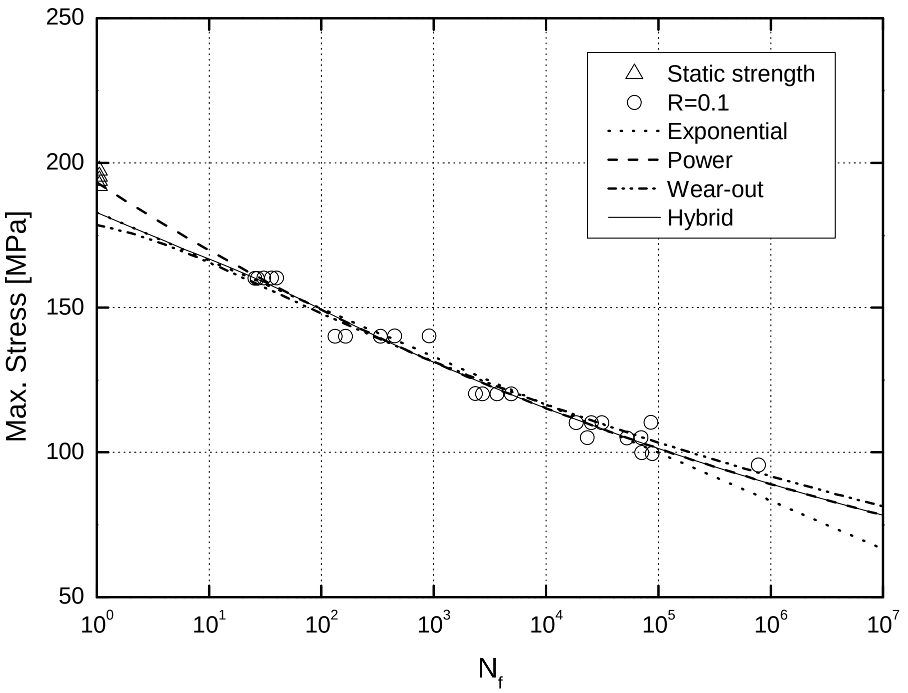

Fig. 4.15. Comparison of hybrid model with other S-N curves for short fiber 30% glass/PEEK fatigue data [5]

### 4.4.5. Pultruded fiber-reinforced adhesively-bonded joints

The introduced hybrid formulation has also been applied for the modeling of the fatigue behavior of pultruded FRP adhesively-bonded joints presented in Chapter 3. The dataset selected for the demonstration of fatigue model applicability relates to the tension-tension fatigue results (*R*=0.1). The resulting S-N curves according to the different fatigue models are shown in Fig. 4.16. All the above-mentioned disadvantages of the examined models are clearly apparent in Fig. 4.16. The power model overestimates the life in the LCF region, the exponential underestimates the life at the HCF region, while the wear-out model fails to converge with the static strength data and is unable to extrapolate any prediction to the LCF region. The hybrid fatigue model produces the most accurate S-N formulation.

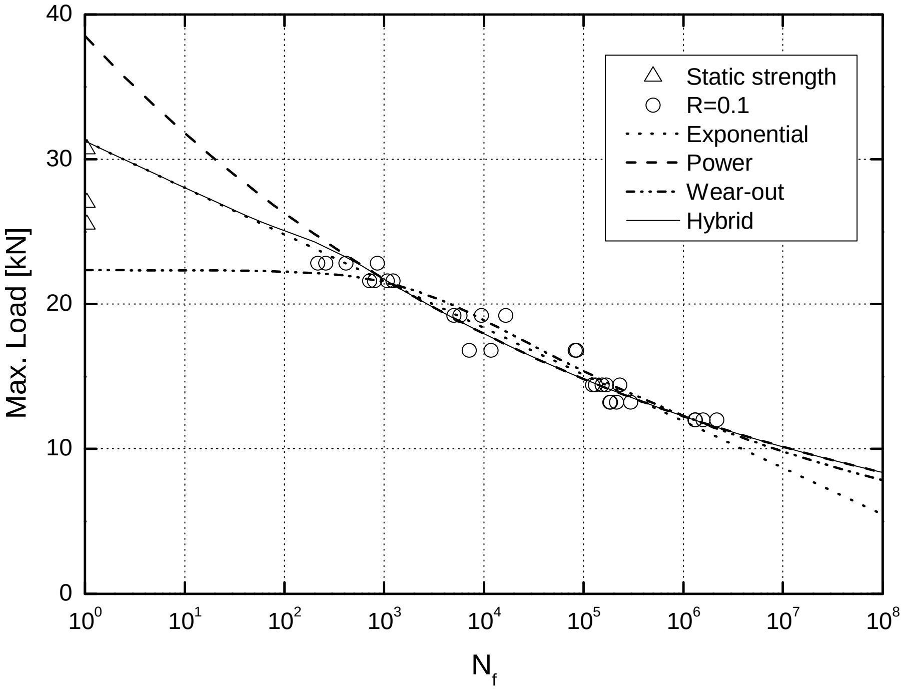

Fig. 4.16. Comparison of hybrid model with other S-N curves for double-lap joints

## 4.5. Discussion

The applicability of the proposed hybrid formulation to a wide range of typical composite materials for different applications, ranging from the wind turbine rotor blade industry to construction, or automotive and aerospace structures, has been validated in the previous section. The performance of the hybrid formulation was graphically and quantitatively (by using the *SSE* index) compared to other, commonly used, fatigue models. A thorough comparison based on several qualitative and quantitative criteria will be made in this section. The appropriateness of each examined fatigue model can be evaluated based on accuracy of modeling, ability to extrapolate and interpolate, number of model parameters, accuracy of parameter estimation, implemented assumptions, sensitivity to the available experimental data, etc.

As shown in Table 4.1, the calculated *SSE*s for the hybrid formulation are the lowest except for two cases (Figs. 4.8, 4.15) where the power model produced the most accurate S-N curve, as it accurately predicted the static strength of the examined material. On average the hybrid model is the most accurate showing substantially lower *SSE* indices, 50% lower than the next best one, the exponential model. The similar *SSE* values obtained for the hybrid formulation and linear regression models were in some cases anticipated since the hybrid formulation was developed based on these models. Accordingly, the results of the hybrid and exponential fatigue models are comparable when the difference between the linear regression models at HCF is small (see e.g. Figs. 4.10, 4.13). The difference between the hybrid and power results is negligible when the difference between the linear regression models in the LCF region is low (Figs. 4.12).

Each of the linear regression models is unable to extrapolate both to the low and high cycle fatigue regions. The exponential was proved more accurate in the LCF region and the power in the HCF region. The wear-out model was proved incapable of extrapolating any lifetime predictions in the LCF region in three out of the ten examined materials when no static strength data was used. On the other hand, the hybrid model, by combining the exponential and power models, is able to accurately simulate the fatigue behavior in both the low and high cycle fatigue regions and successfully extrapolate results in order to estimate the static strength of the examined materials.

With regard to the number of model parameters, the exponential and power models are the simplest, since they both require the estimation of two parameters by simple linear regression analysis. Five parameters are shown in Eq. (4.6) describing the hybrid model. However, the complexity of their estimation is practically the same as for the two aforementioned fatigue models. As mentioned in Section 4.3, one of the parameters, $N_{trans}$, is directly defined by the experimental data, while the remaining four correspond to the parameters of the linear and power models and can be estimated by following the same process as for the individual linear regression models. The wear-out model is the most demanding, since it requires the estimation of four independent parameters via a multi-parameter optimization process: the Weibull shape and scale parameters and the fatigue model parameters.

The accuracy of the estimated parameters of the hybrid model is the same as for the power and exponential fatigue models. For all three methods, a straightforward and simple linear regression analysis is performed, resulting in a very precise estimation of the model parameters. On the other hand, the estimation of the model parameters for the wear-out fatigue model is quite complicated. The parameter estimation is based on the multi-parameter optimization process whose convergence cannot be guaranteed when the static strength data are not considered in the analysis. As presented in Figs. 4.11 and 4.13, the wear-out S-N curves converge with the static data while in Figs. 4.7-4.10 and Figs. 4.14-4.16 the curves intersect the ordinate at lower and in Fig. 4.12 at higher values compared to static strengths.

The wear-out model is based on several assumptions, including the stress life equal rank approach, which compromises the validity of the model when competing failure modes are observed during fatigue life, or between fatigue and static loading. However, the other examined methods resemble mathematical formulations, without any physical meaning, that are fitted to the experimental data without the need to satisfy any assumptions.

Finally, as presented in Section 4.2, the wear-out model is sensitive to the selection of the fatigue data and the presence of data points that do not follow the same trend as the fatigue data. This makes the process sensitive to subjective modeling according to the experience of the user.

## 4.6. Conclusions

A new phenomenological S-N formulation based on the combination of the well-known exponential and power law S-N models for the fatigue life characterization of composite materials and structures was proposed. The modeling efficiency of the new hybrid S-N curve was evaluated by simulating the fatigue behavior of different classes of composite materials and compared to the modeling efficiency of other S-N formulations. The following conclusions can be drawn from this chapter:

- The typical behavior of the well-known exponential and power law S-N models was identified for various composite material systems. The power law model in general overestimates the fatigue life in the LCF region while it fits the experimental data in the HCF region fairly well. On the other hand, the exponential model underestimates the fatigue life at HCF whereas it successfully estimates the lifetime in the LCF region.
- The sensitivity of reliability-based models to the scatter of experimental data was recognized. The strong effect of censoring a few data points on the overall behavior of this type of S-N curve was demonstrated by the analysis of a well-established fatigue database for carbon fiber-reinforced laminates.

- Comparison of the hybrid formulation with the commonly used fatigue models showed the superiority of the new S-N formulation in terms of fitting accuracy. This formulation is no more complex than the linear regression models, since their parameters are used for the establishment of the hybrid S-N curve.
- The continuous hybrid S-N curve equation can be used in fatigue life prediction methodologies to provide a modeling tool for the entire fatigue lifetime. In contrast, two-segment power law or exponential models, or even fitted mathematical equations cannot be easily implemented in design codes since they require subjective selection of fatigue model parameters and cannot be used for extrapolation outside the range of the available fatigue data.
- The accurate modeling achieved by applying the proposed model to different classes of composite materials and structures under different loading conditions proved that the applicability of the model is independent of the material system, loading conditions, failure mode, and range of experimental data.

## 4.7. References

1. Nijssen RPL, Krause O, Philippidis TP. Benchmark of lifetime prediction methodologies, Optimat blades technical report, 2004, OB_TG1_R012 rev.001, http://www.wmc.eu/public_docs/10218_001.pdf
2. Vassilopoulos AP, Nijssen RPL. Fatigue life prediction of composite materials under realistic loading conditions (variable amplitude loading), In: Vassilopoulos AP. (ed.) Fatigue life prediction of composites and composite structures, Woodhead Publishing Limited, 2010.
3. Sendeckyj GP. Fitting models to composite materials fatigue data. In: Test methods and design allowables for fibrous composites, Chamis CC. Ed., ASTM STP 734, American Society for Testing and Materials, 1981, 245–260.
4. Salkind MJ. Fatigue of composites, In: Composite Materials: Testing and Design (second conference), Corten HT. Ed., ASTM STP 497, American Society for Testing and Materials, 1972, 143-169.
5. Mandell JF. Fatigue behavior of short fiber composite materials. In: K.L. Reifsnider, Editor, Fatigue of composite materials, Elsevier, Amsterdam, 1990.

6. Vassilopoulos AP, Georgopoulos EF, Keller T. Comparison of genetic programming with conventional methods for fatigue life modeling of FRP composite materials, Int J Fatigue, 2008;30(9):1634–1645.
7. Mandell JF, McGarry FJ, Huang DD, Li CG. Some effects of matrix and interface properties on the fatigue of short fiber-reinforced thermoplastics, Polym Composite, 1983;4(1):32-39.
8. Bakis CE, Simonds RA, Vick LW, Stinchcomb WW. Matrix toughness, long-term behavior, and damage tolerance of notched graphite fiber-reinforced composite materials. In: Composite Materials: Testing and Design. Garbo SP. Ed., ASTM STP 1059, American Society for Testing and Materials, 1990, 349–370.
9. Aymerich F, Found MS. Response of notched carbon/peek and carbon/epoxy laminates subjected to tension fatigue loading. Fatigue Fract Eng M, 2000;23(8):675-683.
10. Philippidis TP, Vassilopoulos AP. Stiffness reduction of composite laminates under combined cyclic stresses, Adv Compos Lett, 2001;10(3):113-124.
11. Miyano Y, Nakada M, Muki R. Prediction of fatigue life of a conical shaped joint system for reinforced plastics under arbitrary frequency, load ratio and temperature, Mech Time-Depend Mat, 1997;1(2):143-159.
12. Adam T, Fernando G, Dickson RF, Reiter H, Harris B. Fatigue life prediction for hybrid composites. Int J Fatigue, 1989;11(4):233–237.
13. Epaarachchi JA, Clausen PD. An empirical model for fatigue behavior prediction of glass fibre-reinforced plastic composites for various stress ratios and test frequencies, Compos Part A-Appl S, 2003;34(4):313-326.
14. Sarkani S, Michaelov G, Kihl DP, Beach JE. Stochastic fatigue damage accumulation of FRP laminates and joints, J Struct Eng, 1999;125(12):1423-1431.
15. Harik VM, Klinger JR, Bogetti TA. Low-cycle fatigue of unidirectional composites: Bi-linear S-N curves, Int J Fatigue, 2002;24(2-4):455-462.
16. Mu P, Wan X, Zhao M. A new S-N curve model of fiber reinforced plastic composite, Key Eng Mat, 2011;462-463:484-488.
17. Halpin JC, Jerina KL, Johnson TA. Characterization of composites for the purpose of reliability evaluation, In: Analysis of the Test Methods for High Modulus Fibers and Composites, Whitney JM. Ed., ASTM STP 521, American Society for Testing and Materials, 1973, 5-64.

18. Hahn HT, Kim RY. Proof testing of composite materials, J Compos Mater, 1975;9(3):297-311.
19. Whitney JM. Fatigue characterization of composite materials. In: Fatigue in fibrous composite materials, Lauraitis KN. Ed., ASTM STP 723, American Society for Testing and Materials, 1981, 133–151.
20. Vassilopoulos AP, Keller T. Fatigue of fiber reinforced composites, Engineering materials and processes series, Springer, 2011, http://dx.doi.org/10.1007/978-1-84996-181-3.
21. Post NL. Reliability based design methodology incorporating residual strength prediction of structural fiber reinforced polymer composites under stochastic variable amplitude fatigue loading, Virginia Polytechnic Institute and State University, PhD thesis, 2008.
22. Lee LJ, Yang JN, Sheu DY. Prediction of fatigue life for matrix-dominated composite laminates. Compos Sci Technol, 1993;46(1):21–28.
23. Mandell JF, Samborsky DD. DOE/MSU composite material fatigue database. Sandia National Laboratories, SAND97-3002. v. 19; 31st March 2010 < http://windpower.sandia.gov/ >.
24. Nijssen RPL. OptiDAT – fatigue of wind turbine materials database; 2006. <http://www.kc-wmc.nl/optimat_blades/index.htm>.
25. Sendeckyj GP. Life prediction for resin matrix composite materials. In: K.L. Reifsnider, (Ed), Fatigue of composite materials, Elsevier, Amsterdam, 1990.
26. Yang JN, Yang SH, Jones DL. A stiffness-based statistical model for predicting the fatigue life of graphite/epoxy laminates. J Compos Tech Res, 1989;11(4)129-134.
27. Mandell JF, Samborsky DD, Wang L, Wahl NK. New fatigue data for wind turbine blade materials, J Sol Energ-T ASME, 2003;125(4):506-514.
28. Gamstedt EK, Redon O, Brøndsted P. Fatigue dissipation and failure in unidirectional and angle-ply glass fibre/carbon fibre hybrid laminates, Key Eng Mat, 2002;221-222: 35-48.

# 5 Mean load effect

## Abstract

*The effect of mean load on the fatigue behavior of adhesively-bonded pultruded GFRP double-lap joints under constant amplitude loading was experimentally investigated. The joints were examined under nine different stress ratios (R) representing pure tension, compression, and combined tension-compression fatigue loading. A transition of the failure mode, from tensile to compressive, was observed as the mean load decreased from positive to negative values. The slope of the S-N curves derived for R-ratios with positive or negative mean load consistently decreased with increasing mean load. The highest load amplitude corresponded to the R-ratio where the transition of the fatigue failure mode occurred (R=-0.5). The characteristics of the constant life diagram developed for the examined bonded joints are thoroughly discussed. A phenomenological formulation was proposed and its accuracy evaluated by comparisons with the derived experimental data. The comparison of the new formulation with models commonly used for composite materials proved its higher accuracy that is achieved with less implementation effort.*

## 5.1. Introduction

The effect of several critical parameters on the fatigue life of a material under a certain loading condition can be examined when experimental work is performed under this condition. Although the result is useful for the analysis of the examined loading scenario, the experimental effort should be repeated for any other applied loading spectrum. This practice is costly and cannot be followed in practice where numerous different loading patterns are applied on a structural element. Therefore experimental databases are derived for basic loading conditions (e.g. constant amplitude fatigue loading) and appropriate modeling is performed for extrapolation of the experimental evidence to predict the life under other, more complicated, loading conditions.

The stress ratio, the ratio of the minimum to maximum applied cyclic stress ($R=\sigma_{\min}/\sigma_{\max}$), is used to specify the loading type; $0<R<1$ expresses tension-tension (T-T) fatigue, $1<R<+\infty$ represents compression-compression (C-C) fatigue, while $-\infty<R<0$ denotes mixed tension-compression (T-C) fatigue loading that can be tension- or compression-dominated. It is well documented that for a given maximum stress in a tension-tension case, the fatigue life of the composite increases with increasing magnitude of $R$. In compression-compression loading, increasing the magnitude of $R$ reduces the fatigue life of the examined composite [2-6].

The influence of the $R$-ratio on the fatigue behavior of composite materials has been the subject of numerous investigations in the past, e.g. [2-8]. This effect is assessed by using constant life diagrams (CLD). Constant life diagrams reflect the combined effect of mean stress and material strength differential effect on fatigue life, and can be used for estimation of the fatigue life of the material under loading patterns for which no experimental data exist. The main parameters that define a CLD are the cyclic mean stress, stress amplitude and number of fatigue cycles. The CLDs for composite materials are usually shifted towards the tension- or compression-dominated domain, reflecting the degree of strength differential effect of the examined material [8-14]. For laminates exhibiting significantly higher tensile strength than compressive strength, e.g. unidirectional carbon/epoxy laminates [8], the CLD is shifted towards the right, tension-dominated domain. For materials exhibiting higher compressive than tensile fatigue properties, e.g. short- fiber composites [14], the diagram is shifted towards the compression-dominated domain. It has also been reported that this tendency towards one side of the diagram can alter with the number of cycles. Fernando et al. [11] revealed a similar form of constant life curves concerning four different material systems for a fatigue life of $10^5$ cycles. However, a change in the form of the iso-life curves was reported in [8, 10]. The shape of the curves gradually alters from linear to non-linear form with increasing fatigue life.

The classic CLD formulations require that the constant life lines converge to the ultimate tensile stress (UTS) and the ultimate compressive stress (UCS), regardless of the number of loading cycles [15-17]. However, this is an arbitrary simplification originating from the lack of information about the fatigue behavior of the material when no amplitude is applied. In fact, this type of loading cannot be considered as fatigue loading, but rather as creep of the material (constant static load over a short or long period), see e.g. [5, 7]. Although modifications to take the time-dependent material strength into account have been introduced, their integration into CLD formulations requires the adoption of additional assumptions, see e.g. [5, 18], and yet none of these modifications can provide a general model to characterize the fatigue-creep interaction in composite materials.

Although a considerable amount of information exists regarding the *R*-ratio effect on the fatigue life of composite laminates, there is little literature regarding similar investigations for adhesively-bonded structural joints. Experimental studies on joints are based on tensile fatigue loads because they focus on joints exhibiting a cohesive or an adhesive failure. Nevertheless, as shown from several studies, e.g. [19-20], different failure modes can be observed depending on the adherend materials and the joint geometry. Moreover, significant *R*-ratio effects were reported, e.g. [21], especially for pultruded FRP joints in which cracks in the adherend lead the failure process and also different failure modes are observed under tension and compression fatigue (see Section 3.2.2.1) .

The effect of a combination of tensile and compressive loads on the fatigue behavior of adhesively-bonded pultruded GFRP joints has been studied in the present chapter by generating load-life data for a range of *R*-ratios covering all CLD domains. A phenomenological CLD formulation is developed for modeling the *R*-ratio effect taking into account the creep damage with little data required. Although the new formulation is based on a small number of input data it is very accurate, as proved by comparisons with experimental data.

## 5.2. Experimental results

### 5.2.1. Failure modes

Under T-T ($R$=0.5 and $R$=0.9) and T-C ($R$=–0.5) fatigue, the failure mode was similar to that observed under T-T ($R$=0.1). A fiber-tear failure was observed with a dominant crack that initiated from the joint corner of one of the bond lines, between the adhesive and the inner GFRP laminate, and then shifted deeper, between the first and the second mat layers of the inner laminate, and propagated along this path up to failure. Under C-C loading ($R$=2 and $R$=1.1), as under $R$=10, failure occurred within the roving layer of the inner laminate. Under C-T loading ($R$=–2), the failure mode was similar to $R$=–1, as reported in Section 3.2.2.1. Under this loading condition, in addition to the dominant crack along one of the bond lines related to the tensile component of loading, a smaller crack was observed in the middle of the inner laminate at a similar location as for compression fatigue. However, during the fatigue life the dominant crack was propagating and leading the failure process, while the crack created by the compressive component of the applied cyclic load reached a maximum length of 5 mm prior to the failure of the joint. These observations showed that the failure transition occurred beyond the load ratio *R*=–1 in the C-T region, which is consistent with the higher fatigue strength of joints under compressive loading (see Section 3.2.2.2).

### 5.2.2. Fatigue life

The experimental program was designed and maximum load levels were applied in order to obtain representative experimental data in the range between 1 and $10^8$ cycles. The experimental results are presented in Table 5.1. The fatigue life of the examined joints under the applied *R*-ratios is plotted against the cyclic load amplitude in Figs. 5.1 and 5.2 for the experiments under positive and negative mean loads respectively. The data corresponding to loading under *R*=0.1, –1, and 10 were included in these figures for comparative reasons.

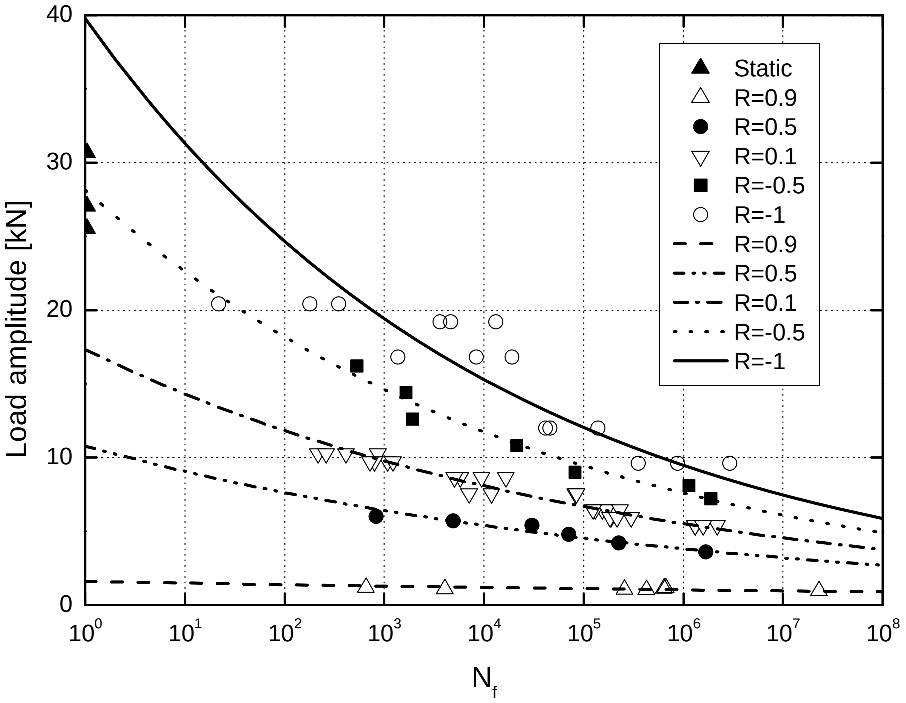

Fig. 5.1. S-N data for tension and tension-dominant fatigue loading

Table 5.1. Constant amplitude fatigue data

| Load ratio ($R$) | Specimen ID | Nominal load level [% of UTL or UCL] | Applied maximum cyclic load [kN] (absolute value) | Cycles to failure, $N_f$ |
|---|---|---|---|---|
| 0.9 | R098901 | 89 | 24.0 | 658 |
| | R098601 | 86 | 23.3 | 666356 |
| | R098401 | 84 | 22.8 | 637004 |
| | R098201 | 82 | 22.0 | 4063 |
| | R098001 | 80 | 21.6 | 257184 |
| | R097801 | 78 | 21.0 | 425510 |
| | R097201 | 72 | 19.3 | 22867961 |
| 0.5 | R059001 | 90 | 24.0 | 832 |
| | R058501 | 85 | 22.8 | 4929 |
| | R058001 | 80 | 21.6 | 30229 |
| | R057001 | 70 | 19.2 | 71410 |
| | R056001 | 60 | 16.8 | 225253 |
| | R055001 | 50 | 14.4 | 1679838 |
| -0.5 | R-058001 | 80 | 21.6 | 533 |
| | R-057001 | 70 | 19.2 | 1660 |
| | R-056001 | 60 | 16.8 | 1924 |
| | R-055001 | 50 | 14.4 | 21472 |
| | R-054001 | 40 | 12.0 | 82510 |
| | R-053801 | 38 | 10.8 | 1141900 |
| | R-053501 | 35 | 9.6 | 1897288 |
| -2 | R-29001 | 90 | 26.1 | 1554 |
| | R-28001 | 80 | 23.2 | 5861 |
| | R-27001 | 70 | 20.3 | 8153 |
| | R-27002 | 70 | 20.3 | 25390 |
| | R-26001 | 60 | 17.4 | 155025 |
| | R-25001 | 50 | 14.5 | 1118434 |
| 2 | R29001 | 90 | 26.1 | 3 |
| | R28501 | 85 | 24.6 | 44743 |
| | R28001 | 80 | 23.2 | 5607 |
| | R27501 | 75 | 21.8 | 22720 |
| | R27001 | 70 | 20.3 | 304338 |
| | R26501 | 65 | 18.9 | 1273000 |
| 1.1 | R1.19301 | 93 | 27.0 | 1 |
| | R1.19302 | 93 | 27.0 | 1453 |
| | R1.19101 | 91 | 26.4 | 229071 |
| | R1.19102 | 91 | 26.4 | 313705 |
| | R1.19001 | 90 | 26.0 | 82056 |
| | R1.18301 | 83 | 24.0 | 341995 |
| | R1.18001 | 80 | 23.0 | 41524855 |

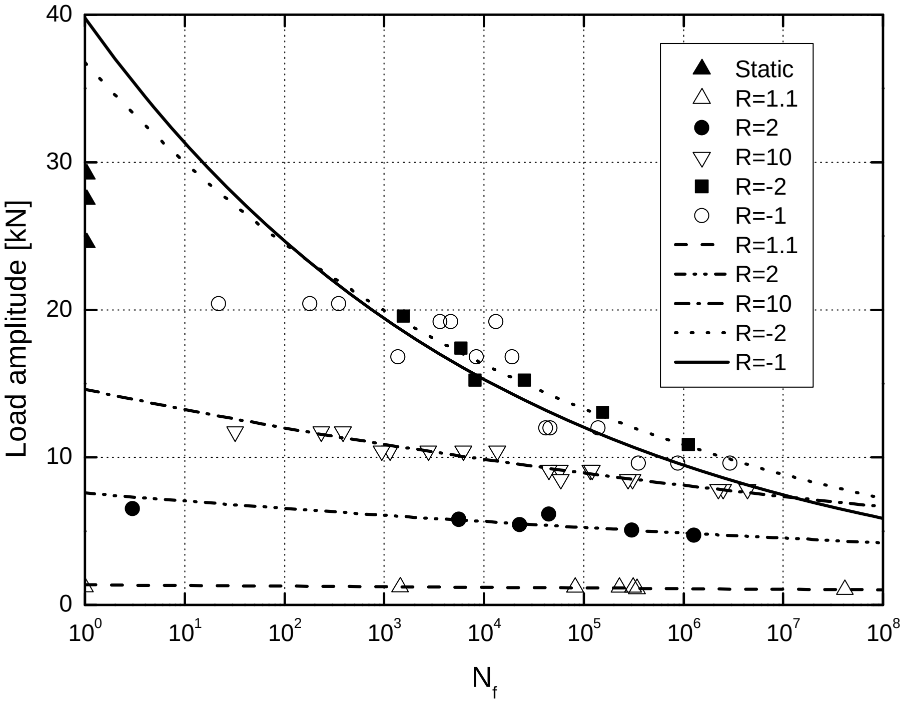

Fig. 5.2. S-N data for compression and compression-dominant fatigue loading

The classic power law relationship was employed to simulate the fatigue behavior:

$$\sigma_a = \sigma_o N^{-k} \tag{5.1}$$

where $\sigma_a$ corresponds to the load amplitude, *N*, to the number of cycles and $\sigma_o$, *k* are model parameters that can be obtained by fitting Eq. (5.1) to the experimental data. The values of parameters $\sigma_o$ and *k* as estimated by a linear regression analysis are shown in Table 5.2. Although the designation "S-N" curves was preserved for convenience, the fatigue data refer to applied load and not to stress levels since the use of a stress value is not meaningful for joints.

Table 5.2. Material constants of Eq. (5.1) for all load ratios

| | ***R*-ratio** | | | | | | | | |
|---|---|---|---|---|---|---|---|---|---|
| | **0.9** | **0.5** | **0.1** | **-0.5** | **-1** | **-2** | **10** | **2** | **1.1** |
| $\sigma_o$ | 1.60 | 10.78 | 17.32 | 28.15 | 39.77 | 36.74 | 14.60 | 7.59 | 1.37 |
| *k* | 0.0314 | 0.0752 | 0.0828 | 0.0949 | 0.1038 | 0.0883 | 0.0426 | 0.0320 | 0.0154 |

The S-N curve for $R$=–1 exhibits the highest slope ($k$=0.1038), demonstrating the sensitivity of the examined joints to reversed loading. As shown in Figs. 5.1-5.2, the fatigue strength of joints decreases under higher $R$-ratios at tensile and tensile-dominated loading. In contrast it decreases under lower $R$-ratios at compression and compression-dominated loading. Under high mean loads (e.g. $R$=0.9 and $R$=1.1), close to the static strength of the joints, the fatigue life is very sensitive to the change of load amplitude and S-N curves become flatter with lower slopes ($k_{(R=0.9)}$=0.0314 and $k_{(R=1.1)}$=0.0154).

However, one exception to this rule is observed when the mean load is decreased from zero, $R$=–1, to a negative level, i.e. $R$=–2. The S-N data for $R$=–2 in Fig. 5.2 is located slightly higher than the fatigue data for $R$=–1. As already explained, although the compressive part of the cyclic load was dominant at this $R$-ratio, the observed failure mode, similar to the reverse loading ($R$=–1), was tensile failure. This behavior occurs due to the higher fatigue strength of the examined joints under compression fatigue. Compared to $R$=–1, a higher load amplitude is required to reach the same maximum load level under $R$=–2. Therefore the highest load amplitude occurs at a load ratio other than $R$=–1 i.e. under a C-T loading condition where a transition in failure occurs from tensile to compressive mode.

### 5.2.3. Constant life diagram

The effect of load ratio on the fatigue life of the examined joints can also be visualized by using constant life diagrams. For the derivation of a CLD, the fatigue data are normally (although not necessarily, see [16]) plotted on the "mean-amplitude" ($\sigma_m$-$\sigma_a$) plane, as radial lines emanating from the origin of the coordinate system. Each radial line represents a single S-N curve under a given $R$-ratio and can be reproduced using the following equation:

$$\sigma_a = \left(\frac{1-R}{1+R}\right)\sigma_m \qquad (5.2)$$

Constant life diagrams are formed by joining in a linear or non-linear way the points (creating iso-life curves) corresponding to the same number of cycles on consecutive radial lines.

The constant life diagram for the examined joint configuration is shown in Fig. 5.3. It is obvious that the CLD is not symmetric with respect to the zero mean cyclic load axis and shifted somewhat towards the compression-dominated domain with the apex corresponding to the S-N curve under $R$=–2.

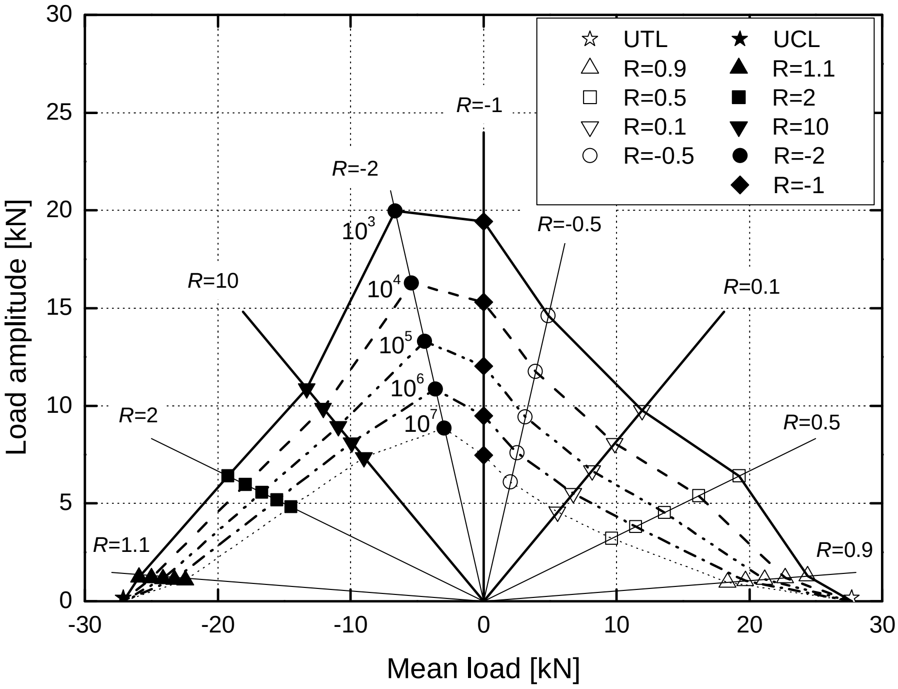

Fig. 5.3. Variation of alternating load vs. mean load at different fatigue lives

This behavior can be attributed to the difference in fatigue strength under tension and compression loading as discussed above (see comments in section 5.2.2 referring to Fig. 5.2). An inflection in the curvature of the iso-life curves is observed. The iso-life curves change from concave to convex when the loading condition shifts from T-T or C-C to combined tension-compression fatigue loading. Moreover it is observed that the ultimate tensile and compressive load (UTL=27.7±2.17 kN and UCL=–27.1±1.92 kN) values are not appropriate for description of the fatigue behavior under zero load amplitude since, as shown in Fig. 5.3, a fatigue-creep interaction occurs under *R*-ratios close to 1 due to the presence of very low amplitude and high mean values that characterize the cyclic loading in this region.

## 5.3. Modeling

The asymmetry of the CLD and the observed fatigue-creep interactions close to the *R*=1 domains prevent the possibility of accurate modeling using simple linear diagram formulations such as the classic Goodman diagram. Based on the characteristics of the constant life diagram for the examined bonded joints, described in the previous section, a semi-empirical CLD formulation is proposed in the form of Eq. (5.3):

$$\sigma_a - \sigma_{(R=-1)} = \sigma_m\left(\alpha\sigma_m^3 + \beta\sigma_m^2 + \gamma\sigma_m + \delta\right) \tag{5.3}$$

where $\sigma_{(R=-1)}$ is the fatigue strength of joints at *R*=–1 and $\alpha$, $\beta$, $\gamma$, and $\delta$ are model parameters. This formulation incorporates both the mean and the amplitude components of the cyclic loading and is a direct function of the number of cycles as shown in Eq. (5.4) that results after substituting Eq. (5.1) into Eq. (5.3):

$$\sigma_o N^{-k} - \sigma_{(R=-1)} = \sigma_m \left(\alpha\sigma_m^3 + \beta\sigma_m^2 + \gamma\sigma_m + \delta\right) \tag{5.4}$$

As deduced from Eq. (5.4), at $\sigma_m = 0$ the fatigue strength is equal to that under reversed loading (*R*=–1):

$$\sigma_o N^{-k} = \sigma_{(R=-1)} \tag{5.5}$$

Eq. (5.3) is actually a fourth order polynomial equation describing constant life lines. Nevertheless, four boundary conditions corresponding to the physical meaning of the constant life diagram must be satisfied in order to determine the model parameters as described in the following.

For the common CLD the ultimate compressive and tensile strengths of the material, which are independent of the number of cycles to failure, usually constitute the upper and lower limits of the mean load ($\sigma_m$) and iso-life curves. This assumption leads to an inadequate modeling of fatigue behavior at high mean load levels as discussed in [15]. To improve the accuracy of the modeling at *R*-ratios close to 1 at zero load amplitude ($\sigma_a = 0$), the two boundaries of the CLD are defined by the creep rupture strength under compression ($\sigma_{cc}$) and tension ($\sigma_{ct}$) instead of the ultimate compressive and tensile strengths ($\sigma_a = 0$ at $\sigma_m = \sigma_{ct}$ and $\sigma_m = \sigma_{cc}$) as shown in Fig. 5.4. Applying these boundary conditions to Eq. (5.3) results in Eqs. (5.6) and (5.7):

$$\left[\sigma_m \left(\alpha\sigma_m^3 + \beta\sigma_m^2 + \gamma\sigma_m + \delta\right) + \sigma_{(R=-1)}\right]_{\sigma_m=\sigma_{ct}} = 0 \tag{5.6}$$

$$\left[\sigma_m \left(\alpha\sigma_m^3 + \beta\sigma_m^2 + \gamma\sigma_m + \delta\right) + \sigma_{(R=-1)}\right]_{\sigma_m=\sigma_{cc}} = 0 \tag{5.7}$$

The fourth order polynomial given in Eq. (5.3) provides the flexibility to simulate the inflection of the iso-life curves described in Section 5.2.3. The parameters of Eq. (5.3) can be determined in such a way that it includes two minima, one maximum and consequently two inflection points bounded by the upper and lower limits of the mean load. To ensure this, since the maximum value of the iso-life curve (polynomial) is between $\sigma_{cc}$ and $\sigma_{ct}$, the minima of the polynomial have to satisfy $\sigma_{cc}$ and $\sigma_{ct}$. Therefore, the first derivative of Eq.

(5.3) with respect to $\sigma_m$ at $\sigma_{ct}$ and $\sigma_{cc}$ must be zero, which leads to two more boundary conditions given in Eqs. (5.8) and (5.9).

$$\left[4\alpha\sigma_m^3+3\beta\sigma_m^2+2\gamma\sigma_m+\delta\right]_{\sigma_m=\sigma_{ct}}=0 \tag{5.8}$$

$$\left[4\alpha\sigma_m^3+3\beta\sigma_m^2+2\gamma\sigma_m+\delta\right]_{\sigma_m=\sigma_{cc}}=0 \tag{5.9}$$

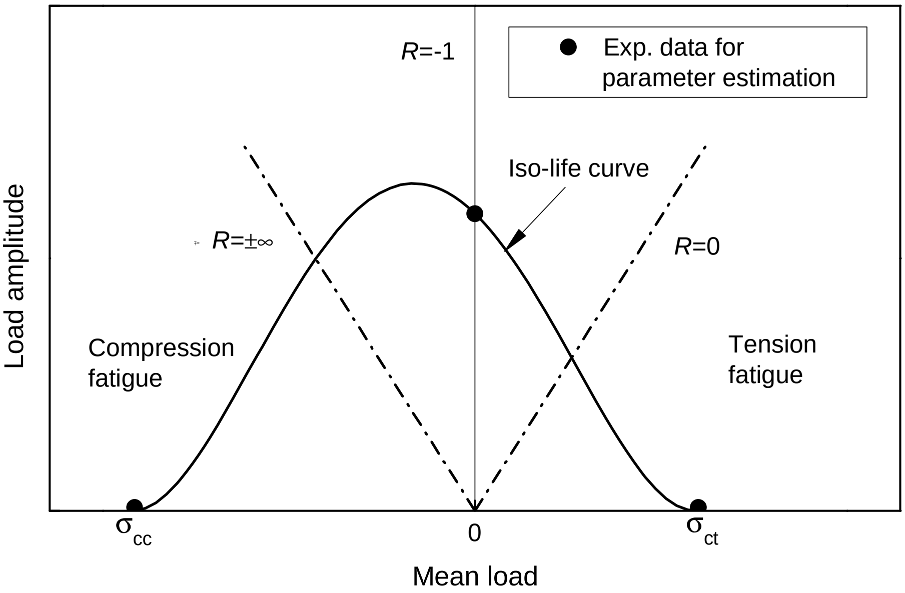

Fig. 5.4. Polynomial iso-life curve and imposed boundary conditions

These boundary conditions allow the derivation of iso-life curves that simulate real material behavior as demonstrated by experimental data by shifting them towards the stronger domain. Furthermore, using the creep rupture strength data instead of static strength data improves existing CLD formulations at high mean load conditions. The four unknown parameters of Eq. (5.3) can be estimated by solving the set of Eqs. (5.6-5.9) as a function of the experimental fatigue data under *R*=–1 and the creep rupture strengths as shown in Eqs. (5.10-5.13):

$$\alpha=\frac{\sigma_{(R=-1)}}{\left(\sigma_{ct}\sigma_{cc}\right)^2} \tag{5.10}$$

$$\beta=\frac{-2\left(\sigma_{ct}+\sigma_{cc}\right)\sigma_{(R=-1)}}{\left(\sigma_{ct}\sigma_{cc}\right)^2} \tag{5.11}$$

$$\gamma=\frac{\left[\left(\sigma_{ct}+\sigma_{cc}\right)^2+2\sigma_{ct}\sigma_{cc}\right]\sigma_{(R=-1)}}{\left(\sigma_{ct}\sigma_{cc}\right)^2} \tag{5.12}$$

$$\delta = \frac{-2\left(\sigma_{ct} + \sigma_{cc}\right)\sigma_{(R=-1)}}{\sigma_{ct}\sigma_{cc}} \tag{5.13}$$

Obviously the resulting parameters are functions of fatigue life and the CLD formulation given by Eq. (5.3) is valid only in the physically acceptable mean load range between the compressive and tensile creep strengths of the joints $\left(\sigma_{cc} \leq \sigma_m \leq \sigma_{ct}\right)$. The accuracy of the proposed model is evaluated by comparisons with the available experimental data and the results of commonly used CLD formulations for composite materials in the following section.

## 5.4. Results and discussion

In addition to the proposed formulation, six existing CLD models extensively used for composite materials were selected and applied to the examined bonded joint fatigue data for comparison. The models are: the linear (LR) [15], the piecewise linear (PWL) [15], the piecewise non-linear (PNL) [16], the Harris (HR) [17, 22-23], the Kawai (KW) [8], and the Boerstra (BR) [24]. The linear CLD can be easily derived using only one set of experimental data usually under reversed loading and assumes a similar failure mode under tension and compression loading. A modified form of the linear Goodman diagram, PWL CLD, is used extensively in the wind turbine rotor blade industry and, although it requires quite large experimental databases, it provides high prediction accuracy. An alternative, the PNL model, recently introduced by the authors [16], can result in more accurate constant life behavior simulations based on fewer experimental data compared to the PWL model.

The Harris CLD requires experimental data comparable with those needed for the application of the piecewise linear model but its implementation requires more computational effort and its precision is based on the accurate estimation of the model parameters [15]. It results in continuous bell-shaped constant life lines calculated by a unified equation that describes the fatigue behavior for both tension and compression loading. The Kawai anisomorphic model can be constructed using only one experimentally derived S-N curve, known as the critical S-N curve. The critical *R*-ratio is defined as the ratio of the compressive strength to the tensile static strength of the examined materials. The multi-slope formulation proposed by Boerstra can be applied to random fatigue data, which do not necessarily belong to a certain S-N curve. However the implementation of this model relies on the solution of a multi-parametric optimization problem for estimation of the five model parameters.

The *CCfatigue* software was used for derivation of all CLDs. The predictive accuracy of the applied CLD models was evaluated by comparing predicted S-N curves with corresponding experimental ones that were not used for estimation of the model parameters. The fatigue data under *R*=0.9 (T-T) and *R*=1.1 (C-C) were used in this work to simulate the combined fatigue-creep behavior of the joints under high mean-low amplitude loading conditions. Constant life diagrams produced by the described models are shown in Figs. 5.5-5.11. Data used for the estimation of model parameters are shown by open triangles, while data used for the model validation are shown by closed circles in all figures. A quantification of the predictive ability of each of the applied models was performed. The coefficients of multiple determination ($R^2$) between the predicted and the experimentally derived S-N curves are shown in Table 5.3.

Table 5.3. Comparison of predictive ability of applied CLD formulations

| | $R^2$ | | | | | | |
|---|---|---|---|---|---|---|---|
| ***R*-ratio** | **POLY** | **LR** | **PWL** | **PNL** | **KW** | **HR** | **BR** |
| **0.5** | 0.930 | 0.537 | 0.921 | 0.839 | 0.493 | 0.800 | 0.940 |
| **0.9** | 0.511 | 0.224 | 0.363 | 0.733 | 0.104 | 0.426 | 0.444 |
| **-0.5** | 0.914 | 0.977 | 0.976 | 0.973 | 0.870 | 0.948 | 0.977 |
| **2** | 0.854 | 0.485 | 0.803 | 0.675 | 0.687 | 0.750 | 0.746 |
| **-2** | 0.905 | 0.552 | 0.708 | 0.815 | 0.872 | 0.838 | 0.723 |
| **1.1** | 0.539 | 0.328 | 0.547 | 0.308 | 0.669 | 0.348 | 0.656 |
| **Average** | 0.775 | 0.517 | 0.720 | 0.724 | 0.616 | 0.685 | 0.748 |
| **Standard deviation** | 0.196 | 0.259 | 0.233 | 0.227 | 0.288 | 0.241 | 0.196 |

The linear model shown in Fig. 5.5, using only fatigue data at *R*=–1, underestimates the fatigue life in all regions except for *R*=–0.5. Comparison of the $R^2$ values in Table 5.3 confirms a good accuracy of the model for this loading condition ($R^2$=0.977). The PWL model, employing three sets of fatigue data (*R*=0.1, –1, and 10), provides more accurate estimations of fatigue life than the linear model (see Fig. 5.6). However, the accuracy of the PWL model under high mean loads is poor. The modified form of this model, the PNL formulation, can appropriately describe the concave upward behavior in the region between *R*=1 and *R*=0.1 (see Fig. 5.7) using the same amount of fatigue data.

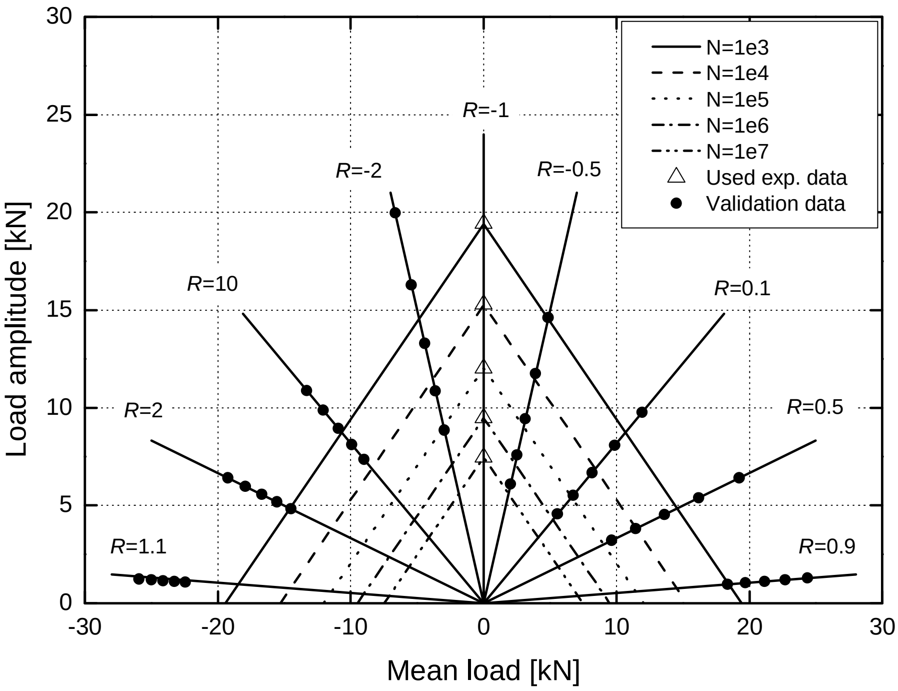

Fig. 5.5. Linear constant life diagram

In this case, the shift of the apex of the iso-life curves toward the negative mean load quadrant at a high number of cycles improves modeling accuracy. On the other hand, the convex shape of the curves between *R*=10 and *R*=1 reduces its accuracy compared to the PWL model, i.e. $R^2$=0.803 and $R^2$=0.675 at *R*=2 for the PWL and PNL models respectively.

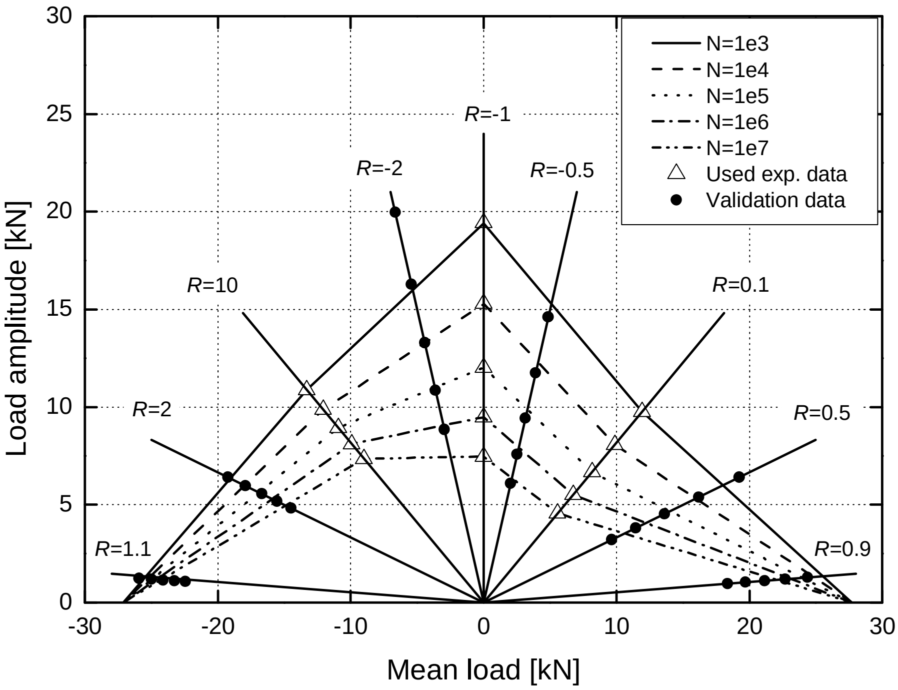

Fig. 5.6. Piecewise linear constant life diagram

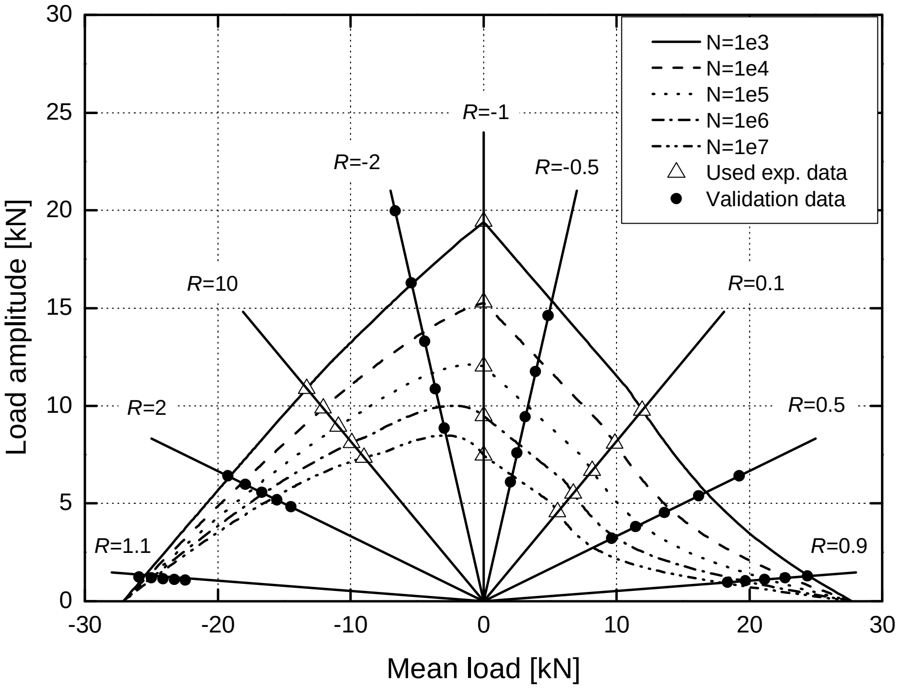

Fig. 5.7. Piecewise non-linear constant life diagram

For Kawai’s anisomorphic model the critical *R*-ratio is calculated as being -0.98. Therefore, the S-N curve under reversed loading (*R*=–1) was considered as the reference one for the derivation of the CLD (see Fig. 5.8).

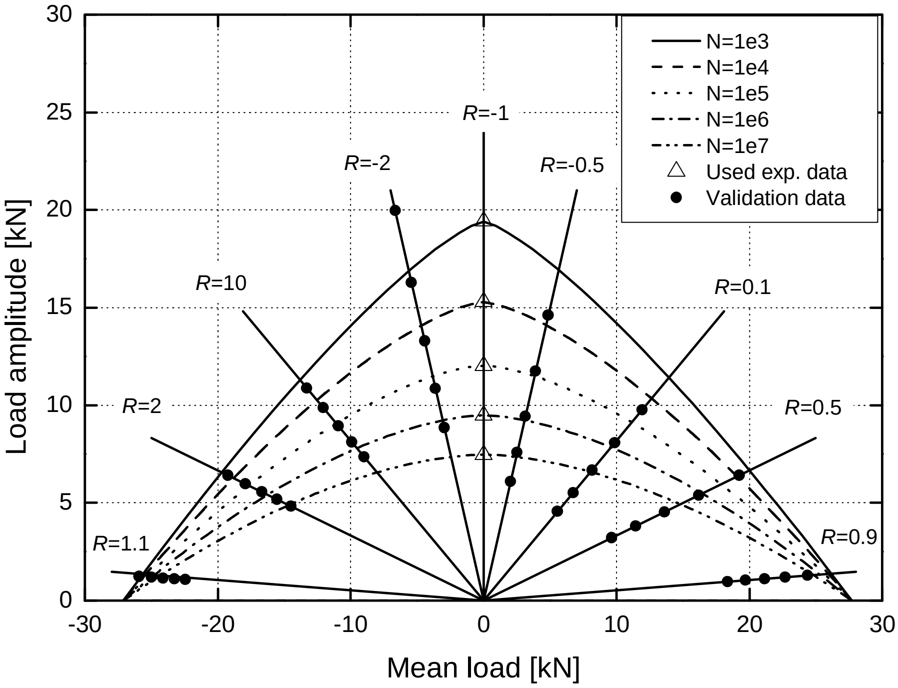

Fig. 5.8. Kawai’s constant life diagram

The obtained CLD, in contrast to the trend of the experimental data, provides convex constant life curves in both the tension- and the compression-dominated domains. Consequently in most regions, except at around *R*=10, the model overestimates the fatigue life and especially at high mean loads produces very poor predictions.

More accurate predictions can be obtained by the bell-shaped equation according to the Harris model (see Fig. 5.9) than those produced by the PWL model. However, application of the model, based on a non-linear fitting of a function to the fatigue data, results in constant life lines that do not satisfy any boundary conditions except at $\sigma_a = 0$ where $\sigma_m = UCS\ and\ UTS$. Therefore, some deviations can be seen even between the derived constant life lines and the experimental data used for estimation of the model parameters.

The use of five parameters for the derivation of the BR constant life diagram makes it very flexible and able to accurately model the fatigue behavior of a large number of different material systems. The average accuracy of Boerstra's CLD ($R^2$=0.748) is one of the highest among the examined models. Nonetheless, the fatigue life in regions susceptible to creep is overestimated. Also, as with the Harris CLD, since the model parameters are calculated based on an optimization process, the CLD only satisfies the boundary conditions at zero load amplitude. Consequently the iso-life lines do not necessarily comply with the experimental data employed for modeling, as shown in Fig. 5.10.

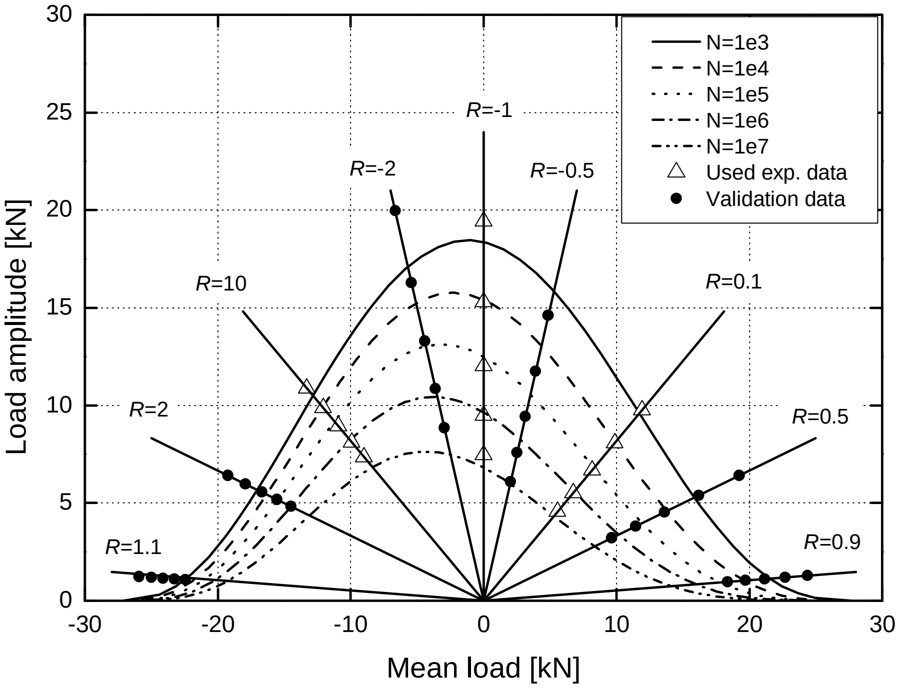

Fig. 5.9. Harris's constant life diagram

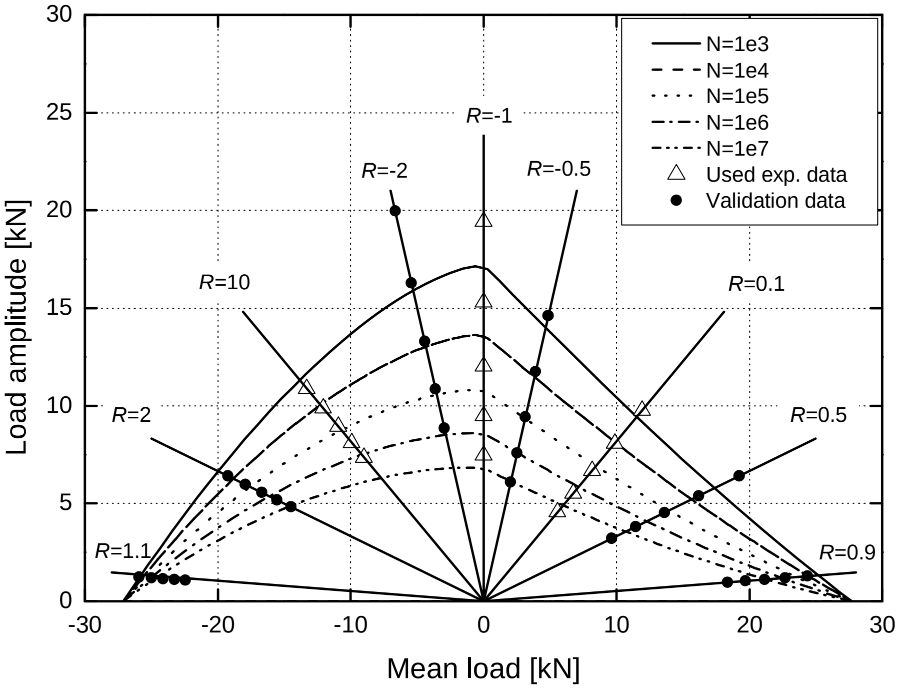

Fig. 5.10. Boerstra’s constant life diagram

The polynomial constant life diagram presented in Fig. 5.11 shows the capability of the introduced CLD model to follow the trend of the experimental data. It is apparent that incorporating the creep rupture strength data (actually the fatigue data under *R*=0.9 (T-T) and *R*=1.1 (C-C)) into the formulation, instead of using the static strength values, improves the accuracy of the model predictions in high mean load regions.

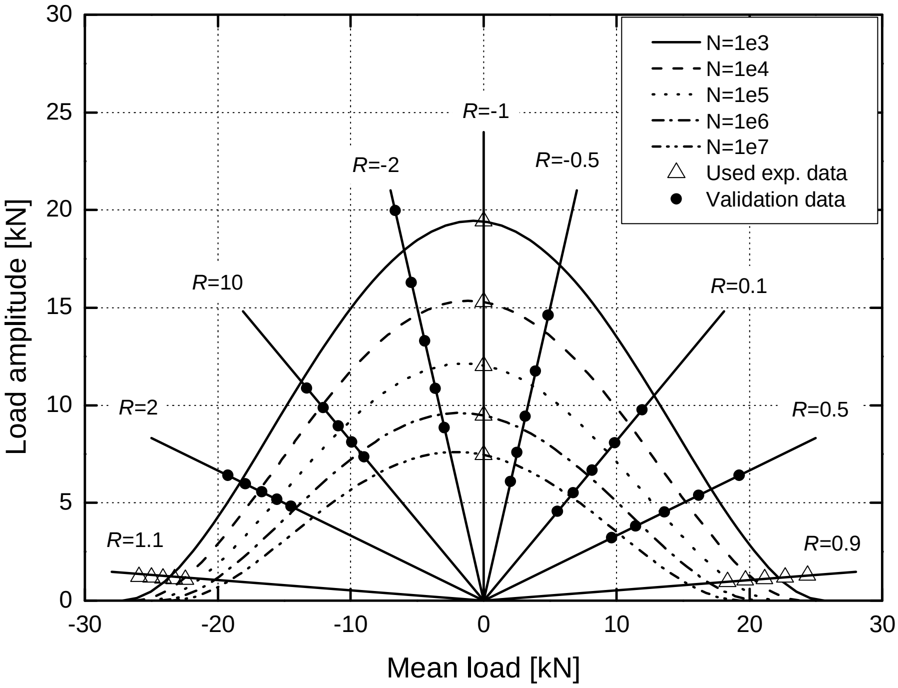

Fig. 5.11. Polynomial constant life diagram

Although under the applied boundary conditions the constant life lines must satisfy the fatigue failure condition under reversed loading (when $\sigma_m = 0,\ \sigma_a = \sigma_{(R=-1)}$), this does not impose a maximum value of the CLD on the radial line representing the S-N curve under *R*=–1. The model allows the diagram to move towards the tension- or compression-dominated domain according to the experimental evidence. The highest average $R^2$ value with the lowest standard deviation obtained for the new CLD formulation, 0.775±0.196 (see Table 5.3), proved the good accuracy and consistency of the model.

## 5.5. Conclusions

The *R*-ratio effect on the fatigue behavior of adhesively-bonded pultruded GFRP double-lap joints was experimentally investigated under different loading conditions. The results showed the high dependency of the fatigue strength on the mean load and therefore the necessity of appropriate modeling of this effect to avoid extensive experimental programs. A new phenomenological model was introduced for derivation of the constant life diagram of the examined bonded joints, providing a tool for the accurate prediction of unknown S-N curves under different loading conditions. The following conclusions can be drawn from this chapter:

- The failure modes of joints under different loading conditions can be classified according to the loading type, i.e. T-T, C-C, and T-C. A transition of the failure mode from tensile to compressive was observed when the mean load was decreased from zero to negative values.
- The increase of the mean load under constant amplitude loading led to an increase of the tensile and compressive fatigue life of the examined joints. The slopes of the S-N curves were decreased by increasing the mean load level.
- The constant life diagram derived for the examined bonded joints was asymmetric and shifted toward the compressive domain. This shift was found to be consistent with the higher fatigue strength of joints under compressive loading.
- The applicability of several CLD formulations developed for composite materials was evaluated for modeling the mean load effect on the fatigue behavior of the examined bonded joints. Although accurate predictions were obtained by some of the applied models, accuracy was not consistent under different loading conditions, especially under *R*-ratios around 1.

- A new phenomenological CLD was proposed for the simulation of the fatigue life of the examined joints taking into account the creep-fatigue interaction. Comparison of the predictions obtained using the new formulation with those of commonly used models for composite materials proved its greater accuracy and reliability under different loading conditions.

## 5.6. References

1. Vassilopoulos AP. Introduction to fatigue life prediction of composite materials and structures: past, present and future prospects. In: Vassilopoulos AP. Editor. Fatigue life prediction of composites and composite structures, Woodhead Publishing Ltd, Oxford, 2010, pp 1–44.
2. Abd Allah MH, Abdin EM, Selmy AI, Khashaba UA. Effect of mean stress on fatigue behavior of GFRP pultruded rod composites, Compos Part A, 1997;28(1):87–91.
3. Mandell JF, Meier U. Effect of stress ratio, frequency and loading time on the tensile fatigue of glass-reinforced epoxy. ASTM STP 813, 1982, pp. 55–77.
4. Ellyin F, El-Kadi H. Effect of stress ratio on the fatigue of unidirectional glass fibre/epoxy composite laminae. Composites, 1994;25(10):917–924.
5. Mallick PK, Zhou Y. Effect of mean stress on the stress-controlled fatigue of a short E-glass fiber reinforced polyamide–6.6, Int J Fatigue, 2004;26(9):941–946.
6. Mandell JF, Samborsky DD. DOE/MSU composite material fatigue database. Sandia National Laboratories, SAND97-3002. v. 19; 31st March 2010 < http://windpower.sandia.gov/ >.
7. Petermann J, Schulte K. The effects of creep and fatigue stress ratio on the long-term behavior of angle-ply CFRP, Compos Struct, 2002;57(1–4):205–210.
8. Kawai M, Koizumi M. Non-linear constant fatigue life diagrams for carbon/epoxy laminates at room temperature, Compos Part A, 2007;38(11):2342–2353.
9. Ramani SV, Williams DP. Notched and unnotched fatigue behavior of angle-ply graphite/epoxy composites. In: Reifsnider KL, Lauraitis KN, editors. Fatigue of filamentary composite materials. ASTM STP 636; 1977, pp. 27–46.
10. Hahn HT. Fatigue behavior and life prediction of composite laminates, Composite Materials: Testing and Design (Fifth Conference), ASTM STP 674 ed. Tsai SW. 1979, 383–417.

11. Fernando G, Dickson RF, Adam T, Reiter H, Harris B. Fatigue behaviour of hybrid composites: part I Carbon/Kevlar hybrids, J Mater Sci, 1988;23(10):3732–3743.
12. Towo AN, Ansell MP. Fatigue of sisal fibre reinforced composites: Constant-life diagrams and hysteresis loop capture, Compos Sci Technol, 2008;68(3–4):915–924.
13. Andersons J, Paramonov Yu. Applicability of empirical models for evaluation of stress ratio effect on the durability of fiber-reinforced creep rupture-susceptible composites, J Mater Sci, 2011;46(6):1705–1713.
14. Silverio Freire RC, Dória Neto AD, De Aquino EMF. Comparative study between ANN models and conventional equation in the analysis of fatigue failure of GFRP, Int J Fatigue, 2009;31(5):831–839.
15. Vassilopoulos AP, Manshadi BD, Keller T. Influence of the constant life diagram formulation on the fatigue life prediction of composite materials, Int J Fatigue, 2010;32(4):659–669.
16. Vassilopoulos AP, Manshadi BD, Keller T. Piecewise non-linear constant life diagram formulation for FRP composite materials, Int J Fatigue, 2010;32(10):1731–1738.
17. Adam T, Fernando G, Dickson RF, Reiter H, Harris B. Fatigue life prediction for hybrid composites, Int J Fatigue, 1989;11(4)233–237.
18. Boller KH. Fatigue properties of fibrous glass-reinforced plastics laminates subjected to various conditions, Mod Plast, 1957;34(10):163–293.
19. Renton WJ, Vinson JR. Fatigue behavior of bonded joints in composite material structures, J Aircraft, 1975;12(5):442-447.
20. Quaresimin M, Ricotta M. Fatigue behaviour and damage evolution of single lap bonded joints in composite material, Compos Sci Technol, 2006;66(2):176-187.
21. Crocombe AD, Richardson G. Assessing stress and mean load effects on the fatigue response of adhesively bonded joints, Int J Adhes Adhes, 1999;19(1):19–27.
22. Gathercole N, Reiter H, Adam T, Harris B. Life prediction for fatigue of T800/5245 carbon fiber composites: I. Constant amplitude loading, Int J Fatigue, 1994;16(8):523–532.
23. Beheshty MH, Harris B. A constant life model of fatigue behavior for carbon fiber composites: the effect of impact damage, Compos Sci Technol, 1998;58(1):9–18.
24. Boerstra GK. The multislope model: a new description for the fatigue strength of glass reinforced plastic, Int J Fatigue, 2007;29(8):1571–1576.

# 6 Block loading

## *Abstract*

*The effect of loading sequence on the fatigue behavior of adhesively-bonded pultruded GFRP double-lap joints was experimentally investigated by applying different tensile and compressive block loading patterns. The observed failure modes were consistent with failure modes under constant amplitude loading. A significant load sequence effect was observed for both tensile and compressive loading. Under tensile loading the transition from low to high load cycles in a two-block loading was more damaging than the high to low sequence. The inverse was observed for compression loading. This behavior was associated with the crack propagation rates and their dependence on loading type. The effect of the number of load transitions in a multi-block loading spectrum was also studied by using different loading sequences. The influence of this loading parameter was found to be more dominant than the sequence effect, which is diminished by increasing the number of transitions.*

## 6.1. Introduction

The complex nature of realistic loading patterns applied to engineering structures necessitates the development of reliable methodologies for the fatigue life prediction of materials and structural components. In many of the methodologies developed for fatigue life prediction, the process of damage accumulation under variable amplitude loading is assumed as being linear and therefore not affected by the load history. The linear Palmgren-Miner rule is therefore usually employed for estimation of the accumulated damage under realistic loading patterns. Although the use of the Palmgren-Miner rule usually leads to accurate life predictions for metals, it has been proved unreliable for composite materials where significant discrepancies between estimated fatigue life and experimental results have been reported [1].

Several experimental investigations of the fatigue behavior of composite laminates show their sensitivity to the loading sequence. Experiments composed of two blocks of constant amplitude loading changing from a low stress level to a higher stress level (L-H sequence) or vice versa (H-L sequence) were usually employed to study the sequence effect in composite materials. However the results obtained from these experiments were not consistent, showing a greater damaging effect due to the L-H sequence, e. g. [1-10] or the opposite behavior, e. g. [11-16] depending on the material and loading parameters.

Several different loading parameters such as the *R*-ratio (the ratio of the minimum to the maximum applied cyclic load) and the cyclic load levels govern the sequence effects [17-20]. Tension or compression loading blocks can produce different damage compared to mixed tension-compression blocks. The difference between the applied load levels in a two-block loading sequence also can be an important parameter as the sequence effect can be magnified when the difference between two load levels is increased, see e.g. [19].

Although numerous publications are dedicated to the study of the sequence effect, explicit explanations regarding the contributing failure mechanisms are very limited [16, 20-22]. The activation of competing failure mechanisms, like initiation mechanisms vs. progressive failure mechanisms or resin cracking vs. fiber breakage or delamination under different stress levels, was considered for the explanation of the sequence effects observed for different types of composite materials [16, 21]. For instance, transverse cracking dominates the failure of cross-ply laminates under high stress levels, while delamination is activated under lower stress levels, see e.g. [16]. Therefore the H-L sequence results in shorter fatigue lifetimes than the L-H sequence since the transverse cracks, created under a high stress level, are potential places for the initiation of delamination. A reverse effect was observed after an experimental investigation of multidirectional carbon/epoxy laminates and explained by the assumption that since most of the applied load is borne by the matrix under low stress levels and by the fibers under high stress levels, the damage mainly involves the growth of microcracks in the matrix throughout the specimen under lower stress levels, which can induce rapid failure in the following high stress level stage [17]. The balance between the damage state and the stress levels and its effect on stress intensity was also proposed as a way of explaining sequence effects in angle ply laminates. The longer life of $[\pm 45]_{2s}$ carbon/epoxy laminates under both L-H and H-L sequences compared to the expected life, characterized by the Palmgren-Miner sum, was thus attributed to the decrease in local stress intensity due to a large number of well distributed matrix cracks when the stress level is decreased [22].

In addition to the loading sequence effect, the significant influence of loading transition and its frequency of occurrence on the fatigue life has been discussed in several investigations [9, 23-25]. The effect of frequent transition of cyclic load level on fatigue life was found to be more significant than the loading sequence effect [9]. The transition effect, as defined by the term “cycle mix”, was introduced for modeling the damage accumulated under block and variable amplitude loading in [23-25].

The load sequence also affects the fatigue behavior of fiber-reinforced polymer (FRP) composite joints, although only a small number of works exist concerning this phenomenon. Similar to composite laminates, several parameters were found to contribute to the loading sequence effect on the fatigue life. A significant load interaction effect (overloads and loading sequence effect) was identified [26] for adhesively-bonded double-lap joints composed of carbon/epoxy laminates and a single-part epoxy adhesive. The crack growth acceleration due to the load interaction was put forward as the main reason for the shorter fatigue life exhibited by the joints under investigation. The cycle mix effect and the variation in mean stress were also investigated and it has been proved that they both affect crack growth acceleration, while overloads were shown to increase the likelihood of fatigue crack initiation.

The above review highlights the significant influence of load interaction on the fatigue behavior of materials and structure under realistic loading patterns. It also shows that this interaction strongly depends on the materials as well as the applied loading spectrum. This work aims to investigate the load sequence effect on the fatigue behavior of adhesively-bonded pultruded GFRP joints. The loading sequence effect, L-H vs. H-L sequences, and also the effect of load transition frequency on the fatigue life of the examined joints are experimentally investigated under both tension and compression loading (experimental program described in Chapter 2). The comparison of the acquired data concerning crack propagation under constant amplitude (CA) and block loading (BL) experiments provides clear insight into the effect of load interaction on the fatigue life of the bonded joints.

## 6.2. Experimental results

### 6.2.1. Failure modes

The observed failure modes were found to be consistent with the failure modes of joints under tensile and compressive constant amplitude loading in Section 3.2.2.1. Under loading sequences composed of tensile loading blocks ($R$=0.1), a dominant crack initiated from the joint corner of one of the bond lines between the adhesive and the inner laminate and then shifted deeper, between the first and second mat layers of the inner laminate, and propagated along this path up to failure. Similarly to the observed failure mode under constant amplitude compression loading at $R$=10, under loading sequences composed of compressive loading blocks, the dominant crack initiated and propagated in the middle of the inner laminate inside the roving layer. Accordingly no visual difference was observed in failure location due to the load interaction, which is a basic required condition for comparison of the BL and CA fatigue data.

### 6.2.2. Block loading results

The fatigue loading matrix and detailed results concerning different loading sequences for tension ($R$=0.1) and compression ($R$=10) fatigue are presented in Tables 6.1-6.2 respectively. The applied number of cycles ($n_1$) and corresponding maximum absolute cyclic load level in the first block ($F_{\max1}$) and the same parameters for the second loading block ($n_2$, $F_{\max2}$) are shown in the same tables. The allowable numbers of cycles corresponding to the constant amplitude loading under each $F_{\max}$ were calculated by fitting a power law model to the experimental data and are indicated by $N_1$ and $N_2$ in Tables 6.1-6.2.

Table 6.1. Two-block loading results at $R$=0.1

| | Specimen ID | $F_{max1}$ [kN] | $n_1$ | $N_1$ | $F_{max2}$ [kN] | $n_2$ | $N_2$ | $D$ |
|---|---|---|---|---|---|---|---|---|
| L-H sequence | R01F30B508001 | 14.4 | 48649 | 142978 | 21.6 | 483 | 1070 | ***0.792*** |
| | R01F30B508002[a] | | 48649 | | | 3 | | ***0.343*** |
| | R01F30B407001 | 12.0 | 456038 | 1291993 | 19.2 | 2592 | 4434 | ***0.938*** |
| | R01F30B407002[a] | | 387598 | | | 9815 | | ***2.514*** |
| | R01F50B407001[b] | | 645996 | | | 3 | | ***0.501*** |
| H-L sequence | R01F30B805001 | 21.6 | 287 | 1070 | 14.4 | 207559 | 142978 | ***1.720*** |
| | R01F30B805002[a] | | 287 | | | 686108 | | ***5.067*** |
| | R01F30B704001 | 19.2 | 1330 | 4434 | 12.0 | 4832688 | 1291993 | ***4.040*** |
| | R01F30B704002[a] | | 1330 | | | 5496607 | | ***4.554*** |
| | R01F50B704001[b] | | 2217 | | | 7329969 | | ***6.173*** |

[a] Specimens instrumented by crack gages

[b] Length of the first block corresponds to 50% of the constant amplitude fatigue life.

Table 6.2. Two-block loading results at $R$=10

| | Specimen ID | $F_{max1}$ [kN][b] | $n_1$ | $N_1$ | $F_{max2}$ [kN][b] | $n_2$ | $N_2$ | $D$ |
|---|---|---|---|---|---|---|---|---|
| L-H sequence | R10F30B607001 | 17.4 | 682023 | 2273411 | 20.3 | 1009548 | 60834 | ***16.895*** |
| | R10F30B607002[a] | | 682023 | | | 1829254 | | ***30.370*** |
| | R10F30B658001 | 18.9 | 104054 | 346848 | 23.2 | 5691 | 2642 | ***2.454*** |
| | R10F30B658002[a] | | 104054 | | | 824363 | | ***312.322*** |
| H-L sequence | R10F30B706001 | 20.3 | 18250 | 60834 | 17.4 | 454047 | 2273411 | ***0.500*** |
| | R10F30B706002[a] | | 18250 | | | 1614479 | | ***1.010*** |
| | R10F30B806501 | 23.2 | 793 | 2642 | 18.9 | 63357 | 346848 | ***0.483*** |
| | R10F30B806502[a] | | 261 | | | 0 | | ***0.099*** |
| | R10F30B806503[a] | | 793 | | | 297046 | | ***1.157*** |

[a] Specimens instrumented by crack gages

[b] Absolute value

The damage index ($D$) was calculated according to the Palmgren-Miner rule as in Eq. (6.1)

$$D = \sum_{i=1}^{k} \frac{n_i}{N_i} \tag{6.1}$$

with $k$ denoting the number of applied loading blocks. According to this model, the specimen under a cyclic loading pattern fails when the damage index reaches 1. In the present study this index was used as a reference value to compare the effect of the parameters being investigated.

Under tensile loading blocks, the calculated damage indices in Table 6.1 for the L-H sequences, independent of load level, are less than one except for one experiment (R01F30B407002) while they are higher than one for the H-L sequences. The results for two joints subjected to the longer first loading blocks, R01F50B407001 and R01F50B704001, were also consistent with the obtained results. The calculated damage indices for different loading sequences are presented in Fig. 6.1 against the ratio of the maximum load of the first block to the second block ($F_{max1}/F_{max2}$). The damage indices corresponding to the L-H sequence are close to or less than one, while for the H-L sequences the $D$ values are higher than one.

In contrast to tensile loading blocks, the loading sequence effect was found more damaging under H-L than L-H compressive loading blocks. The damage index for experiments carried out under the L-H sequence was higher than one, while the H-L sequence led to values of less than or close to one (see Fig. 6.2). The fatigue failure occurred for one of the specimens, R10F30B806502, during the first block before the predetermined number of cycles had been carried out.

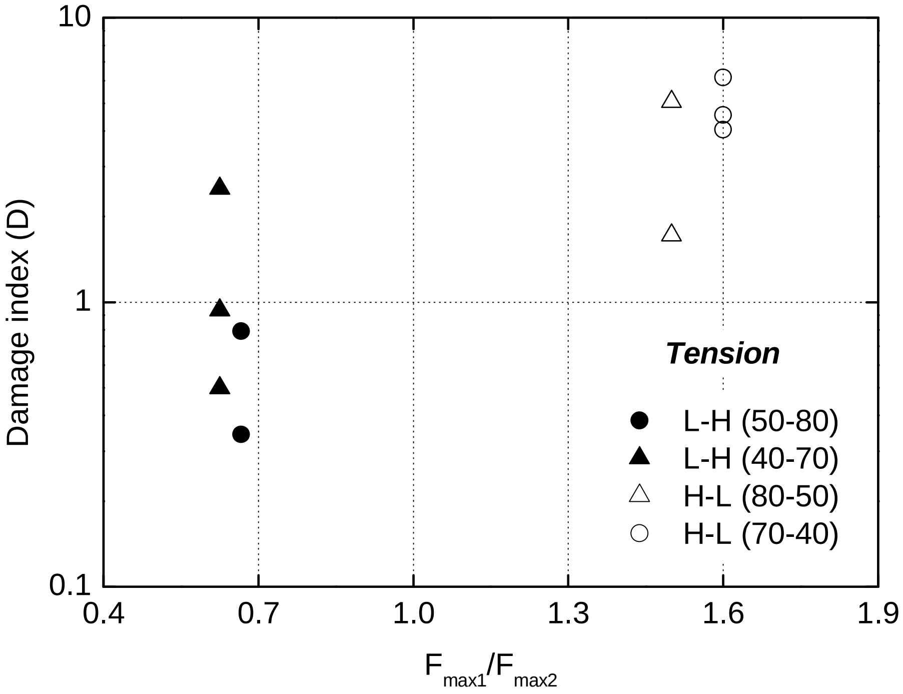

Fig. 6.1. Comparison of calculated damage indices for L-H and H-L sequences composed of tensile loading blocks (*R*=0.1)

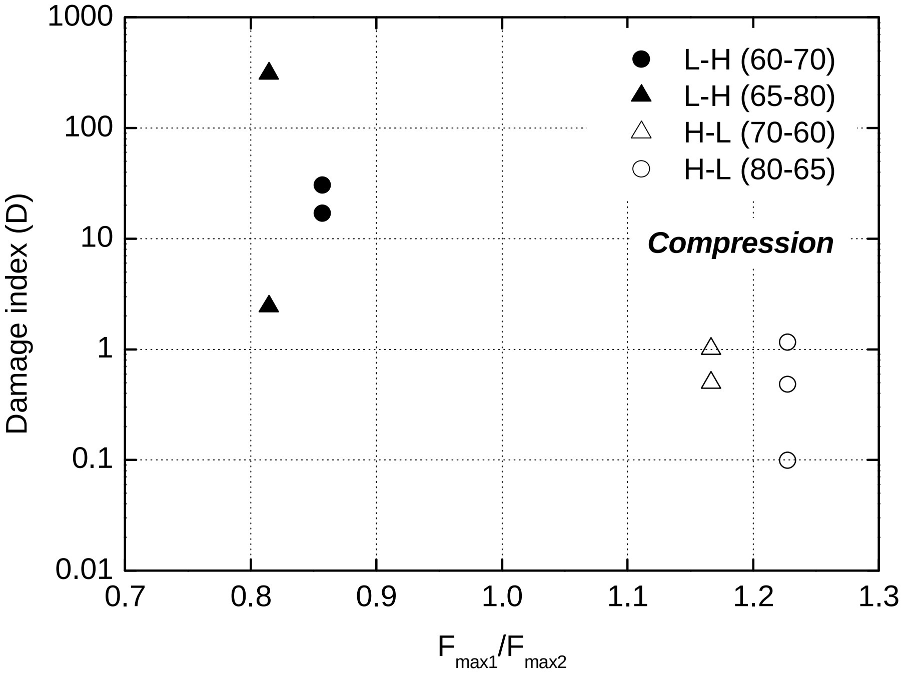

Fig. 6.2. Comparison of calculated damage indices for L-H and H-L sequences composed of compressive loading blocks (*R*=10)

The data acquired from the crack gages concerning the developing crack in the joints provide valuable information regarding the variation in the crack propagation rate during different loading blocks. The calculated crack propagation rate (d$a$/d$N$) based on the incremental polynomial fitting (according to ASTM E647) against the crack length, $a$, is shown in Figs. 6.3-6.6 for tensile and Figs. 6.7-6.10 for compressive loading sequences. The data corresponding to each block are indicated by different symbols. Therefore in all figures the solid circles and triangles are related to the first and second blocks respectively.

The results of the experimental program designed to study the effect of the number of transitions are presented in Tables 6.3 and 6.4 respectively for tensile and compressive loading. The number of cycles in each block ($n_i$), number of blocks ($NB_i$) (number of occurrences of each block), and also the damage indices calculated using the Palmgren-Miner rule given in Eq. (6.1) are shown in these tables. The fatigue failure occurred during both loading blocks, blocks with decimal $NB_i$, independent of load level. The integer part of $NB_i$ denotes the number of transitions ($NT$). The expected constant amplitude fatigue life for each load level can be found in Tables 6.1-6.2. The damage indices for all specimens except one, R01B7040L01, are less than one.

Table 6.3. Multi-block loading results at $R$=0.1

| | Specimen ID | $F_{max1}$ [kN] | $n_1$ | $F_{max2}$ [kN] | $n_2$ | $NB_1$ | $NB_2$ | $D$ |
|---|---|---|---|---|---|---|---|---|
| High Transition | R01B4070H01 | 12.0 | 2914 | 19.2 | 10 | 34 | 34 | ***0.153*** |
| | R01B7040H01 | 19.2 | 10 | 12.0 | 2914 | 164.6 | 164 | ***0.741*** |
| Low Transition | R01B4070L01 | 12.0 | 29140 | 19.2 | 100 | 19 | 18.1 | ***0.837*** |
| | R01B7040L01 | 19.2 | 100 | 12.0 | 29140 | 42.8 | 42 | ***1.913*** |

Table 6.4. Multi-block loading results at $R$=10

| | Specimen ID | $F_{max1}$ [kN]$^a$ | $n_1$ | $F_{max2}$ [kN]$^a$ | $n_2$ | $NB_1$ | $NB_2$ | $D$ |
|---|---|---|---|---|---|---|---|---|
| High Transition | R10B6070H01 | 17.4 | 374 | 20.3 | 10 | 366 | 365.5 | ***0.120*** |
| | R10B7060H01 | 20.3 | 10 | 17.4 | 374 | 730 | 729.5 | ***0.240*** |
| Low Transition | R10B6070L01 | 17.4 | 37400 | 20.3 | 1000 | 8 | 7.1 | ***0.248*** |
| | R10B7060L01 | 20.3 | 1000 | 17.4 | 37400 | 10.9 | 10 | ***0.345*** |

[a] Absolute value

## 6.3. Discussion

### 6.3.1. Loading sequence effect

The fracture data obtained from the BL experiments can be compared with the CA data since similar failure modes were observed under both CA and BL conditions. The crack propagation data under CA loading corresponding to each load level of the BL experiments are shown in Figs. 6.3-6.10 with similar open symbols.

### *6.3.1.1. Tensile loading*

The comparison of the BL with the CA data in Figs. 6.3-6.6 showed that the crack propagation rate during the first block for all loading cases conformed well to the CA data as was expected. However, when the load level was altered and the second block started, a noticeable change compared to the corresponding CA behavior occurred. The analysis of d*a*/d*N* during the second loading block explains the shorter or longer fatigue life compared to the expected lives based on CA data.

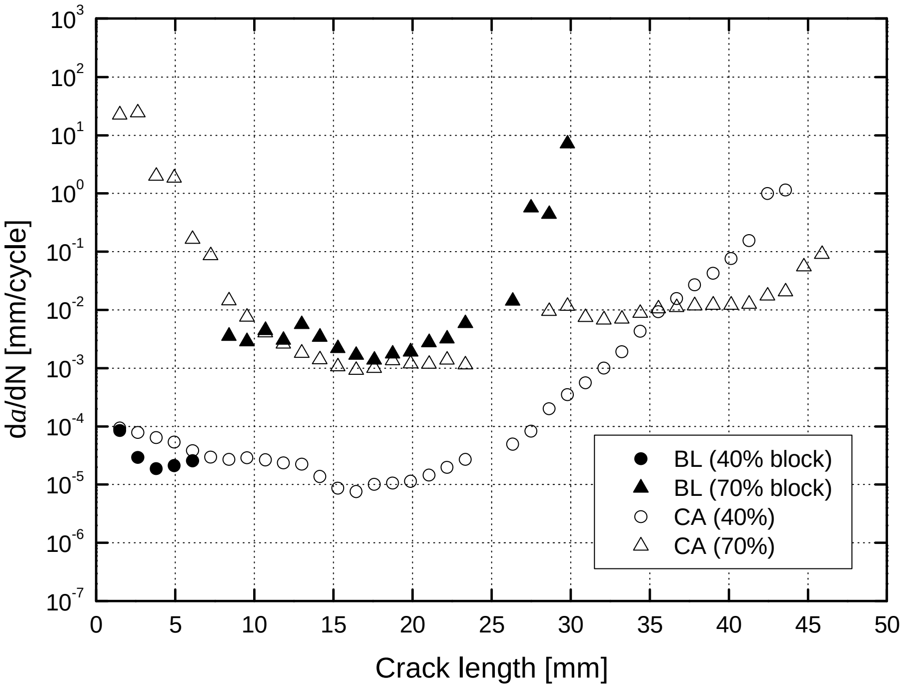

Fig. 6.3. Comparison of crack propagation rate under two-block loading and corresponding CA loading for R01F30B407002

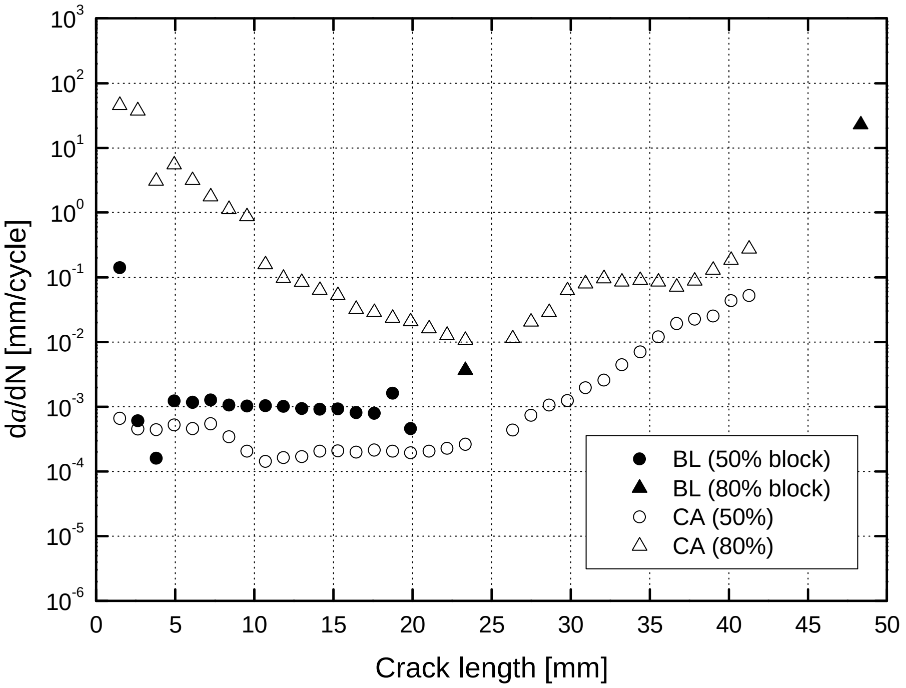

Fig. 6.4. Comparison of crack propagation rate under two-block loading and corresponding CA loading for R01F30B508002

The crack growth acceleration can be seen in Figs. 6.3-6.4 when the load level of the second block is higher than the first block. The d*a*/d*N* during the second block in Fig. 6.3 is slightly higher than the CA results and a rapid nonlinear crack growth occurs earlier, around crack length 25 mm, under block loading. Under the second loading sequence, R01F30B508002, the crack propagated very rapidly (Fig. 6.4) and a sudden rupture occurred when the second load level was applied, similarly to the R01F30B407002.

A retardation effect was identified under the H-L sequences during the second loading block. The crack growth rate decelerated to levels lower than the recorded rate under CA loading as presented in Figs. 6.5-6.6. The retardation effect remains for a long period of time and affects the growth rate till the crack length reaches the rapid nonlinear propagation phase. This behavior leads to fatigue lives longer than the expected life based on the CA data and damage indices higher than one. The retardation effect due to overloads is known for metals and can be attributed to several mechanisms [27]. However, in contrast to what was observed for the examined joints, a progressive reduction in crack growth rate continues in metals over a certain crack growth distance, known as the delay distance, up to a minimum and then starts to increase until it eventually attains the propagation rate before the overload [27].

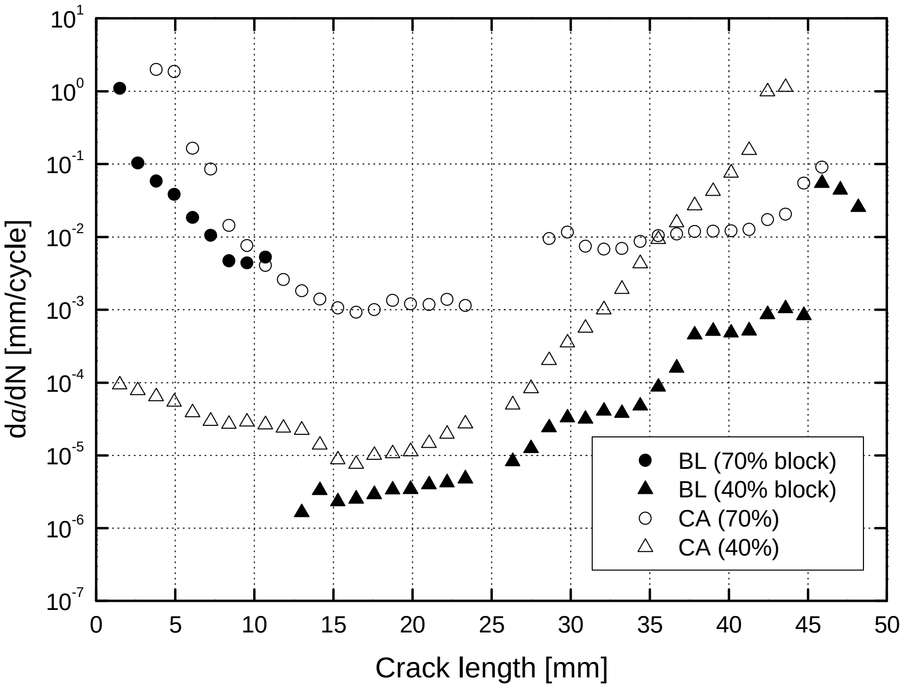

Fig. 6.5. Comparison of crack propagation rate under two-block loading and corresponding CA loading for R01F30B704002

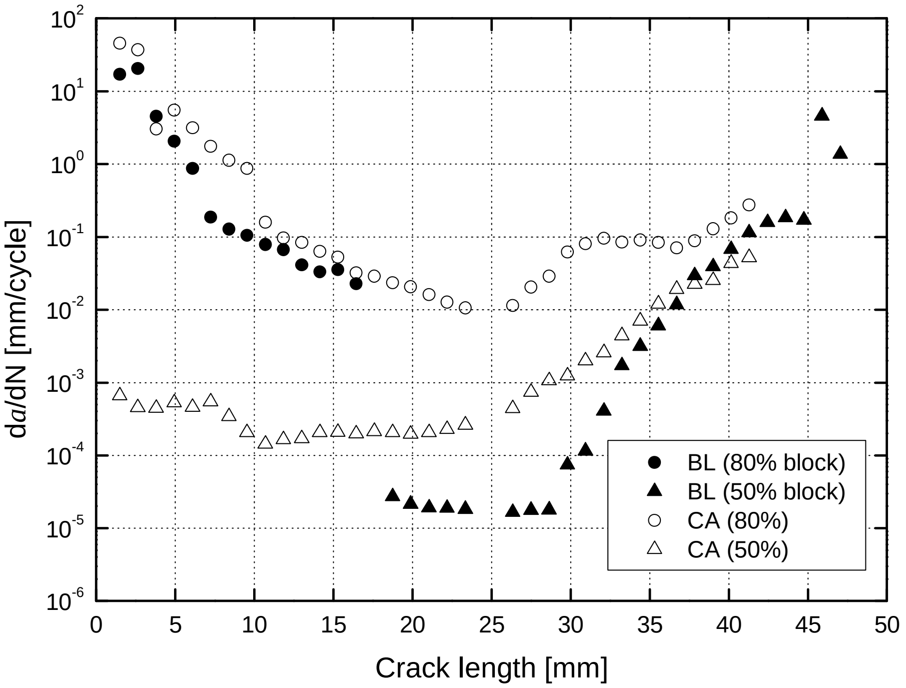

Fig. 6.6. Comparison of crack propagation rate under two-block loading and corresponding CA loading for R01F30B805002

#### *6.3.1.2. Compressive loading*

The crack propagation rate data under compressive loading blocks were compared with the CA data in Figs. 6.7-6.10. Under the L-H sequences (Figs. 6.7 and 6.8), when the load level was increased, the d*a*/d*N* was accelerated over a short crack distance. However, this rate never reached the rate of CA crack propagation under the second load level and slowed down to a rate similar to the CA rate corresponding to the first load level. This behavior clearly explains the extension of the fatigue life under the L-H compressive loading sequence and the calculated damage indices that are significantly higher than one.

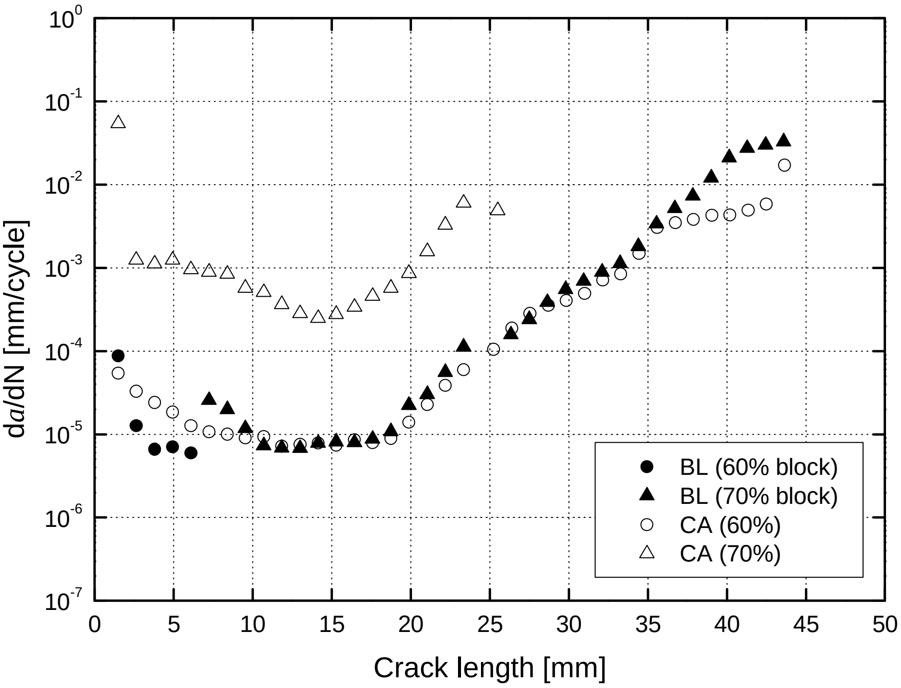

Fig. 6.7. Comparison of crack propagation rate under two-block loading and corresponding CA loading for R10F30B607002

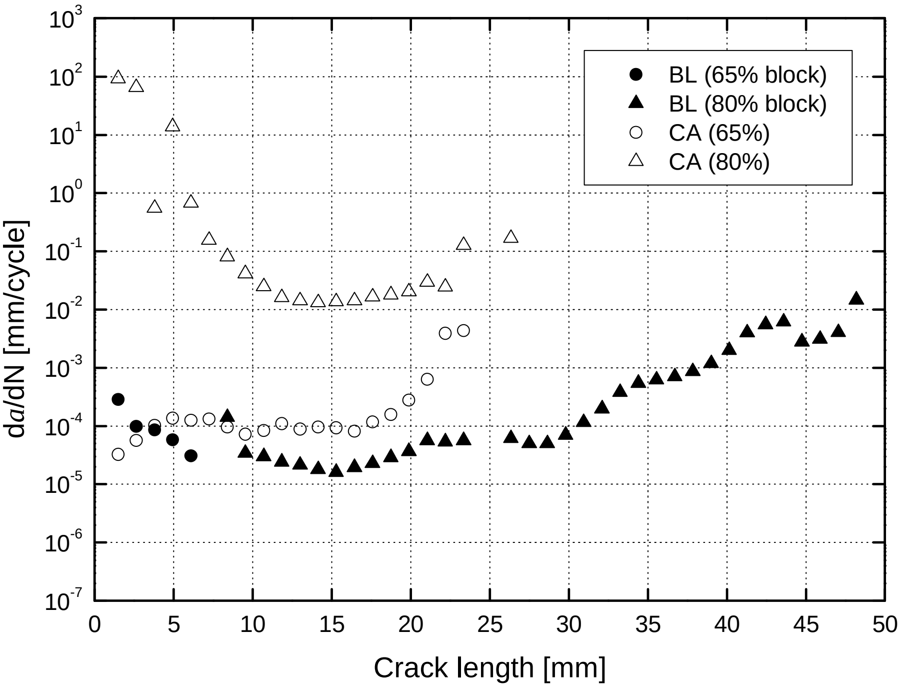

Fig. 6.8. Comparison of crack propagation rate under two-block loading and corresponding CA loading for R10F30B658002

Under the H-L loading blocks a minor sequence effect was observed consistent with the fracture data presented in Figs. 6.9-6.10. The d*a*/d*N* for CA and BL was found to be similar under both load levels, obviously resulting in the damage index close to one.

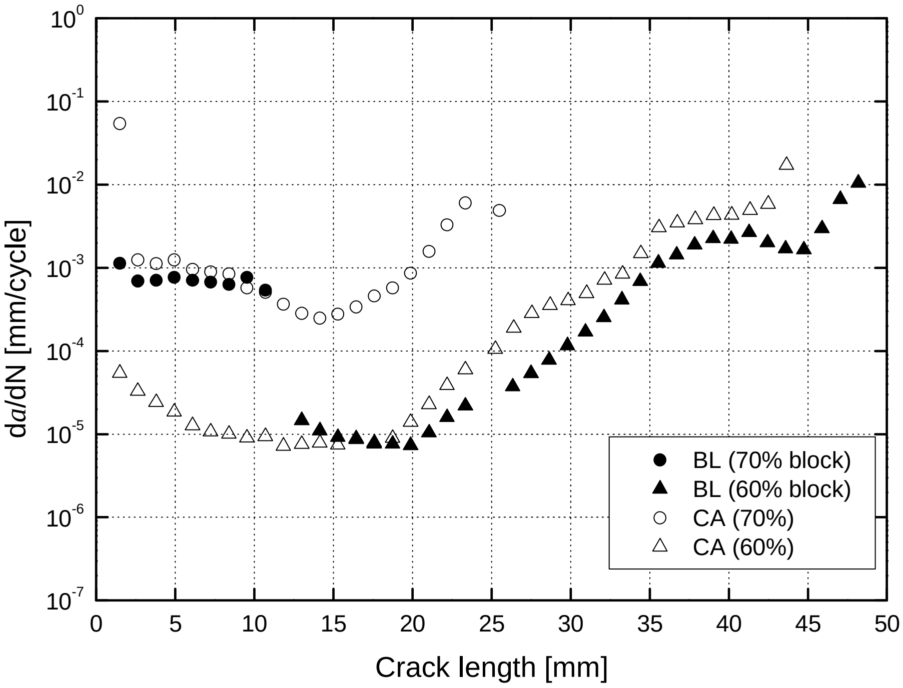

Fig. 6.9. Comparison of crack propagation rate under two-block loading and corresponding CA loading for R10F30B706002

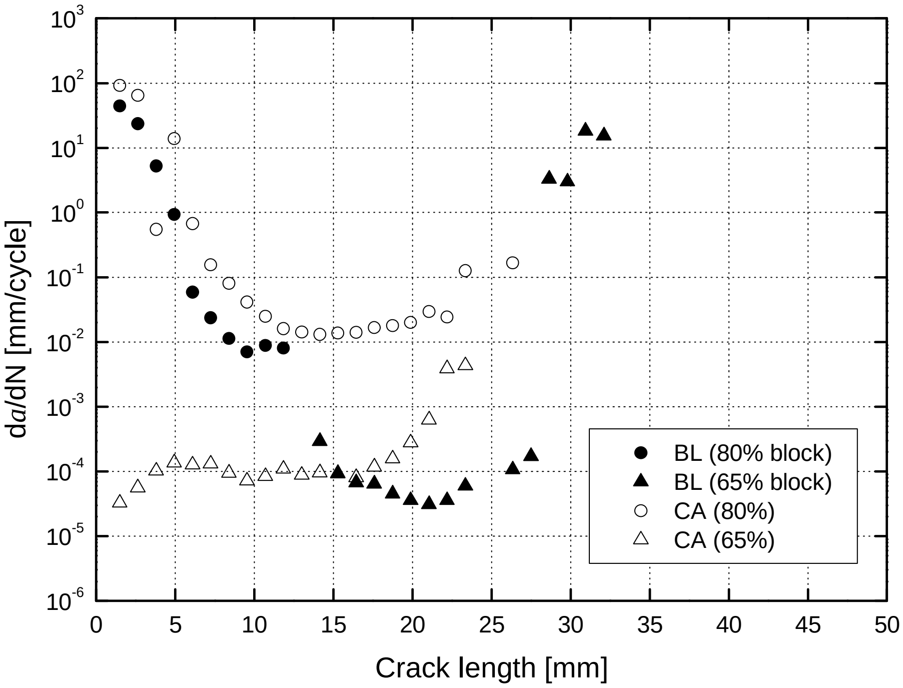

Fig. 6.10. Comparison of crack propagation rate under two-block loading and corresponding CA loading for R10F30B806503

### *6.3.1.3. Failure mode and sequence effect*

The acceleration and retardation of the crack growth rate is due to the damage mechanisms activated under different load levels. Under tensile loading, the dominant crack is located between the first and second mat layers of the laminate, while under compression loading the dominant crack initiates and propagates through the roving layer of the laminates. Between the mat layers, the chopped strands randomly stitched to the 0°/90° fabrics make the material very prone to the initiation of several microcracks and the forming of considerable fiber bridging. The detailed fracture analysis of double cantilever beam (DCB) joints composed of the same pultruded laminates presented in [28] showed that the amount of fiber bridging strongly depends on the location of the crack in the laminate. Based on this research, maximum fiber bridging occurs between the two mat layers with the highest strain energy release rate, while the bridging between the mat and roving layers is less significant. Therefore, for the examined joints, under tension loading the bridging makes a strong contribution to the fracture behavior, while under compression loading the strain energy release rate mainly results from the contribution of the matrix.

Under the H-L tensile loading sequences, when the load level is decreased, the input energy for crack propagation is also decreased, while the fiber bridging developed during the first loading block remains constant. Therefore, the crack propagation rate significantly decreases (see Figs. 6.5-6.6) and leads to a longer fatigue life compared to the life based on the constant amplitude fatigue data. An inverse process occurs under the L-H sequences, i.e. the increase in load levels in the second loading blocks provide the energy required for breaking the fiber bridging developed during the first block and consequently accelerate the crack growth rate (Figs. 6.3-6.4).

Under compressive loading sequences no significant fiber bridging was observed and the failure was dominated by other micro-damage mechanisms. When the H-L loading sequences are applied, since the first block is short (applied for less than 5% of the total life), there is not sufficient time for the development of micro-damage mechanisms. Therefore, the crack propagation rate decreases to the corresponding levels of the constant amplitude experiments, as seen in Figs. 6.9-6.10, when the load is decreased. Under the L-H sequences, the specimens were loaded for a long period under the initial low loading block, allowing the time required for the development of multiple microdamage that governs the joint failure. This damage develops further during the second step (under higher loads), absorbing energy and thus preventing the crack propagation rate from increasing, as presented in Figs. 6.7-6.8, and therefore extending joint lifetime.

### 6.3.1.4. Modeling issues

Several attempts have been made to formulate the effect of loading sequence in composite materials. A comprehensive review of damage accumulation models can be found in [29]. These are mainly the nonlinear damage accumulation models given in Eq. 6.2:

$$D = \sum_{i=1}^{k} \left( \frac{n_i}{N_i} \right)^{\alpha} \tag{6.2}$$

where they provide a nonlinear form of the Palmgren-Miner damage summation rule depending on the exponent $\alpha$, which can be a function of the applied load level and *R*-ratio. The nonlinear form of Palmgren-Miner rule is schematically shown in Fig. 6.11 (dashed lines) compared to the linear form (dotted line).

According to these models, the damage accumulation trend (dashed lines in Fig. 6.11) is a function of the applied stress level. Fig. 6.11 is used as an example to quantitatively describe the nonlinear damage accumulation process in the following. In this figure, when the load level is altered, i.e. from the 1st to the 2nd loading block, the damage accumulation path also changes while the amount of damage remains constant (see solid lines in Fig. 6.11).

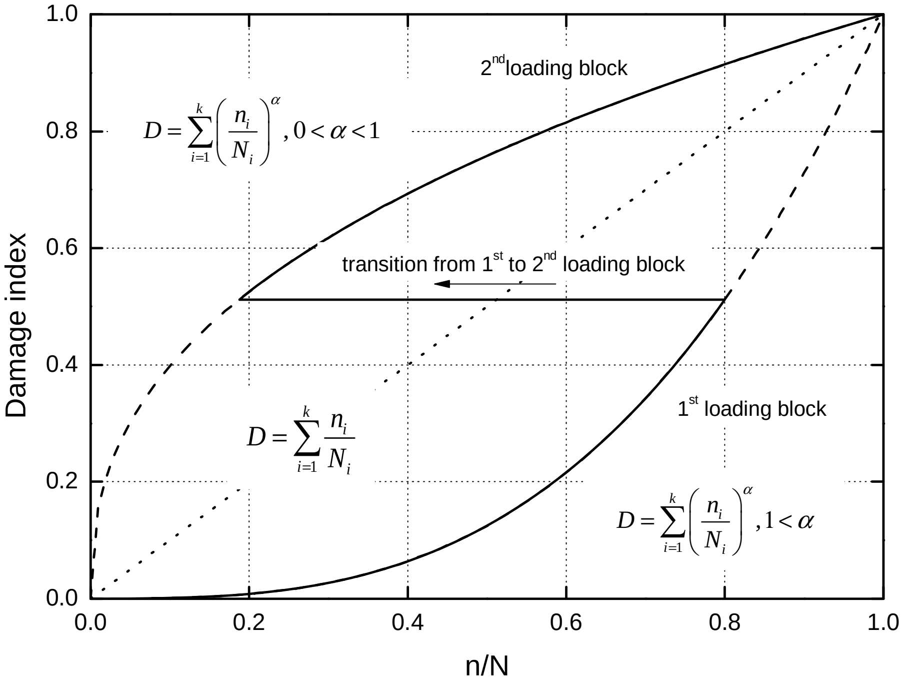

Fig. 6.11. Comparison of linear (dotted line) and nonlinear (dashed lines) damage accumulation models and simulation of two-block loading sequence (solid line)

In this process, although approximately 80% of the total fatigue life occurs during the first block ($n_1/N_1=0.8$), when the load changes, the lifetime that has already occurred is equivalent to 20% of the total fatigue life under the second loading block and the partial damage required to cause failure is ($n_2/N_2=0.8$). Therefore the sum of partial damage ($n_i/N_i$) due to both loading blocks is equal to $D$=1.6. Based on these models, the calculated damage sum in a two-block loading experiment never reaches $D$=2 because the partial damage under each loading block independent of the model exponent is less than one. Although these models have been successfully employed for some composite material systems, they are not able to accurately model the accumulated damage under two-block loading sequences for the examined bonded joints. As shown in Tables 6.1 and 6.2, the damage indices for several cases are greater than two.

Moreover, the fracture mechanics data acquired under different constant amplitude load levels in Section 3.2.2.4 shows a linear correlation between crack length and number of cycles in the range of 10-90% of fatigue life independent of the applied load level. Hence, if the length of the dominant crack in the joint which leads to the final failure is considered as the total damage, the damage accumulation for the examined joints occurs in a linear manner and only a model that takes into account the retardation and acceleration phenomena is able to accurately predict the remaining fatigue life. Therefore the application of nonlinear models to the examined joints not only provides inaccurate results but is also physically meaningless. A detailed testing program including all the parameters involved such as the load level ratio ($L_{max1}/L_{max2}$), length of the first loading block, and applied load ratio ($R$) should be investigated to develop a damage accumulation model that takes load sequence effects into account.

### 6.3.2. Load transition effect

The consistency of the damage indices in Table 6.3 for the tensile loading block shows the strong damaging effect of the number of transitions on the fatigue life in spite of the small number of experimental data and loading cases available. The damage indices decreased for the sequences starting with the high load level (R01B7040xxx) from 1.913 to 0.741 or for sequence R01B4070xxx from 0.837 to 0.153 when the number of transitions was increased. Also for the R01B7040xxx sequence both of these values are lower than the calculated damage index for similar loading conditions but with only one transition (R01FxxB7040xx) i.e. 4.040, 4.554 and 6.173 (given in Table 6.1). Although the applied sequences in these experiments are repeated several times, it seems that there is still a minor effect of the starting loading block consistent with the loading sequence effect discussed in Section 6.3.1. For both high and low transition cases the damage indices corresponding to the experiments starting with higher load levels, 0.741 and 1.913, are greater than the sequences that started with low load levels, i.e. 0.153 and 0.837.

The number of load transitions has a greater damaging effect under compressive fatigue loading. The damage indices given in Table 6.4 for the high transition cases (R10BxxxxH01), independent of the applied load levels, are lower than for the low transition experiments (R10BxxxxL01). Furthermore, the Palmgren-Miner indices for all experiments are less than 0.4, which indicates a stronger effect of the number of loading transitions than the loading sequence effect. In contrast to the tensile fatigue loading, the effect of loading sequence is completely eliminated for compressive loading when the number of transitions is increased.

## 6.4. Conclusions

The effect of loading sequence and number of load transitions on the fatigue behavior of adhesively-bonded pultruded GFRP double-lap joints was experimentally examined under different loading patterns. The results showed a strong sequence effect for a low transition number and its dependency on the type of loading and consequently the failure mode. The following conclusions can be drawn from this chapter:

- The failure modes of bonded joints under different BL patterns were consistent with the failure modes under similar patterns of CA loading.
- A significant loading sequence effect was identified by applying two-block loading sequences. The results showed that the sequence effect is a function of type of loading and the applied load levels. The L-H sequences were found to be more damaging than the H-L sequences under tensile loading, while under compressive loading this trend was reversed.
- The effect of loading sequence on the fatigue life of the examined joints was associated with the crack growth rate during the applied loading blocks. The H-L tensile loading blocks led to retardation of crack growth rate while acceleration was observed under L-H sequences. In contrast, the crack growth rate under L-H compressive loading blocks did not increase significantly when the load level was increased and led to longer fatigue life. However, under the H-L sequences the first loading block did not affect the expected crack propagation rate under the second loading block. The difference in sequence effects under tension and compression was attributed to the difference in failure modes.

- The frequent change of load levels showed a very strong damaging effect compared to the sequence effect. The sequence effect is therefore diminished when the number of transitions is increased. Thus this parameter is more critical than the sequence effect in fatigue life prediction under complex loading patterns.
- The Palmgren-Miner rule was found to be inadequate for estimating the accumulated damage under block loading sequences. However, application of the developed nonlinear models for composite materials is also questionable for the examined bonded joints since the fracture mechanics data show no sign of nonlinear damage accumulation under fatigue loading. Therefore a detailed study including all parameters involved is required in order to develop a reliable damage accumulation model.

## 6.5. References

1. Broutman LJ, Sahu S. A new theory to predict cumulative fatigue damage in fibreglass reinforced plastics, In: Composite materials: testing and design (2nd Conference), pp. 170-188, ASTM STP 497, American Society for Testing and Materials, Philadelphia (1972).
2. Yang JN, Jones DL. Effect of load sequence on the statistical fatigue of composite, AIAA journal, 1980;18(12):1525–1531.
3. Yang JN, Jones DL. Load sequence effects on graphite/epoxy $[\pm 35]_{2s}$ laminates. In: Long-term behavior of composites, pp. 246–262, ASTM STP 813, American Society for Testing and Materials, Philadelphia (1983).
4. Jen MHR, Kau YS, Wu IC. Fatigue damage in a centrally notched composite laminate due to two-step spectrum loading, Int J Fatigue, 1994;16(3):193–201.
5. Found MS, Kanyanga SB. The influence of two-stage loading on the longitudinal splitting of unidirectional carbon-epoxy laminates, Fatigue Fract Engng Mater Struct, 1996;19(1):65–74.
6. Otani N, Song DY. Fatigue life prediction of composite under two-step loading, J Mater Sci, 1997;32(3):755–760.
7. Bartley-Cho J, Lim SG, Hahn HT, Shyprykevich P. Damage Accumulation in Quasi isotropic Graphite/Epoxy Laminates under Constant-Amplitude Fatigue and Block Loading, Compos Sci Technol, 1998;58(9):1535–1547.

8. Wahl NW, Mandell JF, Samborsky DD. Spectrum fatigue lifetime and residual strength for fiberglass laminates in tension, ASME Wind Energy Symposium, AIAA-2001-0025, ASME/AIAA, 2001.
9. Van Paepegem W, Degrieck J. Effects of Load Sequence and Block Loading on the Fatigue Response of Fibre-reinforced Composites, Mech Adv Mater Struct, 2002;9(1):19–35.
10. Hosoi A, Kawada H, Yoshino H. Fatigue characteristic of quasi-isotropic CFRP laminates subjected to variable amplitude cyclic loading of two-stage, Int J Fatigue, 2006;28(10 SPEC. ISS.):1284–1289.
11. Han KS, Abdelmohsen MH. Fatigue Life Scattering of RP/C, Int J of Vehicle Design, Technological advances in Vehicle Design Series, SP6, Designing with Plastics and Advanced Plastic Composites, 1983;218–227.
12. Hwang W, Han KS. Statistical study of strength and fatigue life of composite materials. Composites, 1987;18(1):47–53.
13. Hwang W, Han KS. Fatigue of composite materials – Damage model and life prediction. Composite Materials: Fatigue and Fracture, 2nd Volume. pp. 87–102, ASTM STP 1012, American Society for Testing and Materials, Philadelphia (1989).
14. Lee CH, Jen MHR. Fatigue response and modelling of variable stress amplitude and frequency in AS-4/PEEK composite laminates, Part 1: Experiments, J Compos Mater, 2000;34(11):906–929.
15. Lee CH, Jen MHR. Fatigue response and modelling of variable stress amplitude and frequency in AS-4/PEEK composite laminates, Part 2: Analysis and formulation, J Compos Mater, 2000;34(11):930–953.
16. Gamstedt EK, Sjögren BA. An experimental investigation of the sequence effect in block amplitude loading of cross-ply laminates, Int J Fatigue, 2002;24(2-4):437–446.
17. Adam T, Gathercole N, Reiter H, Harris B. Life prediction for fatigue of T800/5425 carbon-fibre composites: II. Variable amplitude loading, Int J Fatigue, 1994;16(8):533–547.
18. Harris B, Gathercole N, Reiter H, Adam T. Fatigue of carbon-fibre reinforced plastics under block-loading conditions, Compos Part A-Appl S, 1997;28(4):327–337.
19. Lee BL, Liu DS. Cumulative damage of fiber-reinforced elastomer composites under fatigue loading, J Compos Mater, 1994;28(13):1261–1286.

20. Bonnee WJA. NLR investigation of polyester composite materials, C.W. Kensche, Editor, Fatigue of materials and components for wind turbine rotor blades. German Aerospace Establishment, European Commission-EUR 16684 (1996), pp. 39–70.
21. Found MS, Quaresimin M. Two-stage fatigue loading of woven carbon fibre reinforced laminates, Fatigue Fract Engng Mater Struct, 2003;26(1):17–26.
22. Plumtree A, Melo M, Dahl J. Damage evolution in a $[\pm 45]_{2S}$ CFRP laminate under block loading conditions, Int J Fatigue, 2010;32(1):139–145.
23. Schaff JR, Davidson BD. Life prediction methodology for composite structures. Part I. Constant amplitude and two-step level fatigue, J Compos Mater, 1997;31(2):128–157.
24. Schaff JR, Davidson BD. Life prediction methodology for composite structures. Part II - Spectrum fatigue, J Compos Mater, 1997;31(2), 158–181.
25. Filis PA, Farrow IR, Bond IP. Classical fatigue analysis and load cycle mix-event damage accumulation in fibre reinforced laminates, Int J Fatigue, 2004;26(6): 565–573.
26. Erpolat S, Ashcroft IA, Crocombe AD, Abdel-Wahab MM. Fatigue crack growth acceleration due to intermittent overstressing in adhesively bonded CFRP joints, Compos Part A-Appl Sci, 2004;35(10):1175–1183.
27. Suresh S. Fatigue of Materials, Cambridge University Press, 1998.
28. Shahverdi M, Vassilopoulos AP, Keller T. A phenomenological analysis of mode I fracture of adhesively-bonded pultruded GFRP joints, Eng Fract Mech, 2011;78(10):2161–2173.
29. Post NL, Case SW, Lesko JJ. Modeling the variable amplitude fatigue of composite materials: a review and evaluation of the state of the art for spectrum loading, Int J Fatigue, 2008;30(12):2064–2086.

# 7 Variable amplitude loading

## *Abstract*

*The fatigue behavior of adhesively-bonded pultruded GFRP joints subjected to variable amplitude loading patterns was experimentally investigated. The failure mode of the examined joints was found to be similar to that under constant amplitude loading. The acceleration or retardation of the crack propagation rate due to the load interaction effects was thoroughly investigated by monitoring crack propagation during the variable amplitude loading. The fatigue life of the joints was predicted using classic fatigue life prediction methodology. Existing models for characterizing the fatigue behavior of the examined joints were employed together with the linear Palmgren-Miner's rule for the prediction of fatigue life. A simple modification was incorporated into the applied methodology to take into account the load interaction effects introduced under the variable amplitude loading.*

## 7.1. Introduction

Several experimental investigations of the fatigue behavior of composite laminates show their sensitivity to the loading sequence. Experiments composed of two blocks of constant amplitude loading passing from a low stress level to a higher stress level (L-H sequence) or vice versa (H-L sequence) have usually been employed to study the sequence effect in composite materials. However the results obtained from these experiments were not consistent and showed a greater damaging effect due to the L-H sequence, e. g. [1-10] or the opposite behavior, e. g. [11-16] depending on the material and loading parameters. These conclusions are mainly drawn based on comparison with the constant amplitude fatigue life and little information concerning the failure mechanisms that cause sequence effects is available [16-18].

Only a small number of studies have been performed on the variable amplitude (VA) fatigue behavior of bonded joints and they are mainly related to bonded joints with metallic adherends [19-26]. Regardless of the adherend material, the load interaction effects such as load transition, load sequence and overload effects have been reported on in different investigations. The overloads can accelerate the fatigue crack initiation [23] or increase the damaging effect of the following cycles of lower amplitude although their effect is reduced when the number of low amplitude cycles following the overloads is increased [25]. The change of mean load can also accelerate the crack growth in bonded composite joints [23]. The significant damaging effect of introducing a small number of cycles at a higher mean load was also addressed [26]. The load interaction effect was also observed for the examined bonded joints in Section 6.

The aforementioned retardation or acceleration of the fatigue crack growth rate due to load interactions is common for metals, where one dominant crack mainly governs the fracture behavior. In composite materials, which exhibit several contributing fatigue failure mechanisms, identification of a single dominant crack for this investigation is difficult. The situation is less complicated for adhesively-bonded lap joints under cyclic loading however since experimental observation in previous investigations, e.g. [27], showed that in several cases only one dominant crack led to final failure even for joints composed of composite materials. Therefore, for adhesively-bonded joints, the load interaction effects can be correlated with the acceleration or retardation in the propagation rate of the dominant crack, consequently providing explanations regarding the fatigue behavior under VA loading.

The accuracy of available models for the calculation of accumulated damage in materials subjected to fatigue loading depends on the materials and loading conditions. One of the frequently used models for this purpose is the Palmgren-Miner rule due to its simplicity. Based on this model, the damage is accumulated independently of the loading sequence and load history. However, an overestimation of the fatigue life of bonded joints under VA loading by this model was related to the damage acceleration effect due to the load interaction [23, 25, 26, 28]. When applied to bonded wood joints [21], the Palmgren-Miner rule provided fairly conservative results while for CFRP/aluminum scarf joints under random loadings [19] it underestimated and overestimated fatigue life respectively at higher and lower stress levels.

As an alternative to the Palmgren-Miner rule, several conceptually different approaches were introduced for composites and joints based on the stiffness and strength degradation of the materials [29, 30] in order to better describe the damage accumulation in composite materials. Nonetheless, comparative studies between non-linear models and the Palmgren-Miner rule showed no significant improvement of the life prediction [31], and thus the additional experimental effort required for the application of the non-linear models [32] is not justified. In the field of fracture mechanics it was also pointed out that due to the dependency of crack growth on the load history, conventional fracture mechanics based on crack growth integration methods is no longer adequate to predict the VA fatigue life of bonded joints [24].

The concept of the “cycle mix factor” was incorporated into life prediction methodologies [33-35] to take into account the load transition effects on the lifetime estimation of composite laminates. This “cycle mix factor” was determined empirically based on a small number of block loading experiments. A similar concept was presented in [23] for the life prediction of adhesively-bonded composite joints loaded under different variable amplitude spectra. The “cycle mix” effect [23] was employed to explain the observed behavior of the examined joints, and improve the life modeling under variable amplitude spectra. Nevertheless, its use is limited for life prediction since it requires variable amplitude experimental results for estimation of the model parameters.

The above review shows that several parameters significantly affect fatigue behavior under variable amplitude loading. The systematic investigation of the effect of these parameters is therefore necessary for the establishment of reliable fatigue life prediction methodologies. The fatigue behavior of adhesively-bonded pultruded GFRP joints under VA loading is studied in this chapter. The failure process of the examined joints is thoroughly investigated and the acquired data concerning the crack initiation and propagation are analyzed in order to explore the load interaction effects. A phenomenological fatigue life prediction methodology is established, based on the constant amplitude data, and fatigue life predictions are compared with relevant variable amplitude fatigue data. A modification is introduced based on the experimental observation to take into account the effect of load transition on fatigue behavior. Comparison of the theoretical predictions with the experimental data demonstrates the improvement of the methodology thanks to this modification. The experimental program and set-up designed for this study is described in Chapter 2.

## 7.2. Experimental results

### 7.2.1. Failure modes

The failure mode observed for all specimens is shown in Figs. 7.1a and 7.1b for specimens with and without crack gages. A dominant crack initiated from the joint corner of one of the bond lines (upper one in Figs. 7.1a and 7.1b) between the adhesive and the inner laminate and then shifted deeper, between the first and second mat layers of the inner laminate, and propagated along this path up to failure. The cracks observed along the lower bond line and at the left side of the specimen between the adhesive and outer laminate are secondary cracks that occurred only after the failure of the specimen. Since the variable amplitude loading spectrum mainly consisted of tension-tension cycles and comprised only a few cycles crossing the zero level to negative loads (see Fig. 2.8), the failure mode was the same as that under tension-tension constant amplitude loading reported in Section 3.2.2.1.

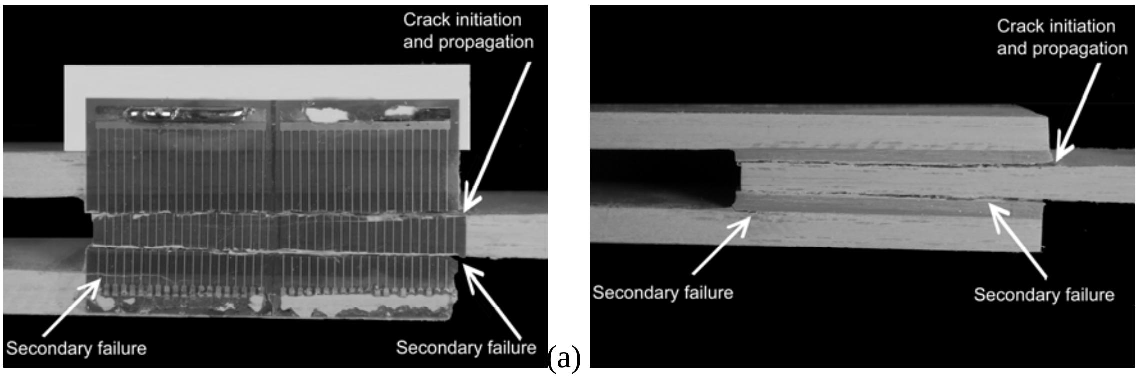

(a) (b)

Fig. 7.1. Failure mode under variable amplitude loading (a) with and (b) without crack gages

### 7.2.2. Fatigue life and crack propagation

The VA fatigue lives obtained for the examined joints under the WISPERX spectrum with different load levels are presented in Table 7.1. The fatigue life is given both in terms of number of spectrum passes ($N_p$), and total number of cycles ($N_f$) to failure. The scatter of fatigue life at 18 kN was relatively high. However no significant difference between failure modes at this load level was observed and therefore all data point were kept in the database. The crack lengths vs. the normalized number of cycles are shown in Fig. 7.2 for one specimen per load level that was equipped with crack gages. A common trend, independent of load level, was observed, showing rapid crack propagation at the beginning (region A), followed by a moderate crack propagation rate represented by a constant slope between ca. 10 and 90%

of fatigue life (region B) and another rapid crack propagation at the end (region C) of the fatigue life.

Table 7.1. Fatigue data under WISPERX spectrum

| Specimen ID | Maximum load level, $F_{max}$ [kN] | No. of spectrum passes to failure, $N_p$ | No. of cycles to failure, $N_f$ |
|---|---|---|---|
| WX2201 | 22.0 | 5.21 | 66805 |
| WX2202 | | 10.26 | 131641 |
| WX2203[a] | | 3.05 | 39091 |
| WX2001 | 20.0 | 23.04 | 295647 |
| WX2002 | | 3.21 | 41142 |
| WX2003[a] | | 14.74 | 189102 |
| WX1801 | 18.0 | 304.74 | 3910140 |
| WX1802 | | 19.12 | 245336 |
| WX1803[a] | | 9.71 | 124628 |
| WX1804 | | 170.92 | 2193086 |
| WX1601 | 16.0 | 201.60 | 2586685 |
| WX1602 | | 80.16 | 1028587 |
| WX1603[a] | | 98.23 | 1260387 |

[a] specimens instrumented by crack gages

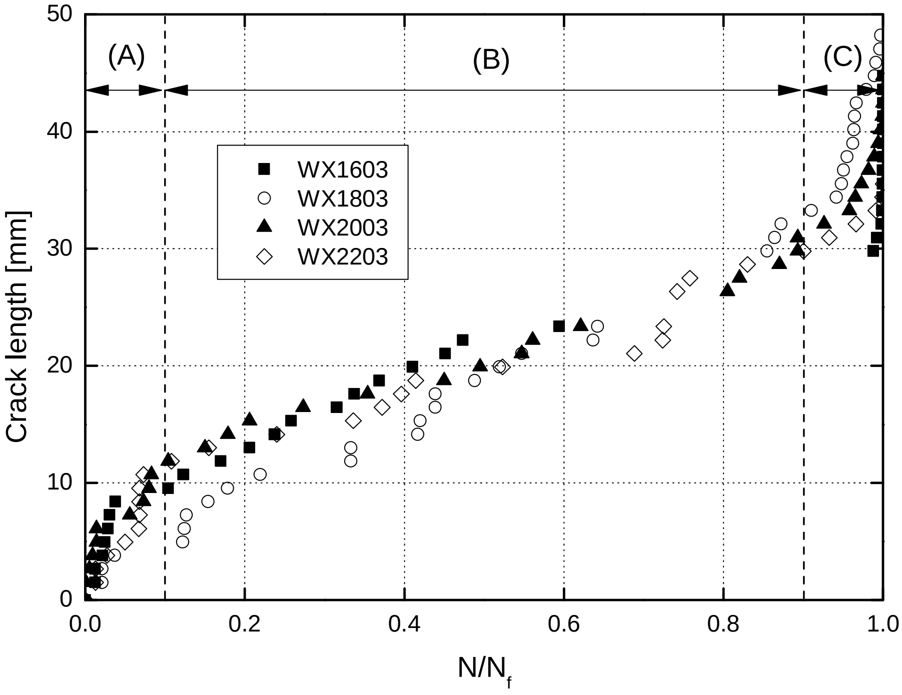

Fig. 7.2. Crack length vs. normalized number of cycles under different load levels

This behavior is similar to the crack propagation observed under constant amplitude loading reported in Section 3.2.2.4 and the similarity shows that this behavior is independent of the applied loading patterns.

Due to the scatter in the fracture mechanics data for composite materials, the incremental polynomial fitting method (according to ASTM E647) is usually preferred to the secant method for the calculation of *da/dN*. Nevertheless, in the present study, the secant method was used to calculate the crack propagation rate to avoid obscuring the possible load interaction effects of the variable amplitude spectrum on the crack propagation rate. According to the secant or point-to-point method, the crack propagation rate is determined by calculating the slope of a straight line connecting two contiguous data points on the *a-N* curve. The details of the derived fracture mechanics data and their relationship with the applied loading spectrum are presented in Figs. 7.3-7.10.

The plots of the crack propagation rate, *da/dN*, against the normalized number of cycles, $N/N_f$, are presented in Figs. 7.3, 7.5, 7.7, and 7.9. They showed a trend consistent with the *a-N* curves presented in Fig. 7.2. The crack propagation rate decreased at the beginning of the life followed by a stable phase with almost constant rate, and finally accelerated at the end of fatigue life. Sharp variations of *da/dN* in the stable phase are likely for composite materials even under constant amplitude loading due to the complex nature of the progressing crack as reported in Section 3.2.2.4. However, the changes observed in the stable phase of crack propagation (region B) were thoroughly analyzed to explore any possible correlation between them and the corresponding periods of the applied spectrum. In Figs. 7.3, 7.5, 7.7, and 7.9, the points that indicate an unusual change in *da/dN*, designated “event”, are marked with capital letters in an ascending order based on the corresponding spectrum passes and the number of cycles they represent. The numbers in brackets denote the spectrum passes of each event. The location of each event in the applied spectrum is shown in Figs. 7.4, 7.6, 7.8, and 7.10.

Fig. 7.3 represents the crack propagation rate under the lowest applied maximum load level (16 kN). Four points marked with letters **A-D** indicate the locations where a significant increase in *da/dN* was observed. Comparison of the loading cycles corresponding to these events, shown in Figs. 7.4a and 7.4b, do not indicate any specific correlation between loading and increase of *da/dN*, except at point **C** where several load transitions occurred before the recording of this increase. However it should be noted that there are several cycles between two adjacent points in Fig. 7.3, e.g. 27450 cycles between point **C** and the previous data point, and the observed increase cannot be directly attributed to the load transitions just before point

**C**. Therefore the variations identified in *da/dN* are attributed to the usual scatter of the fracture data.

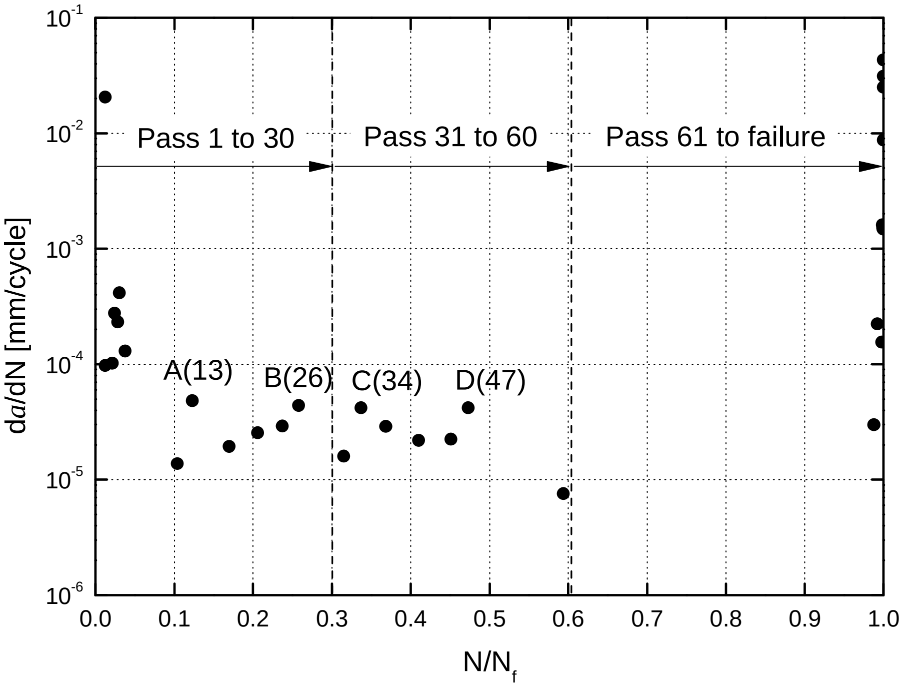

Fig. 7.3. Crack propagation rate vs. normalized number of cycles for WX1603

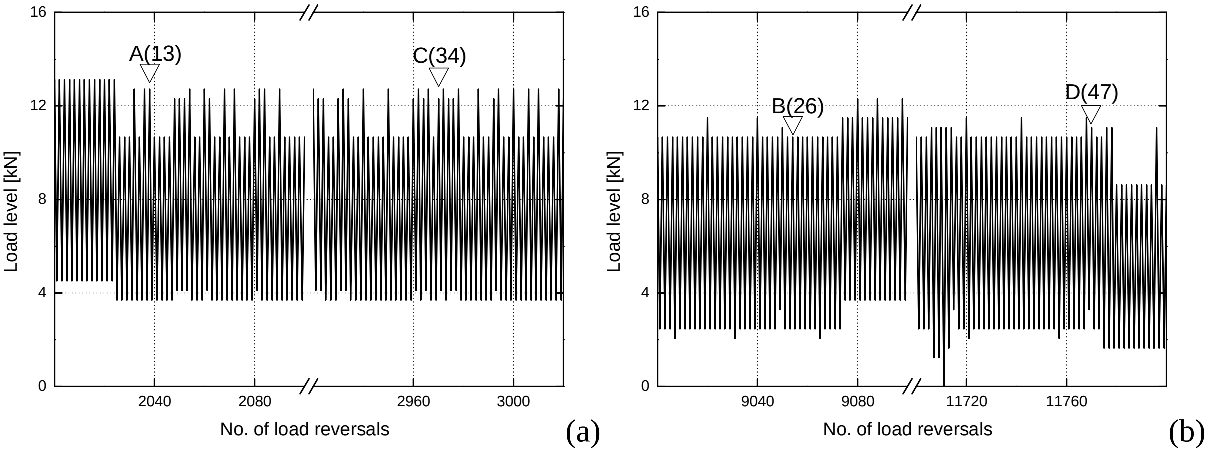

Fig. 7.4. Detailed locations in WISPERX spectrum corresponding to specific events defined in Fig. 7.3 for WX1603

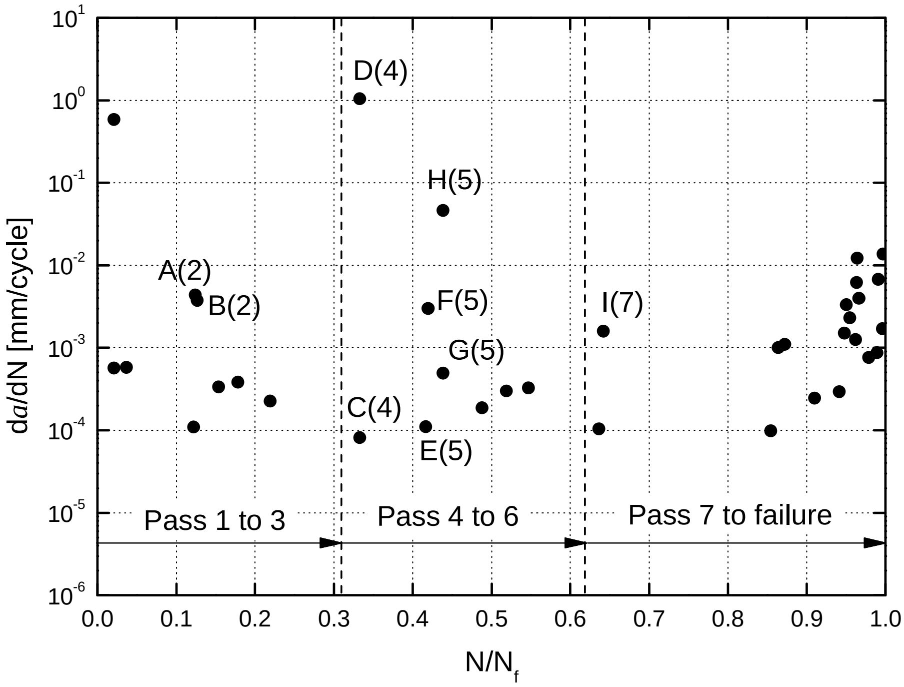

Fig. 7.5. Crack propagation rate vs. normalized number of cycles for WX1803

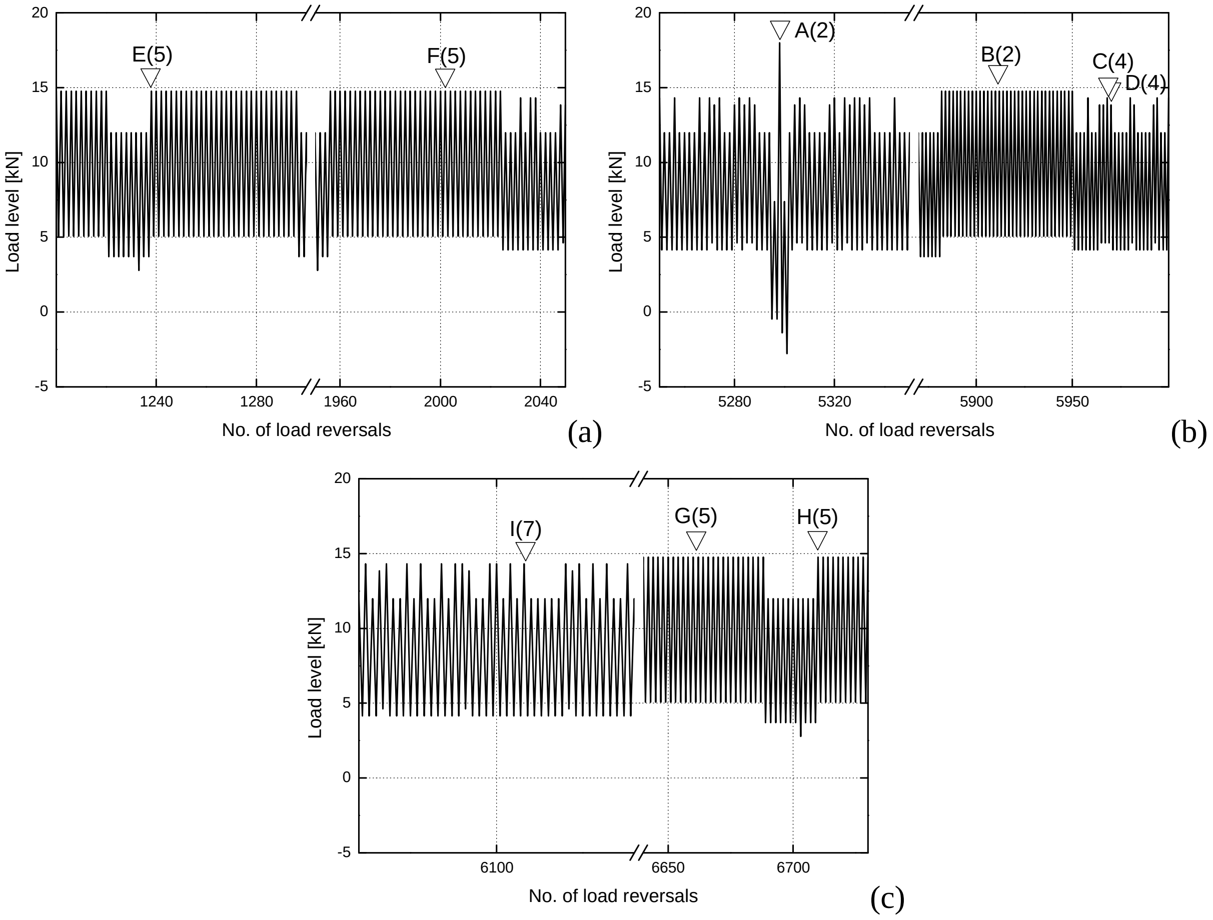

Fig. 7.6. Detailed locations in WISPERX spectrum corresponding to specific events defined in Fig. 7.5 for WX1803

Under the applied spectrum with the maximum load level 18 kN more variations in *da/dN* were observed during the fatigue life and the corresponding locations are denoted with letters **A-I** (see Fig. 7.5). The sudden increase of *da/dN* at point **A** was due to the overload shown in Fig. 7.6b. The high value of *da/dN* at the next data point, **B**, is still attributed to the overload since no particular load variation occurs before point **B** (Fig. 7.6b). The acceleration in *da/dN* between points **C** and **D** occurred after two consecutive load transitions (Fig. 7.6b). At several points, i.e. **C**, **E**, **H**, and **I,** in Figs. 7.6a-c the crack growth was recorded immediately after a load transition. No special characteristic was identified at points **F** and **G**.

A similar behavior is observed at point **D** under the maximum load level 20 kN where the acceleration occurred after several consecutive load transitions with almost 20% increase in maximum load level (see Figs. 7.7 and 7.8a). The event **D** took place 145 cycles after the preceding data point. However no special mechanisms were identified for points **A**-**C** (Figs. 7.8a-b).

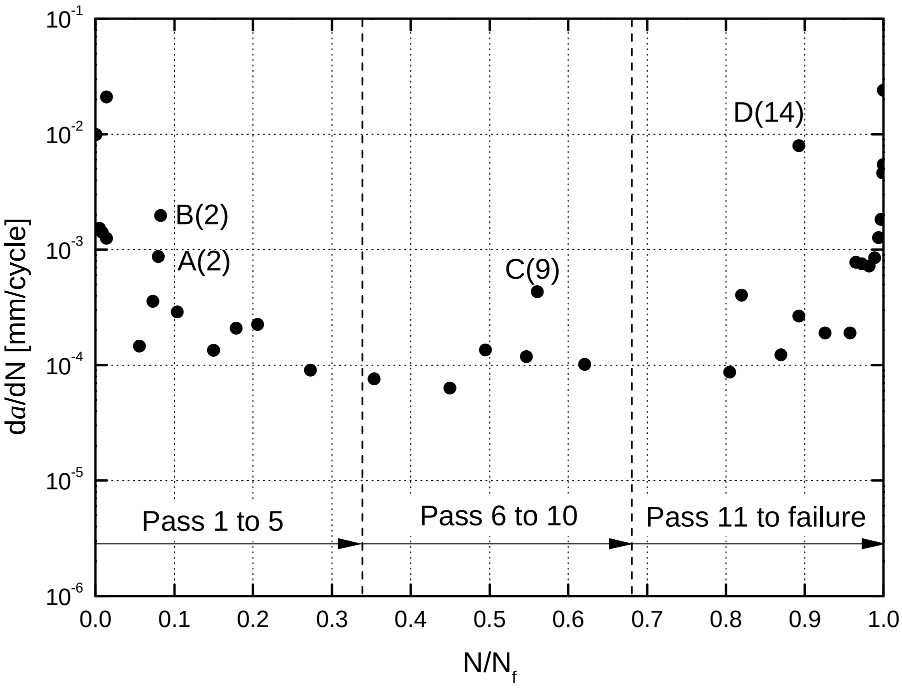

Fig. 7.7. Crack propagation rate vs. normalized number of cycles for WX2003

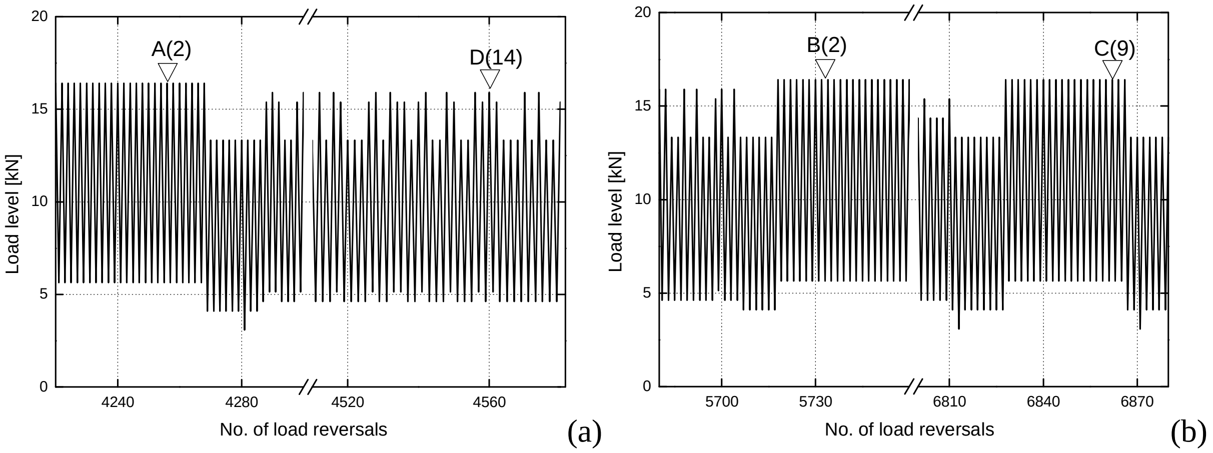

Fig. 7.8. Detailed locations in WISPERX spectrum corresponding to specific events defined in Fig. 7.7 for WX2003

Under the highest maximum load level (22 kN) eight events were identified, as shown in Fig. 7.9. Sudden changes in *da/dN* observed at the beginning of the spectrum coincided with the overload cycles indicated by points **A**, **C**, **E**, and **F** in Fig. 7.10a. Two subsequent events after points **C** and **F**, i.e. **D** and **G**, occurred almost at the same location in the spectrum (Fig. 7.10b) showing that both events, **D** and **G**, still were a consequence of the overload (see also comment regarding Fig. 7.6b).

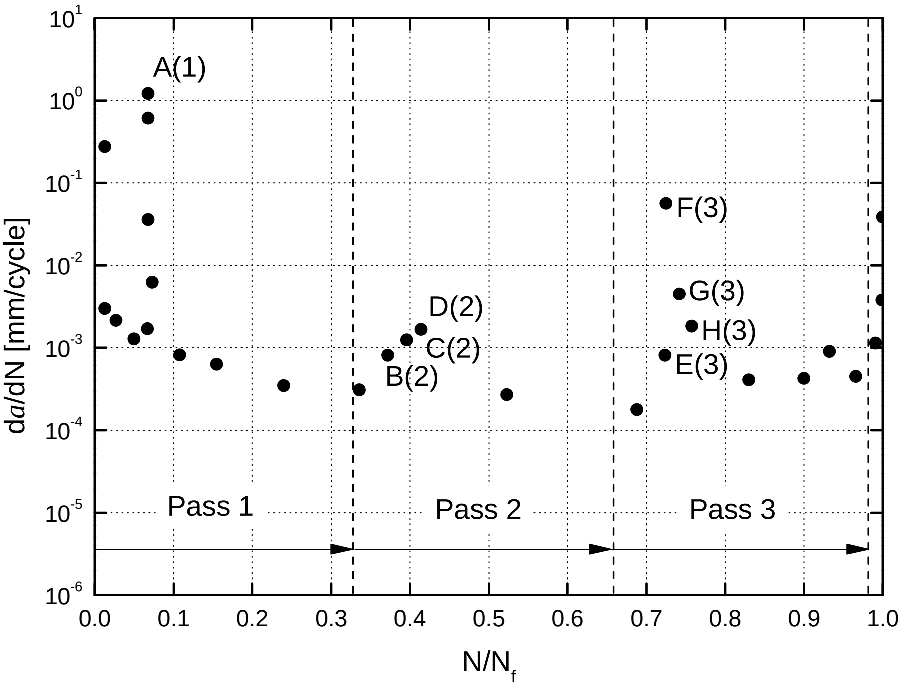

Fig. 7.9. Crack propagation rate vs. normalized number of cycles for WX2203

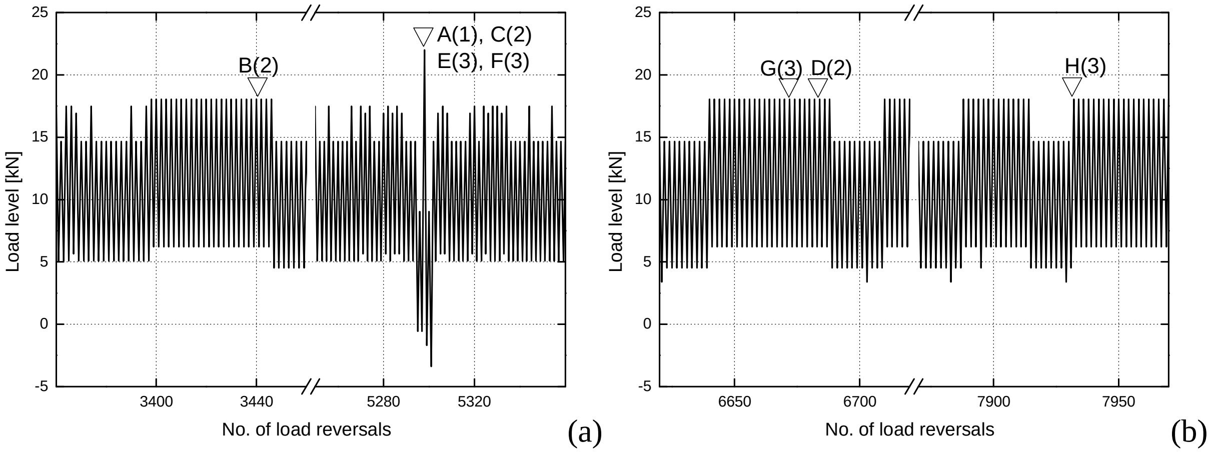

Fig. 7.10. Detailed locations in WISPERX spectrum corresponding to specific events defined in Fig. 7.9 for WX2203

According to the above observations, a sudden increase in the crack propagation rate can be correlated to spectrum overloads. Nevertheless the crack propagation rate returned to the preceding levels after the application of a certain number of additional loading cycles without any observed retardation. Additionally, an increase in *da/dN* after several consecutive load transitions was observed at different locations of the applied spectra (Figs. 7.6b, 7.8a). These interpretations are in agreement with the previous discussion in Chapter 6 where it was reported that frequent load transitions in a block loading spectrum introduced a more damaging effect and obscured the load sequence effects. Therefore, in spite of the various load amplitude changes, the crack growth rate remained almost constant (excluding the sudden jumps due to the overloads) during the stable crack propagation phase (region B in Fig. 7.2) showing a similar trend to that measured under constant amplitude loading.

## 7.3. Modified fatigue life prediction methodology

A modified classic fatigue life prediction methodology was established for estimation of the fatigue life of the examined joints comprising several steps briefly described in the following sections.

### 7.3.1. Cycle-counting methods

Cycle counting is used to summarize irregular load-versus-time histories by providing the number of occurrences of cycles of various sizes. The definition of a cycle varies with the method of cycle counting. Cycle-counting methods known as one-parameter techniques, e.g.

level-crossing counting or peak-counting method, are not applicable for the fatigue analysis of composite materials since they do not consider the significant mean stress effect on lifetime. In the present case, the rainflow counting method, which is a two-parameter method considering both the range and mean value, was used to convert the WISPERX spectrum into blocks of constant amplitude loading. Fig. 7.11 shows the cumulative distribution of loading cycles of the WISPERX spectrum counted by the rainflow method.

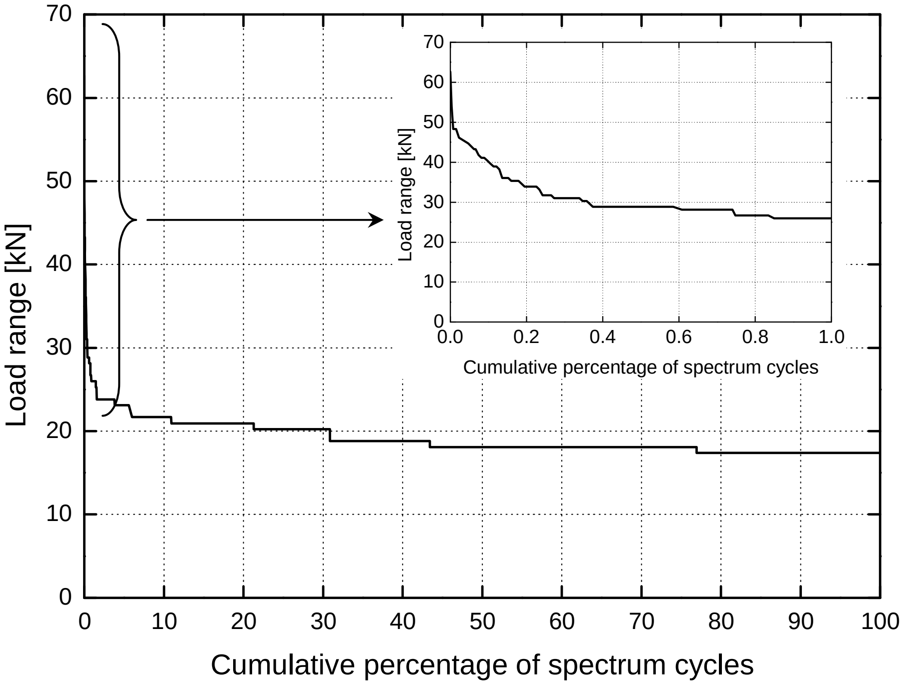

Fig. 7.11. Cumulative spectrum of WISPERX

### 7.3.2. S-N formulations

In Chapter 3, the exponential and power law models were found to be the most appropriate since they are simple and relatively insensitive to the scatter in the experimental data. Nevertheless, the power law model generally overestimates the fatigue life in the Low Cycle Fatigue (LCF) region while it fits the experimental data in the High Cycle Fatigue (HCF) region fairly well. On the other hand, the exponential model underestimates the fatigue life at HCF whereas it successfully estimates the lifetime in the LCF region.

A semi-empirical S-N formulation was developed in Chapter 4, Hybrid S-N, in order to improve the accuracy of these models in the low and high cycle fatigue regions. The constant amplitude fatigue database, employed for the VA life prediction, comprised experiments under three different load ratios, $R$ (the ratio of the minimum to maximum applied cyclic load), i.e. $R$=0.1, -1, and 10 (see Fig. 7.12). The modeling results from the hybrid S-N formulation followed the trend of experimental data in the low and high cycle regions, independent of the *R*-ratio, and this model was therefore used.

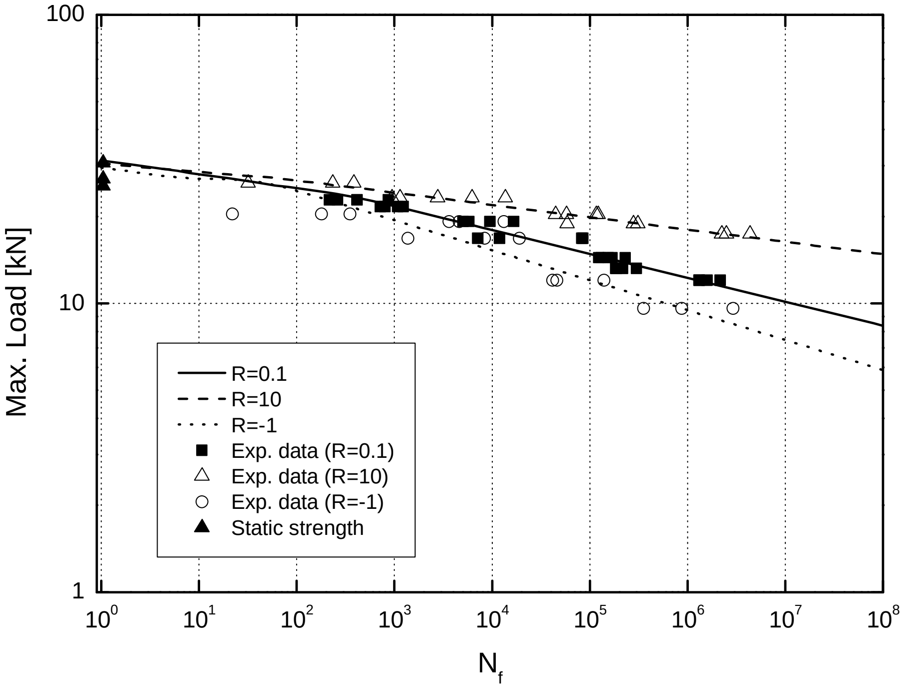

Fig. 7.12. Load-life experimental data and hybrid S-N curves under different loading conditions

### 7.3.3. Constant life diagrams

Constant life diagrams (CLDs) are used in fatigue analysis to take into account the effect of mean stress on the fatigue behavior of composite materials. They provide a tool for the theoretical calculation of S-N curves under, virtually, any constant amplitude loading pattern. The effect of mean load on the fatigue behavior of the examined bonded joints was experimentally investigated under different loading conditions in Chapter 5. The constant life diagram derived for the examined bonded joints was asymmetric and shifted toward the compressive domain.

The CLD formulation proposed in Chapter 5 for modeling the mean load effect on the fatigue behavior of the examined bonded joints (POLY), in addition to three common CLD models for composite materials: the piecewise linear (PWL) [37], the piecewise non-linear (PNL) [38], and the Boerstra (BR) [39], were employed for the estimation of fatigue life under unknown loading conditions. The CLDs constructed based on these formulations are shown in Fig. 7.13a-d. For all CLDs three sets of fatigue data (*R*=0.1, –1, and 10) were employed for modeling. Data used for the estimation of model parameters are designated by open triangles, while data used for the model validation are designated by closed circles in all figures.

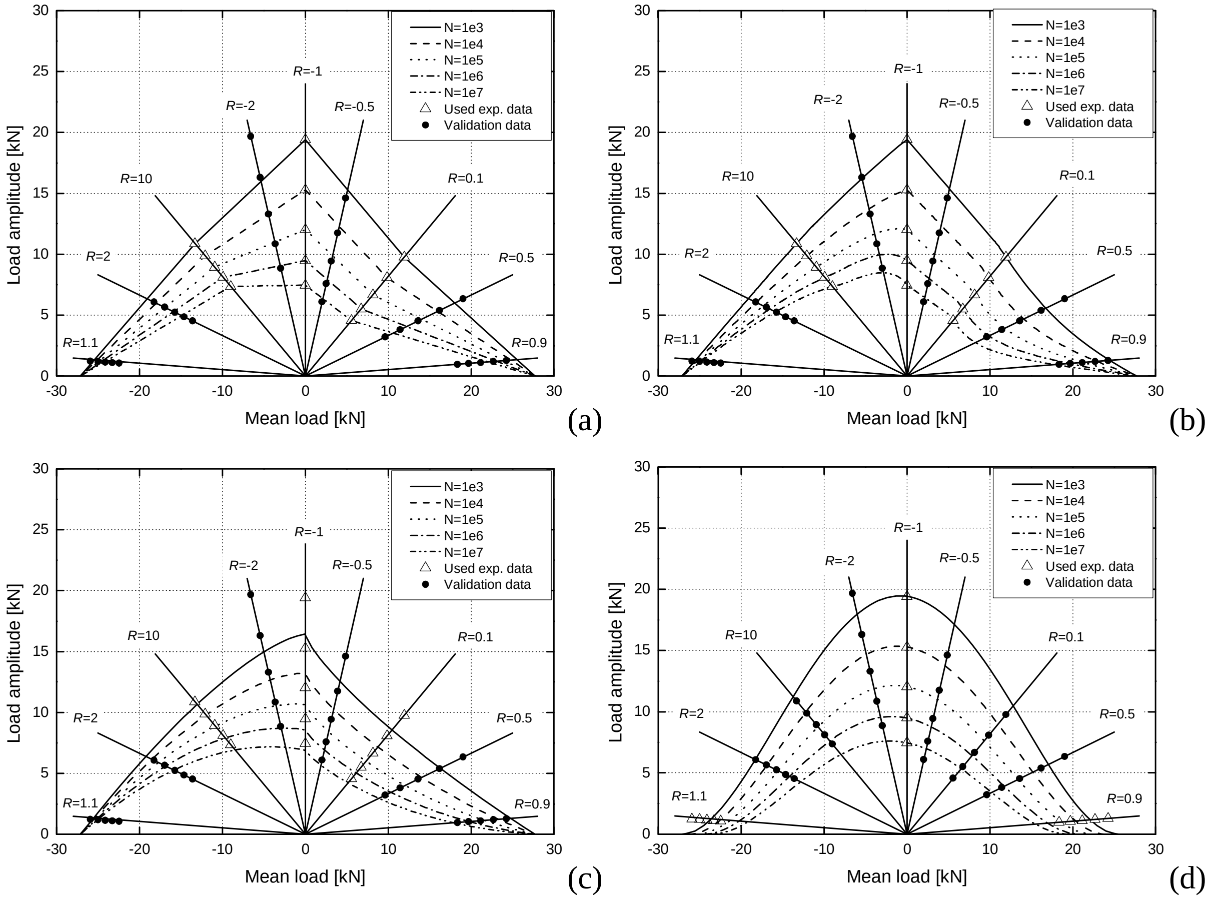

Fig. 7.13. Piecewise linear (a), piecewise nonlinear (b), Boerstra (c), and Polynomial (d) constant life diagrams

## 7.3.4. Damage summation

The last step of the presented methodology concerns the damage summation. The linear Palmgren-Miner rule, although presenting certain disadvantages as discussed in Section 7.1, was used as the damage accumulation rule. The linear Palmgren-Miner rule is presented in Eq. (7.1) for *k* loading blocks:

$$D = \sum_{i=1}^{k} \frac{n_i}{N_i} \qquad (7.1)$$

where $D$ is the damage index and $n_i$ and $N_i$ are the applied number of cycles in each loading block and the allowable number of cycles under the applied load level respectively. Based on this model, the specimen under a cyclic loading pattern fails when the damage index reaches one.

### 7.3.5. Effect of frequent load transition

The previous study of the examined bonded joints in Chapter 6 showed that the fatigue behavior of these structural components is sensitive to the loading sequence. Also, it was concluded that the frequent change of maximum load level (load transition), which is an inherent characteristic of a VA spectrum, has a detrimental effect that obscures the loading sequence effects. However, the load transition and sequence effects are not explicitly considered in the existing classic life prediction methodologies. A simple approach to take into account the effect of the number of load transitions was incorporated into the life prediction methodology to provide a more realistic prediction.

A new fatigue damage parameter is defined based on the number of load transitions under fatigue loading. The damage introduced by this parameter can be determined based on a small number of simple block loading experiments such as those presented in Chapter 6. A load transition is counted in the spectrum when the increase of the maximum load level in two consecutive cycles is more than 20% of the maximum load of the first cycle. This definition is based on the experimental evidence from block and variable amplitude loading. Under block loading, as presented in Chapter 6, the minimum variation in load level between different loading blocks was 50%. However, as discussed in Section 7.2.2, smaller variations, even of 20%, can also cause similar damaging effects. According to the described approach, the deviation of the Palmgren-Miner damage index from unity is assumed to be due to the load transition effect. The damage introduced due to each transition in the block loading, $D_{trans}$, is defined as Eq. (7.2),

$$D_{trans} = (1 - D)/NT \qquad (7.2)$$

where $NT$ denotes the number of transitions in the applied block loading and $D$ is the corresponding Palmgren-Miner damage index.

The block loading (tension-tension) experimental results from Chapter 6, showing the number of transitions ($NT$) and estimated damage indices ($D$), are presented in Table 7.2 together with the $D_{trans}$ calculated according to Eq. (7.2). The variation of $D_{trans}$ against the number of transitions is shown in Fig. 7.14. Although only a small number of experimental data were used, $D_{trans}$ exhibits a decreasing trend with the increase of the number of transitions following the power law relationship given in Eq. (7.3).

$$D_{trans} = 0.0775 NT^{-0.6442} \qquad (7.3)$$

Table 7.2. Calculated damage per transition for different type of loading

| Type of loading | No. of transitions ($NT$) | Damage/transition ($D_{trans}$) |
|---|---|---|
| Two-block / L-H | 1 | 0.062 |
| Multi-block / L-H (Low transition) | 19 | 0.009 |
| Multi-block / L-H (High transition) | 34 | 0.025 |
| Multi-block / H-L (High transition) | 165 | 0.002 |

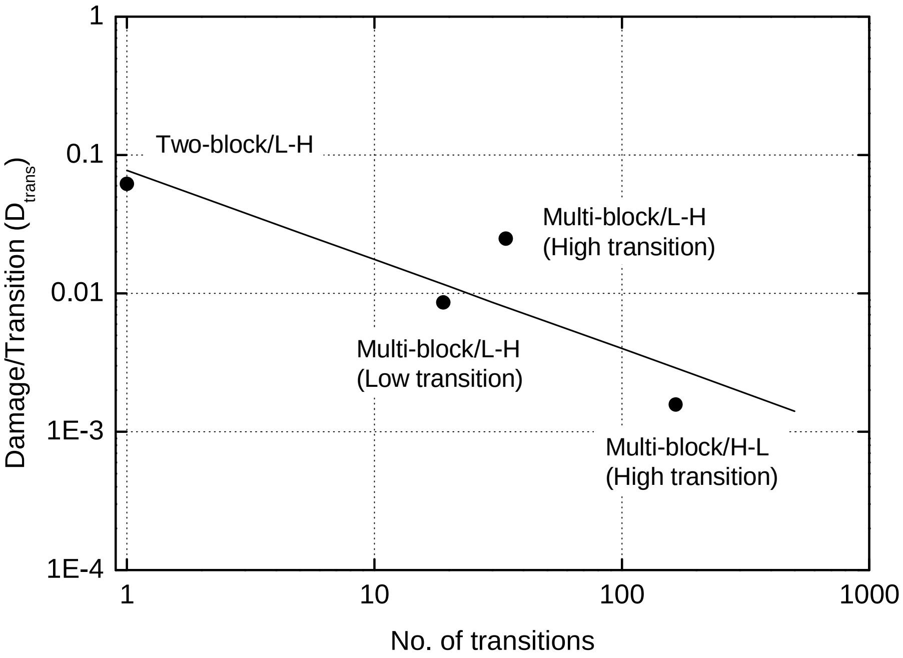

Fig. 7.14. Variation of introduced damage per load transition with number of load transitions

If the relationship between $D_{trans}$ and $NT$ is defined, the damage due to the transition effect of variable amplitude spectra can be calculated. The total number of transitions in a variable amplitude experiment is equal to the number of spectrum passes to failure (*passes*), as predicted by the Palmgren-Miner rule, multiplied by the number of transitions in each spectrum ($NT_{pass}$), see Eq. (7.4).

$$NT = passes \times NT_{pass} \tag{7.4}$$

Therefore, the damage due to one transition ($D_{trans}$) is calculated using Eq. (7.3) and consequently the total damage due to the load transitions in one spectrum ($D_{trans}^{pass}$) is calculated using Eq. (7.5):

$$D_{trans}^{pass} = NT_{pass} \times D_{trans} \tag{7.5}$$

Accordingly, a modified damage index ($D_{mod}^{pass}$) and fatigue life (*passes<sub></sub>*$_{mod}$), in terms of number of spectrum passes, ($passes_{mod}$) can be calculated using Eqs. (7.6) and (7.7).

$$D_{mod}^{pass} = D^{pass} + D_{trans}^{pass} \tag{7.6}$$

$$passes_{mod} = \frac{1}{D_{mod}^{pass}} \tag{7.7}$$

## 7.4. Results and discussion

The similarity between the failure modes under constant, block, and variable amplitude loading facilitates the use of constant amplitude and block loading fatigue data for the prediction of fatigue life under variable amplitude loading. The fatigue life under the WISPERX spectrum predicted by the existing classic methodology (excluding the effect of frequent load transitions) is compared with the experimental data in Fig. 7.15.

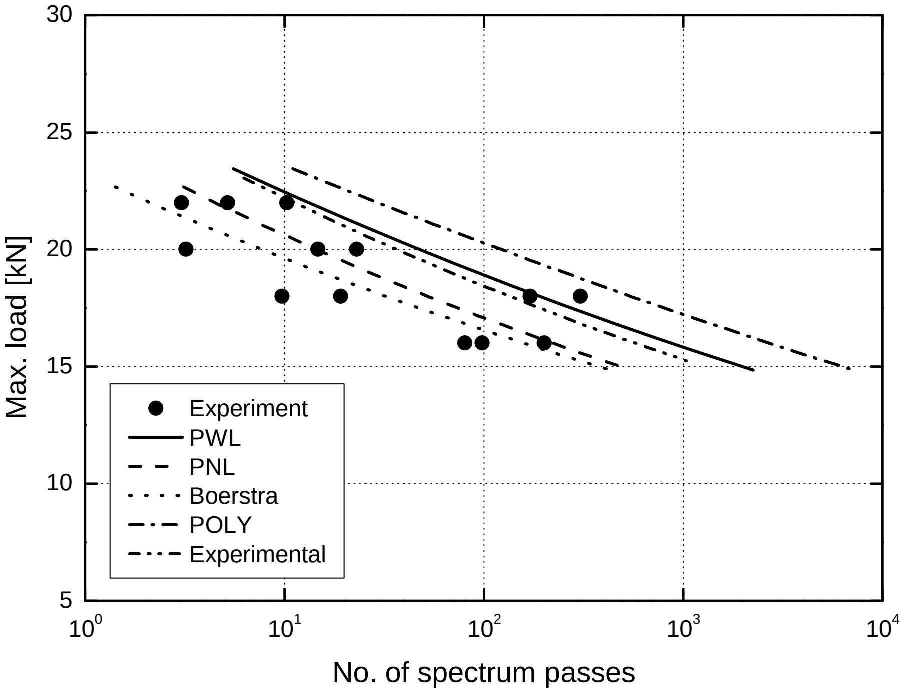

Fig. 7.15. Comparison of life prediction of bonded joints under WISPERX spectrum using different CLDs with experimental data

The curves represent the predictions obtained from using the above mentioned CLDs and also the experimental constant life diagram (PWL CLD constructed using all *R*-ratios). The VA fatigue life predictions using each CLD is conservative or not depending on the degree of conservatism presented by the corresponding CLD model in the relevant regions, as shown in Fig. 7.13a-d. These regions correspond to the locations of loading blocks of constant amplitude counted by the rainflow method, as presented in the mean-amplitude diagram for the WISPERX spectrum in Fig. 7.16. The loading blocks are mainly clustered around the $R$=0 and the average of their $R$-ratios is $R$=0.247. The graph clearly shows that the accuracy of CLD models in the region between $R$=0.5 and $R$=-1 (-1<$R$<0.5) is critical for the appropriate interpretation of the results. The comparisons in Fig. 7.13a-d show that the Boerstra CLD is conservative in the range -1<$R$<0.5 and the PNL CLD in the range 0<$R$<0.5. The PWL CLD is fairly accurate in the range -1<$R$<0.5 and the POLY CLD provides to a certain extent a non-conservative prediction in the right quarter.

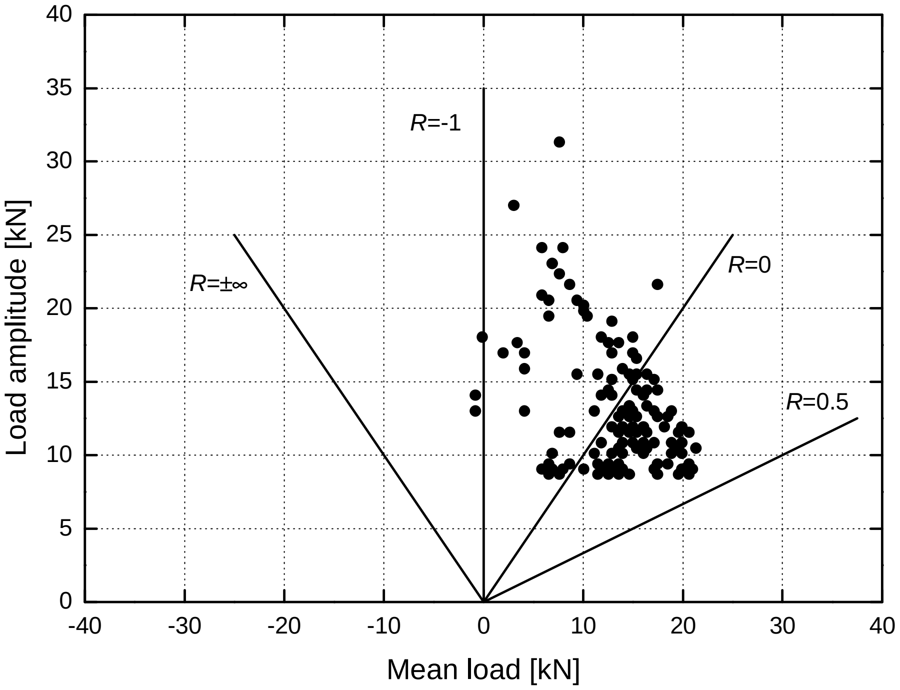

Fig. 7.16. Distribution of constant amplitude blocks for rainflow-counted WISPERX spectrum

However, the conservative models, Boerstra and PNL, provide accurate life predictions while the life predictions of the accurate model (PWL) and the experimental CLD (as the most accurate CLD, since it is based on the entire database) overestimate the fatigue life, especially in the HCF region. This can be attributed to the load interaction effects under variable amplitude loading. In the applied classic life prediction methodology the load interaction effect is neglected. The VA spectrum is simply converted to the constant amplitude loading blocks and all information concerning the loading sequence effect and load transitions is discarded.

The modified life predictions (*passes*$_{mod}$) including the introduced damage due to the load transitions, as described in the previous section, are shown in Fig. 7.17. The obtained life predictions are consistent with the accuracy of the CLD models in contrast to the previous ones. The Boerstra and PNL formulations provide conservative life predictions, the PWL fairly accurate, while the POLY formulation leads to relatively non-conservative life predictions.

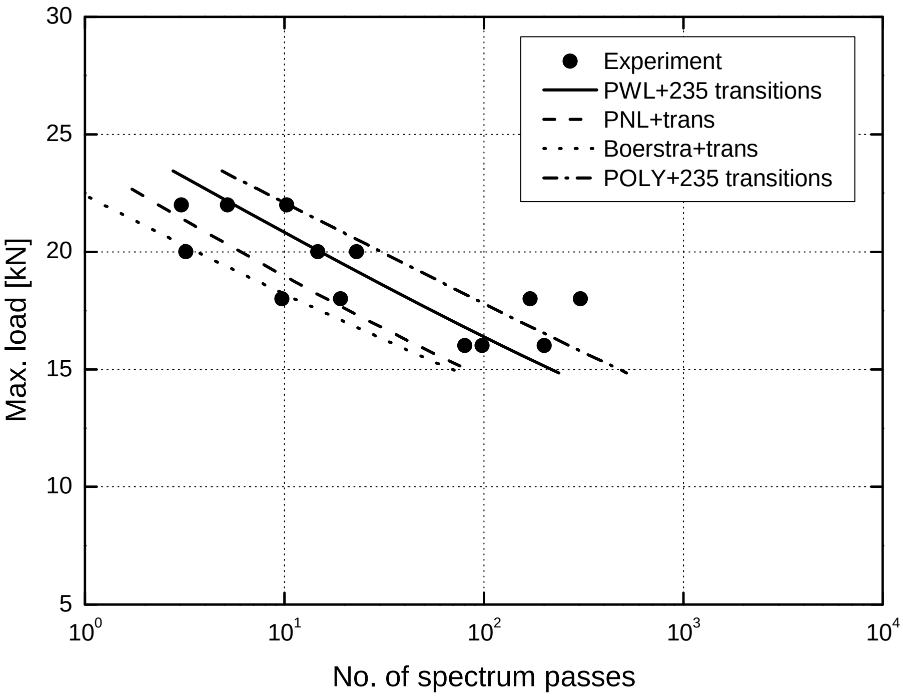

Fig. 7.17. Comparison of corrected life prediction of bonded joints under WISPERX spectrum using different CLDs with experimental data

The number of transitions counted in the applied spectrum, WISPERX, based on the definition mentioned in the previous section is 235. The sensitivity of the applied modification to the number of load transitions is analyzed using the PWL CLD in Fig. 7.18. The number of transitions in the WISPERX spectrum according to a 20%, 30% and 40% increase in maximum load level in two consecutive cycles was $NTS$=235, $NTS$=85 and $NTS$=37 respectively. As shown in Fig. 7.18, by increasing the number of transitions the estimated variable amplitude fatigue life is reduced. Nevertheless, this reduction is much less than the life reduction obtained when the transition effect is incorporated into the life prediction algorithm.

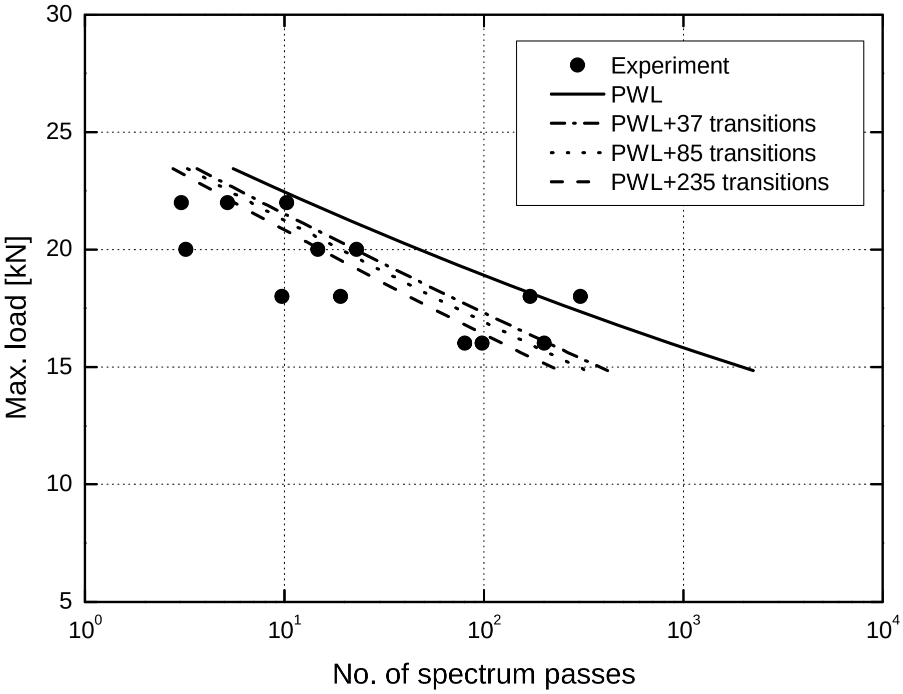

Fig. 7.18. Comparison of corrected life prediction using PWL CLD with different number of transitions

## 7.5. Conclusions

The fatigue behavior of adhesively-bonded pultruded GFRP double-lap joints under variable amplitude loading conditions was experimentally investigated. The crack propagation data recorded during the cyclic loading were used to analyze the effects of load interactions on the variable amplitude fatigue behavior of the examined joints. A simple modification of the damage summation rule was proposed to improve the accuracy of the classic life prediction method. The modified method can accurately predict fatigue life under variable amplitude loading patterns using only a small number of constant amplitude and block loading experimental data. The following conclusions can be drawn from this chapter:

- The failure mode of bonded joints under variable amplitude loading patterns was the same as the previously identified failure modes under constant amplitude loading, allowing the CA loading experimental results to be used for prediction of the fatigue life of the examined joints under variable amplitude loading.
- Three stages in the crack propagation behavior of the examined bonded joints under VA loading were identified: rapid crack propagation at the beginning, a stable phase in the middle and another accelerated phase at the end of the fatigue life. This behavior is similar to that exhibited under constant and block loading.

- The crack propagation rate was correlated to the applied loading spectrum. Under higher load levels, where the fatigue life was limited to a small number of spectrum passes, an acceleration in crack propagation due to the overloads was observed. However, the crack propagation rate decreased to the previous rate after a short period.
- In spite of the presence of loading sequence effects under two-stage block loading for the examined bonded joints, the crack propagation rate was almost stable during 80% of the fatigue life. This behavior was attributed to the frequent change of the load level under variable amplitude loading, which accelerates the crack propagation rate and obscures the potential retardation and/or acceleration of the crack propagation rate due to the loading sequence effects.
- An inconsistency was identified between the accuracy of the constant life diagram formulation used and the corresponding life predictions, indicating the existence of another damage parameter related to the detrimental effect of frequent load transition. A simple modification of the damage summation rule by using a few block loading experiments to take this effect into account in the life prediction methodology resulted in significant improvement of the predictions.

## 7.6. References

1. Broutman LJ, Sahu S. A new theory to predict cumulative fatigue damage in fiberglass reinforced plastics. In: Composite materials: Testing and design (Second conference), ASTM STP 497. Philadelphia (1972), ASTM, pp. 170–188.
2. Yang JN, Jones DL. Effect of load sequence on the statistical fatigue of composite, AIAA journal, 1980;18(12):1525–1531.
3. Yang JN, Jones DL. Load sequence effects on graphite/epoxy $[\pm 35]_{2s}$ laminates. In: Long-term behavior of composites, STP 813, ASTM, Philadelphia (1983), pp. 246–262.
4. Jen MHR, Kau YS, Wu IC. Fatigue damage in a centrally notched composite laminate due to two-step spectrum loading. Int J Fatigue, 1994;16(3):193–201.
5. Found MS, Kanyanga SB. The influence of two-stage loading on the longitudinal splitting of unidirectional carbon-epoxy laminates, Fatigue Fract Engng Mater Struct, 1996;19(1):65–74.
6. Otani N, Song DY. Fatigue life prediction of composite under two-step loading, J Mater Sci, 1997;32(3):755–760.

7. Bartley-Cho J, Lim SG, Hahn HT, Shyprykevich P. Damage accumulation in quasi isotropic Graphite/Epoxy laminates under constant-amplitude fatigue and block loading, Compos Sci Technol, 1998;58(9):1535–1547.
8. Wahl NW, Mandell JF, Samborsky DD. Spectrum fatigue lifetime and residual strength for fiberglass laminates in tension, 2001 ASME Wind Energy Symposium, AIAA-2001-0025, ASME/AIAA, (2001).
9. Van Paepegem W, Degrieck J. (2002). Effects of load sequence and block loading on the fatigue response of fibre-reinforced composites. Mech Adv Mater Struc, 2002;9(1):19–35.
10. Hosoi A, Kawada H, Yoshino H. Fatigue characteristic of quasi-isotropic CFRP laminates subjected to variable amplitude cyclic loading of two-stage. Int J Fatigue, 2006;28(10 SPEC ISS):1284–1289.
11. Han KS, Abdelmohsen MH. Fatigue Life Scattering of RP/C, Int J of Vehicle Design, Technological advances in Vehicle Design Series, SP6, Designing with Plastics and Advanced Plastic Composites, 1983;218–227.
12. Hwang W, Han KS. Statistical study of strength and fatigue life of composite materials. Composites, 1987;18(1):47–53.
13. Hwang W, Han KS. Fatigue of composite materials – Damage model and life prediction. Composite Materials: Fatigue and Fracture, 2nd Volume. ASTM STP 1012, American Society for Testing and Materials, Philadelphia (1989), pp. 87–102.
14. Lee CH, Jen MHR. Fatigue response and modelling of variable stress amplitude and frequency in AS-4/PEEK composite laminates, Part 1: Experiments, J Compos Mater, 2000;34(11):906–929.
15. Lee CH, Jen MHR. Fatigue response and modelling of variable stress amplitude and frequency in AS-4/PEEK composite laminates, Part 2: Analysis and formulation, J Compos Mater, 2000;34(11):930–953.
16. Gamstedt EK, Sjögren BA. An experimental investigation of the sequence effect in block amplitude loading of cross-ply laminates, Int J Fatigue, 2002;24(2-4):437–446.
17. Found MS, Quaresimin M. Two-stage fatigue loading of woven carbon fibre reinforced laminates, Fatigue Fract Eng M, 2003;26(1):17–26.
18. Plumtree A, Melo M, Dahl J. Damage evolution in a [±45]2S CFRP laminate under block loading conditions, Int J Fatigue, 2010;32(1):139–145.
19. Smith MA, Hardy R. Fatigue research on bonded carbon fibre composite/metal joints, Composites, 1977;8(4):255–261.

20. Jeans LL, Grimes GC, Kan HP. Fatigue sensitivity of composite structure for fighter aircraft, J Aircraft, 1983;20(2):102–110.
21. Bond IP, Ansell MP. Fatigue properties of jointed wood composites: Part II Life prediction analysis for variable amplitude loading, J Mater Sci, 1998;33(16):4121–4129.
22. Sarkani S, Michaelov G, Kihl DP, Beach JE. Stochastic fatigue damage accumulation of FRP laminates and joints, J Struct Eng, 1999;125(12):1423–1431.
23. Erpolat S, Ashcroft IA, Crocombe AD, Abdel-Wahab MM. A study of adhesively bonded joints subjected to constant and variable amplitude fatigue. Int J Fatigue 2004;26(11):1189–1196.
24. Ashcroft IA. A simple model to predict crack growth in bonded joints and laminates under variable-amplitude fatigue, J Strain Anal Eng, 2004;39(6):707–716.
25. Nolting AE, Underhill PR, DuQuesnay DL. Variable amplitude fatigue of bonded aluminum joints, Int J Fatigue, 2008;30(1):178–187.
26. Shenoy V, Ashcroft IA, Critchlow GW, Crocombe AD. Fracture mechanics and damage mechanics based fatigue lifetime prediction of adhesively bonded joints subjected to variable amplitude fatigue, Eng Fract Mech, 2010;77 (7):1073–1090.
27. Zhang Y, Vassilopoulos AP, Keller T. Fracture of adhesively-bonded pultruded GFRP joints under constant amplitude fatigue loading. Int J Fatigue, 2010;32(7):979–987.
28. Yang JN, Du S. An exploratory study into the fatigue of composites under spectrum loading, J Compos Mater, 1983;17(6)511–526.
29. Halpin JC, Jerina KL, Johnson TA. Characteristics of composites for the purpose of reliability prediction. Analysis of test methods for high modulus fibers and composites. ASTM, West Conshohocken, p. 5–64, 1973.
30. Yang JN, Yang SH, Jones DL. A stiffness-based statistical model for predicting the fatigue life of graphite/epoxy laminates, J Comp Technol Res, 1989;11(4):129–134.
31. Read RJCL, Shenoi RA. A review of fatigue damage modeling in the context of marine FRP laminates, Marine Struct, 1995;8(3):257–278.
32. Passipoularidis VA, Philippidis TP. A study of factors affecting life prediction of composites under spectrum loading, Int J Fatigue, 2009;31(3):408–417.
33. Schaff JR, Davidson BD. Life prediction methodology for composite structures. Part I. Constant amplitude and two-step level fatigue, J Compos Mater, 1997;31(2):128–157.
34. Schaff JR, Davidson BD. Life prediction methodology for composite structures, Part II - Spectrum fatigue, J Compos Mater, 1997;31(2):158–181.

35. Filis PA, Farrow IR, Bond IP. Classical fatigue analysis and load cycle mix-event damage accumulation in fibre reinforced laminates, Int J Fatigue, 2004;26(6):565–573.
36. ten Have AA. WISPER and WISPERX: Summary paper describing their backgrounds, derivation and statistics, American Society of Mechanical Engineers, Solar Energy Division, 1993, p. 169-178.
37. Vassilopoulos AP, Manshadi BD, Keller T. Influence of the constant life diagram formulation on the fatigue life prediction of composite materials. Int J Fatigue, 2010;32(4):659–669.
38. Vassilopoulos AP, Manshadi BD, Keller T. Piecewise non-linear constant life diagram formulation for FRP composite materials. Int J Fatigue, 2010;32(10):1731–1738.
39. Boerstra GK. The multislope model: a new description for the fatigue strength of glass reinforced plastic, Int J Fatigue, 2007;29(8):1571–1576.

# 8 Conclusions and future work

## 8.1. Conclusions

This section presents the principal conclusions drawn from the research described in this thesis. The main conclusions are categorized for experimental and analytical investigations in the following sections.

### 8.1.1. Experimental investigations

The fatigue behavior of adhesively-bonded pultruded GFRP double-lap joints was experimentally examined under constant amplitude, block, and variable amplitude loadings. The results showed the high dependency of fatigue strength on loading parameters such as the mean load level, loading sequence, and load transition. A consistent correlation was found between the effects of these parameters and observed failure modes. The conclusions drawn from the experimental investigations are the following:

- The behavior of the examined joints was different under quasi-static tension and compression loading. This difference was associated with the layered architecture of the adherends, which led to different failure modes under tension and compression loading. Under tensile loading, the failure was dominated by cracks in the mat layers of the inner laminate (fiber-tear failure) while under compression, failure occurred in the roving layer in the middle of the inner laminate. The effect of loading rate on the stiffness and strength of DLJs was insignificant and a similar failure was observed under low and high loading rates.

- The fatigue failure modes of the DLJ joints under different constant amplitude loading patterns (different *R*-ratios) were found to be similar to the failure modes observed under quasi-static loads. A transition in the failure mode from tensile to compressive was observed when the mean of the cyclic load was decreased from zero to negative values. The failure modes under block and variable amplitude loading patterns were consistent with the failure modes under similar patterns of constant amplitude loading. The similarity of the failure modes enables the correlation of the block and variable amplitude data with the constant amplitude results.
- The fatigue behavior of the examined DLJs was more sensitive to tensile loading than to compressive loading. The increase of the mean load under constant amplitude loading led to an increase in the tensile and compressive fatigue life of the examined joints. The slopes of the S-N curves were decreased by increasing the mean load level.
- A general trend was identified regarding crack propagation behavior under constant and variable amplitude loading; fast crack growth at the beginning, up to around 10%, stable phase in the middle (10-90%), and accelerated phase at the end of (90-100%) the fatigue life. The similar crack propagation trend in DLJs under constant and variable amplitude loading showed that this behavior was independent of the applied loading patterns.
- The FCG curves derived under three load ratios ($R$=0.1, $R$=-1, and $R$=10) based on linear elastic fracture mechanics showed that this approach is capable of differentiating and characterizing fracture behavior for different failure modes. Among the FCG curves derived for different *R*-ratios, the steepest one occurred at $R$=10 since the crack propagated in the roving layer without significant fiber bridging. On the other hand, significant fiber bridging was associated with cracks that propagated between the mat layers of the inner laminates of the joints examined under $R$=0.1 and -1. However, the bridging fibers broke during the closing of the crack during the compressive component of each cycle under $R$=-1 and the corresponding FCG curve therefore had a lower slope than the FCG curve for $R$=0.1.

- The effect of loading sequence on fatigue life was found to be very significant. This effect was dependent on the loading type (tension or compression) and the applied load levels. The L-H (low-high) sequences led to shorter fatigue lives compared to H-L sequences under tensile loading. The reverse trend was observed under compressive loading. The effect of loading sequence on the fatigue life was associated with the crack growth rate during the block loading experiments and explained with the help of the observed failure modes. However, when frequent changes of load level occur, the abovementioned effect of loading sequence is diminished. This argument is also applicable for variable amplitude loading where a continuous – cycle-by-cycle – change of load levels appears. Therefore a relatively stable crack growth rate under variable amplitude loading during 80% of the fatigue life, despite the loading sequence effects, was observed confirming this conclusion.

### 8.1.2. Analytical investigations

The modeling for the variable amplitude fatigue life prediction was performed using the classic stress-life approach. The attempt to characterize constant amplitude fatigue behavior revealed the shortcomings of existing S-N models. A new S-N model was therefore developed to overcome these deficiencies. The effort to model the parameters involved in the variable amplitude loading such as the mean load and load transition effects also led to a new CLD formulation to model the mean load effect and a simple method to take into account the effect of frequent load transitions in the life prediction methodology. A life prediction methodology was established based on the developed models and modifications to predict the variable amplitude fatigue life of the bonded joints. A new computational tool, designated *CCfatigue*, was developed to integrate the different steps of this methodology. The conclusions drawn from the modeling phase are discussed in the following:

- The extrapolation of different S-N models for the modeling of fatigue behavior in the low- and high-cycle (LCF and HCF) fatigue regions inconsistently overestimated or underestimated the fatigue life. The analysis performed concerning the influence of including static strength data for the derivation of S-N curves showed that this approach improved the fatigue life estimation in the LCF region. However, the slopes of the S-N curves were negatively affected by this modification and the use of static data for derivation of the S-N curves is thus not recommended except for models developed based on the relationship between static and fatigue data. The reliability-based models were found to be very sensitive to the scatter of experimental data since the overall behavior of this type of S-N curve was strongly affected by censoring a few data points. The exponential and power law models were found to be the most appropriate, since they are simple and relatively insensitive to the scatter in the experimental data. Nevertheless, none of the studied models could adequately characterize the fatigue behavior of the examined bonded GFRP joints over the entire life range.

- The new hybrid S-N formulation developed in the present work exhibited better fitting accuracy than the commonly used fatigue models in low- and high-cycle fatigue regions while the formulation was not more complex than the linear regression models, since their parameters were used to establish the hybrid S-N curve. Also the continuous form of the hybrid S-N curve equation, in contrast to the two-segment models, makes it more convenient for use in fatigue life prediction methodologies for characterization of the entire fatigue lifetime. The accurate fitting of the hybrid S-N curve applied to different classes of composite materials and structures under different loading conditions proved its independency of the material system, loading conditions, failure mode, and range of experimental data.
- An asymmetric constant life diagram (CLD), shifted toward the compressive domain, was derived for the examined bonded joints. This shift was attributed to the higher fatigue strength of joints under compressive loading. The evaluation of different CLD formulations developed for composite materials for modeling the mean load effect showed their inconsistency under different loading conditions, especially under *R*-ratios around 1. The phenomenological CLD proposed here to take into account the creep-fatigue interaction provided greater accuracy and reliability compared to models commonly used for composite materials.
- The Linear Palmgren-Miner damage accumulation rule was found to be inadequate to model the fatigue life under block loading experiments. The application of the developed nonlinear models for composite materials is also questionable for the examined bonded joints since the fracture mechanics data showed no indication of nonlinear damage accumulation under fatigue loading. Therefore a detailed experimental program is required to study all parameters involved in order to develop a reliable damage accumulation model.
- The established fatigue life prediction methodology provided a relatively accurate estimation of fatigue life under variable amplitude loading patterns using only a

limited amount of constant amplitude experimental data. The accuracy of the prediction strongly depended on the selection of the appropriate constant life diagram. However, an inconsistency was identified between the accuracy of the CLDs and predicted VA fatigue lives. The predictions using the conservative CLDs provided more accurate results than the exact CLDs, suggesting the existence of another damaging parameter in addition to the linear accumulation model. This discrepancy was attributed to the damaging effect of the frequent load transition in the VA loading spectrum as previously identified in the BL investigation. A simple modification was proposed to include this effect in the life prediction methodology. The final results proved the significant improvement of the predictions using this modification.

- The analysis performed using the *CCfatigue* software proved its capability for the reliable calculation of the fatigue life of a composite material system and structures. The software contains several modules for the solution of the individual steps of a classic stress-life fatigue life prediction methodology, including the models developed in this work and models commonly used for composite materials and therefore enables the benchmarking processes for the comparison of different methods for the solution of the various tasks of the methodology. Since a commonly accepted complete fatigue theory does not yet exist, this software can assist the development process of a unified fatigue life prediction methodology, such as developing hybrid methods combining fatigue stress with strength and stiffness degradation measurements.

## 8.2. Original contributions

The original contributions of the present work to the project topic are summarized in the following:

- The behavior of adhesively-bonded FRP joints under quasi-static, constant and variable amplitude fatigue, and block loading was experimentally investigated. The information derived from these experiments led an exploration of the loading parameters that significantly influence fatigue behavior and therefore must be considered in the fatigue life prediction methodologies developed for bonded FRP joints under realistic loading patterns.
- The deficiencies of S-N formulations commonly used for modeling the constant amplitude fatigue behavior of materials and structures were highlighted, in particular the sensitivity of reliability-based models to the scatter of the experimental data. A

new semi-empirical S-N model was developed to overcome the shortcomings of these models and its applicability to a wide range of composite materials was proven.

- A new constant life diagram was established to model the mean load effect on the fatigue behavior of the examined bonded joints and resolve the limitations of the common CLD models, especially the consideration of the fatigue-creep interaction at high mean loads. The proposed model with a simple implementation procedure and a small amount of experimental data required for the modeling showed a better performance than the other models.
- The non-conservative life prediction results that were derived by the established classic life prediction methodology were attributed to the load transition in the variable amplitude loading that is skewed during the cycle counting. A modified Palmgren-Miner-like damage accumulation model was introduced in order to take this effect into account and therefore improve the life predictions under variable amplitude loading.
- A classic stress-life fatigue life prediction methodology was established using the developed models and applied to the adhesively-bonded FRP joints. New software was developed to incorporate different steps of this methodology. The accuracy of this methodology for predicting variable amplitude fatigue life was validated with the data acquired in experimental investigation.

## 8.3. Recommendations for future research

In spite of the research already performed on the fatigue behavior of bonded FRP joints, several more investigations should be carried out in order to provide a reliable basis for engineers to consider the fatigue approach in the designing of bonded joints. The recommendations for future research to complement the present study are discussed in the following.

### 8.3.1. Modeling of fatigue-creep interaction

In the classic constant life diagrams that are used to model the mean stress effect, the constant life lines converge to the ultimate tensile and compressive strength of materials regardless of the number of cycles. This simplification is due to the lack of information about the fatigue behavior when the cyclic amplitude is close or equal to zero. In fact, under this type of loading the material is subjected to creep rather than fatigue loading and therefore a fatigue-creep interaction can occur at high mean stresses. The hitherto performed modifications cannot provide a general model to characterize the fatigue-creep interaction in composite materials. The model developed in the present research showed that taking into account the fatigue-creep interaction significantly improves the accuracy of the constant life diagram, especially at high mean stress loadings. However this model requires some data in the high mean stress regions. The development of a CLD formulation that also considers the fatigue-creep interaction using the traditionally available fatigue data ($R$=0.1 and $R$=0.5) can significantly improve the performance of stress-life prediction methodologies used for composite materials.

### 8.3.2. Investigation of loading parameters

The effect of several loading parameters such as mean load, loading sequence, and load transitions were found to be very significant on the variable amplitude fatigue behavior of the examined bonded joints. Nevertheless, due to the variety of loading cases that occurs in a realistic loading pattern, many more investigations are required to explore other parameters involved in this process. These investigations can be carried out using simple appropriately designed loading block experiments. Finally the contribution of these parameters to fatigue failure can be examined using different variable amplitude loading patterns including narrow- and wide-band spectrums.

### 8.3.3. Development of damage accumulation models

The damage accumulation model employed in the present work was a linear model independent of the loading type. Although the predictions obtained using established methodology were accurate, the linear damage accumulation model was inadequate to estimate the damage sum under block and variable amplitude loading. The simple modification such as the model proposed in Section 7.4 showed that it is possible to develop a damage accumulation model that takes into account the dominant loading parameters involved in the fatigue life. Therefore a systematic experimental program supported by more sophisticated experimental investigations, such as the microscopy of the fracture surface and the area at the vicinity of the crack tip, can make a significant contribution to the development of these type of models.

# Annex 1

## *CCfatigue software*

### A1.1. Introduction

The fatigue behavior of modern engineering components and structures is considered to be very important in recent damage analysis procedures. Most engineering structures involve parts subjected to fluctuating loads and, as is widely accepted, the majority of all structural failures occur due to a fatigue mechanism, whereas purely static loading is rarely observed. As a result, fatigue analysis has become necessary for a growing number of companies and design teams.

A considerable number of fatigue theories and methodologies have therefore been developed, based on empirical, phenomenological modeling, or on the quantification of specific damage metrics, such as the residual strength and/or stiffness of the examined material or structural element. However, the influence of the method selection on the fatigue life prediction of composite materials under variable amplitude must be thoroughly examined. This effect can be investigated by using well established fatigue life prediction methodologies like the one presented in [1]. This kind of articulated methodology that sequentially solves the different problems that arise in a life prediction scheme can be used for the benchmarking of different modules and evaluation of their predicting capabilities.

A computational tool, designated *CCfatigue*, developed in [2], is presented in this Annex. This software assists the rapid interchange between modules in a complete methodology and the evaluation of their effect on the life prediction result. A small number of commercial solutions addressing this problem are available, e.g. [3, 4], but they mainly provide tools for work carried out in the environment of a large private company and do not concern composite materials. In many cases however, the needs of universities, research centers, and smaller firms are generally different from those that can be covered by the software products offered. This implies customization that is very difficult if not impossible from a commercial point of view. Given the current state of engineering software packages, modifying or extending the code requires that users have a thorough knowledge of the data structures, their procedures and the extent to which they affect specific portions of the code. The possibility of reusing code from other sources is also limited because data structures vary widely between programs. On the other hand, in-house software development forces researchers to devote part of their research time to developing and testing software instead of concentrating on their main scientific tasks. The aim of this tool is to create a generic software framework that will enable rapid prototyping of various life prediction schemes.

The *CCfatigue* software provides a relatively easy way to link customized components developed by users and researchers separately. The philosophy of this software framework was initially presented in [5]. In the form presented here, the software can be used as a powerful design tool but also as a research tool for the validation of in-house developed methods and benchmarking processes to assess the effectiveness of different modules. The first version of the software framework in the form of a windows-based user-friendly application is presented here.

## A1.2. Software framework

The estimation of fatigue life based on the so-called classic fatigue life prediction methodologies comprises the following tasks [1]:

- Cycle counting, to convert variable amplitude (VA) time series into blocks of certain numbers of cycles that correspond to constant amplitude and mean values.
- Interpretation of fatigue data to determine and apply the proper S-N formulation according to the examined material.

- Selection of the proper formulation in order to take the mean stress effect on the fatigue life of the examined material into account.
- Use of the proper fatigue failure criterion to calculate the allowable number of cycles for each block that results after cycle counting.
- Calculate the sum of the partial damage caused to the material by each of the applied loading blocks estimated by the cycle counting method.

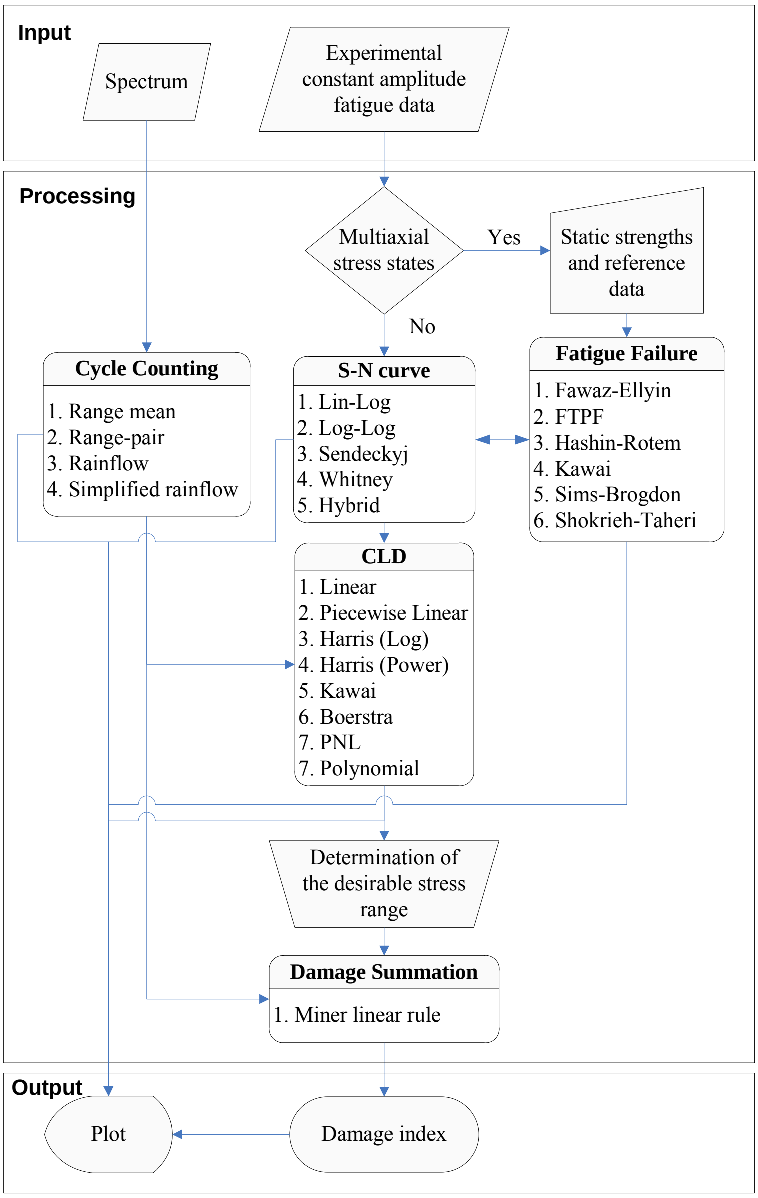
Input
Spectrum
Experimental constant amplitude fatigue data
Processing
Multiaxial stress states
Yes
No
Static strengths and reference data
Cycle Counting
1. Range mean
2. Range-pair
3. Rainflow
4. Simplified rainflow
S-N curve
1. Lin-Log
2. Log-Log
3. Sendeckyj
4. Whitney
5. Hybrid
Fatigue Failure
1. Fawaz-Ellyin
2. FTPF
3. Hashin-Rotem
4. Kawai
5. Sims-Brogdon
6. Shokrieh-Taheri
CLD
1. Linear
2. Piecewise Linear
3. Harris (Log)
4. Harris (Power)
5. Kawai
6. Boerstra
7. PNL
7. Polynomial
Determination of the desirable stress range
Damage Summation
1. Miner linear rule
Output
Plot
Damage index

Fig. A1.1. *CCfatigue* software flowchart

The software library contains a considerable number of solutions for each of the aforementioned steps of the methodology. The *CCfatigue* framework is thus capable of predicting the fatigue life of a number of different material systems under different loading conditions. The flowchart presented in Fig. A1.1 schematically shows the process used for predicting the Palmgren-Miner's damage index for a variable amplitude fatigue problem. The five distinctive steps of the methodology are presented in the section showing the data processing part of the software framework.

The software framework and modules are briefly introduced in this paragraph. The welcome page is shown in Fig. A1.2 and the five successive steps can be seen on the left hand side of this screen shot. The user can run each step independently of the others, select the desired solver from those available in the software library and obtain the solution. The data structure of the output file of each step has been designed in a way that it can be used as the input file for the following step. The implementation of the software for the life prediction of the selected materials and evaluation of the fatigue failure theories are presented in the following sections. An explanation of each one of the steps of the methodology and a brief discussion about the developed solvers follows.

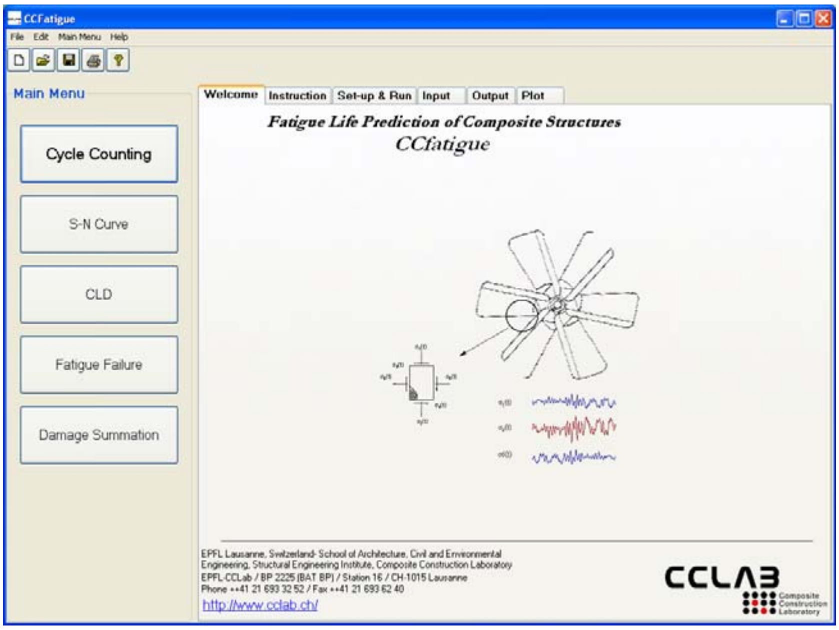

*Fatigue Life Prediction of Composite Structures*
*CCfatigue*

EPFL Lausanne, Switzerland- School of Architecture, Civil and Environmental Engineering, Structural Engineering Institute, Composite Construction Laboratory
EPFL-CCLab / BP 2225 (BAT BP) / Station 16 / CH-1015 Lausanne
Phone ++41 21 693 32 52 / Fax ++41 21 693 62 40
http://www.cclab.ch/

Fig. A1.2. Welcome page of *CCfatigue* software.

### A1.2.1. Cycle-counting methods

Cycle counting is used to summarize irregular load-versus-time histories by providing the number of occurrences of cycles of various sizes. The definition of a cycle varies with the method of cycle counting. A significant number of cycle counting techniques have been proposed over the last 30 years, e.g. ASTM E1049, with rainflow counting being the most widely used. Cycle-counting methods known as one-parameter techniques, e.g. level-crossing counting or peak-counting methods, are not applicable for the fatigue analysis of composite materials since they do not consider the significant mean stress effect on lifetime. Based on the previous comments, it can be concluded that - according to the application and material used - the appropriate cycle-counting technique should be selected very carefully.

In the current version of the fatigue analysis software, four cycle-counting techniques were programmed and are ready for use: simple range counting, range-pair counting, rainflow counting, and simplified rainflow counting. A comparison of the application of different cycle-counting algorithms for measurement of the number of cycles of a fatigue spectrum (MWISPERX [1]) is presented in Fig. A1.3.

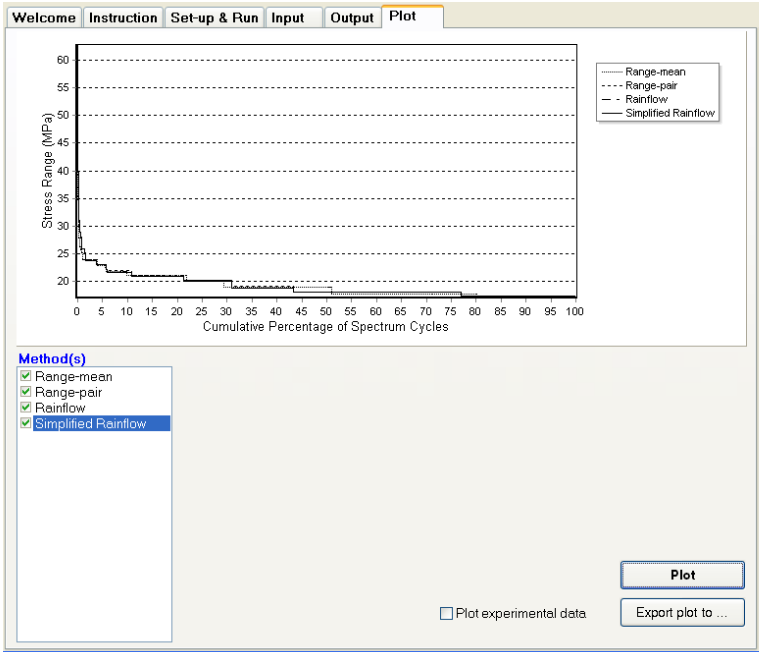
Welcome
Instruction
Set-up & Run
Input
Output
Plot
Stress Range (MPa)
60
55
50
45
40
35
30
25
20
0 5 10 15 20 25 30 35 40 45 50 55 60 65 70 75 80 85 90 95 100
Cumulative Percentage of Spectrum Cycles
Range-mean
Range-pair
Rainflow
Simplified Rainflow
Plot
Export plot to ...

Method(s)

☑ Range-mean
☑ Range-pair
☑ Rainflow
☑ Simplified Rainflow

☐ Plot experimental data

Fig. A1.3. Comparison of cumulative spectra resulting from different cycle-counting methods, MWISPERX time series [1]

### A1.2.2. S-N formulations

Traditionally, constant amplitude fatigue data are plotted on the S-N plane. The number of cycles to failure is plotted on the abscissa, and the stress parameter on the ordinate. However, as mentioned in ASTM E739, the stress level must be considered as the independent variable, whereas the corresponding number of cycles to failure must be the dependent one. This is how the fatigue data has been used here for the estimation of the derived S-N curve parameters. The selection of the fatigue model is very important for any fatigue analysis. The fatigue model expresses the experimental data in terms of theoretical equations which are subsequently used for any calculations. Therefore, the correlation between theory and test values is of paramount importance. A number of different types of fatigue models (or types of

S-N curves) were presented in the literature, with the most “famous” being the semi-logarithmic (called also Lin-Log) and the logarithmic (Log-Log) relationships. Based on these, it is assumed that the logarithm of the loading cycles is linearly dependent on the cyclic stress parameter or its logarithm. In addition to these, two other more sophisticated models that also take into account the reliability of the derived S-N curves and the hybrid S-N curve in Chapter 4 were implemented in the current version of *CCfatigue*. A demonstration of the software output S-N curves is graphically presented in Fig. A1.4.

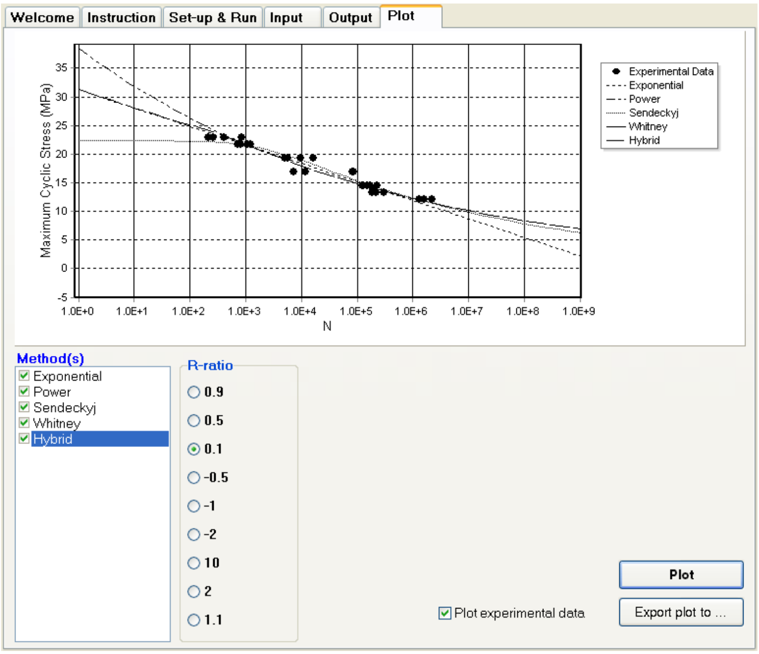
Welcome
Instruction
Set-up & Run
Input
Output
Plot
Maximum Cyclic Stress (MPa)
35
30
25
20
15
10
5
0
-5
1.0E+0
1.0E+1
1.0E+2
1.0E+3
1.0E+4
1.0E+5
1.0E+6
1.0E+7
1.0E+8
1.0E+9
N
Experimental Data
Exponential
Power
Sendeckyj
Whitney
Hybrid
Plot
Export plot to ...

Method(s)
☑ Exponential
☑ Power
☑ Sendeckyj
☑ Whitney
☑ Hybrid

R-ratio
○ 0.9
○ 0.5
● 0.1
○ -0.5
○ -1
○ -2
○ 10
○ 2
○ 1.1

☑ Plot experimental data

Fig. A1.4. Different types of S-N curves produced by *CCfatigue*

### A1.2.3 Constant life diagrams

Constant life diagrams (CLDs) are used in fatigue analysis in order to take into account the effect of mean stress on the fatigue behavior of composite materials. They provide a mean for the theoretical calculation of S-N curves under, virtually, any constant loading pattern. Several types of CLD formulations have been presented in previous work [6, 7]. Eight methods were implemented in this version of the software: two linear types - the commonly used “piecewise linear” CLD (similar to the standard Goodman diagram) and a modified “linear” diagram that takes into account the effect of creep under R-ratios ($R=\sigma_{min}/\sigma_{max}$) close to unity, and three non-linear ones: the “Harris” diagram (two versions of which have been modeled), the anisomorphic “Kawai” diagram, and the one proposed by Boerstra. The CLD model developed in Chapter 5 was also included in the software. A graphical representation of different Kawai and Harris diagrams is presented in Fig. A1.5.

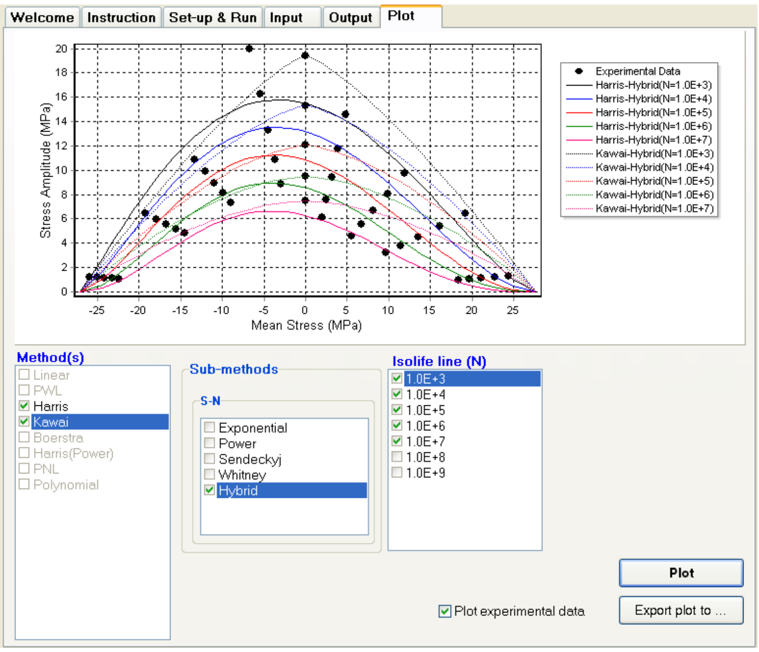
Welcome
Instruction
Set-up & Run
Input
Output
Plot
Stress Amplitude (MPa)
Mean Stress (MPa)
20
18
16
14
12
10
8
6
4
2
0
-25
-20
-15
-10
-5
0
5
10
15
20
25
● Experimental Data
Harris-Hybrid(N=1.0E+3)
Harris-Hybrid(N=1.0E+4)
Harris-Hybrid(N=1.0E+5)
Harris-Hybrid(N=1.0E+6)
Harris-Hybrid(N=1.0E+7)
Kawai-Hybrid(N=1.0E+3)
Kawai-Hybrid(N=1.0E+4)
Kawai-Hybrid(N=1.0E+5)
Kawai-Hybrid(N=1.0E+6)
Kawai-Hybrid(N=1.0E+7)
Plot
Export plot to ...

Method(s)
☐ Linear
☐ PWL
☑ Harris
☑ Kawai
☐ Boerstra
☐ Harris(Power)
☐ PNL
☐ Polynomial

Sub-methods
S-N
☐ Exponential
☐ Power
☐ Sendeckyj
☐ Whitney
☑ Hybrid

Isolife line (N)
☑ 1.0E+3
☑ 1.0E+4
☑ 1.0E+5
☑ 1.0E+6
☑ 1.0E+7
☐ 1.0E+8
☐ 1.0E+9

☑ Plot experimental data

Fig. A1.5. Typical piecewise linear and Harris CLDs derived by *CCfatigue*

### A1.2.4 Fatigue failure criteria

In the case of uniaxial stress states, this step can be omitted as selection of the appropriate S-N and CLD formulations suffices to take into account the effect of any possible variable amplitude loading pattern. However, when the loading or the resulting stress field is complex, constant life diagrams must be available for all strength parameters of the material in its symmetry directions, and the aforementioned interpolation procedure must be performed separately for all the plane stress tensor components. Their interaction in determining failure is then taken into account by considering multiaxial fatigue strength criteria. Six models were implemented in *CCfatigue* to cover as many concepts that deal with this problem as possible. Three of the selected models can be characterized as the macroscopic fatigue strength criteria, which are usually generalizations of known static failure theories for taking factors relevant to the fatigue life of the structure into account, such as number of cycles and loading frequency. The Hashin-Rotem (HR) [8], Sims-Brogdon (SB) [9] and Failure Tensor Polynomial in Fatigue (FTPF) [10, 11] are representative models of this class. However, the HR is limited to materials for which a discrimination can be made between fiber and matrix failure modes. It is basically applicable for unidirectional composite materials. The SB is a modification of the Tsai-Hill static criterion to take into account fatigue parameters, such as number of cycles, loading frequency etc., by replacing the static strengths with the corresponding fatigue functions. The FTPF was formulated on the same basis, although the Tsai-Hahn static criterion [12] was used instead of the Tsai-Hill and therefore the different tensile and compressive strengths were considered in the formulation.

Two more criteria, one proposed by Kawai (KW) [13] and the second by Fawaz and Ellyin (FWE) [14], seem very promising since they include the stress ratio in their formulation and can therefore be used without the need for any CLD and consequently are based on limited databases. According to [13] the KW model is able to predict the off-axis fatigue behavior of carbon- and glass fiber-reinforced composites under constant amplitude loading with positive mean values. The FWE criterion does not have any restrictions and can easily be used for prediction of the fatigue life of any unidirectional or multidirectional composite laminate provided that one S-N curve is available for use as reference, as well as the static strength of the examined material along the principal directions. The sixth model, introduced by Shokrieh and Taheri (ST) [15], is based on a strain energy concept and its use is also limited to the modeling of the off-axis fatigue behavior of unidirectional materials.

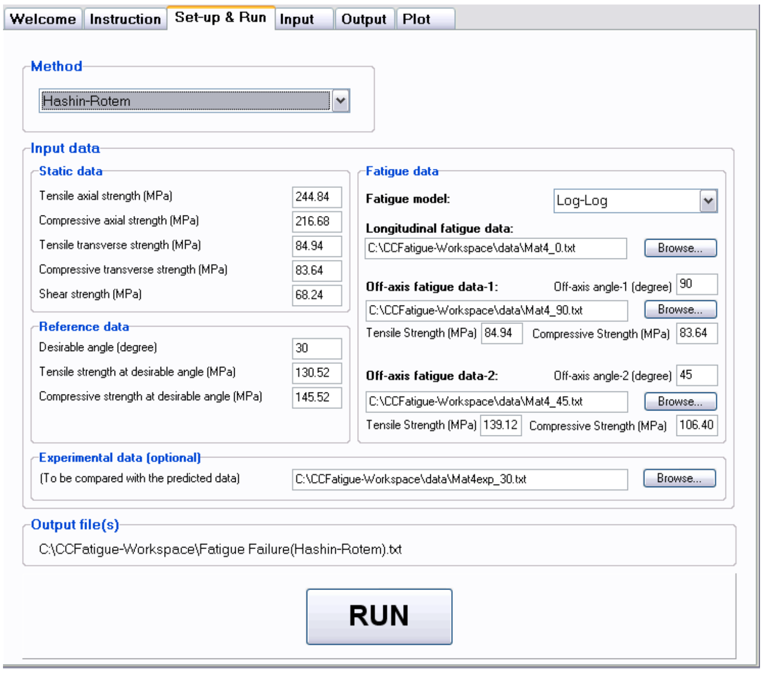

Method: Hashin-Rotem

Input data

Static data
Tensile axial strength (MPa) 244.84
Compressive axial strength (MPa) 216.68
Tensile transverse strength (MPa) 84.94
Compressive transverse strength (MPa) 83.64
Shear strength (MPa) 68.24

Reference data
Desirable angle (degree) 30
Tensile strength at desirable angle (MPa) 130.52
Compressive strength at desirable angle (MPa) 145.52

Fatigue data
Fatigue model: Log-Log
Longitudinal fatigue data: C:\CCFatigue-Workspace\data\Mat4_0.txt
Off-axis fatigue data-1: Off-axis angle-1 (degree) 90
C:\CCFatigue-Workspace\data\Mat4_90.txt
Tensile Strength (MPa) 84.94 Compressive Strength (MPa) 83.64
Off-axis fatigue data-2: Off-axis angle-2 (degree) 45
C:\CCFatigue-Workspace\data\Mat4_45.txt
Tensile Strength (MPa) 139.12 Compressive Strength (MPa) 106.40

Experimental data (optional)
(To be compared with the predicted data) C:\CCFatigue-Workspace\data\Mat4exp_30.txt

Output file(s)
C:\CCFatigue-Workspace\Fatigue Failure(Hashin-Rotem).txt

Fig. A1.6. *CCfatigue* interface for setup of fatigue failure solver

Although other models can be found in the literature, those selected here have been proved more accurate than others, e.g. see [10, 16], they can be easily implemented in *CCfatigue* and fatigue databases exist in the literature for the evaluation of their accuracy. The *CCfatigue* interface for the selection of the appropriate fatigue failure theory and input of the requested parameters is presented in Fig. A1.6 (The HR criterion is used for the demonstration). The static tensile and compressive strengths of the material are required as input together with three S-N curves (normally those corresponding to the fatigue functions of the material along the longitudinal and the transverse directions and under shear).

### A1.2.5 Damage summation

The last step of the *CCfatigue* software, presented in Fig. A1.7, concerns the ultimate damage summation. As presented, the combination of the solvers for the solution of each step of the articulated methodology can be selected in the interface. A fatigue damage index is the output of this module, corresponding to the damage accumulated in the material after the application of the selected fatigue spectrum. In the present version of the software the linear Palmgren-Miner rule is implemented. An investigation of the life prediction ability of the Palmgren-Miner rule in comparison with different damage accumulation metrics was presented in [17]. In some cases other more sophisticated rules provided more accurate results, however, the simplicity of the Palmgren-Miner rule and its applicability based on the minimum of experimental data impose its use.

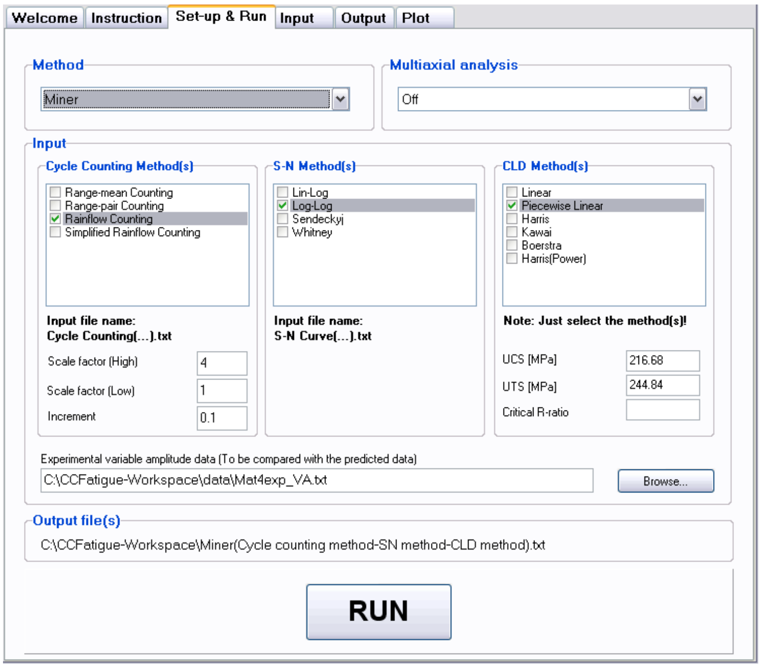

Method: Miner

Multiaxial analysis: Off

Input

Cycle Counting Method(s)
☐ Range-mean Counting
☐ Range-pair Counting
☑ Rainflow Counting
☐ Simplified Rainflow Counting

Input file name:
Cycle Counting(...).txt

Scale factor (High): 4
Scale factor (Low): 1
Increment: 0.1

S-N Method(s)
☐ Lin-Log
☑ Log-Log
☐ Sendeckyj
☐ Whitney

Input file name:
S-N Curve(...).txt

CLD Method(s)
☐ Linear
☑ Piecewise Linear
☐ Harris
☐ Kawai
☐ Boerstra
☐ Harris(Power)

Note: Just select the method(s)!

UCS [MPa]: 216.68
UTS [MPa]: 244.84
Critical R-ratio:

Experimental variable amplitude data (To be compared with the predicted data)
C:\CCFatigue-Workspace\data\Mat4exp_VA.txt

Output file(s)
C:\CCFatigue-Workspace\Miner(Cycle counting method-SN method-CLD method).txt

Fig. A1.7. Fatigue life prediction estimation based on selected modules

### A1.2.6 References

1. Philippidis TP, Vassilopoulos AP. Life prediction methodology for GFRP laminates under spectrum loading, Compos Part A–Appl S, 2004;35(6):657–666.

2. Vassilopoulos AP, Sarfaraz R, Manshadi BD, Keller T. A computational tool for the life prediction of GFRP laminates under irregular complex stress states: influence of the fatigue failure criterion, Comput Mater Sci, 2010;49(3):483-491.
3. http://www.ffatigue.net/index.php?task=home&l=en
4. http://www.ncode.com/Product.aspx?Product_ID=90
5. Vassilopoulos AP. A new software framework for fatigue life prediction of composite materials under irregular loading, Adv Compos Lett, 2006;15(1):23-29.
6. Vassilopoulos AP, Manshadi BD, Keller T. Influence of the constant life diagram formulation on the fatigue life prediction of composite materials, Int J Fatigue, 2010;32(4):659–669.
7. Vassilopoulos AP, Manshadi BD, Keller T. Piecewise non-linear constant life diagram formulation for FRP composite materials, Int J Fatigue, 2010;32(10):1731–1738.
8. Hashin Z, Rotem A. A fatigue failure criterion for fibre-reinforced materials, J Compos Mater, 1973;7(4):448–464.
9. Sims DF, Brogdon VH. Fatigue behaviour of composites under different loading modes. Fatigue of filamentary materials, ASTM STP 636, 1977, p. 185–205.
10. Philippidis TP, Vassilopoulos AP. Fatigue strength prediction under multiaxial stress, J Compos Mater, 1999;33(17):1578–1599.
11. Philippidis TP, Vassilopoulos AP. Complex stress state effect on fatigue life of GRP laminates. Part II, Theoretical formulation, Int J Fatigue, 2002;24(8):825–830.
12. Tsai SW, Hahn HT. Introduction to Composite Materials, Technomic, 1980.
13. Kawai M. A phenomenological model for off-axis fatigue behavior of unidirectional polymer matrix composites under different stress ratios, Compos Part A–Appl S, 2004;35(7–8):955–963.
14. Fawaz Z, Ellyin F. Fatigue failure model for fibre-reinforced materials under general loading conditions, J Compos Mater, 1994;28(15):1432–1451.
15. Shokrieh MM, Taheri-Behrooz F. A unified fatigue life model based on energy method, Compos Struct, 2006;75(1-4):444–450.
16. Quaresimin M, Susmel L, Talerja R. Fatigue behaviour and life assessment of composite laminates under multiaxial loadings, Int J Fatigue, 2010;32(1):2-16.
17. Passipoularidis VA, Philippidis TP. A study of factors affecting life prediction of composites under spectrum loading, Int J Fatigue, 2009;31(3):408–417.

# Annex2

## Pultruded GFRP laminates

### A2.1. Overview

Pultruded GFRP laminates, supplied by Fiberline A/S, Denmark, consisted of E-glass fibers and isophthalic polyester resin were used for fabrication of bonded joints. The fiber architecture and fiber content of the laminates was determined by burn-off experiments. An estimation of the nominal thickness of each layer was derived by optical microscopy. Tensile mechanical properties of laminates were determined by using tension experiments on pultruded laminates.

### A2.2. Burn-off

The burn-off experiments on three specimens cut from the long laminates were carried out according to test method I – procedure G of the ASTM D3171-09. The specimens were kept for 5 hours at 600$^{o}$C in an electric oven. The fiber volume fraction was calculated according to the fiber density of 2560 kg/m$^3$ specified by the manufacturer and weight of specimens before and after resin burn-off (see Fig. A2.1). The detail results of burn-off tests are presented in Table A2.1. Typical architecture of laminates is also shown in Fig. A2.2.

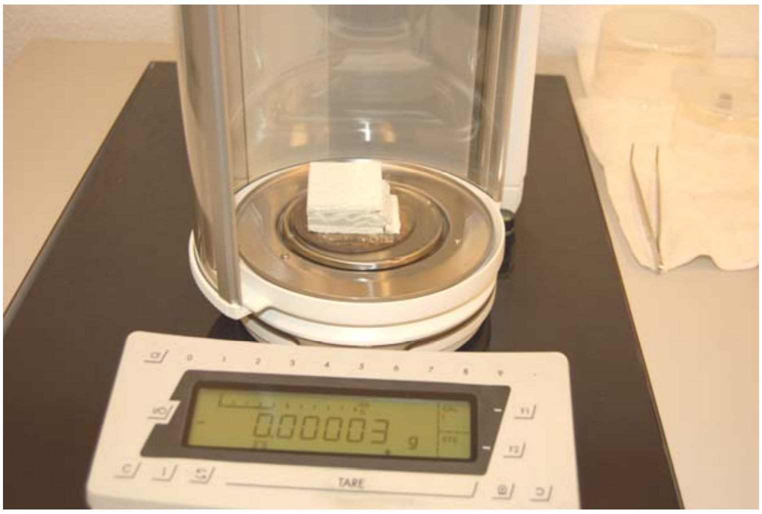

Fig. A2.1. Weight measurement of specimens after burn off

Table A2.1. Burn-off test results

| | **Specimen No.** | | |
|---|---|---|---|
| | **1** | **2** | **3** |
| Dimension [mm] | 39.25 x 40.30 x 5.90 | 39.60 x 40.60 x 5.90 | 39.40 x 40.40 x 5.80 |
| Volume [$mm^3$] | 9332.47 | 9485.78 | 9232.21 |
| Initial mass [gr] | 15.64514 | 16.34446 | 15.61177 |
| Final mass (after burn-off) [gr] | 10.03253 | 10.35031 | 10.25169 |
| Volume of fiber [$mm^3$] | 3.96543 | 4.09103 | 4.05205 |
| Fiber volume fraction | **42.49** | **43.13** | **43.89** |
| Fiber weight fraction | 64.13 | 63.33 | 65.67 |

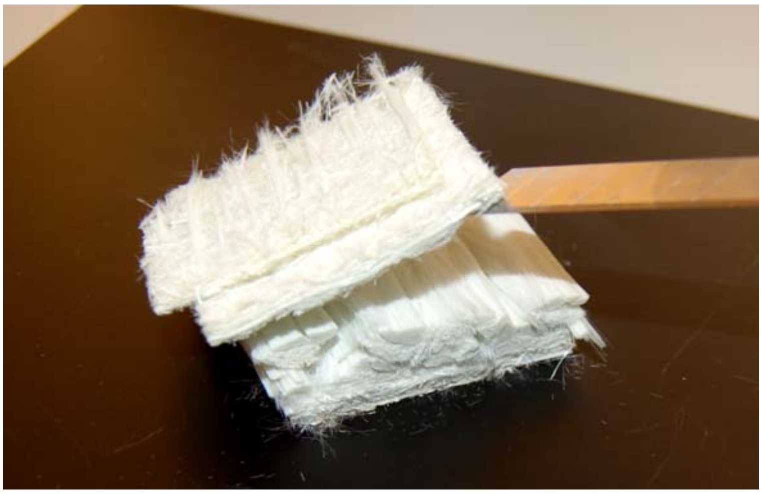

Fig. A2.2. Typical architecture of laminates after burn-off

## A2.3. Optical microscopy

Optical microscopy of cross section of laminates was performed in Laboratory of Mechanical Metallurgy (LMM) in EPFL. The preparation procedure for samples to be examined by an optical microscope is explained in the following:

1. Pultruded GFRP laminates were cut into small pieces.
2. Each piece was placed in a circular plastic mold (25-mm inner diameter) with the surface to be investigated facing downwards. A colorless epoxy resin (Epofix) was mixed at a resin-to-hardener ratio of 25:3 and poured onto the laminate piece in the mold.
3. The samples were placed in a vacuum chamber connected to a vacuum pump and air bubbles inside the sample were sucked out.
4. The samples were left to cure for 24 hours while subjected to a pressure of 2.5 bar.
5. The samples were removed from the mold and polished manually using polishing papers. The surface to be investigated was then polished by a high-speed polishing machine using discs with different roughnesses. In order to obtain a good finish of the sample surface, diamond discs of up to three microns were used. The final specimens are shown in Fig. A2.3.

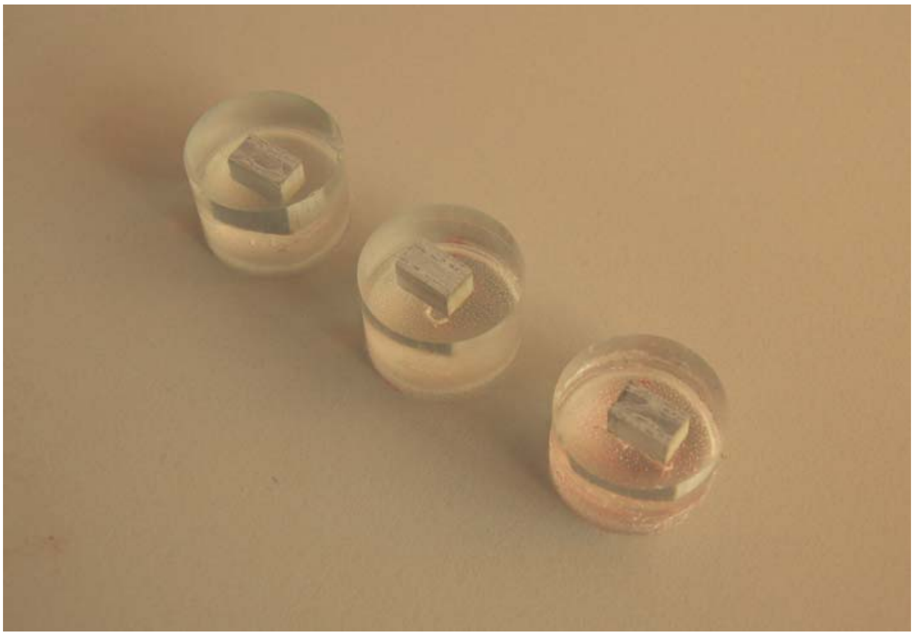

Fig. A2.3. Polished specimens for optical microscopy

After preparation, the samples were placed under the optical microscope (ZEISS – Axioplan2 shown in Fig. A2.4).

Fig. A2.4. Polished specimens for optical microscopy

The apertures and optical lenses (focusing) were adjusted to obtain the best contrast and resolution results. Fig. A2.5. shows the microscopic view of examined pultruded laminates. The presented cross section in this figure is perpendicular to pultrusion direction. An estimation of the nominal thickness of each layer is also given in Fig. A2.5.

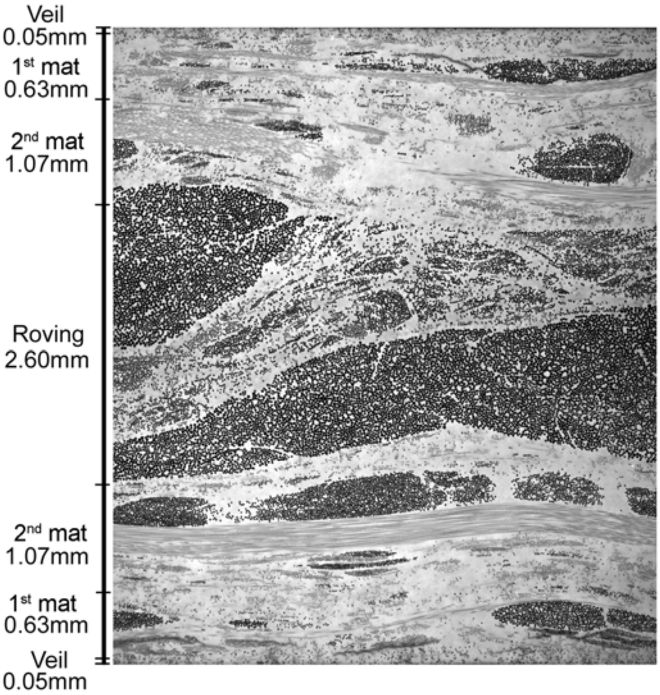
Veil
0.05mm
1st mat
0.63mm
2nd mat
1.07mm
Roving
2.60mm
2nd mat
1.07mm
1st mat
0.63mm
Veil
0.05mm

Fig. A2.5. Microscopic view of laminates

## A2.4. Tensile experiments

The longitudinal strength and Young's modulus of the GFRP laminate were obtained from tensile experiments, according to ASTM D3039-08. Three specimens were prepared and instrumented with two strain gages (type 1-LY18-6/120) in longitudinal direction (front and back face) and one in transverse direction for determination of Poisson's ratio, as shown in Fig. A2.6. The width of long laminates was 40 mm. The total length of specimens, cut from long laminates, were 450 mm with the gage length of 150 mm.

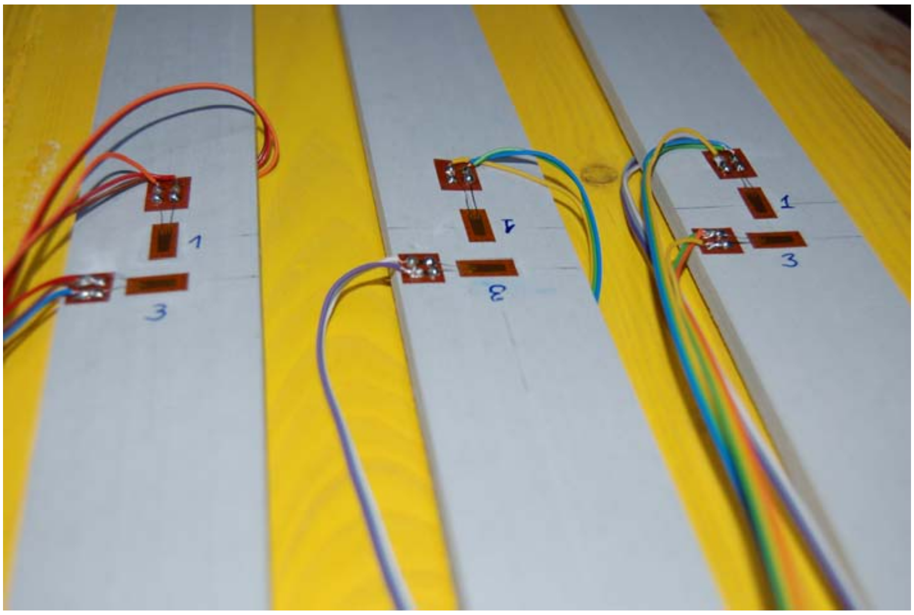

Fig. A2.6. Instrumentation of 6 mm thick laminates with 3 strain gages

All experiments were carried out on a Zwick universal 500kN machine (Fig. A2.7) under laboratory conditions (23±5°C and 50±10% RH). Quasi-static tensile experiments were performed under displacement-control mode with a ramp rate of 2 mm/min. Typical failure of examined laminates is shown in Fig. A2.8. Details of experimental data for different specimens are presented in Table A2.2. The derived stress-strain curves are presented in Figs. A2.9-A2.11. The value of stress was calculated based on the load recorded from the machine and the average cross section of laminates (average of three measurements).

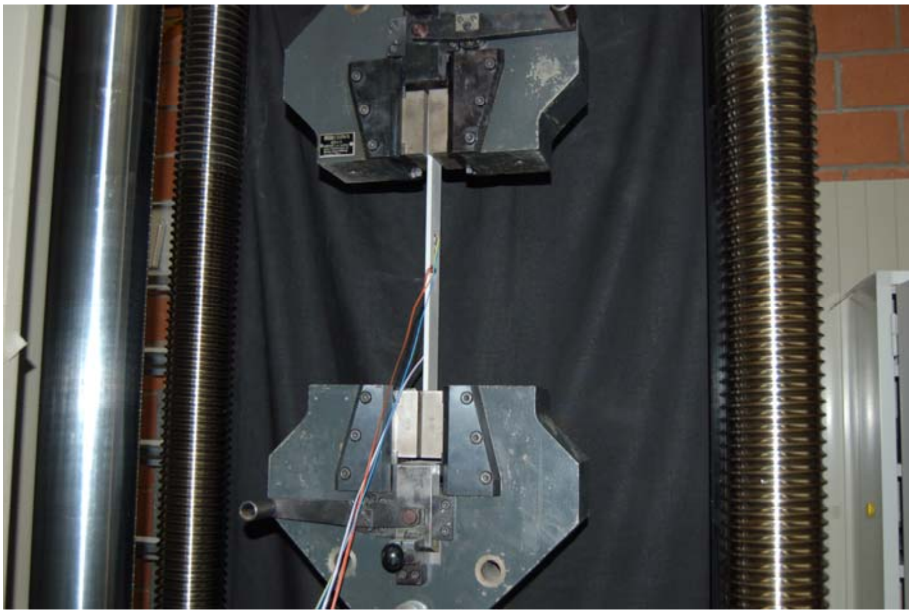

Fig. A2.7. Zwich universal 500 kN machine for tension experiments

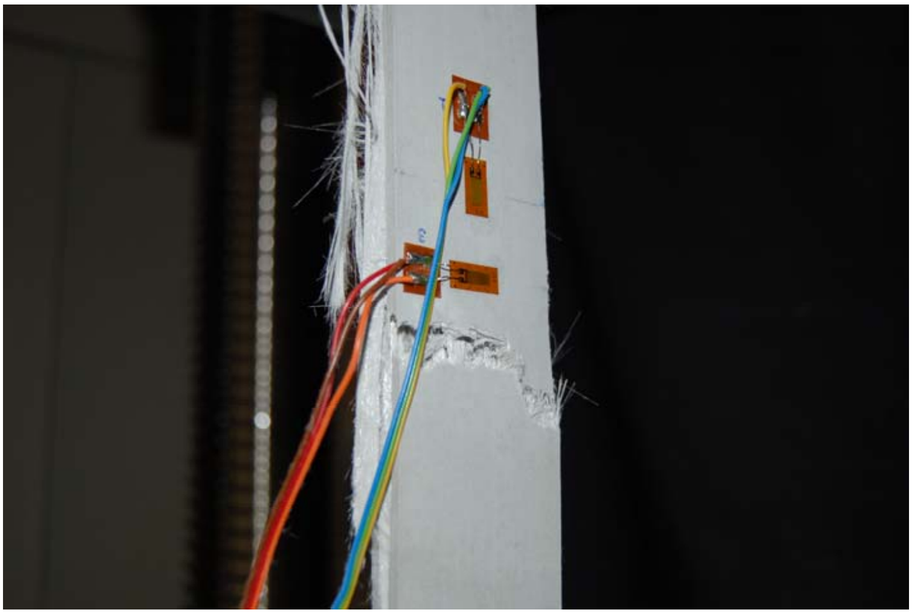

Fig. A2.8. Typical tensile failure of laminates

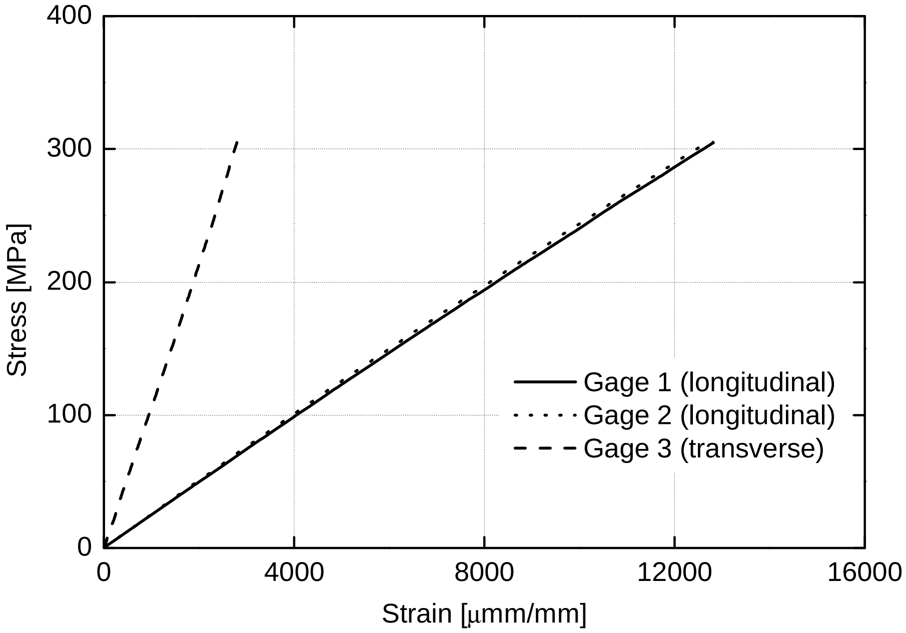

Fig. A2.9. Strain-stress curve derived by strain gages – Specimen No. 1

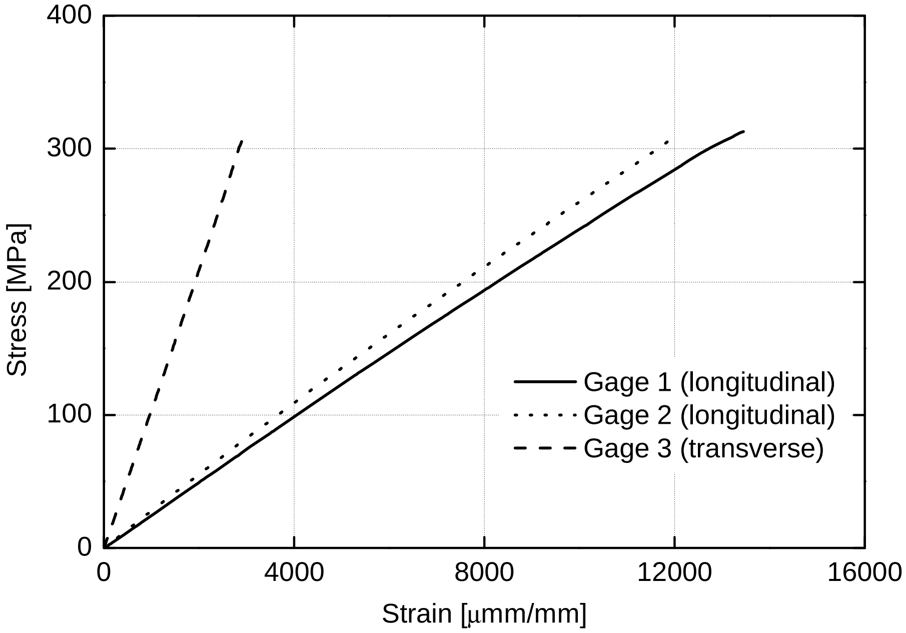

Fig. A2.10. Strain-stress curve derived by strain gages – Specimen No. 2

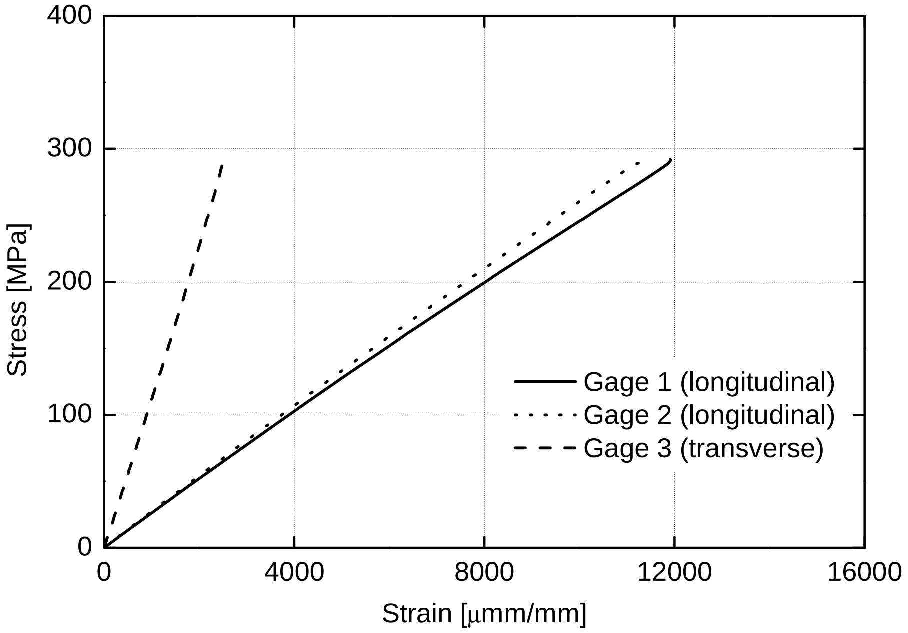

Fig. A2.11. Strain-stress curve derived by strain gages – Specimen No. 3

Table. A2.2. Longitudinal tensile test results for pultruded laminates

| | Specimen No. | | |
|---|---|---|---|
| | 1 | 2 | 3 |
| Average thickness [mm] | 6.22 | 6.12 | 6.14 |
| Average width [mm] | 40.71 | 41.02 | 40.83 |
| Average area [mm$^2$] | 253.22 | 251.04 | 250.70 |
| Maximum load [kN] | 77.24 | 78.56 | 76.34 |
| Tensile strength [Mpa] | 305.04 | 312.94 | 304.51 |
| Longitudinal strain at start point[a] | 999.1 | 1006.6 | 1010 |
| Transverse strain at start point | 240.5 | 237.7 | 237.7 |
| Load at start point [kN] | 6.32 | 6.12 | 6.62 |
| Stress at start point [MPa] | 24.96 | 24.38 | 26.41 |
| Longitudinal strain at end point[a] | 3032 | 3012.6 | 3018 |
| Transverse strain at end point | 710.2 | 722.4 | 702.8 |
| Load at end point [MPa] | 19 | 18.66 | 19.52 |
| Stress at end point [Mpa] | 75.03 | 74.33 | 77.86 |
| Tensile chord modulus of elasticity [Gpa] | 24.63 | 24.90 | 25.63 |
| Poisson’s ratio | 0.23 | 0.24 | 0.23 |
| **Modulus of Elasticity [Gpa]** | | | |
| • Average | | **25.05** | |
| • Standard deviation | | 0.514 | |
| • Coefficient of variation | | 2.05 | |
| **Poisson’s ratio** | | | |
| • Average | | **0.23** | |
| • Standard deviation | | 0.006 | |
| • Coefficient of variation | | 2.53 | |
| **Tensile strength [Mpa]** | | | |
| • Average | | **307.49** | |
| • Standard deviation | | 4.719 | |
| • Coefficient of variation | | 1.53 | |

[a] For definition of start and end point see ASTM D3039

# Annex 3

## Double-lap joints quasi-static loading

### A3.1. Overview

Quasi-static tensile and compressive experiments were performed under two different loading modes: A displacement-control mode with a ramp rate of 1 mm/min – designated the low loading rate (LLR) – and a load-control mode with a ramp rate of around 350 kN/s – designated the high loading rate (HLR). The loading rate selected for the load-control mode is similar to the highest loading rate applied during fatigue loading. Five specimens under tensile loading and LLR and three samples per loading condition for the other cases, i.e. tension-HLR, compression-HLR and compression-LLR, were examined. All experiments were carried out on an INSTRON 8800 servohydraulic machine (see Fig. A3.1) under laboratory conditions (23±5°C and 50±10% RH).

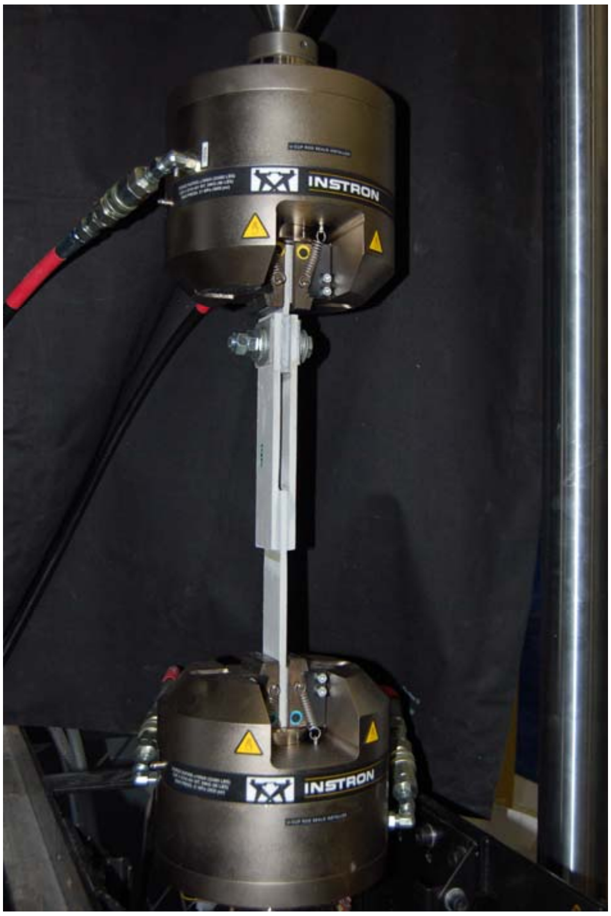

Fig. A3.1. INSTRON 8800 servohydraulic 100 kN machine and a double lap joint installed for experiment

## A3.2. Tension experiments

### A3.2.1. Failure mode

The observed failure mode was a fiber-tear failure as presented in Fig. A3.2 for a specimen tested under tensile loads. A dominant crack initiated from the joint corner of one of the bond lines – the upper in this figure – between the adhesive and the inner laminate and then shifted deeper, between the first and the second mat layers of the inner laminate, and propagated along this path up to failure.

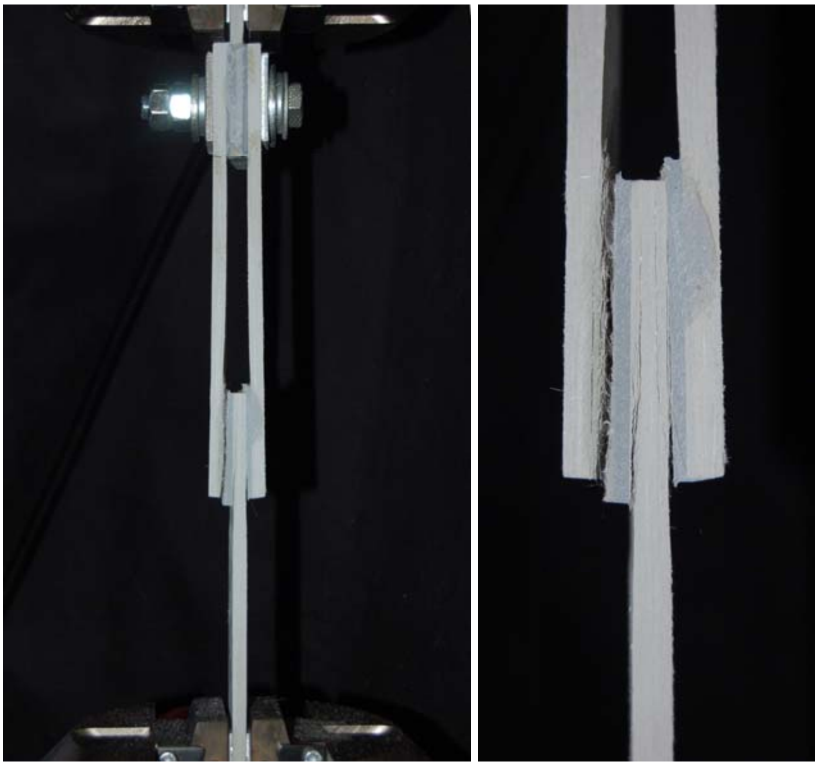

Fig. A3.2. Failure of double lap joint under quasi-static tensile loading

### A3.2.2. Load-displacement curve

The load-displacement curves derived by the machine for tension experiments are shown in Figs. A3.3 and A3.4 for LLR and HLR experiments respectively.

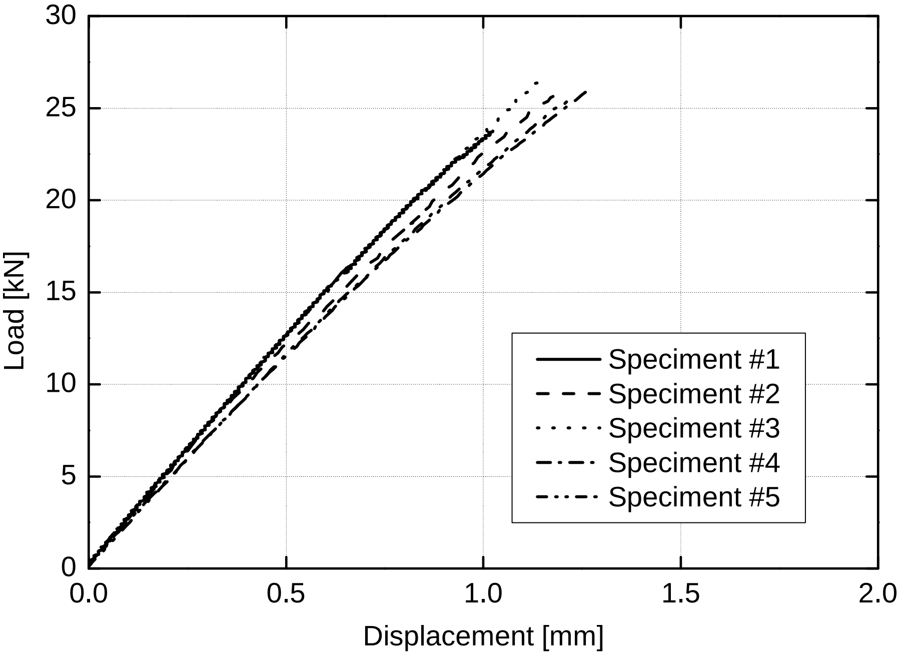

Fig. A3.3. Load-displacement curves for tension experiments under LLR

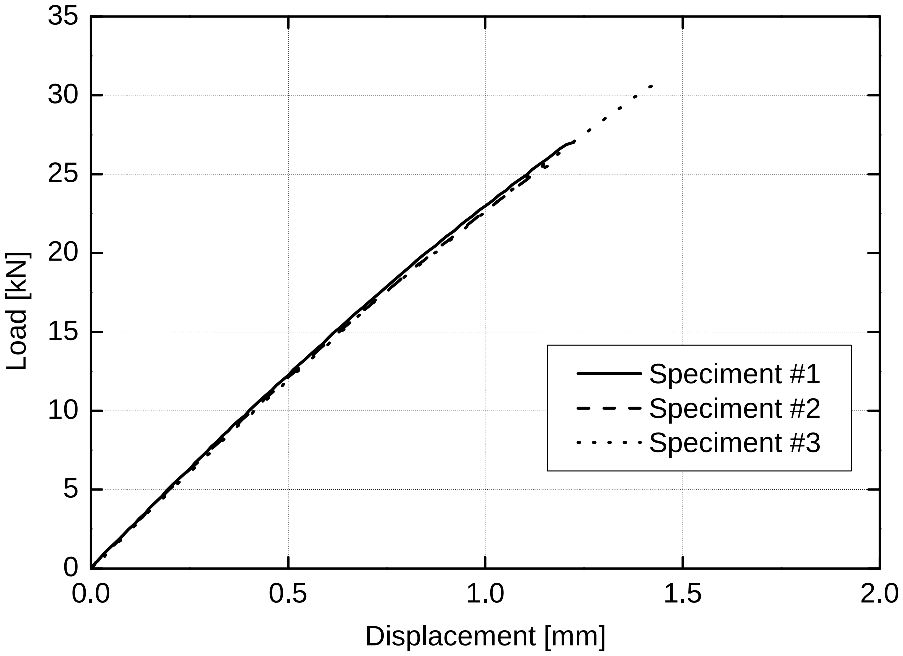

Fig. A3.4. Load-displacement curves for tension experiments under HLR

### A3.2.3. Stiffness and failure load

The examined DLJs showed an almost linear load-elongation behavior up to a brittle failure under tension independent of the applied loading rate. The failure loads recorded for the examined joints are presented in Table A3.1. The calculated tensile stiffness of joints is presented in Table A3.2.

Table A3.1. Ultimate load [kN] of tension experiments

| | **Specimen No.** | | | | | **Averaged Ultimate Load [kN]** | **Standard deviation** |
|---|---|---|---|---|---|---|---|
| | **1** | **2** | **3** | **4** | **5** | | |
| **Low loading rate (LLR)** | 23.8 | 25.9 | 26.7 | 25.9 | 25.4 | 25.5 | 0.97 |
| **High loading rate (HLR)** | 27.0 | 25.5 | 30.7 | --- | --- | 27.7 | 2.17 |

Table A3.2. Stiffness [kN/mm] of tension experiments

| | **Specimen No.** | | | | | **Averaged Stiffness [kN/mm]** | **Standard deviation** |
|---|---|---|---|---|---|---|---|
| | **1** | **2** | **3** | **4** | **5** | | |
| **Low loading rate (LLR)** | 26.5 | 26.1 | 26.9 | 23.3 | 23.2 | 25.2 | 1.61 |
| **High loading rate (HLR)** | 24.9 | 24.6 | 24.2 | --- | --- | 24.6 | 0.28 |

## A3.3. Compression experiments

### A3.3.1. Failure mode

The observed failure mode as presented in Fig. A3.5 for a specimen tested under compression was different. The dominant crack initiated and propagated from the right side of the inner laminate (as shown in Fig. A3.5) inside the roving layer.

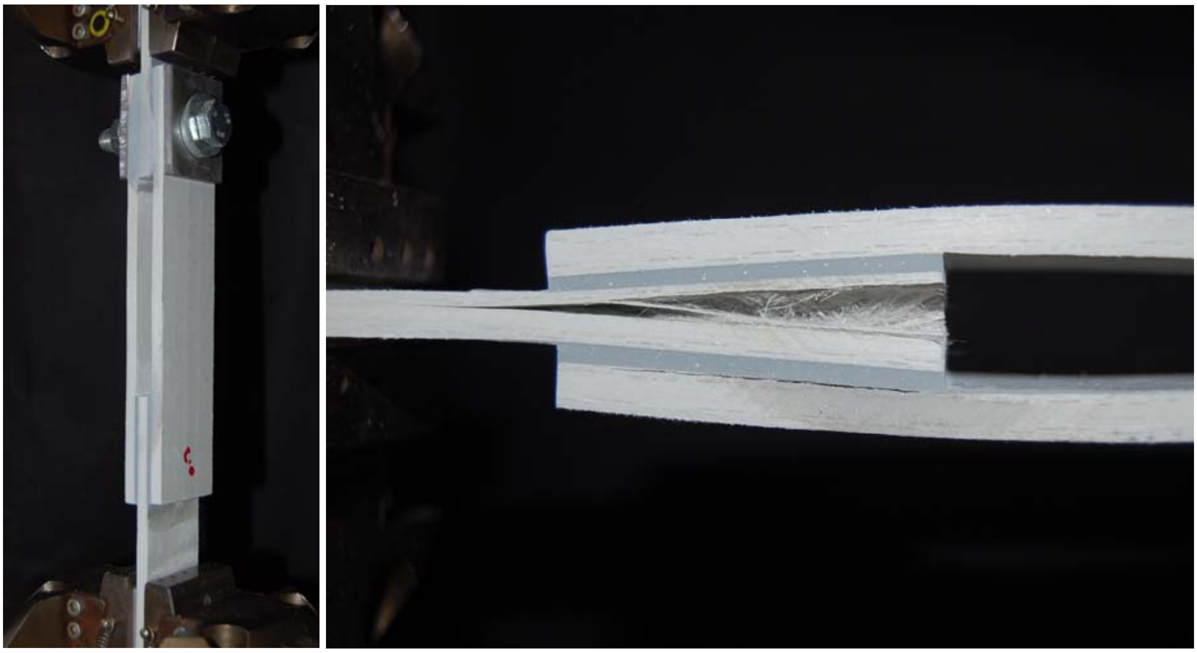

Fig. A3.5. Failure of double lap joint under quasi-static tensile loading

### A3.3.2. Load-displacement curve

The load-displacement curves derived by the machine for compression experiments are shown in Figs. A3.6 and A3.7 for LLR and HLR experiments respectively.

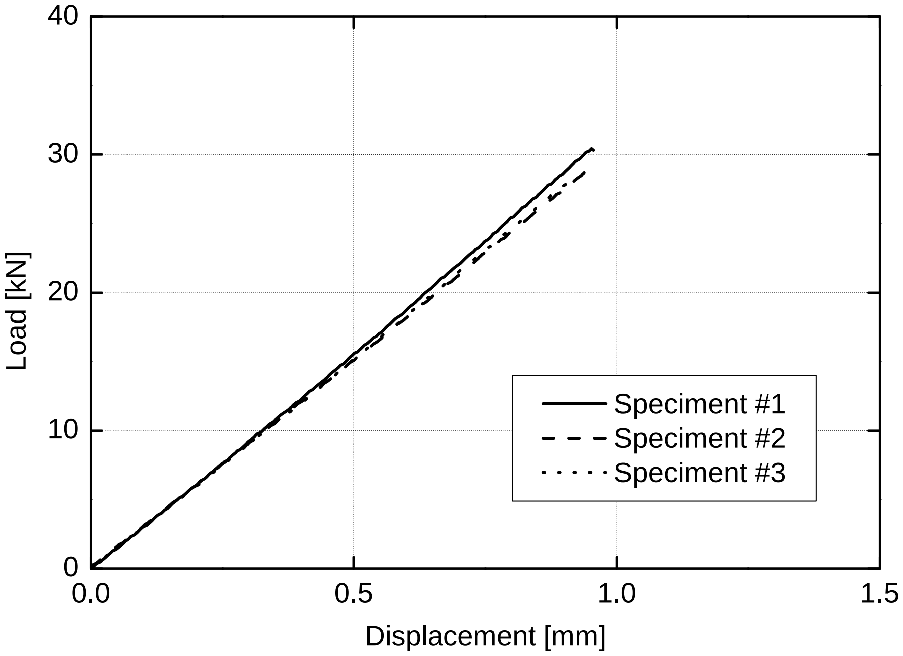

Fig. A3.6. Load-displacement curves for compression experiments under LLR

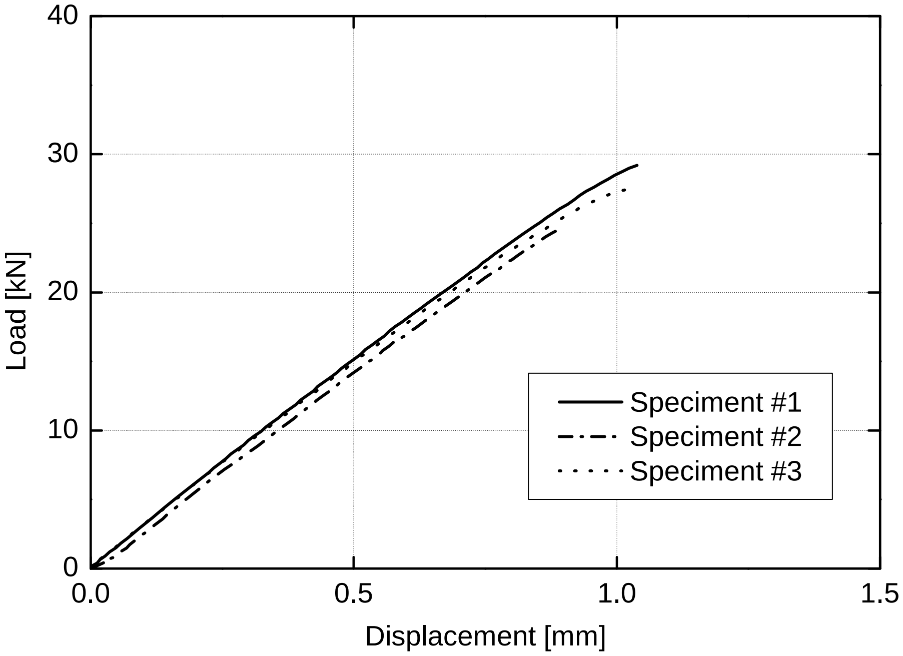

Fig. A3.7. Load-displacement curves for compression experiments under HLR

### A3.3.3. Stiffness and failure load

The examined DLJs showed an almost linear load-elongation behavior up to a brittle failure under compression independent of the applied loading rate. The compressive failure loads recorded and the calculated stiffness for the examined joints are presented in Tables A3.3 and A3.4.

Table A3.3. Ultimate load [kN] of compression experiments

| | Specimen No. | | | Averaged Ultimate Load [kN] | Standard deviation |
|---|---|---|---|---|---|
| | **1** | **2** | **3** | | |
| **Low loading rate (LLR)** | -30.4 | -28.8 | -27.8 | -29.0 | 1.07 |
| **High loading rate (HLR)** | -29.2 | -24.5 | -27.5 | -27.1 | 1.92 |

Table A3.4. Stiffness [kN/mm] of compression experiments

| | Specimen No. | | | Averaged Stiffness [kN/mm] | Standard deviation |
|---|---|---|---|---|---|
| | **1** | **2** | **3** | | |
| **Low loading rate (LLR)** | 31.1 | 30.2 | 30.3 | 30.5 | 0.39 |
| **High loading rate (HLR)** | 30.7 | 29.6 | 30.5 | 30.2 | 0.46 |

# *Curriculum Vitae*

## Roohollah SARFARAZ KHABBAZ

Data of birth: 24 Dec. 1979

Nationality: Iranian

### EDUCATION

| | |
|---|---|
| **2008-2012** | ***Ph.D.:*** Composite Construction Laboratory (CCLAB), Swiss Federal Institute of Technology Lausanne (EPFL), Lausanne, Switzerland |
| **2003-2005** | ***M.Sc.:*** Aerospace Engineering, Sharif University of Technology, Tehran, Iran. |
| **1998-2003** | ***B.Sc.:*** Aerospace Engineering, Sharif University of Technology, Tehran, Iran. |

### PROFESSIONAL EXPERIENCE

**2007-2008** *Puya Turbine Co., Iran*

**Project manager (part time)**

Maintenance of turbochargers of diesel locomotives

**2002-2007** *Fanavaran Ghader Co., Iran*

**Project manager (part time and full time)**

Engineering, Procurement, and Construction of the auxiliary units of the Iranian gas trunk line stations for the National Iranian Gas Company (NIGC) under the license of SIEMENS turbo-machinery division.

## PUBLICATIONS

### *Journal papers*

1. Sarfaraz R, Vassilopoulos AP, Keller T. Modeling the constant amplitude fatigue behavior of adhesively-bonded pultruded GFRP joints, Journal of Adhesion Science and Technology, Journal of Adhesion Science and Technology, DOI:10.1080/01694243.2012.727158.
2. Sarfaraz R, Vassilopoulos AP, Keller T. Experimental investigation and modeling of mean load effect on fatigue behavior of adhesively-bonded pultruded GFRP joints, International Journal of Fatigue, 2012;44:245-252.
3. Sarfaraz R, Vassilopoulos AP, Keller T. A hybrid S-N formulation for fatigue life modeling of composite materials and structures, Composite Part A-Applied Science, 2012;43(3):445-453.
4. Sarfaraz R, Vassilopoulos AP, Keller T. Experimental investigation of fatigue behavior of adhesively-bonded pultruded GFRP joints under different load ratios, International Journal of Fatigue, 2011;33(11):1451-1460.
5. Vassilopoulos AP, Sarfaraz R, Manshadi BD, Keller T. A computational tool for the life prediction of GFRP laminates under irregular complex stress states: influence of the fatigue failure criterion, Computational Materials Science, 2010;49(3):483-491.
6. Fayazbakhsh K, Abedian A, Dehghan Manshadi B, Sarfaraz R. Introducing a novel method for materials selection in mechanical design using Z-transformation in statistics for normalization of material properties, Materials & Design, 2009;30(10):4396-4404.
7. Sarfaraz R, Dehghan Manshadi B, Abedian A, Mahmudi R. A simplified fuzzy logic approach for materials selection in mechanical engineering design, Materials & Design, 2009;30(3):687-697.
8. Sarfaraz R, Dehghan Manshadi B, Abedian A. Non-linear analysis of FGM plates under pressure loads using higher-order shear deformation theories, Composite Structures, 2009;89(3):333-496.

## *Conference papers*

1. Sarfaraz R, Vassilopoulos AP, Keller T. Phenomenological modeling of the fatigue life of adhesively-bonded joints, 10th International Conference on Durability of Composite Systems (DURACOSYS-2012), Brussels, Belgium, 17-19 September, 2012.
2. Sarfaraz R, Vassilopoulos AP, Keller T. Influence of the mean load effect interpretation on the fatigue life prediction of GFRP structural joints, In proceeding of the 15th European Conference on Composite Materials (ECCM15), Venice, Italy, 24-28 June, 2012.
3. Sarfaraz R, Vassilopoulos AP, Keller T. Fatigue life behavior of adhesively-bonded pultruded FRP joints under tensile and compressive loading, In proceeding of the 4th international conference on the durability and sustainability of fibre reinforced polymer (FRP) composites for construction and rehabilitation (CDCC-11), pp. 229-236 , Quebec City, Canada, 20-22 July, 2011.
4. Sarfaraz R, Dehghan Manshadi B, Abedian A, Mahmudi R. Materials Selection for Spar of a Human Powered Aircraft (HPA) Using a Simplified Fuzzy Logic Approach, In proceeding of the 7th Iranian Aerospace Society Conference (Aero2008), pp. 55-56, Sharif University of Technology, Tehran, Iran. 19-21 February, 2008.